(1)

VOLUME II

RESEARCH AND DEVELOPMENT

IN SUPPORT OF THE

SURFACE CHEMISTRY BRANCH

GEO-CENTERS, INC.

GC-TR-88-1639

VOLUME II

RESEARCH AND DEVELOPMENT

IN SUPPORT OF THE

SURFACE CHEMISTRY BRANCH

FINAL REPORT

PREPARED FOR
NAVAL RESEARCH LABORATORY
4555 OVERLOOK DRIVE, S.W.
WASHINGTON, D.C. 20375-5000
UNDER CONTRACT NUMBER N00014-86-C-2096

PREPARED BY
GEO-CENTERS, INC.
7 WELLS AVENUE
NEWTON CENTRE, MA 02159

JUNE 1988

GEO-CENTERS, INC.

UNCLASSIFIED
SECURITY CLASSIFICATION OF THIS PAGE

REPORT DOCUMENTATION PAGE

1a. REPORT SECURITY CLASSIFICATION UNCLASSIFIED	1b. RESTRICTIVE MARKINGS
2a. SECURITY CLASSIFICATION AUTHORITY	3. DISTRIBUTION/AVAILABILITY OF REPORT Approved for public release; distribution unlimited.
2b. DECLASSIFICATION/DOWNGRADING SCHEDULE	
4. PERFORMING ORGANIZATION REPORT NUMBER(S) GC-TR-88-1639	5. MONITORING ORGANIZATION REPORT NUMBER(S)
6a. NAME OF PERFORMING ORGANIZATION GEO-CENTERS, INC. — 6b. OFFICE SYMBOL (If applicable): Code 6170	7a. NAME OF MONITORING ORGANIZATION
6c. ADDRESS (City, State, and ZIP Code) 7 Wells Avenue Newton Centre, MA 02159	7b. ADDRESS (City, State, and ZIP Code)
8a. NAME OF FUNDING/SPONSORING ORGANIZATION Naval Research Laboratory — 8b. OFFICE SYMBOL (If applicable): Code 6170	9. PROCUREMENT INSTRUMENT IDENTIFICATION NUMBER Contract Number N00014-86-C-2096
8c. ADDRESS (City, State, and ZIP Code) 4555 Overlook Avenue, S.W. Washington, DC 20375-5000	10. SOURCE OF FUNDING NUMBERS PROGRAM ELEMENT NO. — PROJECT NO. — TASK NO. — WORK UNIT ACCESSION NO.

11. TITLE (Include Security Classification)
Research and Development in Support of the Surface Chemistry Branch (U)

12. PERSONAL AUTHOR(S)
D. Ballantine

13a. TYPE OF REPORT	13b. TIME COVERED	14. DATE OF REPORT (Year, Month, Day)	15. PAGE COUNT
Final	FROM 12/85 TO 4/88	June 1988	750

16. SUPPLEMENTARY NOTATION

17. COSATI CODES			18. SUBJECT TERMS (Continue on reverse if necessary and identify by block number)
FIELD	GROUP	SUB-GROUP	Surface analysis, surface modification and tribological characterization, chemical microsensors, air purification and detection, ~~electrochemical~~

19. ABSTRACT (Continue on reverse if necessary and identify by block number)

GEO-CENTERS, INC. programs in support of the Naval Research Laboratory Surface Chemistry Branch of the Chemistry Division have addressed problems dealing with the properties of and chemistry occurring on/at surfaces and interfaces. Of particular interest to the Navy are the programs and advances described below:

Modified ceramic and metal surfaces demonstrated significant improvements in tribological characteristics such as friction and wear resistance. In addition to the characterization and analysis of these materials, a large materials database was compiled. This information will assist in identifying important factors affecting stress propagation and tribological performance, and will aid in the development of models.

(Continued on back of sheet)

20. DISTRIBUTION/AVAILABILITY OF ABSTRACT	21. ABSTRACT SECURITY CLASSIFICATION
☒ UNCLASSIFIED/UNLIMITED ☐ SAME AS RPT. ☐ DTIC USERS	UNCLASSIFIED
22a. NAME OF RESPONSIBLE INDIVIDUAL Dr. James S. Murday	22b. TELEPHONE (Include Area Code) (202) 767-3550 — 22c. OFFICE SYMBOL Code 6170

DD FORM 1473, 84 MAR — 83 APR edition may be used until exhausted. All other editions are obsolete.

SECURITY CLASSIFICATION OF THIS PAGE
UNCLASSIFIED

FINAL REPORT

FOR

GEO-CENTERS SUBCONTRACT NO.
GC-87-1639-002

DEVELOPMENT OF CHEMICAL DETECTORS

SUBMITTED BY

MICROSENSOR SYSTEMS, INC.
P.O. BOX 90
FAIRFAX, VA 22030

JUNE 1988

TABLE OF CONTENTS

page

I. TASK REVIEW 4

II. SUMMARY OF WORK PERFORMED 5

III. FUTURE RESEARCH RECOMMENDATIONS 7

IV. APPENDIX OF WRITTEN REPORTS 8

A. SAW Hardware Development

1) 112 MHz 4 SAW Array Instrument
2) 52 MHz Dual SAW Vapor Sensor Hardware
3) 158 MHz Dual SAW Vapor Sensor Hardware
4) A Study of SAW Oscillator Performance: SAW Resonators vs. SAW Delay Lines

B. Research Papers Published in the Proceedings of the 1986 U.S. Army CRDEC Conference on Chemical Defense Research

1) "Poly(ethylene maleate) Variants for SAW Microsensor Coating Study"
2) "Limits of Chemical Microsensor Technology"
3) "Chemiresistor Vapor Sensor Coatings: Structure and Properties"
4) "Sorption Kinetics Measured by Surface Acoustic Wave Shifts"

C. Research Papers Published in the Proceedings of the 1987 U.S. Army CRDEC Conference on Chemical Defense Research

1) "Correlation of SAW Vapor Sensor Responses with Partition Coefficients"

2) "Synthesis and Evaluation of Hexafluorodimethylcarbinol Functionalized Polymers as SAW Sensor Coatings"

D. Optical Waveguide Research

1) "Optical Waveguide Humidity Detector"

E. SAW / Chemiresistor Studies

1) "Simultaneous Electrical Conductivity and Piezoelectric Mass Measurements on Iodine Doped Phthalocyanine Langmuir-Blodgett Films"

2) "Surface Acoustic Wave Sensors, Chemiresistor Sensors and Hybrids Using Both Techniques Simultaneously to Detect Vapors"

F. SAW Coating Studies

1) "Correlation of SAW Device Coating Responses with Solubility Properties and Chemical Structure Using Pattern Recognition"

2) "Determination of Partition Coefficients from Surface Acoustic Wave Vapor Sensor Responses and Correlation with Gas-Liquid Chromatographic Partition Coefficients"

3) "The Use of Partition Coefficients and Solubility Properties to Understand and Predict SAW Vapor Sensor Behavior"

G. Vapor Generation Systems

1) "An Automated Vapor Generation and Data Collection Instrument for the Evaluation of Chemical Microsensors"

2) "VG-7000 Automatic Vapor Generation System Operating Manual"

I. TASK REVIEW

The objective of this project was to develop novel chemical sensor devices in support of programs at the U.S. Naval Research Laboratory's Surface Chemistry Branch. The project involved extensive collaboration with scientists employed by Geo-Centers, Inc. and the U.S. Naval Research Lab. During the course of his program Microsensor Systems, Inc. focussed its efforts on the following tasks:

1) The design, fabrication, and evaluation of model sensors based on surface acoustic wave (SAW), optical waveguide and chemiresistor technologies.

2) Design, fabrication, and operation of automated vapor generation systems and the operation of these systems to permit he rapid testing of chemical microsensor devices and chemically selective coatings developed as part of this program.

II. SUMMARY OF WORK PERFORMED

During the period from 1 January 1986 to May 1988, Microsensor Systems, Inc. supplied Geo-Centers, Inc. with a broad spectrum of hardware and services in support of the Chemical Detector Development program at the U.S. Naval research Laboratory. The highlights of work performed in each significant category are described here. Detailed reports of the work performed and results obtained are provided in the Appendix.

A) SAW Hardware

The SAW vapor sensor was the primary sensor technology being developed in this program. Microsensor Systems, Inc. fabricated several different SAW sensor configurations that could be used in the laboratory to evaluate selective coating performance. These included a 52 MHz dual SAW delay line oscillator and a 158 MHz dual delay line oscillator. These two SAW devices were the primary vehicles used to conduct chemical sensor coating development at NRL. Descriptions of the devices, the supporting RF electronic hardware and operating instructions for these devices are contained in the Appendix. Microsensor Systems, Inc. also fabricated a field portable 4 SAW array instrument using 112 MHz dual SAW delay line oscillators. This instrument contained a built in air sampling pump. scrubber and solenoid valves to permit the periodic sampling of ambient air. The instrument provided frequency data to an Apple IIe data acquisition computer equipped with a four channel frequency counter. The 4 SAW array sensor was tested at NRL and sent to the U.S. Army CRDEC Lab for evaluation with chemical agents and simulants. Finally, Microsensor Systems, Inc. conducted a study to compare the relative performance of SAW oscillators built with the delay line and resonator configurations.

B) Chemical Sensor Development and Evaluation

All of the chemical sensors explored in this program require a chemically selective coating. Thus, the development of coatings and the evaluation of their relative performance was an important focal point of this program. All of the chemically selective coatings were intended for use in the field of chemical defense and most of this work was reported at the annual Conference on Chemical Defense Research sponsored by the U.S. Army Chemical Research, Development, and Engineering Center (CRDEC) at Edgewood, MD. Microsensor Systems, Inc. participated in this research effort by fabricating SAW and chemiresistor sensor devices and related electronics, applying candidate coatings to the sensor devices, evaluating the sensor responses to challenge vapors, and designing experiments to test hypotheses.

C) Automatic Vapor Generation Systems

Perhaps the most labor intensive aspect of the chemical sensor development program at NRL was chemical vapor testing of the devices. Detailed evaluation of sensor performance demands that each sensor be exposed to a significant number of different gases under varying conditions of concentration, composition, temperature, and flow rate. Considerable effort was expended to fabricate fully automated systems that could provide a dozen source vapors, singly or as binary mixtures. The final vapor generator fabricated for this program (i.e. "VG-7000") offered fully programmable concentrations over a range of 5 orders of magnitude. The use of a novel digital pneumatic pulse width modulation scheme minimized the carrier gas consumption to a mere 700 sccm while permitting simple, gravimetrically calibrated bubbler vapor sources to be used. Complex experiment sequences could be readily programmed to permit days of unattended operation.

III. FUTURE RESEARCH RECOMMENDATIONS

The chemical sensor development program was highly successful in several areas. These successes serve as an obvious guide to promising research programs for the future. Specific areas that should be given attention in the future are itemized below.

1) The chemically selective coating research conducted in this program led to a considerably clearer understanding of how SAW coatings and vapors interact. The solubility parameter models that were investigated during this research will most certainly prove to be valuable to chemical sensor developers and these models deserve further investigation. Further exploitation of hydrogen bonding interactions could prove to be a particularly interesting facet of future research.

2) The ability of chemical sensor arrays to discriminate among a variety of analyte vapors was unambiguously established during the course of this work. Further development of SAW array sensors should be an important priority for future research.

3) SAW resonators were shown to be a superior sensor device compared to SAW delay lines, owing to the higher frequency stability exhibited by the resonators. Development of SAW resonator vapor sensor devices would certainly be worthwhile in the future.

APPENDIX OF WRITTEN REPORTS

A. SAW Hardware Development

112 MHz 4 SAW Array Instrument

52 MHz Dual SAW Vapor Sensor Hardware

158 MHz Dual SAW Vapor Sensor Hardware

A Study of SAW Oscillator Performance: SAW Resonators vs. SAW Delay Lines

APPENDIX OF WRITTEN REPORTS

B. Research Papers Published in the Proceedings of the 1986 U.S. Army CRDEC Conference on Chemical Defense Research

"Poly(ethylene maleate) Variants for SAW Microsensor Coating Study"

A.W. Snow, D.S. Ballantine, T. Whitney, W.R. Barger, M. Klusty, H. Wohltjen, J. Grate, D. Chaput,

Proceedings of the 1986 U.S. Army CRDEC Conference on Chemical Defense Research, 18-21 Nov. 1986, (CRDEC-SP-87008) pp. 695-703.

"Limits of Chemical Microsensor Technology",

J.S. Murday, S. Caras, H. Wohltjen,

Proceedings of the 1986 U.S. Army CRDEC Conference on Chemical Defense Research, 18-21 Nov. 1986, (CRDEC-SP-87008) pp. 405-413.

"Chemiresistor Vapor Sensor Coatings: Structure and Properties"

W.R. Barger, A.W. Snow, J.L. Dote, R. Price, M. Klusty, and H. Wohltjen,

Proceedings of the 1986 U.S. Army CRDEC Conference on Chemical Defense Research, 18-21 Nov. 1986, (CRDEC-SP-87008) pp. 863-868.

"Sorption Kinetics Measured by Surface Acoustic Wave Shifts"

D. L. Bartley, D. Dominguez, W.R. Barger, A.W. Snow, and H. Wohltjen,

Proceedings of the 1986 U.S. Army CRDEC Conference on Chemical Defense Research, 18-21 Nov. 1986, (CRDEC-SP-87008) pp. 825-830.

APPENDIX OF WRITTEN REPORTS

C. Research Papers Published in the Proceedings of the 1987 U.S. Army CRDEC Conference on Chemical Defense Research

"Correlation of SAW Vapor Sensor Responses with Partition Coefficients"

J.W. Grate, A.W. Snow, D.S. Ballantine, H. Wohltjen, M.H. Abraham, R.A. Mcgill, and P. Sasson

Proceedings of the 1987 U.S. Army CRDEC Conference on Chemical Defense Research, 17-20 Nov. 1987, (CRDEC-SP-88013) pp. 297-303.

"Synthesis and Evaluation of Hexafluorodimethylcarbinol Functionalized Polymers as SAW Sensor Coatings"

L.G. Sprague, A.W Snow, R.L. Soulen, J. Lint, H. wohltjen, D.S. Ballantine, J.W. Grate

Proceedings of the 1987 U.S. Army CRDEC Conference on Chemical Defense Research, 17-20 Nov. 1987, (CRDEC-SP-88013) pp. 1241-1251.

APPENDIX OF WRITTEN REPORTS

D. Optical Waveguide Research

"Optical Waveguide Humidity Detector"

D.S. Ballantine and H. Wohltjen

Analytical Chemistry, 1986, 58, pp. 2883 -2885

APPENDIX OF WRITTEN REPORTS

E. SAW / Chemiresistor Studies

"Simultaneous Electrical Conductivity and Piezoelectric Mass Measurements on Iodine Doped Phthalocyanine Langmuir-Blodgett Films"

A.W. Snow, W.R. Barger, M. Klusty, H. Wohltjen, and N.L. Jarvis

Langmuir, 1986, 2, pp 513-519.

"Surface Acoustic Wave Sensors, Chemiresistor Sensors and Hybrids Using Both Techniques Simultaneously to Detect Vapors"

W. R. Barger, M. Klusty, A.W. Snow, J.W. Grate, D.S. Ballantine, and H. Wohltjen

Proceedings of the Symposium on Sensor Science and Technology, April 6 - 8, 1987, Case Western Reserve Univ., B. Schumm, C.C. Liu, R.A. Powers, and E.B. Yeager eds., The Electrochemical Soc. Proceedings Volume 87-15, pp. 198-217. (Lib. of Cong. # 87-83041)

APPENDIX OF WRITTEN REPORTS

F. SAW Coating Studies

"Correlation of SAW Device Coating Responses with Solubility Properties and Chemical Structure Using Pattern Recognition"

D.S. Ballantine, S.L. Rose, J.W. Grate, and H. Wohltjen

Analytical Chemistry, 1986, 58, pp 3058-3066.

"Determination of Partition Coefficients from Surface Acoustic Wave Vapor Sensor Responses and Correlation with Gas-Liquid Chromatographic Partition Coefficients"

J.W. Grate, A.W. Snow, D.S. Ballantine, H. Wohltjen, M.H. Abraham, R.A. McGill, and P. Sasson

Analytical Chemistry, 1988, 60, pp. 869-875.

"The Use of Partition Coefficients and Solubility Properties to Understand and Predict SAW Vapor Sensor Behavior"

J.W. Grate, A.W. Snow, D.S. Ballantine, H. Wohltjen, M.H. Abraham, R.A. McGill, and P. Sasson

Proceedings of the International Conference on Solid State Sensors and Actuators, "Transducers '87", Tokyo, Japan, June 6-9, 1987

APPENDIX OF WRITTEN REPORTS

G. Vapor Generation Systems

"An Automated Vapor Generation and Data Collection Instrument for the Evaluation of Chemical Microsensors"

J.W. Grate, D.S. Ballantine, H. Wohltjen

Sensors and Actuators, 11, (1987) pp. 173-188.

"VG-7000 Automatic Vapor Generation System Operating Manual"

THE U.S. NAVAL RESEARCH LABORATORY

SURFACE ACOUSTIC WAVE VAPOR SENSOR SYSTEM

CONTENTS

I. System Description

II. Set Up Procedure

III. Operating Procedure

I. SYSTEM DESCRIPTION

The Surface Acoustic Wave (SAW) vapor sensor system consists of an array of four 112 MHz dual delay line oscillators. Each oscillator device has one side coated with a selective organic film chosen for its ability to absorb organophosphorus compounds (i.e "G" agents or their simulants). In addition to the four SAW devices and their associated RF support electronics, the system also contains regulated DC power supplies to permit operation from 120 Volt 60 Hz power sources, interface electronics for communication with an APPLE II microcomputer, an air pump to draw ambient air across the sensors, an air scrubber to provide a source of clean, dry reference air, and a solenoid valve with TTL drive electronics.

In normal operation the SAW sensors provide a signal which is the difference frequency between the clean and coated oscillator of each sensor. This signal is processed into a TTL compatible pulse train whose frequency is determined by four frequency counters which are plugged directly into the APPLE II interface slots #1,2,3,and4. The difference frequencies obtained from each sensor are usually in the range of 100 to 800 kilohertz. Ambient air is drawn across each sensor with suction from a small (but very noisy) air pump. An electric solenoid valve is used to control the air exposed to the sensors. This valve is controlled through a cable which is plugged into the APPLE II game controller interface socket. It can select either ambient air or ambient air which has been scrubbed with Drierite and charcoal. By switching back and forth between these two sources of air it is possible to obtain accurate compensation of baseline drift. This system works on a three minute cycle in which the sensors are

exposed to scrubbed reference air for one minute, contaminated(perhaps) ambient air for one minute, and scrubbed reference air for the final minute. The APPLE II computer controls the sequencing of the measurement, the acquisition and processing of experimental data, and printing (on paper) and storage (on disk) of the results of each three minute measurement. The system can run unattended until the disk is full of data. Approximately 80 three minute measurements can be stored (i.e. 80 disk files). Thus a minimum of four hours of unattended operation is possible.

The experimental results are available in hardcopy which is not easily interpreted at a glance. It was not possible to develop more elegant data processing software in the time available. Therefore, it is important that the disks containing the raw data be returned to NRL after the field test so that the results can be worked up into human compatible form (i.e. graphs and pictures).

MICROSENSOR SYSTEMS, INC.

SURFACE ACOUSTIC WAVE VAPOR SENSOR ARRAY

112 MHz

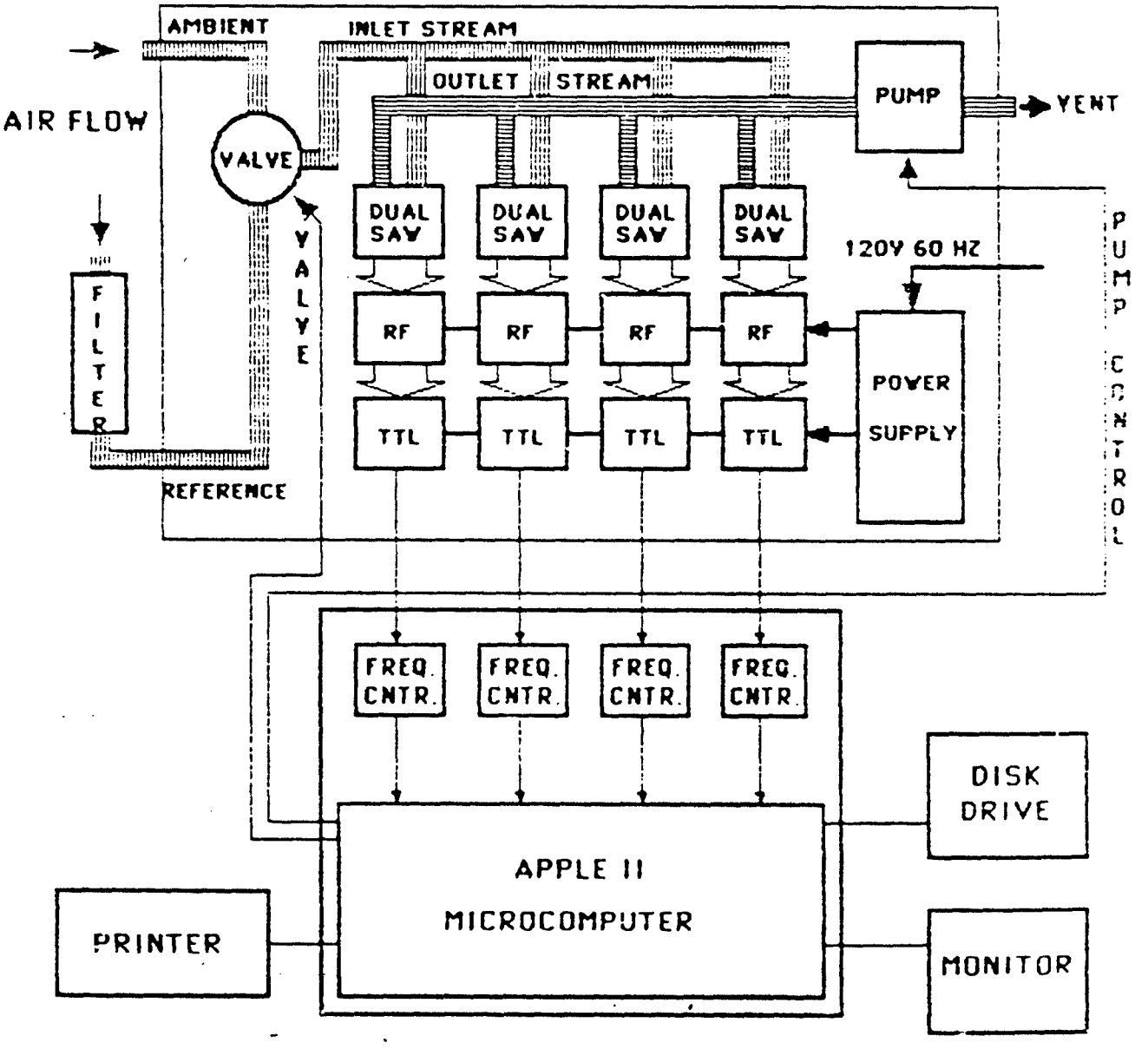

DUAL SAW
VAPOR SENSOR

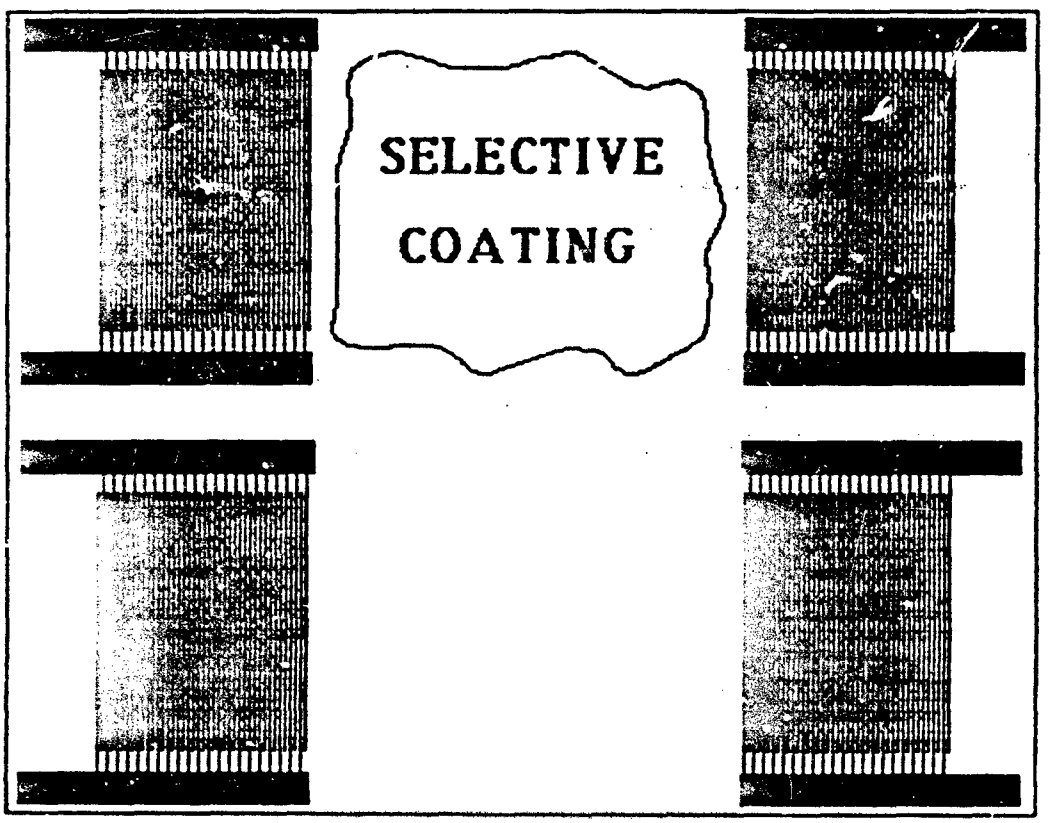

II. SET UP PROCEDURE

Putting the SAW vapor sensor to work is straightforward. The following sequence can be performed to get things going.

1. Position the Equipment.

The APPLE II microcomputer,printer,display,disk drive, and SAW sensor package must all be located near to each other since the connecting cables are all rather short. The sensor package will be placed on top of the APPLE II. The display, printer, and disk drive will have to be placed on either side of the computer. The sensor package power supplies get hot and need adequate ventilation.

2. Plug in Cables and Interface Cards.

The following interface cards must be plugged into the APPLE II:

a. Four Frequency Counter Cards : Slots #1,2,3,and 4.

b. Printer interface card : Slot #5.

c. Disk Controller card : Slot #6

Slots #0 and #7 will be empty.

The following cables must be plugged into the APPLE II:

a. Cable from sensor package to Game Controller socket. (NOTE: be careful of polarity !)

b. Cable from APPLE II video output to display monitor.

c. Disk Controller cable from interface to disk drive.

d. Printer cable from interface to printer.

e. Power cable from 120v 60 Hz outlet to APPLE II power supply.

The following cables must be connected to the sensor package:

a. Cable from APPLE II frequency counters. (Thick black bundle)

b. Power cable to 120 v 60 Hz power outlet.

3. Attach Air Connections to Sensor Package.

a. Connect ambient air sampling line to 1/8" SWAGELOK ambient air inlet connector. Air presented to the sensor inlet must not be pressurized. It must be at ambient pressure.

b. Connect air scrubber to 1/8" SWAGELOK scrubber inlet. The scrubber should be examined daily. If the indicating Drierite has turned from blue to pink over 90% of the length of the Drierite bed then it must be replenished along with the charcoal. This will probably be required every 8 hours the system is pumping air.

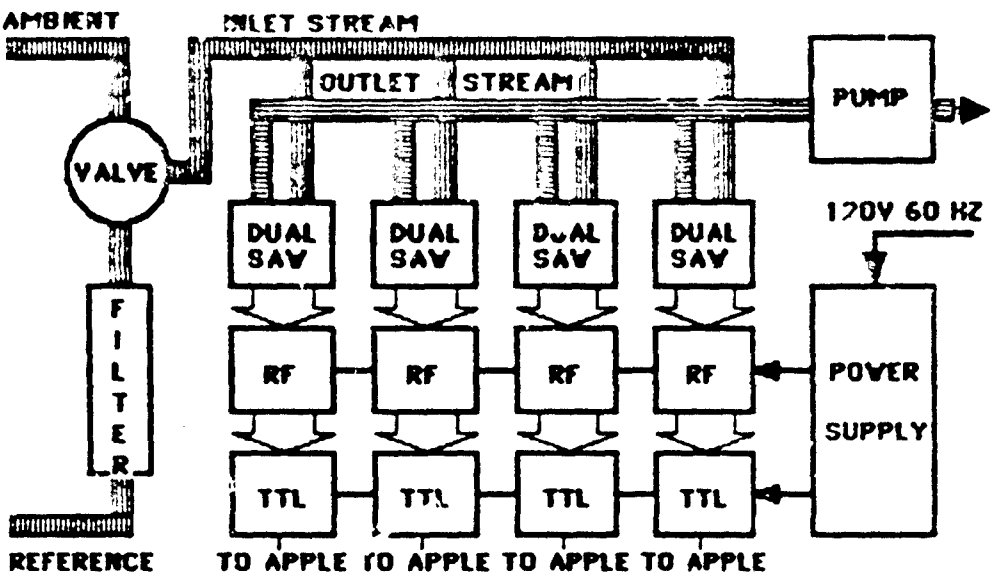
AMBIENT
INLET STREAM
OUTLET STREAM
PUMP
VALVE
DUAL SAW
DUAL SAW
DUAL SAW
DUAL SAW
120V 60 HZ
FILTER
RF
RF
RF
RF
POWER SUPPLY
TTL
TTL
TTL
TTL
REFERENCE
TO APPLE
TO APPLE
TO APPLE
TO APPLE

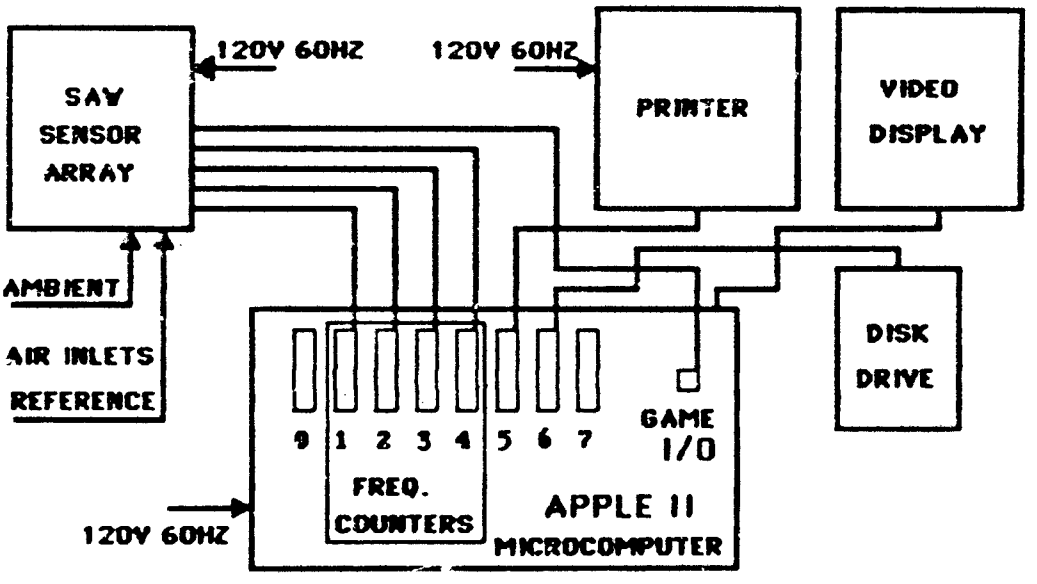
SAW
SENSOR
ARRAY
120V 60HZ
120V 60HZ
PRINTER
VIDEO
DISPLAY
AMBIENT
AIR INLETS
REFERENCE
DISK
DRIVE
0 1 2 3 4 5 6 7
GAME
I/O
FREQ.
COUNTERS
APPLE II
MICROCOMPUTER
120V 60HZ

III. OPERATING PROCEDURE

Once the system has been set up it should be double checked before power is applied. When satisfied that everything is OK, then the system can be powered up. The order is not critical but the following switches must be turned "ON":

a. Power switch on sensor package (near fuse).
b. Video display power.
c. Printer power. (Also, make sure printer is "ON LINE" or the system will hang up until it is on line).
d. APPLE II power switch.

Turning on the APPLE II power will automatically cause it to "boot" itself by loading programs from disk. Once the cursor appears on the display it is a good idea to look at the "CATALOG" of the disk. If the catalog indicates the diskette has many data files on it (e.g. more than 20) then a new diskette should be used if more than a few hours of data is to be taken.

To start the vapor sensor it is necessary to type the following commands (always in CAPITAL LETTERS followed by hitting the "Return" key):

]RUN CRDC SAW

The disk will run for a few seconds and then a few questions will appear on the monitor screen which ask for date, file name, and some descriptive information. Enter whatever is appropriate as long as the entry

is less than about 100 characters long. Hit "return" to proceed after each question. The only critical entry is the file name. Care must be taken not to duplicate previously used names unless the previous files are expendable. The system will print a few things on the printer (make sure it's "ON LINE" !) and then will proceed to take data from the SAW sensors. The computer will take about a minutes worth of data to get things started and then will begin its 3 minute measurement cycle. At the end of each cycle, the computer will save the raw data in a disk file and print some processed results on the printer.

To stop the system at any time, hit the escape key (marked "ESC")

If things are really going wild, hit the control (marked "CTRL") and Reset keys simultaneously. Then start over by typing RUN CRDC SAW.

Thats all there is to it. Once the system is set up all that is required is to turn on the power switches and start the APPLE II data acquisition program (CRDC SAW).

Problems, complaints, and inquiries should be brought to the attention of

Hank Wohltjen

(703) 250-5336 (Microsensor Systems, Inc.)

(202) 767-2536 (Naval Research Lab)

(703) 250-7932 (Home)

```
]LIST

1   REM ***********************************
2   REM *
3   REM *      S A W T E S T
4   REM *
5   REM *
6   REM *
7   REM *            .
8   REM *
9   REM *            BY
10   REM *
11   REM * MICROSENSOR SYSTEMS
12   REM *          INC.
13   REM *       P.O. BOX 90
14   REM *    FAIRFAX,VIRGINIA
15   REM *          22030
19   REM *
20   REM ***********************************
101   REM *
102   REM *    SLOT ASSIGNMENTS
104   REM *
105   REM *
106   REM *   SLOT#0 = 80 COLUMN CARD (OPTIONAL)
107   REM *   SLOT#1 = FREQ.COUNTER #1
108   REM *   SLOT#2 = FREQ.COUNTER #2
109   REM *   SLOT#3 = FREQ.COUNTER #3
110   REM *   SLOT#4 = FREQ.COUNTER #4
111   REM *   SLOT#5 = PRINTER INTERFACE
112   REM *   SLOT#6 = DISK CONTROLLER
113   REM *   SLOT#7 = <EMPTY>
199   REM
200   REM
990   REM ************************
991   REM *
992   REM *    INIT PARAMETERS
993   REM *
999   REM ************************
1000   HIMEM: 32000
1010   TEXT
1020   HOME
1030   DIM RF(3,220)
1040   DIM B1%(4,10)
1050   DIM B2%(4,10)
1060   DIM B3%(4,10)
1100   DIM FR(4,12)
1110   DIM FF(4,10)
1120   DIM FA(10)
1130   DIM X1(5)
1140   DIM X2(5)
1150   DIM Y1(5)
1160   DIM Y2(5)
1170   DIM SIG(5)
1200 T% = 0
1210 N = 0
1220 BB = 20
1230 DU = 0
1240 FS = 1000
1250 CY = 0
1300 A = 49296
```

```
1396  REM *
1397  REM *          TURN SOLENOID OFF
1398  REM *(LOGIC 1 ON GAME PIN #15)
1399  REM *
1400 ZZ =  PEEK (49241)
1416  REM *
1417  REM *          TURN PUMP ON
1418  REM *(LOGIC 0 ON GAME PIN #14)
1419  REM *
1420 ZZ =  PEEK (49242)
1500  PRINT
1510  PRINT
1520  PRINT "    SAW DATA ACQUISITION PROGRAM"
1527  REM *
1528  REM * INPUT EXP. PARAMETERS
1529  REM *
1530  GOSUB 51000
1531  REM *  PRINT HEADER
1533  GOSUB 52000
1535  HOME : VTAB 5: HTAB 7
1540  PRINT "   TURN ON SAW SENSORS"
1550  PRINT : PRINT
1555  HTAB 5
1560  PRINT "  SYSTEM WARMUP IN PROGRESS";
1980  REM *
1982  REM *
1990  REM **********************
1991  REM *
1992  REM *
1993  REM *   MAIN PROGRAM
1994  REM *
1995  REM *
1997  REM **********************
1998  REM *
1999  REM *
2000  FOR N = 1 TO 7
2005 GG = 0
2010  GOSUB 25000
2020  NEXT N
2070  HOME
2097  REM *
2098  REM ************************
2099  REM *
2100 PP = 0
2115 T% = 0
2120 T = 0
2130 SO = 5
2140 SF = 10
2150 SE = 15
2159  REM *
2190 GG = 1
2207  REM *
2208  REM **********************
2209  REM *
2210  REM *  MODULATE & ACQUIRE
2211  REM *
2213  REM **********************
2214  REM *
2220  FOR N = 1 TO SE
2222  VTAB 24: HTAB 5
2223  IF N = 1 THEN  PRINT "PURGING ";
2225 PP = PP + 1
```

```
2225  REM *
2227  REM * TURN SOLENOID ON
2228  REM *
2230  IF N = SO THEN ZZ =  PEEK (49240): PRINT "SAMPLING";
2236  REM *
2237  REM * TURN SOLENOID OFF
2238  REM *
2239  REM *
2240  IF N = SF THEN ZZ =  PEEK (49241): PRINT "PURGING ";
2257  REM *
2258  REM * GRAB SAW FREQS.
2259  REM *
2260  GOSUB 25000
2266  REM *
2267  REM *  CHECK STATUS OF ESC
2268  REM *
2270  GOSUB 30000
2280  NEXT N
2295  REM *
2296  REM *********************
2297  REM *
2298  REM * COMPUTE PEAK SIZE
2299  REM *
2300  GOSUB 35000
2367  REM *
2368  REM * SAVE DATA ON DISK
2369  REM *
2370  GOSUB 53000
2497  REM *
2498  REM *  PRINT RESULTS
2499  REM *
2800  GOSUB 36000
3000  GOTO 2100
3990  REM *
3992  REM *
4000  REM *
4001  REM *
4990  REM ***********************
4992  REM *
4993  REM *   ERROR HANDLER
4995  REM *
4999  REM ***********************
5000  TEXT
5005  HOME
5010  PRINT : PRINT
5020 JL =  PEEK (222)
5022  PRINT : PRINT
5024  PRINT : PRINT
5030  PRINT "ERROR # =  ";JL
5031  PRINT : PRINT "ERROR #9 MEANS DISK FULL"
5033  PRINT : PRINT
5040  PRINT "INSERT ANOTHER DISK IF REQUIRED"
5045  PRINT : PRINT
5046  PRINT : PRINT
5050  INPUT "PRESS RETURN....";H$
5060  GOTO 53000
9999  END
25000  REM ******************************
25001  REM *
25002  REM *   FREQUENCY DATA ACQUISITION
25003  REM *          ROUTINE
25004  REM *
25005  REM *       D=FREQUENCY
25006  REM *
25009  REM *
25019  REM ******************************
25020  REM  *
25030 A = 49296
25050 KK = 0
25060  VTAB 15: HTAB 10
25070  PRINT "REAL TIME DATA";
25080  VTAB 17: HTAB 3
25090  PRINT "ELAPSED TIME   SAW FREQ.      DELTA";
25092  VTAB 18: HTAB 3
25094  PRINT "------------   ---------      -----";
25100 ZZ =  PEEK (A)
25200  IF ZZ = 255 THEN  GOTO 25100
25400 KK = KK + 1
```

```
25497  REM *
25498  REM ******************
25499  REM *
25500 B1%(1,KK) =  PEEK (49298)
25502 B2%(1,KK) =  PEEK (49299)
25504 B3%(1,KK) =  PEEK (49300)
25506 ZZ =  PEEK (49302)
25510 B1%(2,KK) =  PEEK (49314)
25512 B2%(2,KK) =  PEEK (49315)
25514 B3%(2,KK) =  PEEK (49316)
25516 ZZ =  PEEK (49318)
25520 B1%(3,KK) =  PEEK (49330)
25522 B2%(3,KK) =  PEEK (49331)
25524 B3%(3,KK) =  PEEK (49332)
25526 ZZ =  PEEK (49334)
25530 B1%(4,KK) =  PEEK (49346)
25532 B2%(4,KK) =  PEEK (49347)
25534 B3%(4,KK) =  PEEK (49348)
25536 ZZ =  PEEK (49350)
25597  REM *
25598  REM ******************
25599  REM *
25600 ZZ =  PEEK (A)
25610  IF ZZ = 127 THEN  GOTO 25600
25690  REM *
25693  REM ******************
25696  REM *
25710  IF KK = 2 THEN  GOSUB 28000
25720  IF KK = 3 THEN  GOSUB 27000
25740  IF KK = 4 THEN  GOSUB 29000
25790  IF KK < 10 THEN  GOTO 25100
25800  IF KK = 10 THEN  GOSUB 26000
25900  GOSUB 31000
25990  RETURN
26000  REM ******************
26003  REM *
26004  REM *  CALC. AVG. FREQ.
26009  REM *
26010  REM ******************
26100  FOR I = 0 TO 3
26110 AV = 0
26120  FOR J = 2 TO 10 STEP 2
26130 AV = AV + FR(I,J)
26140  NEXT J
26150 FA(I) = AV / 4
26300  NEXT I
26990  RETURN
27000  REM ******************
27003  REM *
27005  REM *  PRINT RESULTS
27009  REM *
27010  REM ******************
27100  HTAB 5
27110  VTAB 21
27120  PRINT T;" MIN.  ";
27200  FOR I = 0 TO 3
27210  VTAB (21 + I)
27215  HTAB 18
27220  PRINT "@";I;"=        ";
27230  HTAB 22
27240  PRINT F(I);
27300  NEXT I
27800 T% = T% + 2
27820 T = T% / 10
27900  IF T > 5.8 THEN T = 0
27990  RETURN
```

```
28000  REM ****************
28002  REM *
28005  REM *  5 POINT SMOOTH
28009  REM *
28010  REM ****************
28100  FOR I = 0 TO 3
28300 FF(I,5) = FF(I,4)
28310 FF(I,4) = FF(I,3)
28320 FF(I,3) = FF(I,2)
28330 FF(I,2) = FF(I,1)
28340 FF(I,1) = FA(I)
28500 F(I) = FF(I,1) + FF(I,2) + FF(I,3) + FF(I,4) + FF(I,5)
28600 F(I) =  INT (F(I) / 5)
28700  NEXT I
28990  RETURN
29000  REM ******************
29001  REM *
29005  REM *  FIND DERIVATIVE
29009  REM *
29010  REM ******************
29100  FOR I = 0 TO 3
29200 D(I) = F(I) - OF(I)
29300 OF(I) = F(I)
29330  HTAB 33
29340  VTAB (21 + I)
29350  PRINT "       ";
29360  HTAB 32
29380  PRINT D(I);
29400  NEXT I
29990  RETURN
30000  REM ******************************
30001  REM *
30003  REM *     STATUS CHECKER
30004  REM *
30010  REM *
30019  REM ******************************
30250 IN =  PEEK (49152): POKE 49168,0
30260  IF IN <  > 155 THEN  RETURN
30267  TEXT : HOME
30270  VTAB 21
30272  INPUT "STORE DATA AND QUIT ? (Y OR N) : ";J$
30275  IF J$ = "Y" THEN  GOSUB 53000: END
30276  INPUT "COLLECT MORE DATA ? (Y OR N) : ";Q$
30277  IF Q$ = "N" THEN  END
30278  HOME
30280  RETURN
30289  REM  ************************
30290  REM  *
30291  REM  *      PLOT DATA
30292  REM  *
30293  REM  ************************
30300  IF GG = 0 THEN  RETURN
30333  RETURN
30400  FOR I = 0 TO 3
30480 D = D(I)
30500 Y = BB - 20 * (D / FS)
30510  IF Y < 0 THEN Y = 0
30520  IF Y > 40 THEN Y = 40
30560  PLOT N,Y
30800  NEXT I
30900  RETURN
```

```
31000  REM ********************
31001  REM *
31005  REM *  REASSIGN DATA
31009  REM *
31010  REM ********************
31100  FOR I = 0 TO 3
31120 RF(I,PP) = FA(I)
31200  FOR J = 1 TO 10
31300 FR(I,J) = (B1%(I + 1,J) * 65536) + (B2%(I + 1,J) * 256) + B3%(I + 1
      ,J)
31400  NEXT J
31440 FR(I,1) = FR(I,2)
31500  NEXT I
31990  RETURN
35000  REM ***********************
35001  REM *
35003  REM *   COMPUTE PEAK SIZE
35009  REM *
35010  REM ***********************
35100 SP = 0
35200  FOR I = 0 TO 3
35300 SS = 0:ES = 0:IS = 0:CC = 0
35400 SS = RF(I,SO) + RF(I,(SO - 1))
35430 SS = SS / 2
35500 ES = RF(I,(SF + 2)) + RF(I,(SF + 3))
35530 ES = ES / 2
35600 SL = (ES - SS) / ((SF - SO) + 2)
35700  FOR J = (SO + 1) TO (SF + 1)
35710 CC = CC + 1
35720 IS = IS + (RF(I,J) - (SS) - (SL * CC))
35730  NEXT J
35800 SIG(I) =  INT (IS / CC)
35900  NEXT I
35990  RETURN
36000  REM ********************
36001  REM *
36005  REM *   PRINT RESULTS
36009  REM *
36010  REM ********************
36020 CY = CY + 1
36025  PRINT  CHR$ (4);"PR#5"
36030  PRINT N$; TAB( 12);SIG(0); TAB( 12);SIG(1); TAB( 12);SIG(2); TAB(
     12);SIG(3)
36035  PRINT
36040  PRINT  CHR$ (4);"PR#0"
36050  HOME
36055  VTAB 2: HTAB 5
36060  PRINT "3 MINUTE SAMPLE & PURGE RESULTS"
36070  VTAB 4: HTAB 16
36080  PRINT "CYCLE #";CY
36090  PRINT
36100  PRINT
36200  FOR I = 0 TO 3
36300  PRINT "SENSOR #";I;" PEAK HEIGHT (HZ) = ";SIG(I)
36400  NEXT I
36990  RETURN
```

```
50000  REM ******************************
50001  REM *
50002  REM *    COORDINATE PLOTTER
50003  REM *
50004  REM *
50010  REM ******************************
50080 GG = 1
50085  RETURN
50090  HCOLOR= 7
50100  HOME
50110  HGR2
50120  HPLOT 0,0 TO 0,159
50130  HPLOT 0,79 TO 200,79
50200  FOR Q = 0 TO 159 STEP 15.9
50210  HPLOT 0,Q TO 3,Q
50220  NEXT Q
50300  FOR Q = 0 TO 200 STEP 20
50310  HPLOT Q,77 TO Q,81
50320  NEXT Q
50900  RETURN
51000  REM ******************************
51001  REM *
51004  REM *   INPUT EXPERIMENTAL
51005  REM *       PARAMETERS
51019  REM *
51020  REM ******************************
51100  VTAB 21: HTAB 1
51110  INPUT "DATE                    : ";M$
51120  INPUT "FILE NAME               : ";F$
51140  INPUT "DESCRIPTION             : ";A$
51150  INPUT "TEST ATMOSPHERE         : ";P$
51900  RETURN
52000  REM ******************************
52001  REM *
52004  REM *   OUTPUT EXPERIMENTAL
52005  REM *      PARAMETERS
52019  REM *
52020  REM ******************************
52100  PRINT  CHR$ (4);"PR#5"
52110  PRINT "            S A W  D A T A  S U M M A R Y"
52120  PRINT
52140  PRINT
52142  PRINT "DATE          : ";M$
52148  PRINT "ATMOSPHERE    : ";P$
52160  PRINT "FILE NAME     : ";F$
52180  PRINT "DESCRIPTION   : ";A$
52230  PRINT : PRINT : PRINT
52240  PRINT "SENSOR 0 : ABIETIC ACID                          (70 KHZ)
52250  PRINT "SENSOR 1 : POLYAMIDOXIME                         (98 KHZ)
52260  PRINT "SENSOR 2 : POLY(ETHYLENE MALEATE)                (90 KHZ)
52270  PRINT "SENSOR 3 : FLUORO POLYOL                         (107 KHZ)"
52280  PRINT : PRINT : PRINT
52290  PRINT "    FREQUENCY SHIFT (HZ) AFTER 3 MIN. EXPOSE AND PURGE CYCL
    E"
52295  PRINT
52300  PRINT "FILE NAME   SENSOR 0    SENSOR 1    SENSOR 2    SENSOR 3"
52305  PRINT "---------   --------    --------    --------    --------"
52320  PRINT
52340  PRINT
52800  PRINT  CHR$ (4);"PR#0"
52900  RETURN
53000  REM ******************************
53001  REM *
```

```
53005  REM *
53005  REM *    DISK STORAGE ROUTINE
53019  REM *
53020  REM ****************************
53027  REM *
53028  REM *   TURN OFF SOLENOID
53029  REM *
53030 ZZ =  PEEK (49241)
53040 DU = DU + 1
53050  ONERR  GOTO 3000
53100  HOME
53180  VTAB 22: HTAB 7
53190  PRINT "DATA BEING STORED ON DISK"
53200 D$ =  CHR$ (4)
53220 N$ = F$ + "." +  STR$ (DU)
53240  PRINT D$;"OPEN ";N$
53260  PRINT D$;"DELETE ";N$
53280  PRINT D$;"OPEN ";N$
53300  PRINT D$;"WRITE ";N$
53310  PRINT PP
53320  PRINT M$
53330  PRINT P$
53340  PRINT N$
53350  PRINT A$
53360  PRINT SO
53370  PRINT SF
53380  PRINT SE
53500  FOR J = 0 TO 3
53520  FOR I = 1 TO PP
53540  PRINT RF(J,I)
53560  NEXT I
53580  NEXT J
53600  PRINT D$;"CLOSE ";N$
53800  VTAB 22: HTAB 7
53820  PRINT "
53990  RETURN

]
```

MICROSENSOR SYSTEMS, INC.

52 MHz
SURFACE ACOUSTIC WAVE
VAPOR SENSOR

INCLUDING:

a) 52 MHz DUAL SAW DELAY LINE (PART NO. SD-52-A (OR B))

b) DEVICE MOUNTING FIXTURE
POWER SUPPLY
RF ELECTRONICS SYSTEM
(PART NO. CEM-52)

JANUARY 1987

GENERAL SAW VAPOR SENSOR CONSIDERATIONS

Theoretical Model of SAW Sensor Response

The signal provided by a SAW oscillator vapor sensor can be described by the following theoretical equation (4):

$$\Delta f = (k_1 + k_2) f_0^2 \; h\rho' - k_2 f_0^2 \; h \left(\frac{4\mu'}{V_r^2} \left(\frac{\lambda' + \mu'}{\lambda' + 2\mu'} \right) \right) \qquad (1)$$

where Δf is the SAW oscillator frequency change produced by the vapor absorbed into the coating, k_1 and k_2 are material constants for the piezoelectric substrate, f_0 is the unperturbed resonant frequency of the SAW oscillator, h is the coating thickness, ρ' is the coating density, μ' is the shear modulus and λ' is the Lame' constant of the coating, and V_r is the Rayleigh wave velocity in the piezoelectric substrate (3159 m/sec for Y-X Quartz). This relationship assumes that the SAW device coating is isotropic and non-piezoelectric and that the coating covers 100% of the delay line surface. Furthermore, the relationship is valid only for very thin films (e.g. less than 0.2% of the acoustic wavelength thick). For thicker films, equation 1 can only provide estimates of the signal magnitude. When organic coatings are employed, it is often found that the second term of equation 1 is negligible because the shear elastic modulus of the coating (μ') is small compared to the square of the Rayleigh wave velocity (V_r). Under these conditions, equation 1 reduces to:

$$\Delta f = (k_1 + k_2) f_0^2 \; h\rho' \qquad (2)$$

For Y-X Quartz SAW devices, $k_1 = -9.33 \times 10^{-8}$ $m^2 \cdot sec/kg$ and $k_2 = -4.16 \times 10^{-8}$ $m^2 \cdot sec/kg$. The product of the coating thickness (h) and its density (ρ') is the mass per unit area on the device surface. Equation 2 predicts that the signal obtained from a given mass loading (h ρ' product) will increase with the square of the operating frequency of the SAW oscillator. Furthermore, operating frequency determines the size of the device since it imposes size requirements on the interdigital electrodes used to generate the Rayleigh surface wave. As the operating frequency increases, the device area (and cost) decreases. Higher operating frequencies permit thinner coatings to be employed with a corresponding improvement in response time since vapor diffusion into the coating will be quicker. Higher operating frequencies also result in greater baseline noise that hinders detection at the lowest concentrations. All of these considerations result in a set of scaling laws (detailed in reference 6) that can offer guidance in predicting the ultimate performance capabilities of SAW vapor sensor technology. The key assumption in these predictions is that the sensitivity increases

with the square of the frequency. Several experimental studies have indicated that this assumption is valid.

SAW Vapor Sensor System Description

The SAW devices employed in this system have a nominal frequency of 52 MHz. In fact, the devices are capable of operating at a number of resonant modes in the frequency range of 50 to 54 MHz. A dominant resonance is often observed at 52.3 MHz. A dual SAW delay line oscillator configuration is employed in the system. In this design, two SAW delay lines are fabricated on the same substrate. One delay line is coated with the chemically selective film and the other is left uncoated. The frequencies of the two delay line oscillators are mixed to provide a frequency equal to the difference of the two oscillator frequencies. In principle, frequency drifts caused by ambient temperature and pressure fluctuations experienced by the SAW device are compensated by this scheme. (Note: mechanical stresses imposed by thermal expansion of mounting fixture in this particular system can cause uncompensated drift.) This approach affords the additional advantage that the difference frequency is much lower (e.g. a hundred KHz) than the frequency of the oscillators themselves (i.e. 52 MHz). This makes it much easier to measure the SAW vapor response using inexpensive, digital counter circuitry. Theoretically, when a clean device is in the system the two delay lines on that device should resonate at exactly the same frequency and the difference frequency should be 0 Hz. In practice the two delay lines are not exactly the same, nor are the matching networks associated with the RF electronic system. As a result the two, uncoated delay lines typically resonate at slightly different frequencies thereby providing a non zero difference frequency. In fact, this nonzero difference frequency is desireable since it keeps the two oscillators from "locking" on to each other. The appearance of a zero output frequency is usually indicative of an oscillator malfunction due to faulty electrical connections, excessive mass loading, or shorted device electrodes. The existence of a nonzero output frequency from the mixer can cause confusion when an inexperienced person is attempting to coat the device. Coating one side of the device (e.g. delay line #1) will cause the frequency to increase while coating the opposite side of the device (i.e. delay line #2) will cause the frequency to decrease. It is usually desireable to coat the side that causes the frequency to increase (i.e. the lower frequency oscillator) since the system becomes erratic when the difference frequency approaches within about 10 KHz of zero. Care must be taken to make sure that the uncoated, reference delay line is indeed clean after the other side has been coated. Contamination present on the reference device will produce a signal that is subtracted from that produced by the coated side. Wiping the reference side of the device with a Q-tip soaked in solvent is sometimes useful to guarantee its cleanliness.

The actual design of the 52 MHz dual SAW vapor sensor device is illustrated in figure 1 & 2. The device is available in two configurations. Part number SD-52-A has a common ground connection for each of the four SAW interdigital transducers. This permits easier installation of the device into the holder. Part number SD-52-B has a

separate ground connection for each transducer and is attractive when simultaneous mass and conductivity measurements are to be performed. The separate ground minimizes RF noise pickup by the sensitive electrometer circuitry used to measure conductivity in very weakly conducting films. The "chips" are fabricated on ST-Quartz using gold metallization on top of a thin adhesion layer of tungsten/titanium. The electrode configuration was selected to provide a reasonably high resonant Q and a substantial area of bare quartz available for the coating. The entire surface of each SAW delay line is uniformly sensitive to materials placed there and application of films over the metal electrodes is fine unless the film material is conductive. In normal applications it is desireable to coat 100% of the delay line surface (including the electrodes) since this results in the greatest sensitivity. Coating only 50% of the device surface will yield a frequency shift that is only half of that predicted by the theoretical equations. Overall size of the chip is 1.5cm x 2.5 cm.

The mass detection limit of the SAW device depends on the signal to noise ratio provided by the sensor. The signal produced for a given mass loading is determined by the operating frequency of the device and the percentage of active area used. The noise is determined by the SAW oscillator stability. A frequency stability of 1 part in 10^7 measured over a 1 second interval is typically achievable with this system. This translates into a baseline noise level of less than +/- 5 Hertz RMS for the 52 MHz oscillator. Significant improvements in the stability of the oscillator may be possible through redesign of the SAW device and the mounting fixture.

The present system does respond to pressure and temperature and flow rate fluctuations. These effects are largely due to the inferior SAW mounting fixture employed in this system and are not intrinsic to the SAW concept. When vapors are to be exposed to the SAW sensor it is desireable that a flow rate in the range of 10 - 500 cc / min be employed. There is a small effect of flow rate on the difference frequency obtained from the system.

SAW Coating Procedure

Any number of methods can be used to apply chemically selective coatings to the surface of the SAW device. These methods include deposition from solutions applied by microsyringes, Q-tips, and brushes, spin casting, dipping, spraying by air brush, Langmuir-Blodgett film transfer, plasma deposition, sputtering, evaporation, sublimation, etc. A convenient technique for research applications is air brushing.

Coating application can be accomplished by spraying through a small mask positioned over the active area of the delay line to be coated. A dilute solution of the coating material dissolved in a volatile solvent works quite well. The spray can then be used to coat the device while the difference frequency is monitored with an oscilloscope and frequency counter. Multiple short bursts of the spray onto the device surface result in a coating that can produce a total frequency shift of 100 KHz or more. The device should be allowed to sit in clean, dry air for about 12 hours prior to testing.

REFERENCES

1. W. King Jr., Analytical Chemistry, 36, 1964, pp 1735-1733.

2. J. F. Alder, and J.J. McCallum, "Piezoelectric Crystals for Mass and Chemical Measurements", The Analyst, 108 (1291) 1983, pp 1169-1189.

3. A. Bryant, D.L. Lee, and J.F. Vetelino, "A Surface Acoustic Wave Gas Detector", Proc. IEEE 1981 Ultrasonics Symposium, pp 171-174.

4. H. Wohltjen, "Mechanism of Operation and Design Considerations for Surface Acoustic Wave Vapor Sensors", Sensors and Actuators, 1984, pp 307-325.

5. A. Snow, and H. Wohltjen, "Poly(ethylene maleate) - Cyclopentadiene: A Model Reactive Polymer-Vapor System for Evaluation of a SAW Microsensor", Analytical Chemistry, 56(8), 1984, pp 1411-1416.

6. H. Wohltjen, A. Snow, and D. Ballantine, "The Selective Detection of Vapors Using Surface Acoustic Wave Devices", Proc. of the Int. Conf. on Solid State Sensors and Actuators - Transducers '85, Philadelphia PA, June 11-14, 1985, IEEE Cat. No. CH2127-9/85/0000-0066, pp 66-70.

7. J. Hlavay, and G.G. Guilbault, "Applications of the Piezoelectric Crystal Detector in Analytical Chemistry", Analytical Chemistry, 49(13), 1977, pp1890-1898.

PROCEDURE
FOR SAW DEVICE PREPARATION AND MOUNTING

I. CLEAN THE DEVICE

a) Rinse SAW device with solvent (e.g. acetone or CH_3Cl.....cleaning the device in a Soxhlet extractor is suggested if every trace of a previous coating must be removed).

b) Place device in electronic grade isopropanol and clean ultrasonically for 10 min.

c) Dry the device by standing on edge on clean blotter paper. (Handle the device by the edges only.)

d) For storage, stand the device on its edge in a clean, glass tube with a clean cover.

II. MEASURE THE ELECTRODE RESISTANCE

(Sometimes the SAW interdigital (IDT) electrodes pick up contaminant particles that short them out.)

a) Select the highest resistance scale on an Ohmeter.

b) Check each of the 4 IDT electrodes for shorts between the fingers by measuring the resistance between the fingers. Do this by touching the ohmeter probes to the two gold bus bars associated with each IDT.
(NOTE: This procedure requires a steady hand and needle sharp ohmeter probes. If the probes are inadvertently dragged across the IDT then irreparable damage can be done to the device.

c) If the resistance between the fingers is measurable (i.e. less than about 1 Megohm) then the cleaning process must be repeated.
(NOTE: Sometimes careful wiping of the IDT with a solvent moistened Q-Tip can eliminate the difficulty.)

III. CLEAN THE DEVICE HOLDER

a) Blow out the empty holder with clean, filtered air (or "DUST-OFF" fluorocarbon propellant).

b) Visually inspect the holder for debris.
(Dirt and grit that accumulates in the device holder can provide a sharp point that cleaves the device when pressure is applied during the clamping process.)

IV. CLEAN THE ELECTRICAL CONTACT CLIPS (OCCASIONALLY)

a) Remove the clips.

b) Clean them in solvent (e.g. acetone).

c) Ultrasonically clean in isopropanol bath for 10 minutes. Air dry.

V. MOUNT THE DEVICE IN THE HOLDER

(It is a good idea to be seated, relaxed, and undisturbed during this procedure.)

a) Loosen the clamping screws in the device holder and turn the clips to permit the device to drop freely into the well.

b) Visually inspect the well to make sure that it is free of debris.

c) Place the SAW device in the well and make sure it is flat against the bottom.

d) With tweezers, rotate each clip to contact the gold pads for each electrode. (Pay particular attention to the clips which must provide ground connections to the four center pads.....These connections can be troublesome.)

e) Tighten the screws using a jeweler's screwdriver. *Use care* so that it cannot be dropped onto the device. It is sometimes helpful to use another screwdriver or tweezers to hold the clip in position while tightening the screws. Tighten only enough so that the clips do not move freely when nudged with the tweezers.

VI. CHECK THE ELECTRICAL CONTINUITY OF EACH CONNECTION

a) Measure the resistance from each gold pad of the SAW device to the top of the screw on its contact clip. (*Be careful ! Do not allow the probes to slip onto the electrodes.*) A resistance of less than 5 ohms should be measured.

b) If good contact is not observed, then loosen and retighten the screws as required to obtain less than 5 ohms.

c) Measure the resistance between the grounding screw heads (labeiled "G" on the pictorial diagram) and ground (e.g. the chassis). Also measure the resistance between the IDT connector screw heads (labelled "A,B,C, & D" on the pictorial diagram) and the corresponding point (i.e. "A,B,C &D") on the IDT tuning inductor. Each connection should show a resistance less than 5 ohms. If they don't, then the contact between the screw and the metal contact nut on the reverse side of the circuit board is bad and should be cleaned or otherwise corrected. (Some graphite placed on the screw threads can help.)

d) Measure the resistance between the IDT connector screw heads (labelled "A,B,C, & D" on the pictorial diagram) and ground. The resistance should be greater than 1 Megohm. If it is less than 1 Meg then the IDT electrodes are contaminated and cleaning is necessary.

VII. TURN ON THE POWER

Once the SAW device has been installed into the holder and good electrical connections have been established, then the system can be powered up.

a) Turn on power switch.

b) Observe the system output signal (i.e. difference frequency) on an oscilloscope. A stable waveform (about 5 V p-p) in the frequency range of about 10 KHz to 200 KHz should be observed. If the waveform is not stable then the tuning capacitors (shown in the pictorial diagram) can be adjusted to improve the stability.

MICROSENSOR SYSTEMS, INC.

PART NO. SD-52-A/B
(52 MHz DUAL SAW DELAY LINE)

HANDLING INSTRUCTIONS

The SD-52-A/B SAW dual delay lines are shipped with a photoresist coating to prevent damage to the gold microelectrodes. Before use, the devices must be gently removed from the sticky tape that holds them together and then rinsed with a solvent (e.g. acetone) to remove the photoresist. It is recommended that they be rinsed a second time with electronic grade isopropanol and allowed to drip dry by supporting the device on an edge while resting on a piece of absorbent paper. This will prevent any spotting of the device surface by impurities in the solvent. The devices can also be cleaned in an ultrasonic cleaner. With care the devices can be coated and cleaned many times for reuse.

Prior to using any SAW delay line, one should ALWAYS measure the resistance of the electrodes to make sure that electrical shorting has not occured. A conventional volt-ohmmeter (VOM) connected to an electrode should indicate a resistance greater than a Megohm. Lower resistances occur when the electrode is contaminated with ionic impurities, moisture, or other things that can bridge between the electrode "fingers". When low electrode resistances are observed, cleaning is recommended. Rubbing the electrodes with a solvent wetted Q-tip is acceptable. Persistent shorts can be "blown out" by connecting the electrode to a 24 Volt power source. This procedure will cause the shorted "finger" to melt like a fuse. While this may destroy a small part of the electrode it usually does not result in any noticeable degradation of SAW device performance.

Breakage is perhaps the most serious problem encountered with large SAW delay lines. Quartz is very brittle and will break if excessive forces are applied to the device.

MICROSENSOR SYSTEMS, INC.

52 MHz
DUAL SAW DELAY LINE OSCILLATOR
SYSTEM DIAGRAM

CEM - 52

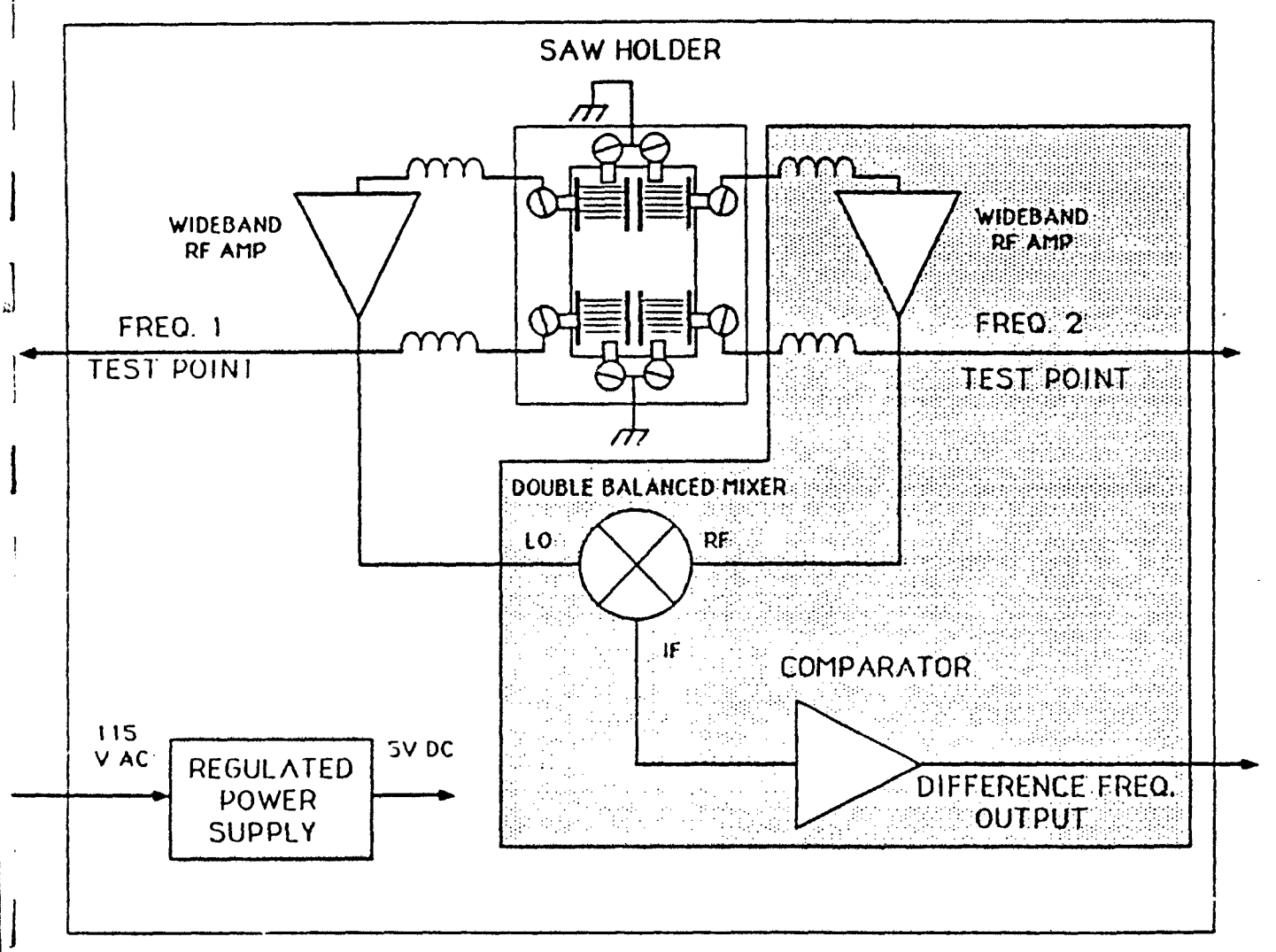

NOTE: SHADED AREA IS DELETED WHEN SIMULTANEOUS SAW FREQUENCY / CONDUCTIVITY MEASUREMENTS ARE REQUIRED.

CEM-52 SAW VAPOR SENSOR CHASSIS LAYOUT

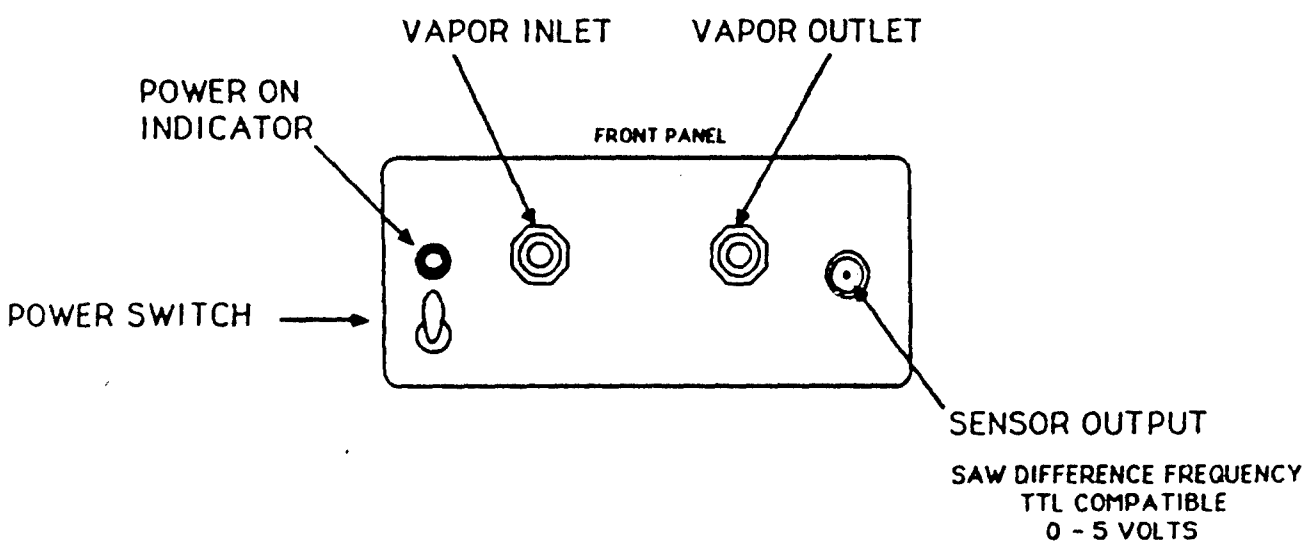

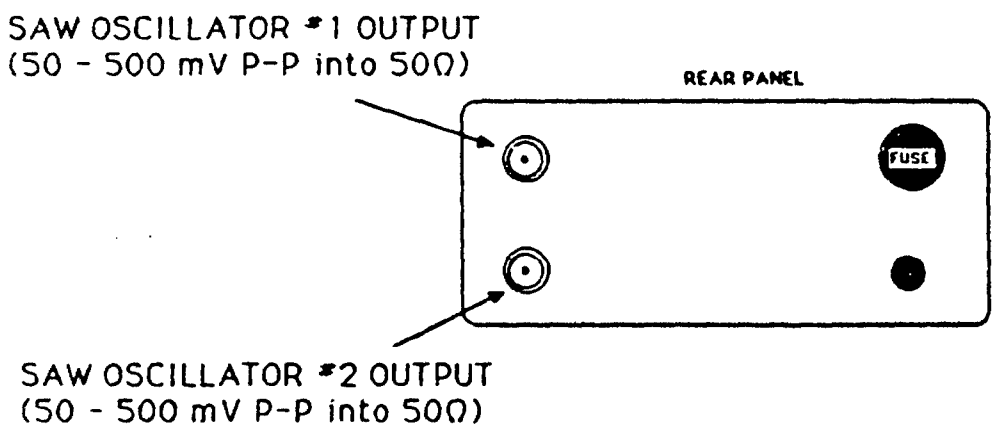

MICROSENSOR SYSTEMS, INC.

52 MHz
DUAL SAW DELAY LINE OSCILLATOR
PICTORIAL DIAGRAM

TUNING CAP.

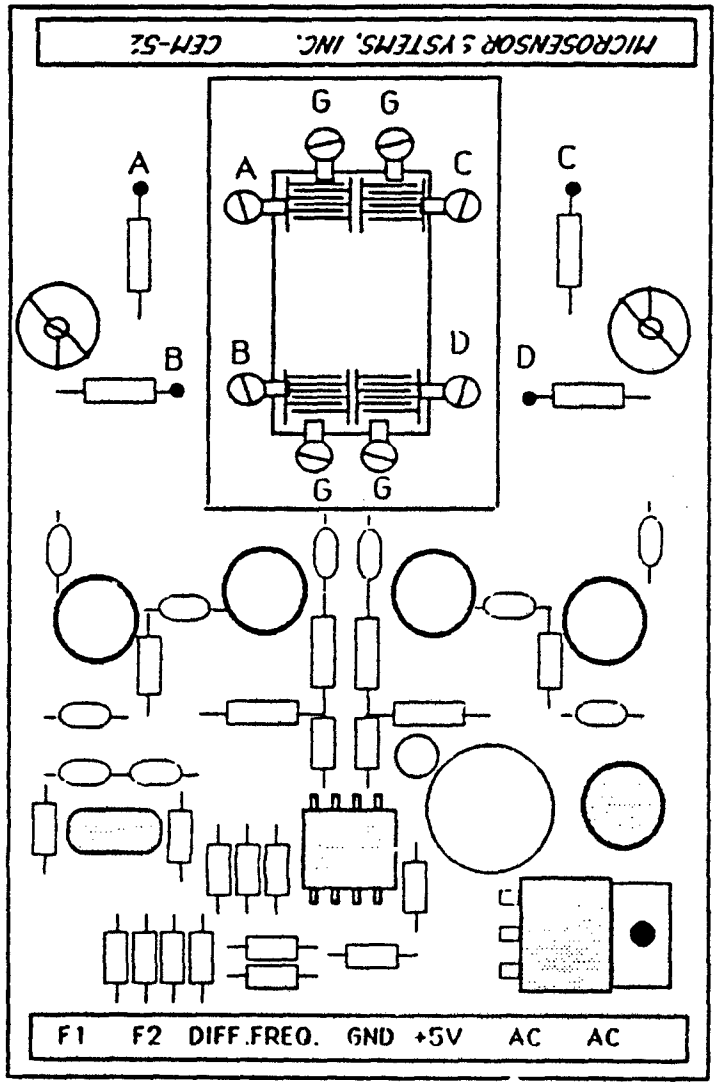

TUNING CAP.

MICROSENSOR SYSTEMS, INC.

52 MHz DUAL SAW DELAY LINE

(PART NO. SD- 52 - A)

COMMON GROUND

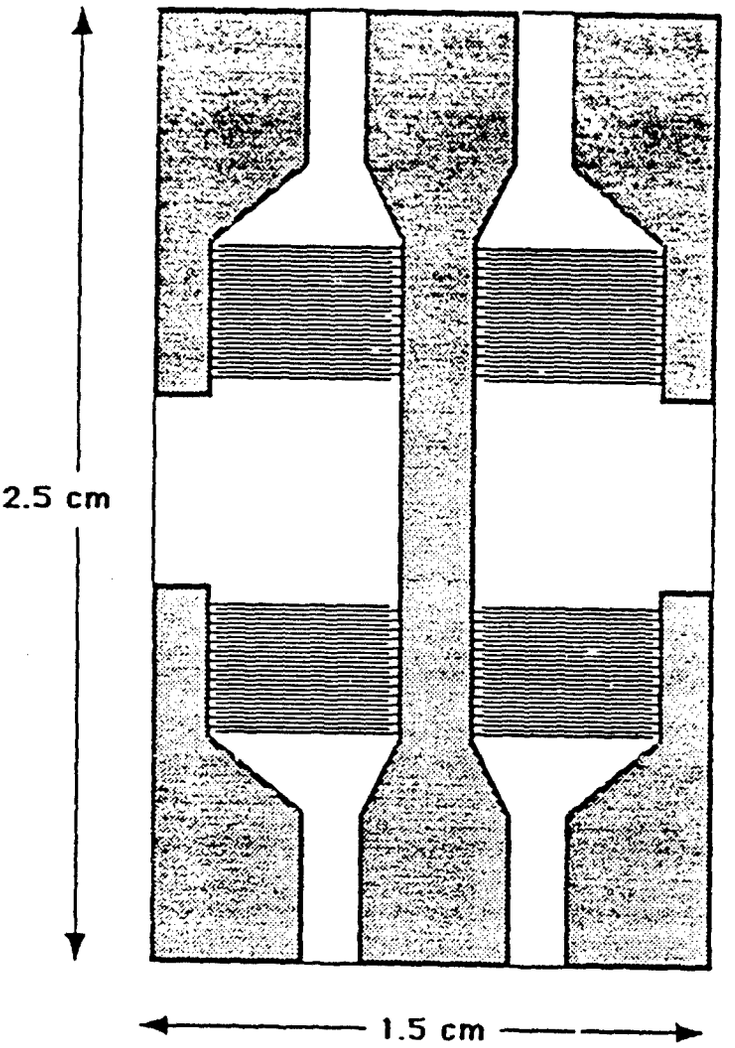

ELECTRODE MATERIAL	:	GOLD
SUBSTRATE MATERIAL	:	ST-QUARTZ
FINGER WIDTH	:	15 MICRONS
FINGER SPACING	:	15 MICRONS
NO. OF FINGER PAIRS	:	50
ACOUSTIC APERTURE	:	4800 MICRONS

MICROSENSOR SYSTEMS, INC.

52 MHz DUAL SAW DELAY LINE ELECTRICAL CONNECTIONS

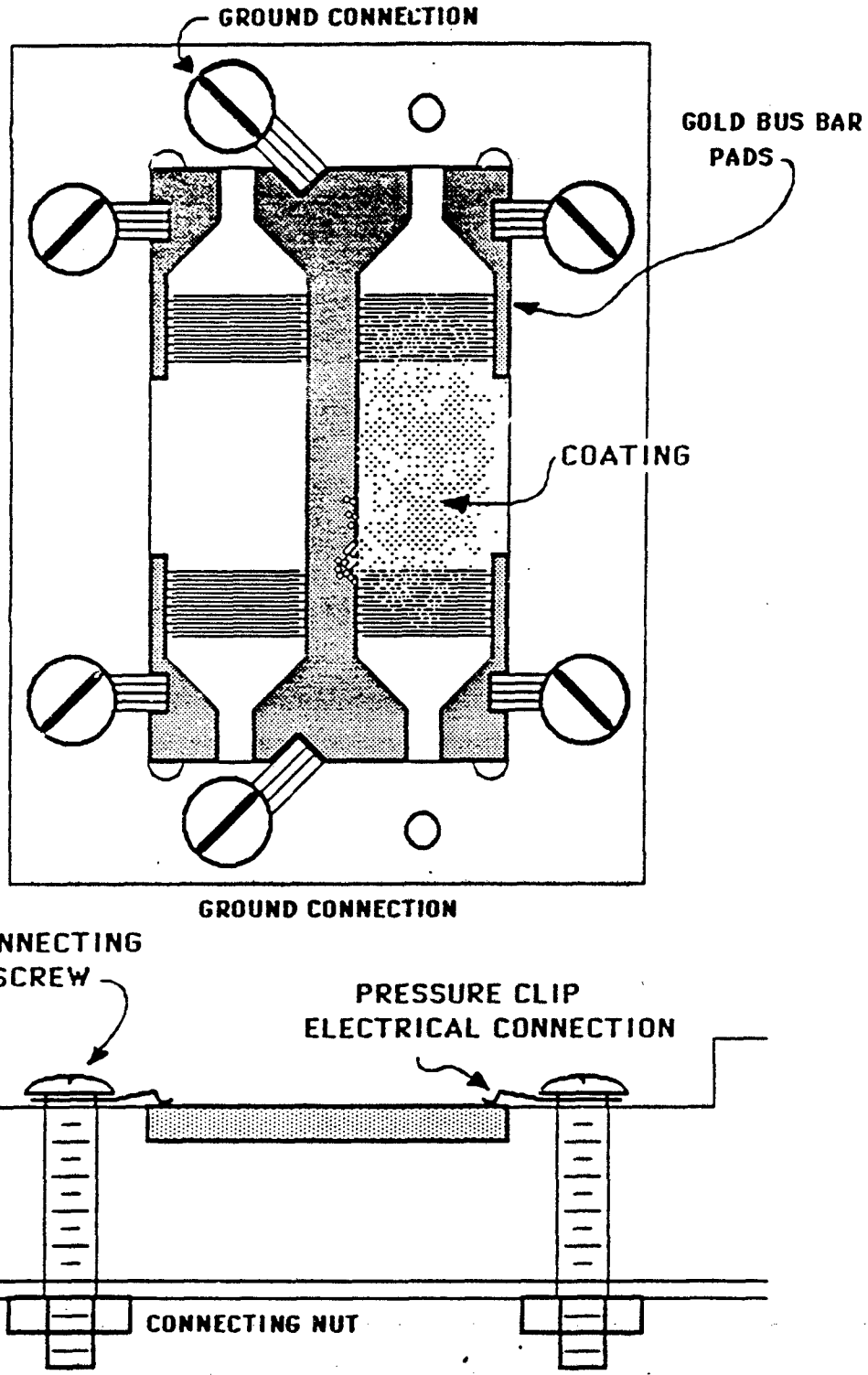

TOP VIEW

SIDE VIEW

MICROSENSOR SYSTEMS, INC.

52 MHz DUAL SAW DELAY LINE

(PART NO. SD- 52 - B)

SEPARATE GROUNDS

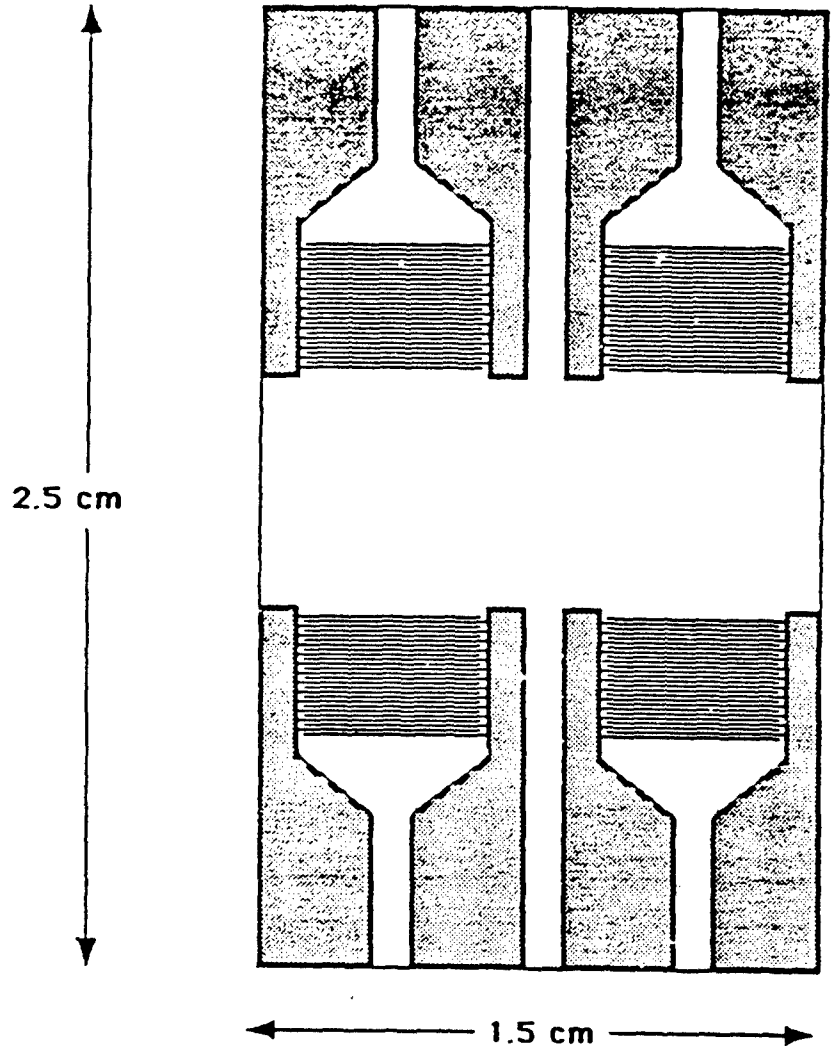

ELECTRODE MATERIAL	:	GOLD
SUBSTRATE MATERIAL	:	ST-QUARTZ
FINGER WIDTH	:	15 MICRONS
FINGER SPACING	:	15 MICRONS
NO. OF FINGER PAIRS	:	50
ACOUSTIC APERTURE	:	4800 MICRONS

MICROSENSOR SYSTEMS, INC.

52 MHz DUAL SAW DELAY LINE ELECTRICAL CONNECTIONS

TOP VIEW

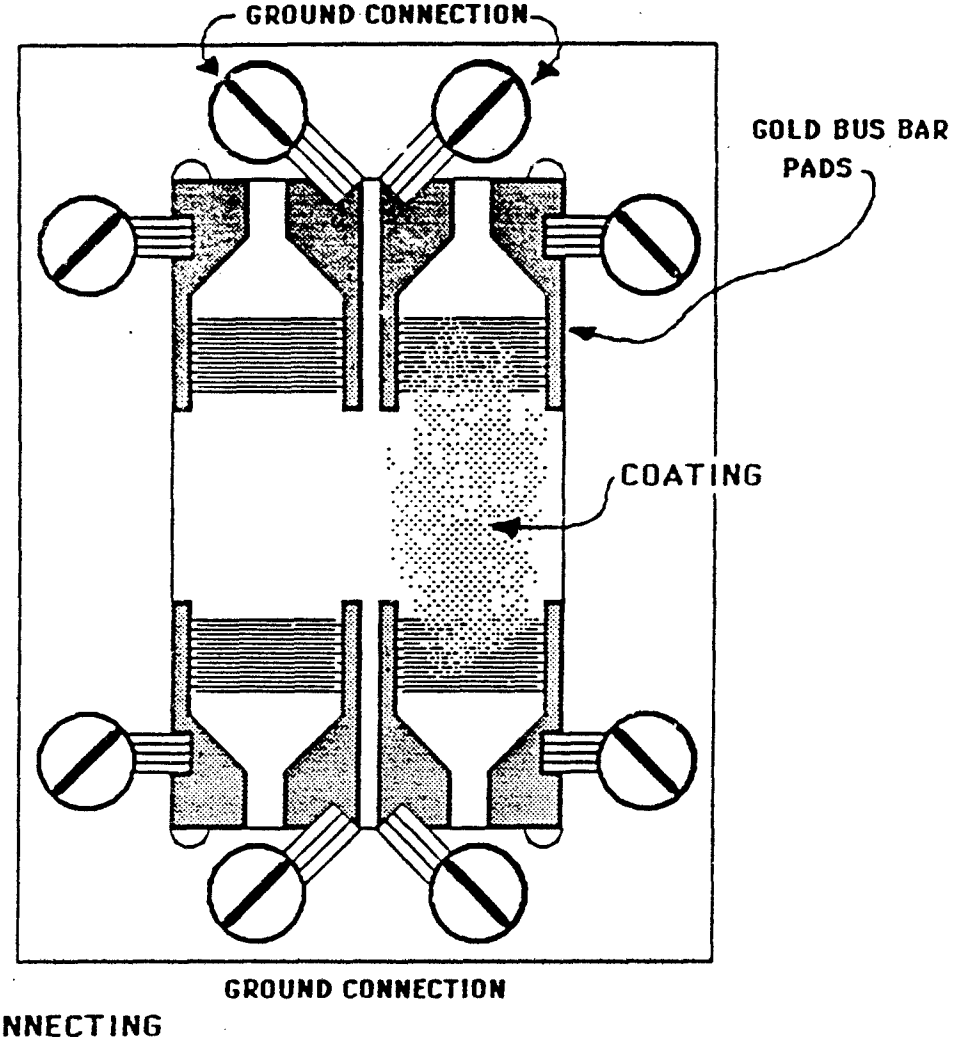

SIDE VIEW

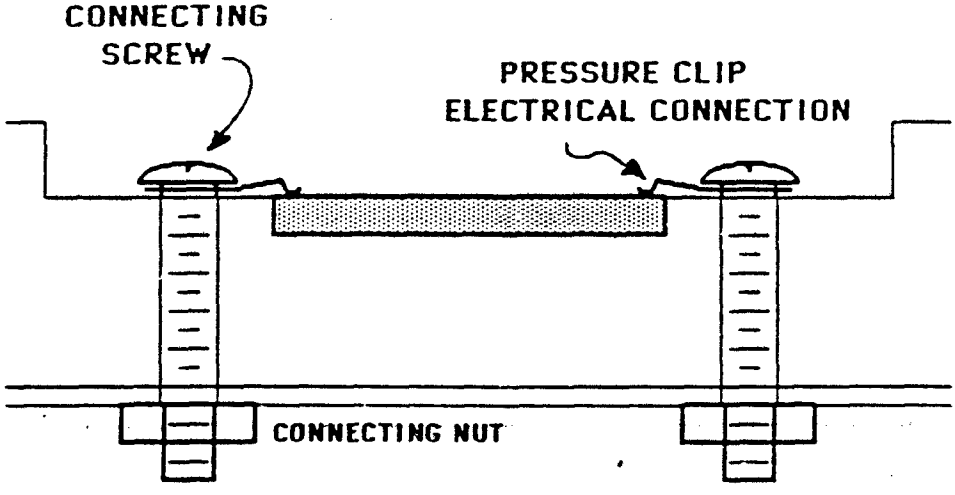

MICROSENSOR SYSTEMS, INC.

RFM-158 A

158 MHZ
SAW DEVICE RF ELECTRONICS MODULE

OPERATING DESCRIPTION

JANUARY 1987

GENERAL SAW VAPOR SENSOR CONSIDERATIONS

Theoretical Model of SAW Sensor Response

The signal provided by a SAW oscillator vapor sensor can be described by the following theoretical equation (4):

$$\Delta f = (k_1 + k_2)\, f_0^2\, h\, \rho' - k_2\, f_0^2\, h \left(\frac{4\mu'}{V_r^2} \left(\frac{\lambda' + \mu'}{\lambda' + 2\mu'} \right) \right) \qquad (1)$$

where Δf is the SAW oscillator frequency change produced by the vapor absorbed into the coating, k_1 and k_2 are material constants for the piezoelectric substrate, f_0 is the unperturbed resonant frequency of the SAW oscillator, h is the coating thickness, ρ' is the coating density, μ' is the shear modulus and λ' is the Lame' constant of the coating, and V_r is the Rayleigh wave velocity in the piezoelectric substrate (3159 m/sec for Y-X Quartz). This relationship assumes that the SAW device coating is isotropic and non-piezoelectric and that the coating covers 100% of the delay line surface. Furthermore, the relationship is valid only for very thin films (e.g. less than 0.2% of the acoustic wavelength thick). For thicker films, equation 1 can only provide estimates of the signal magnitude. When organic coatings are employed, it is often found that the second term of equation 1 is negligible because the shear elastic modulus of the coating (μ') is small compared to the square of the Rayleigh wave velocity (V_r). Under these conditions, equation 1 reduces to:

$$\Delta f = (k_1 + k_2)\, f_0^2\, h\, \rho' \qquad (2)$$

For Y-X Quartz SAW devices, $k_1 = -9.33 \times 10^{-8}$ m^2·sec/kg and $k_2 = -4.16 \times 10^{-8}$ m^2·sec/kg. The product of the coating thickness (h) and its density (ρ') is the mass per unit area on the device surface. Equation 2 predicts that the signal obtained from a given mass loading (h ρ' product) will increase with the square of the operating frequency of the SAW oscillator. Furthermore, operating frequency determines the size of the device since it imposes size requirements on the interdigital electrodes used to generate the Rayleigh surface wave. As the operating frequency increases, the device area (and cost) decreases. Higher operating frequencies permit thinner coatings to be employed with a corresponding improvement in response time since vapor diffusion into the coating will be quicker. Higher operating frequencies also result in greater baseline noise that hinders detection at the lowest concentrations. The key assumption in these predictions is that the sensitivity increases with the square of the frequency. Several experimental studies have indicated that this assumption is valid.

SAW VAPOR SENSOR SYSTEM DESCRIPTION

The SAW devices employed in this system have a nominal frequency of 158 MHz. A dual SAW delay line oscillator configuration is employed in the system. In this design, two SAW delay lines are fabricated on the same substrate. One delay line is coated with the chemically selective film and the other is left uncoated. The frequencies of the two delay line oscillators are mixed to provide a frequency equal to the difference of the two oscillator frequencies. In principle, frequency drifts caused by ambient temperature and pressure fluctuations experienced by the SAW device are compensated by this scheme. (Note: unsymmetrical mechanical stresses imposed by thermal expansion of device package can cause uncompensated drift.) This approach affords the additional advantage that the difference frequency is much lower (e.g. a hundred KHz) than the frequency of the oscillators themselves (i.e. 158 MHz). This makes it much easier to measure the SAW vapor response using inexpensive, digital counter circuitry. Theoretically, when a clean device is in the system the two delay lines on that device should resonate at exactly the same frequency and the difference frequency should be 0 Hz. In practice the two delay lines are not exactly the same, nor are the matching networks associated with the RF electronic system. As a result the two, uncoated delay lines typically resonate at slightly different frequencies thereby providing a non zero difference frequency. In fact, this nonzero difference frequency is desireable since it keeps the two oscillators from "locking" on to each other. The appearance of a zero output frequency is usually indicative of an oscillator malfunction due to faulty electrical connections or excessive mass loading. The existence of a nonzero output frequency from the mixer can cause confusion when an inexperienced person is attempting to coat the device. Coating one side of the device (e.g. delay line #1) will cause the frequency to increase while coating the opposite side of the device (i.e. delay line #2) will cause the frequency to decrease. It is usually desireable to coat the side that causes the frequency to increase (i.e. the lower frequency oscillator) since the system becomes erratic when the difference frequency approaches within about 10 KHz of zero. Care must be taken to make sure that the uncoated, reference delay line is indeed clean after the other side has been coated. Contamination present on the reference device will produce a signal that is subtracted from that produced by the coated side. Wiping the reference side of the device with a Q-tip soaked in solvent is sometimes useful to guarantee its cleanliness.

The mass detection limit of the SAW device depends on the signal to noise ratio provided by the sensor. The signal produced for a given mass loading is determined by the operating frequency of the device and the percentage of active area used. The noise is determined by the SAW oscillator stability. A frequency stability of 1 part in 10^7 measured over a 1 second interval is typically achievable with this system. This translates into a baseline noise level of less than ± 16 Hertz RMS for the 158 MHz oscillator.

The device intended to be used with the RFM-158A is the Microsensor Systems, Inc.

MICROSENSOR SYSTEMS, INC.

158 MHz DUAL SAW DEVICE

SD-158-A

TO-8 Header / 0.600" Diameter
12 Pin Package

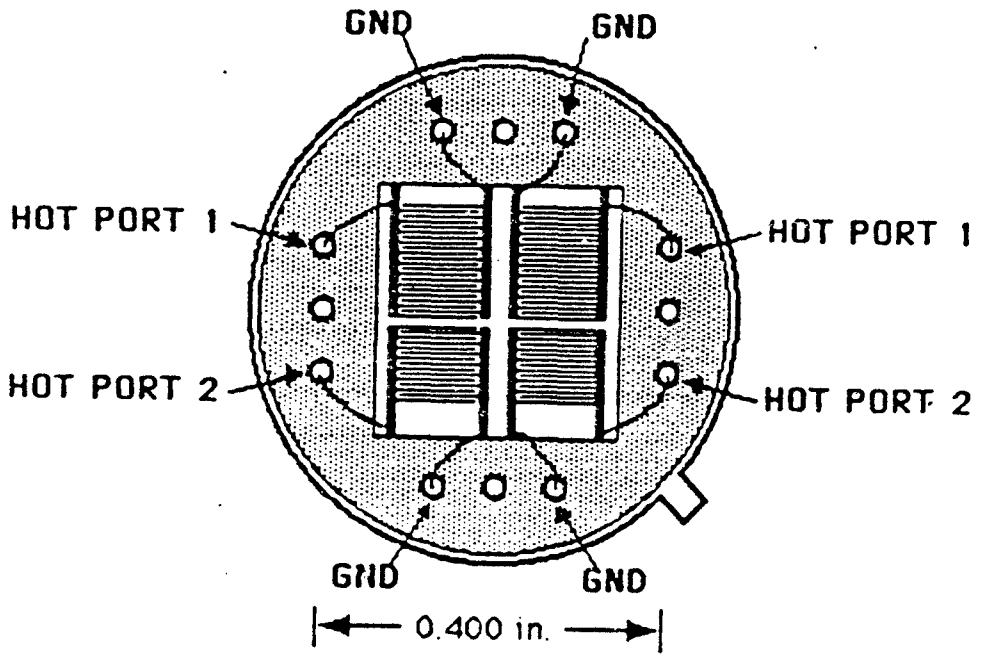

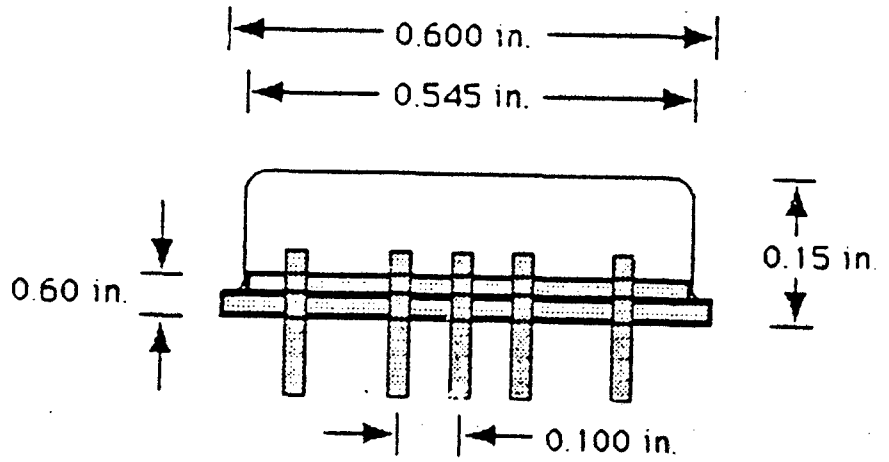

158 MHz dual SAW (part no SD-158-A). This device is packaged in a gold plated 12 pin 0.600 inch diameter TO-8 package. The SAW "chip" contains two individual 158 SAW delay lines. One of the delay lines is used as a reference and is not coated. The electrical connections to the SAW device are made through 12 pins on the bottom of the SAW package. Only 8 of these pins are used and they are attached to the SAW device by gold wire bonds. A detailed drawing of this device is shown in figure 1. The SAW device plugs into the RF electronics module for use. It is important to observe the proper position of the tab on the SAW device when inserting into the RF module. The tab must face towards the lower right hand corner of the module as shown on figure 1 If the SAW device is not properly inserted, it will not function correctly. The following precautions should be observed when plugging a SAW device into the module:

1. **TURN OFF POWER TO THE SAW RF MODULE WHEN INSERTING THE SAW DEVICE.**

2. **OBSERVE THE PROPER POSITION OF THE TAB ON THE SAW DEVICE WHEN INSERTING INTO RF MODULE SOCKET.**

Coated SAW devices are sealed and require no special handling precautions. SAW devices that are not coated require additional care to prevent damage. The devices are packaged with a lid designed to fit over the device. These lids are not attached until after a coating is applied and can fall off if not handled correctly. (Lid sealing is normally accomplished using epoxy cement after drilling holes in the lid for vapor circulation.) The fine gold wire electrical connections to the SAW device can be damaged if care is not taken when the lid is removed.

Care should be used when removing the SAW device from the socket on the RF electronics module to prevent damage to the connecting pins. It is recommended that the SAW device be removed by prying the device from underneath using a small screwdriver, awl, or similar object. The device should be raised by prying first at the corner beneath the tab on the SAW device and then alternating with the opposite corner.

SAW COATING APPLICATION

A number of methods can be used to apply chemically selective coatings to the surface of the SAW device. These methods include deposition from solutions applied by microsyringes, Q-tips, and brushes, spin casting, dipping, spraying by air brush, Langmuir-Blodgett film transfer, plasma deposition, sputtering, evaporation, sublimation, etc. A particularly convenient technique for research applications is air brushing.

Coating application can be accomplished by spraying through a small mask positioned over the active area of the delay line to be coated. A dilute solution of the coating material dissolved in a volatile solvent works quite well. The spray can then be used to coat the device while the difference frequency is monitored with an oscilloscope and frequency counter. Multiple short bursts of the spray onto the device surface result in a coating that can produce a total frequency shift of 100 KHz or more. The device should be allowed to sit in clean, dry air for about 12 hours prior to testing.

The entire surface of each SAW delay line is uniformly sensitive to materials placed there and application of films over the metal electrodes is fine. In normal applications it is desireable to coat 100% of the delay line surface (including the electrodes) since this results in the greatest sensitivity. Coating only 50% of the device surface will yield a frequency shift that is only half of that predicted by the theoretical equations. Overall size of the chip is 0.5 cm x 0.5 cm. The active area of each delay line is approximately 0.2 cm x 0.4 cm.

RF ELECTRONICS MODULE CONNECTIONS

The RF electronics module contains VHF amplifiers that allow the dual SAW device to function as two independent delay line oscillators. These two oscillators generate signals that are mixed electronically to provide a signal whose frequency is the difference between the two oscillator frequencies. This difference frequency is processed by a comparator circuit to provide a TTL compatible signal. The power input (+5 Volts) and output (freq. 1, freq. 2, and freq.1 - freq. 2) for this module is provided through a 6-pin edge connector. The function of each of these pins is as follows:

Pin 1: This pin connects to the ground plane of the SAW module.
Pin 2: The signal from this pin is the frequency difference between the two SAW delay lines. (5V P-P square wave...drives one LS TTL load).
Pin 3: The RF output from channel 1 (the uncoated side) of the SAW device is available on this pin. (around 200 mV P-P @ 158 MHz).
Pin 4: The RF output from channel 2 (the coated side) of the SAW device is available on this pin. (around 200 mV P-P @ 158 MHz).
Pin 5: This pin is used to supply power to the SAW module (+5 V @50mA DC).
Pin 6: This pin connects to the ground plane of the SAW module.

It should be noted that the RF outputs on pins #3 & 4 are not buffered. Connections to these pins can perturb the oscillator frequencies. For device coating it is very desireable to monitor all frequencies as the coating is being applied in order to get an accurate estimate of coating thickness. An RF buffer amplifier / power supply / coating fixture that is designed for use with the RFM-158 is available from Microsensor Systems, Inc. (part no. SPM-158)

MICROSENSOR SYSTEMS, INC.

158 MHz DUAL SAW DELAY LINE OSCILLATOR PICTORIAL DIAGRAM

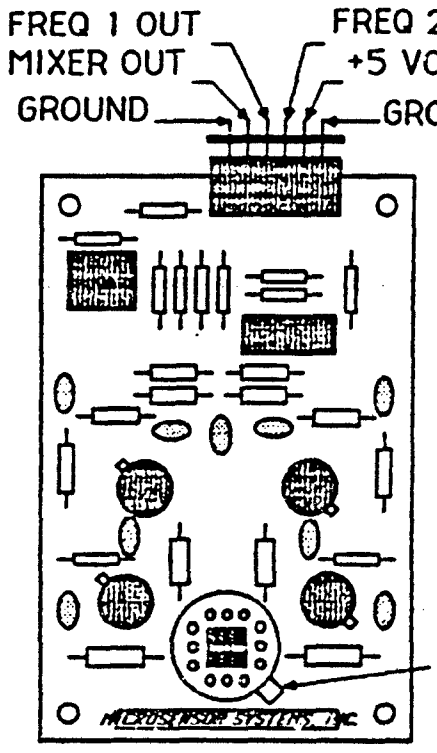

MICROSENSOR SYSTEMS, INC.

158 MHz
DUAL SAW DELAY LINE OSCILLATOR

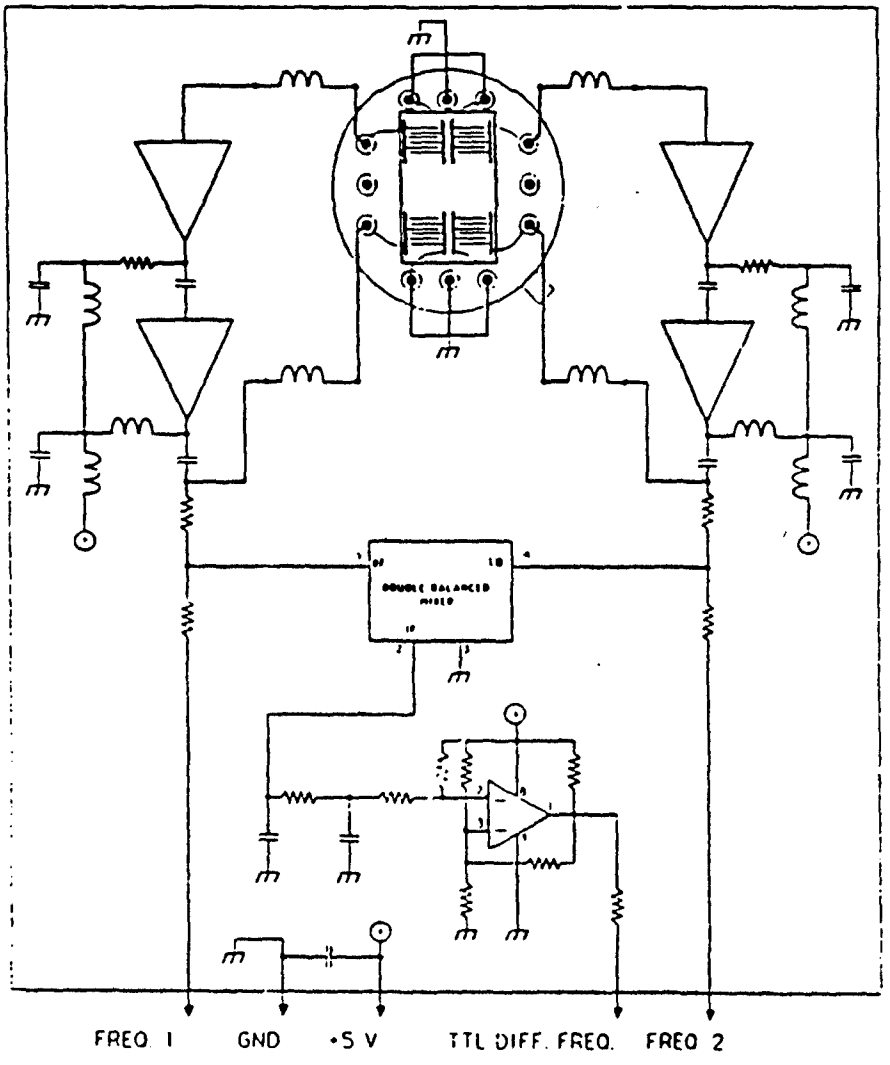

USAF / NRL RESEARCH PROGRAM

A STUDY OF SURFACE ACOUSTIC WAVE DEVICE OSCILLATOR PERFORMANCE:

SAW RESONATORS VS SAW DELAY LINES

PROGRESS REPORT

25 SEPTEMBER, 1987

PREPARED BY

HANK WOHLTJEN

MICROSENSOR SYSTEMS, INC.
FAIRFAX, VA

CONTENTS

		PAGE
1.	INTRODUCTION	3
2.	MEASURES OF SAW OSCILLATOR NOISE	4
3.	EXPERIMENTAL PROCEDURE	6
4.	RESULTS	7
5.	DISCUSSION	10
6.	APPENDICES	11

APPENDIX A. (SAW Device Data Sheets)
APPENDIX B. (SAW Vapor Response Data)
APPENDIX C. (Experimental NoiseData)

1. INTRODUCTION

Surface Acoustic Wave (SAW) devices are being developed as sensors for a variety of applications. The most common SAW device configuration for sensors is the SAW oscillator in which the physical or chemical property of interest perturbs the Rayleigh wave propagation velocity, resulting in a corresponding shift in the resonant frequency of the SAW controlled oscillator. These devices are especially attractive in chemical vapor sensing applications because of their relatively high surface mass sensitivity. For example, at a Rayleigh wave frequency of 158 MHz on ST-quartz, a SAW oscillator exhibits a sensitivity of approximately 32 Hz/nanogram/cm^2. This magnitude of sensitivity is predicted theoretically and has been experimentally verified using Langmuir-Blodgett films of known mass density. The detection limit of the device is determined by this sensitivity and the characteristic noise level exhibited by the device. A typical 158 MHz SAW delay line oscillator produces 16 Hz of "noise" which suggests that 1 nanogram/cm^2 would be detected with a signal to noise ratio of 2. Clearly, a dramatic reduction in the detection limit of SAW vapor sensors can be realized if the effective frequency noise of the SAW controlled oscillator can be reduced.

SAW oscillator noise (i.e. the random fluctuations in the SAW oscillator frequency that are uncorrellated with the frequency shifts produced by the chemical species being measured) is related to the resonant "Q" of the SAW device. Devices having higher Q provide a more stable resonant frequency and hence lower noise. There are two SAW device configurations that are used in the vast majority of SAW controlled oscillators. These are the delay line and the resonator (figure 1). Both devices should exhibit the same mass sensitivity but the resonator is well known for its superior noise performance. Up to this time the majority of SAW vapor sensor devices have used the delay line configuration.

The objective of this study was to quantify the noise levels of several SAW delay lines and resonators (both coated and uncoated) in order to learn if SAW resonators could afford any significant performance advantage in chemical sensor applications.

2-PORT SAW RESONATOR

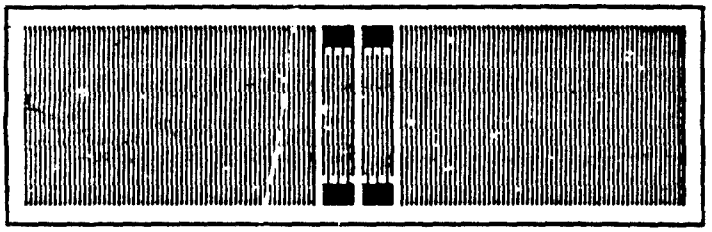

SAW DELAY LINE

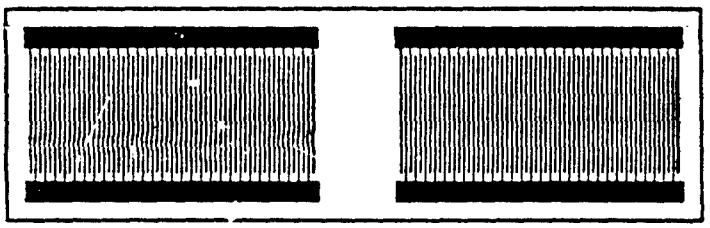

FIGURE 1.

2 MEASURES OF SAW OSCILLATOR NOISE

The measurement of noise in any physical system is usually complicated by the fact that the noise is not truly random (i.e. "white") but rather has a distinctive spectral distribution. Furthermore, the experimental measurements are often conducted under conditions in which all variables (e.g. temperature, atmospheric presssure, etc.) are not perfectly controlled and result in systematic drift superimposed on the intrinsic noise of the oscillator. Two methods have been used in this study to characterize the noise generated by SAW oscillators.

Root Mean Square (RMS) of Linear Least Square Fit Residuals

This method is somewhat unconventional but provides a measure that correllates closely with the signal processing commonly employed with SAW vapor sensors. In this method, the frequency (or difference frequency) of an unperturbed SAW oscillator is recorded at regular time intervals over some fixed time period (e.g. 1 minute). A linear least squares fit is performed on this data set. The least squares fit line is then assumed to represent the average value of the signal over the measurement period. The difference between the actual signal value and the average signal (as determined by the least squares fit line) is calculated and saved as a set of residual differences. The standard deviation of these residuals (as calculated using the relationship shown below) is used to describe the root-mean-square (RMS) noise level of the SAW sensor.

$$\sigma(N) = \left(\frac{1}{N-1} \sum_{k=1}^{N} (y_k - \bar{y})^2 \right)^{1/2}$$

where $\sigma(N)$ is the Standard Deviation

N is the Number of measurements

$\bar{y}$ is the average value of the signal

y_k is the value of the signal at time k

The slope of the linear least squares fit line is indicative of the drift exhibited by the SAW oscillator. This method is relevant to practical SAW vapor sensors since baseline drift compensation schemes are commonly employed (e.g. frequent rezeroing of the baseline) and it is only the "high frequency" noise as represented by the residuals that presents a barrier to signal detection. When the SAW oscillator drift is non-linear with time, this method of characterizing oscillator noise can be misleading since it will overestimate the noise level of the device. Nevertheless, using the root-mean-square of least square fit residuals as a measure of SAW oscillator performance has proved to be very convenient and informative particularly because it separates out the noise and drift components.

Allan Variance

The most commonly employed measure of SAW oscillator performance is Allan variance. It is fundamentally superior to methods that measure standard deviation because it makes no assumptions about the spectral distribution of the oscillator noise. Indeed, the ratio of the standard deviation to the Allan variance of the SAW oscillator frequency can provide a useful diagnostic measure of the type noise exhibited by the oscillator (e.g. random, flicker, flicker-walk, etc.). The Allan variance is calculated by using the following relationship:

$$\sigma_y(\tau_o) = \left(\frac{1}{2(N-1)} \sum_{k=1}^{N-1} (y_{k+1} - y_k)^2 \right)^{1/2}$$

where $\sigma_y(\tau_o)$ is the Allan Variance of samples taken every τ_o sec

N is the Number of measurements

y_{k+1} is the normalized value of the signal at time k+1

y_k is the normalized value of the signal at time k

The normalized signal values are obtained by subtracting the instantaneous frequency from some starting reference frequency and dividing the difference by the starting frequency value.

3. EXPERIMENTAL PROCEDURE

The accurate comparison of SAW delay line oscillator performance and SAW resonator oscillator performance is not straightforward. This is due to the fact that there are many ways to configure the device design and supporting electronics for each type of oscillator to optimize one performance characteristic at the expense of others. The approach taken in this study was to utilize several existing SAW delay line and SAW resonator designs that are representative of presently available technology. The devices used in this study were:

1) 158 MHz dual SAW delay line (Microsensor P/N SD-158-A)
2) 229.25 MHz 2-port SAW resonator (SAWTEK P/N 851080)
3) 401 MHz 2-port SAW resonator (SAWTEK P/N 850999)
4) 668 MHz 2-port SAW resonator (SAWTEK P/N 850883)

The following experimental conditions were maintained for all devices studied:

- Devices were fabricated on ST-quartz with aluminum metallization.
- Devices were mounted in commercial packages with epoxy and connected via gold wire bonds.
- Oscillators were "burned in" for more than 72 hours prior to testing.
- Oscillators were warmed up for 24 hours prior to making noise measurements.
- The same RF amplifier system was used for each oscillator. Only the series tuning inductors were different from oscillator to oscillator.
- A dual oscillator configuration was used to provide a low frequency difference signal.

A schematic of the SAW oscillator RF electronics used in this study is shown in figure 2. Variable inductors were used to provide a series match to the RF amplifiers. The SAW frequency data was collected using a four channel digital frequency counter interfaced to a Macintosh data acquisition computer (Microsensor Systems, Inc. Model DAS-158). SAW oscillator frequencies were measured once every 2 seconds with a precision of ±1 Hertz. An experiment duration of 1 minute was chosen. The Allan variance and the root-mean-square of least square fit residuals was calculated for each data set. A total of ten trials were conducted with each sensor to obtain a representative average RMS noise and Allan variance for each device. All four SAW oscillators were run simultaneously from the same power supply during the course of these measurements.

The 158 MHz dual SAW delay line and the 668 MHz SAW resonator were coated with fluoropolyol (by air-brushing) to determine the extent to which the coating degrades the noise performance of the SAW oscillators. Noise trials were conducted as before except that the devices were purged with clean, dry air while being measured. These devices were then exposed to DMMP (using a Microsensor Systems, Inc. Model VG-7000 vapor generation system) to determine the magnitude of vapor response.

DUAL SAW OSCILLATOR

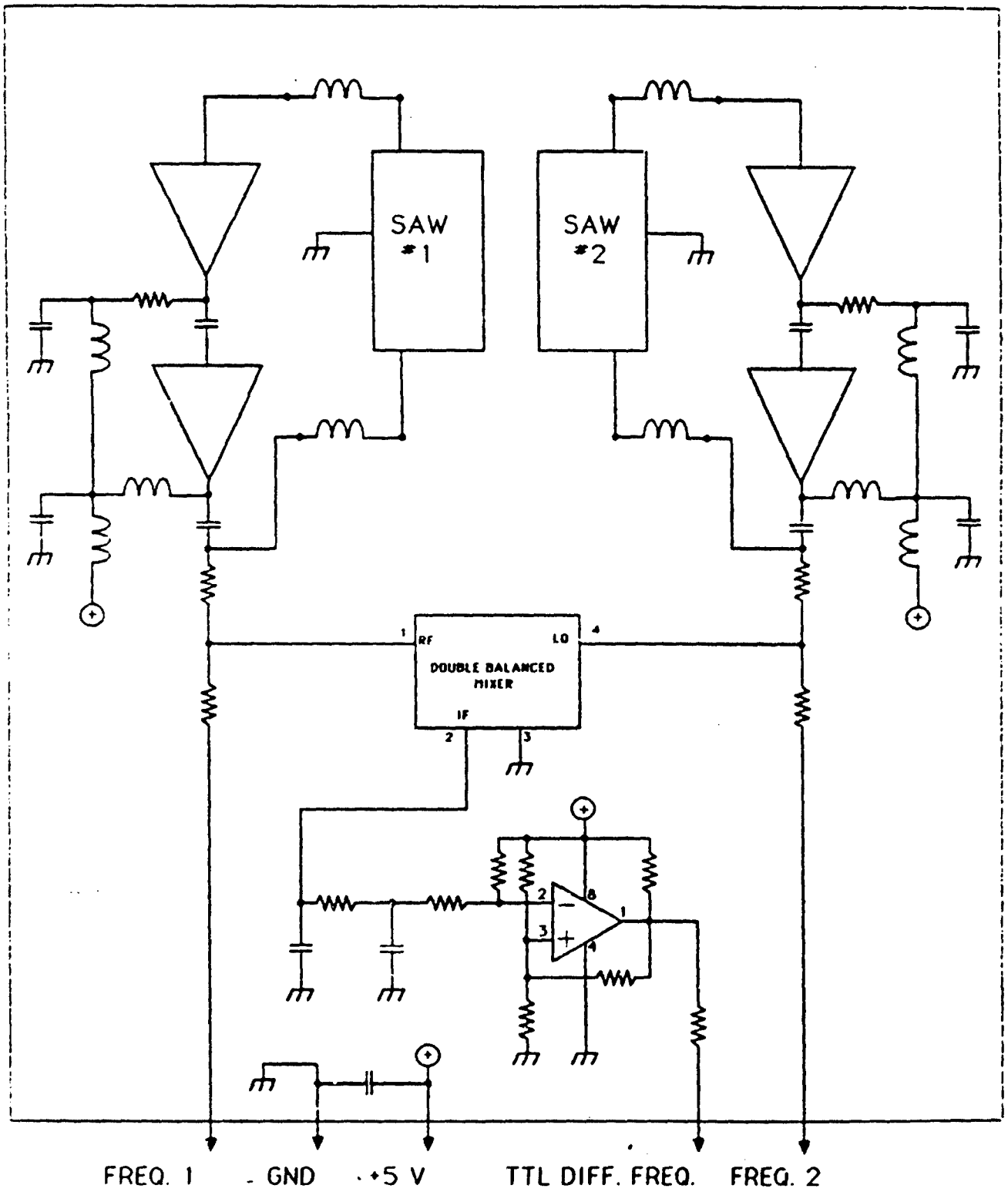

FIGURE 3.

4. RESULTS

Noise Measurements

The results of these SAW oscillator noise measurements are presented in Table 1. The raw experimental data used to prepare Table 1 is available in Appendix B.

Table 1.

MEASURED NOISE PERFORMANCE OF SAW OSCILLATORS

Average Results of 10 Measurements Trials
(1 measurement every 2 seconds for 60 seconds)

Uncoated Devices in Sealed Package

DEVICE	RMS NOISE (Hz)	DRIFT (Hz/min)	ALLAN VARIANCE
158 MHz Delay Line	2.8	0.4	1.5 E -08
229 MHz Resonator	4.3	-8.8	1.6 E -08
401 MHz Resonator	3.3	-9.9	4.8 E -09
668 MHz Resonator	1.0	-0.1	1.1 E -09

Coated Devices with Air Purge

DEVICE	RMS NOISE (Hz)	DRIFT (Hz/min)	ALLAN VARIANCE
158 MHz Delay Line	10.1	5.1	4.4 E -08
316 MHz Delay Line	20+ (typical)	----	----
668 MHz Resonator	14.7	6.5	7.8 E -09

Coated SAW Device Ageing

It is well known that SAW vapor sensors work best when they are allowed to "age" at least overnight after being coated with a vapor sensitive polymer film. The "ageing" of a 668 MHz coated SAW resonator was observed experimentally by making periodic noise measurements on the device immediately after coating application. The results (illustrated in figure 3) show a dramatic increase in the noise level following the coating application. The uncoated device exhibited an Allan variance of 1.1 E -09 prior to coating. Thirty minutes after coating the same device produced an Allan variance of 2.7 E -07, more than 100 times more noisy. As shown in figure 3, the device eventually aged so that after 70 hours, an Allan variance of 7.8 E -09 was measured.

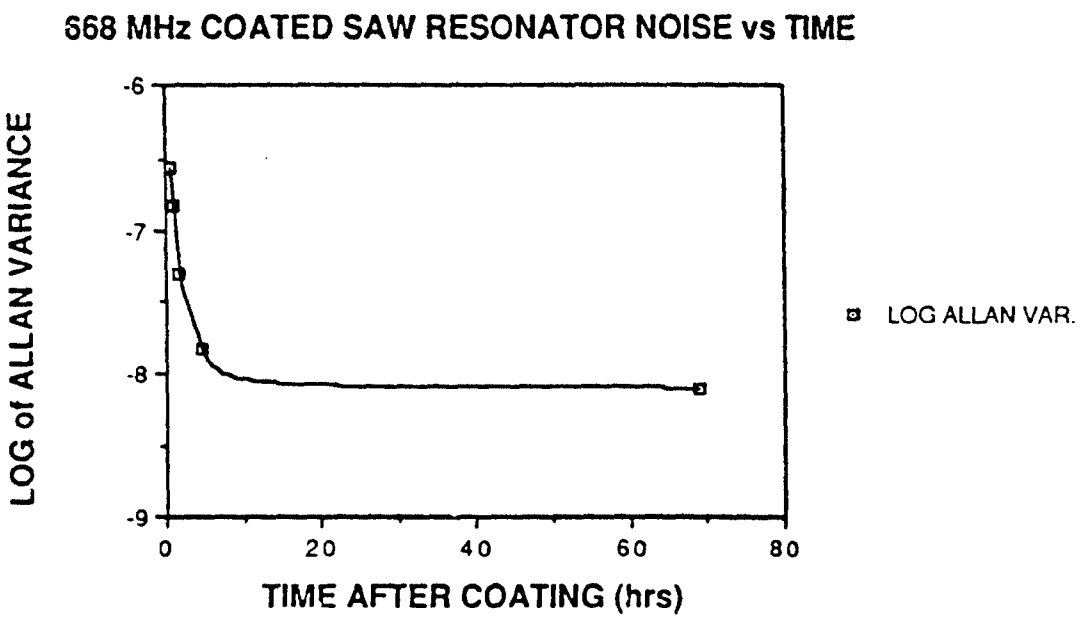

Figure 3.

Vapor Exposure

As a final investigation, the coated 158 MHz dual SAW device and the 668 MHz SAW resonator were exposed to low concentrations of dimethylmethylphosphonate (DMMP) vapor to verify that the coatings responded as expected. For unknown reasons, the 668 MHz device did not respond to DMMP (i.e. no measurable response was observed at a DMMP concentration of 2.8 mg/m^3). A second 668 MHz resonator was then coated carefully with fluoropolyol and exposed again to DMMP. This device performed as expected. The magnitudes of sensor response are tabulated below.

Table 2.

MEASURED SAW OSCILLATOR VAPOR RESPONSE

Fluoropolyol coating exposed to DMMP Vapor @ 25 °C

DEVICE	COATING THICKNESS (KHz)	VAPOR RESPONSE (Hz/mg/m^3)
158 MHz Delay Line	252	564
668 MHz Resonator	451	1085

5. DISCUSSION

One surprising trend is evident in the data presented in Table 1. As the SAW resonator frequencies increase from 229 to 401 to 668 MHz, the RMS oscillator noise (and Allan variance) *decreases*. This is certainly not the commonly observed behavior in which noise *increases* roughly linearly with frequency. The reasons for this contrary behavior are not known but it is likely that the 229 and 401 MHz resonators are not performing well with the particular RF amplifier circuitry used in this study. The performance exhibited by the 668 MHz resonator was very good and is certainly more consistent with published reports of SAW resonator stability. The 158 MHz dual SAW delay line is optimized with the RF amplifier circuitry and exhibited noise levels that were typical of good SAW delay line oscillators. Indeed, the 158 MHz device investigated in this study was quiter than many that we have used in recent years. Since it is apparent that, of the resonators, the 668 MHz device was performing the best, comparisons between it and the 158 MHz dual delay line were further examined by coating and vapor exposure.

The noise levels demonstrated by the uncoated 158 MHz delay line and 668 MHz resonator show that the resonator is clearly superior. The resonator offered RMS noise levels of 1 Hz and an Allan variance of 1.1 E -09 in contrast to 2.8 Hz and 1.5 E -08 for the 158 MHz device. A 668 MHz SAW delay line would be expected to exhibit a n RMS noise level of about 11 Hz, more than 10 times greater than the resonator.

Coating of the SAW devices results in a marked increase in oscillator noise. The RMS noise is increased by 4 fold on the 158 MHz delay line and by 14 fold on the 668 MHz resonator. The Allan variance of the delay line increased by 3 fold while that of the resonator increased by 7 fold. It is likely that the resonator electronic circuitry could be optimized to make the noise increase correspond more closely to that exhibited by the delay line. In spite of the un-optimized electronics, the coated 668 MHz resonator still offers a smaller noise level and higher vapor sensitivity than the 158 MHz delay line.

It appears that SAW resonators do offer attractive advantages for vapor sensing applications. Further work to develop a SAW resonator electronics system that is optimized for coated performance may yield a sensor capable of vapor detection limits several times lower than those achieved by delay line devices.

APPENDIX A.

SAW RESONATOR DEVICE DATA SHEETS

APPLICATION		REVISIONS			
NEXT ASSY	USED ON	LTR	DESCRIPTION	DATE	APPROVED
	851080	A	CHGE. FREQ. .295/.250; SEE ECO # 846	8-6-84	

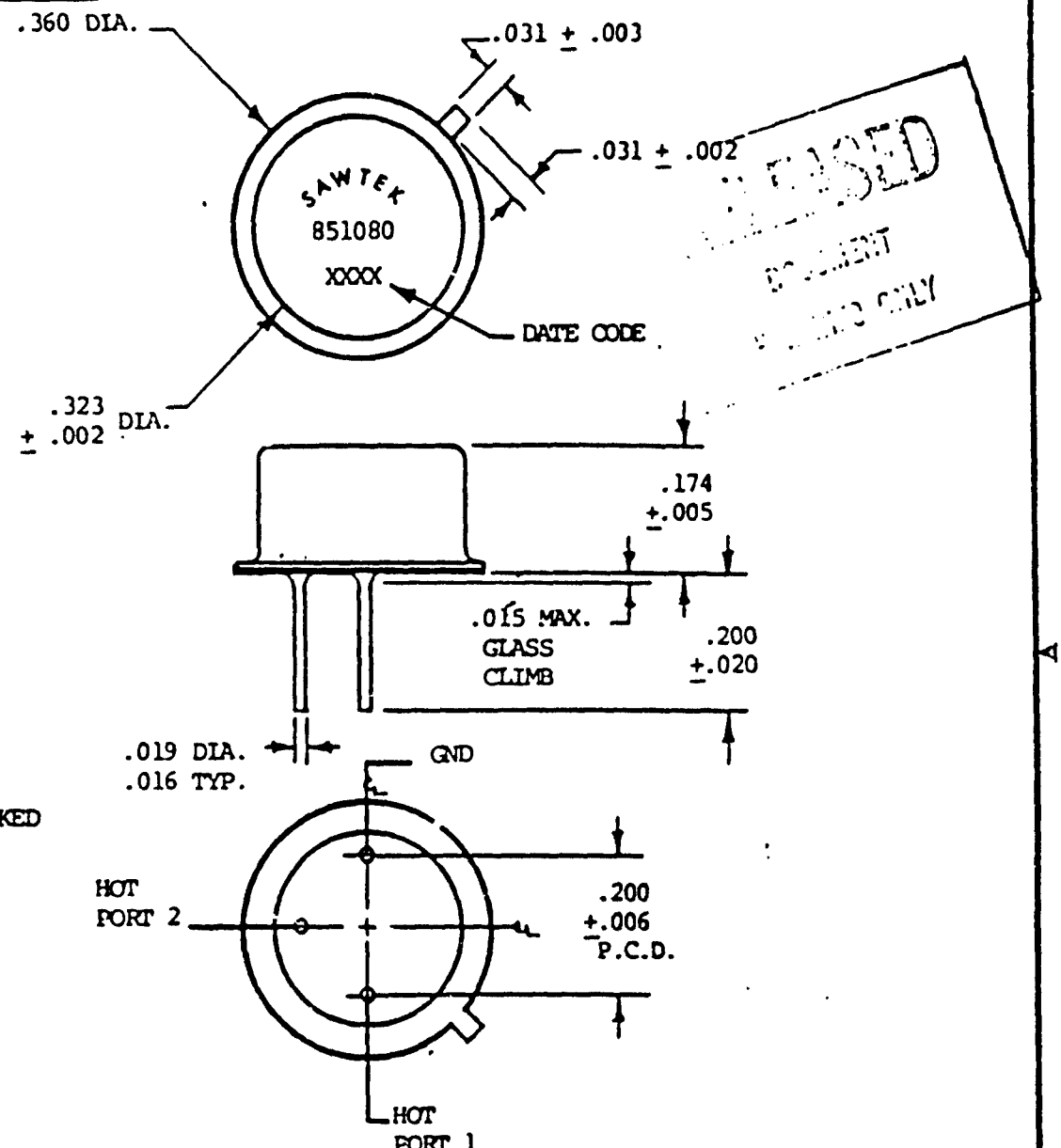

NOTES:

1. PINS ARE NOT MARKED ON FILTER; FOR REFERENCE ONLY

ESS OTHERWISE SPECIFIED ENSIONS ARE IN INCHES TOLERANCE ON ± DEC. ANGLES ±.010	DRAWING STARTED DATE	SAWTEK INC.
ERIAL:	DRAWN M. ELLIS 11-7-83	OUTLINE AND MARKING, 229.250 MHz, 2 PORT, 180° PHASE RESONATOR
	CHECKED	
	ENGR B. Horton 11-7-83	
SH:	MFG. T. Hurst 11-7-83	SIZE A / CODE IDENT NO. 58068 / DWG. NO. 851080
	Q.C. J. C. Magnes 11-7-83	SCALE 4/1 / SHEET

SAWTEK INC.

229.3 MHZ SINGLE-POLE TWO-PORT SAW RESONATOR

(P/N 851080)

TYPICAL PERFORMANCE

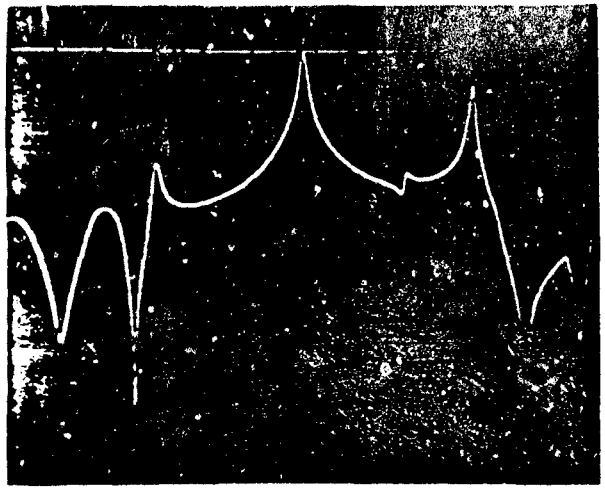

10 DB/DIV

200 KHZ/DIV

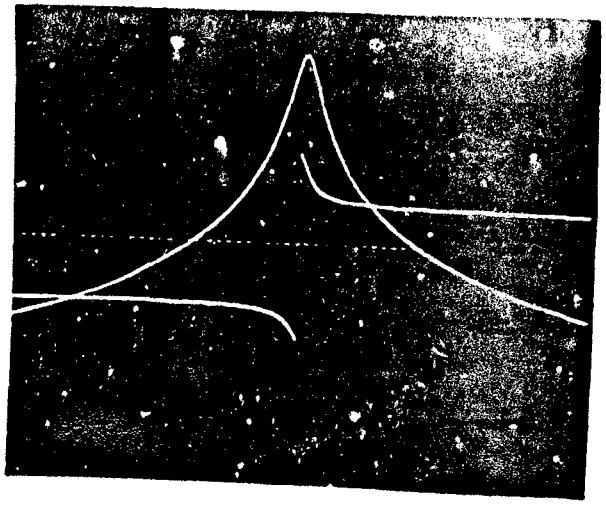

5 DB/DIV
90°/DIV

50 KHZ/DIV

ELECTRICAL

CENTER FREQUENCY	= 229.3 MHZ
INSERTION LOSS	= 7.0 DB
INSERTION PHASE	= 180° (NOMINAL)
LOADED Q (50Ω)	= 11,000
SPURIOUS REJECTION	= 7.1 DB
PACKAGE	= TO-5

1/13/84

APPLICATION		REVISIONS			
NEXT ASSY	USED ON	LTR	DESCRIPTION	DATE	APPROVED
	850999				

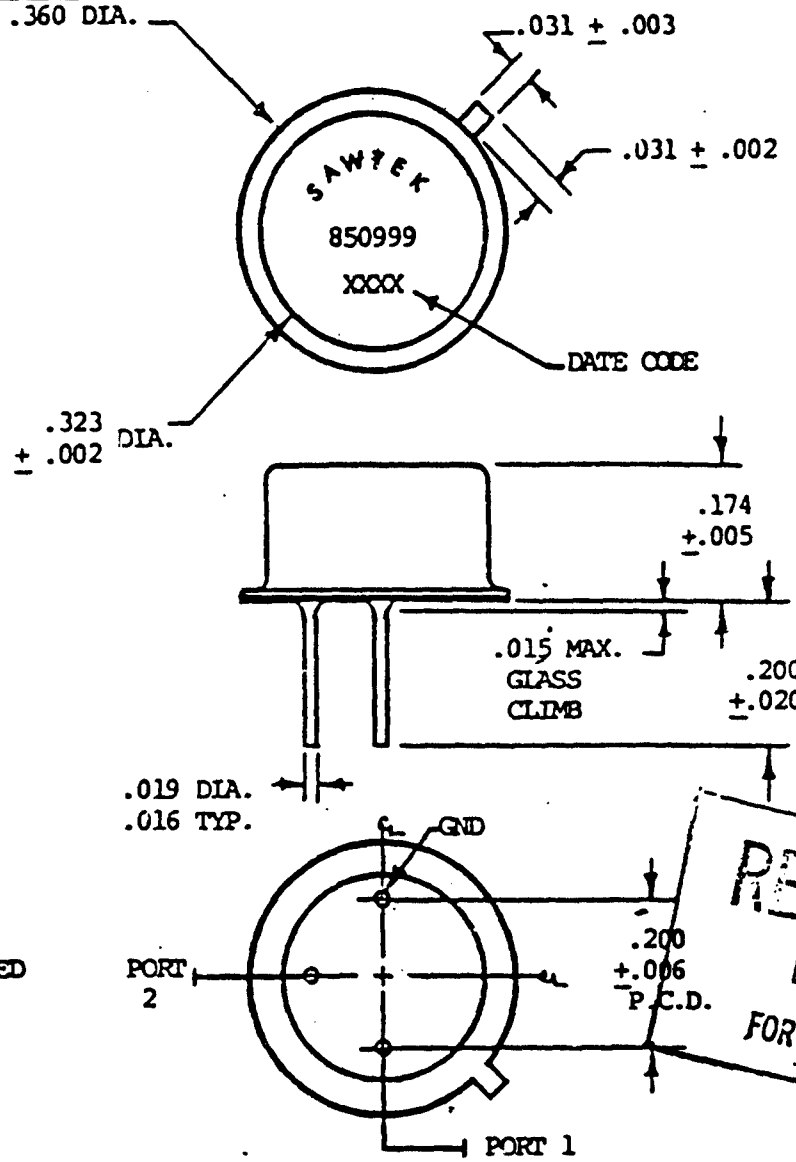

NOTES:

1. PINS ARE NOT MARKED ON FILTER; FOR REFERENCE ONLY

SS OTHERWISE SPECIFIED NSIONS ARE IN INCHES TOLERANCE ON DEC ±.010 ANGLES	DRAWING STARTED DATE	SAWTEK INC.		
RIAL:	DRAWN M.ELLIS 10-18-83	OUTLINE AND MARKING, 401 MHz RESONATOR		
	CHECKED			
	ENGR P. Kinsel 10.A.83			
H:	MFG. J Thorpe 10.19.83	SIZE A	CODE IDENT NO. 58068	DWG. NO. 850999
	Q.C. J C. Maynes 10/19/83	SCALE 4/1		SHEET

SAWTEK INC.
401 MHz SINGLE-POLE TWO-PORT SAW RESONATOR
(P/N 850999)
TYPICAL PERFORMANCE

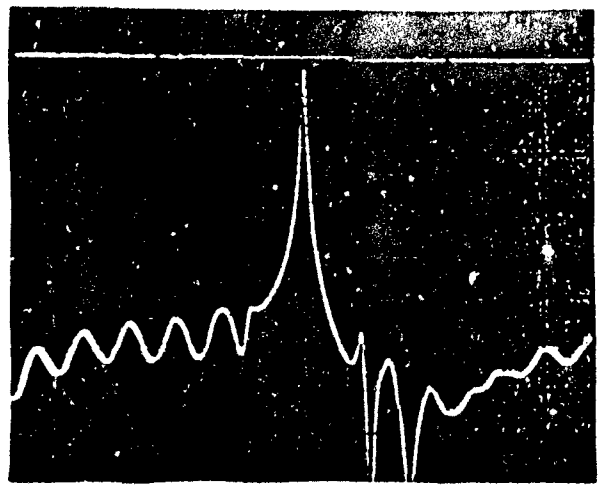

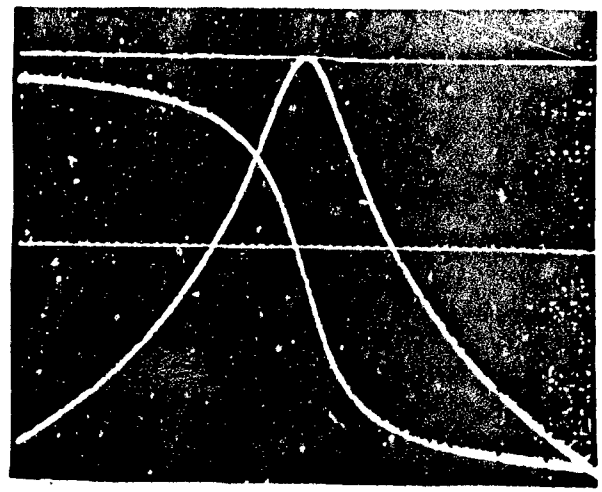

ELECTRICAL

CENTER FREQUENCY	=	401.024 MHz
INSERTION LOSS	=	-12 DB
INSERTION PHASE	=	0° (NOMINAL)
LOADED Q (50Ω)	=	7000
SPURIOUS REJECTION	=	15 DB
PACKAGE	=	TO-5

APPLICATION		REVISIONS			
NEXT ASSY	USED ON	LTR	DESCRIPTION	DATE	APPROVED
	850883	A	CHANGE DIM. + ADD BOTTOM VIEW, ECO 0572	11-7-83	gam

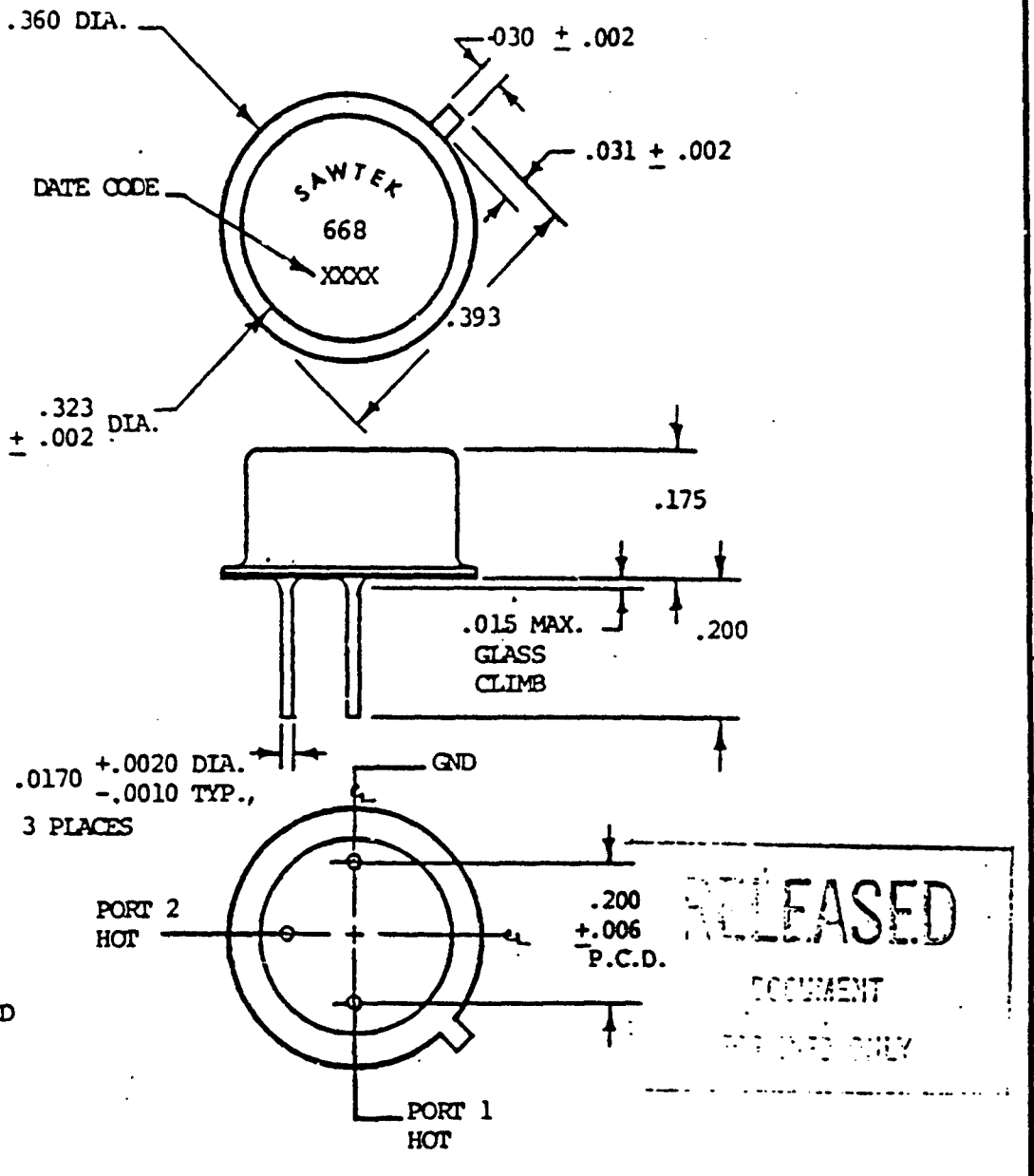

NOTES:

MARKING PER MIL-STD-202, METHOD 215, EPOXY INK

PINS ARE NOT MARKED ON FILTER; FOR REFERENCE ONLY

SS OTHERWISE SPECIFIED NSIONS ARE IN INCHES TOLERANCE ON DEC ±.005 ANGLES	DRAWING STARTED DATE	SAWTEK INC.		
RIAL:	DRAWN M. ELLIS 11-7-83	OUTLINE AND MARKING, 668 MHz RESONATOR		
	CHECKED C. Arnold 11-8-83			
SH:	ENGR			
	MFG T. Short 11-8-83	SIZE A	CODE IDENT NO. 58068	DWG. NO. 850883
	Q.C. L. R. McGuyer 11-7-83	SCALE 4/1		SHEET

CATV TWO-PORT SAW RESONATOR (P/N 850883, 850860, 850861)

TYPICAL PERFORMANCE

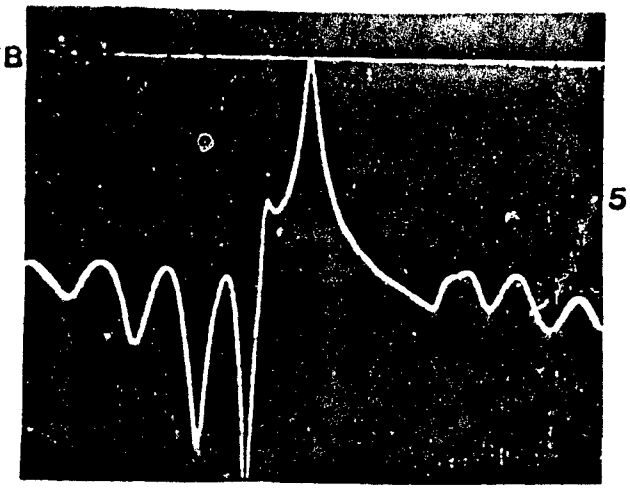

850 KHz/div.

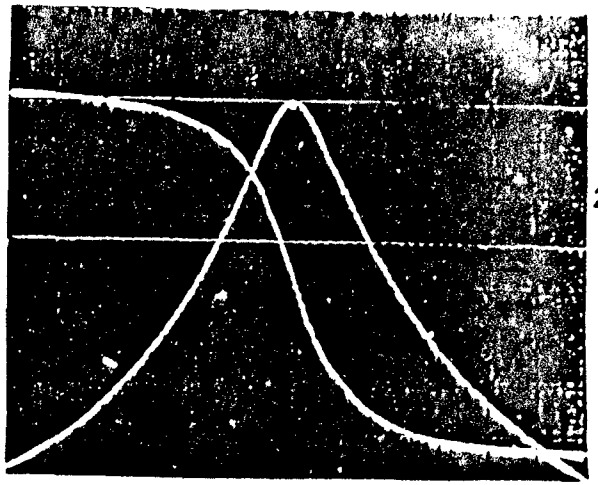

75 KHz/div.

ELECTRICAL

CENTER FREQUENCY	= 668.0, 674.0, 680.0 MHz
INSERTION LOSS	= 10.0 dB
LOADED Q (50Ω)	= 4500
SPURIOUS REJECTION	= 15 dB
DRIVE LEVEL	= ≤15 dBm
PACKAGE	= TO-5

STABILITY

OPERATING TEMP. RANGE (NOTE)	STABILITY vs. TEMP. (Ref. 25° C)
15° C to 40° C	±17 KHz
10° C to 110° C	±25 KHz
0° C to 120° C	±50 KHz
AGING	≤10 ppm/yr

NOTE: NON-OVENIZED APPLICATION ASSUMED, $T_O = 60 \pm 5°C$

POL(ETHYLENE MALEATE) VARIANTS FOR SAW MICROSENSOR COATING STUDY

A.W. Snow[1], D.S. Ballantine, T. Whitney, W.R. Barger
M. Klusty, H. Wohltjen, J. Grate, D. Chaput

ABSTRACT

A series of 11 polyester coatings, structurally related to poly(ethylene maleate), PEM, were synthesized, characterized and evaluated for relative sensitivity to dimethyl methylphosphonate, DMMP, vapor. Characterization included IR and NMR spectroscopies, DSC, MW measurements and solubility parameters. Surface acoustic wave, SAW, vapor response measurements with 112 and 52 MHz devices indicated all of the polyester coatings have ppm level DMMP vapor sensitivity and the sensitivity variation between coatings was within one order of magnitude. PEM and PPM were the most sensitive coatings. Crystalline polymers had lower sensitivity than amorphous polymers. Relative sensitivity did not correlate with DMMP-coating solubility parameter match.

INTRODUCTION

Microsensor coatings with highly sensitive, reversible and selective absorptions for particular vapors are critical to the successful development of electronic chemical microsensors. In this work, coatings which have a specific interaction with nerve agent simulants are being investigated using a surface acoustic wave (SAW) device. The SAW device detects extremely small gravimetric changes in a coating (i.e., vapor absorption and desorption) by registering a frequency shift in the resonance of the piezoelectric substrate. Approaches to the design of coating chemical structure involve selection and incorporation of an appropriate functional group to serve as a vapor receptor site and the thermodynamic considerations of solubility interactions. Previous work from this laboratory has employed a model reactive polymer-vapor system based on the Diels-Alder reaction between poly(ethylene maleate) and cyclopentadiene[2], a series of amidoxime functionalized poly(butadiene-co-acrylonitrile) coatings[3] and a comparative study of homopolymer coatings from N-vinylimidazole and 4(5)-vinylimidazole[4]. From this work, useful information has evolved regarding effect of intrinsic simulant vapor pressure, discrimination of chemisorption from physisorption, effect of coating glass transition temperature and match between polymer coating and vapor solubility parameters. When sensitivity to the simulant DMMP is

considered, PEM has been one of the most sensitive coatings tested. This sensitivity is not currently understood. The approach of the present work is synthesize and characterize a structurally systematic series of maleic anhydride related polyesters with the objective of improving on PEM-phosphonate ester simulant sensitivity and of obtaining additional insight to the coating-vapor interaction. This includes twelve different polyesters, chemical characterization (structure, molecular weight, T_g, T_m, and solubility parameter) and two types of SAW testing against DMMP. The structures of the polyesters and their characterization data are presented in Table 1.

EXPERIMENTAL

All reagents and solvents were of reagent grade quality, purchased commercially and used without further purification unless otherwise noted. Infrared and ^1H NMR spectroscopic data were obtained respectively with Perkin-Elmer 1430 and Varian EM390 spectrometers. Glass transition temperatures and melting points were determined by differential scanning calorimetry with a Dupont 1090 Thermal Analyzer and a 910 Differential Scanning Calorimeter (heating rate 10°C/min, nitrogen atmosphere). Molecular weight measurements were made by vapor pressure osometry using a Wescan Molecular Weight Apparatus Model 232A (chloroform solutions, 30°C, benzil calibration). Polymer density measurements were made by density matching with heptane-carbon tetrachloride mixtures. Solubility parameters were determined from group molar attraction constants (COO ester, 302 $(cal\ cm^3)\cdot^5\ mole^{-1}$; $-CH_2-$, 124; $-CH_3$, 209; =CH-, 103; =C-, -90; -Cl, 265; o-phenylene, 610). Inert atmosphere dilution of DMMP vapor and SAW frequency response measurements were made as described in companion papers for 112 MHz[5] and 52 MHz[6].

Polymerization apparatus consisted of a 25 ml pear-shaped, two-neck flask fitted with a miniature Dean-Stark trap, condenser, nitrogen inlet and 3/8 x 1/4 in. magnetic stirring bar. The condensed byproduct (water, methanol or ethylene glycol) was distilled into the trap at atmospheric pressure under nitrogen or at reduced pressure as the temperature was increased to 170°C followed by application of vacuum with further heating. For each polymerization ethylene glycol was purified by distillation with toluene azeotrope.

Poly(ethylene oxalate), PEOX, was prepared by reacting 5.00 g dimethyloxalate (recrystallized) with 2.89 g ethylene glycol catalyzed by 0.04 g p-toluene sulfonic acid, PTSA, at 140 to 150°C for 2.5 hr. followed by heating to 170-180°C under vacuum for 3 hrs. Attempted dissolution of the product in $CHCl_3$ resulted in dispersed of an opaque white solid. This product was filtered and purified by 7 acetonitrile extractions[7]. Yield

0.55 g MP 149-153°C (lit 157-159°C[7]). IR (neat) 2997, 2968, 2897, 1778, 1748, 1469, 1260, 1044, 889, 778 cm^{-1}. NMR (DMSO-d_6) δ 4.52 (S, CH_2). Density 1.555. MW 2000.

Poly(ethylene malonate), PEMo, was prepared by reacting 5.00 g dimethymalonate with 4.71 g ethylene glycol catalyzed by 0.04 g PTSA at 170°C for 1.25 hr. followed by heating at 170°C under vacuum for 1 hr. The temperature was advanced to 200°C and additional ethylene glycol removed over the second hour. The temperature was then increased to 210-220°C for a 3.5 hr. period. The product was purified by dissolution in 4 ml $CHCl_3$ and precipitation into 350 ml CH_3OH. Yield 3.62 g. IR (neat) 2970, 1755, 1740, 1450, 1415, 1380, 1335, 1280, 1150, 1045, 985, 870 cm^{-1}. NMR ($CDCl_3$) δ 3.41 (S, 1H), 4.36 (S, 2H). Density 1.446. MW 497.

Poly(ethylene succinate), PES, was prepared by reacting 3.14 g succinic anhydride (recrystallized) with 1.95 g ethylene glycol catalyzed by 0.05 g PTSA in 2 ml C_6H_5Cl (distilled) with 2 ml toluene (for azeotroping water byproduct) at 125 to 130°C for 5 hr. The temperature was then raised to 170°C for 8 hr. with 3 displacements of 2 ml C_6H_5Cl. The vacuum was then applied for 3 hr. The product was purified by dissolution in 30 ml $CHCl_3$, filtered and precipitated into 200 ml ether. Yield 2.96 g. MP 95-97°C. IR (KBr) 2970, 2940, 1737, 1390, 1220, 1168 cm^{-1}. NMR ($CDCl_3$) δ 2.65 (S, 1H) 4.31 (S, 1H). Density 1.357. MW 2180.

Poly(ethylene maleate), PEM; was prepared as previously described[2]. Density 1.353. MW 2470.

Dimethylacetylene dicarboxylate, DMADC, was prepared by reacting 24.5 g acetylene dicarboxylic acid, 100 ml methanol and 50 ml sulfuric acid at 20°C[8]. The reaction was worked up by adding the mixture to a saturated NaCl solution at 0°C followed by separation of the oil and ether extraction. The combined oil and ether extracts were extracted with 5% $NaHCO_3$, dried and vacuum distilled (80-83°C/8 torr). Yield 20.5 g. IR (neat) 2961, 2829, 1731, 1440, 1270, 1047, 898, 750. 680 cm^{-1}. NMR ($CDCl_3$) δ 3.86 (S, CH_3).

Dimethylmethoxyfumerate, DMMF, and dimethyl-α,α-dimethoxysuccinate, DMDMS, were prepared by an identical procedure to DMADC except the temperature was increased to 60°C. After distillation of the DMADC, the DMMF solidified in the condenser (90-95°C/9 torr). After collection of the DMFF, the DMDMS was distilled and collected as a liquid (100-110°C/1 torr). For DMMF: MP = 97°C. IR (KBr) 3100, 3002, 2948, 2857, 1733, 1670, 1645, 1445, 1345, 1260, 1220, 1105, 1030, 780. NMR ($CDCl_3$) δ 3.77 (S, 3H), 3.84 (S, 3H), 3.90 (S, 3H), 6.02 (S, 1H). MW 185 (calc 174). For DMDMS: IR (neat) 3000, 2950, 2840, 1745, 1630, 1440, 1205. NMR ($CDCl_3$) δ 3.00 (S, 2H), 3.30 (S, 3H), 3.69 (S, 3H), 3.873 (S, 3H). MW 207 (calc 206).

Polymers from dimethylacetylene dicarboxylate and ethylene glycol, PEADC 1:1 and 2:1, were prepared by reacting 5.00 g DMADC with 1.75 g ethylene glycol (for PEADC 1:1) and with 3.50 g ethylene glycol (for PEADC 2:1) catalyzed by 0.03 g PTSA at 140-150°C for 2 hr. followed heating to 170-180°C under vacuum for 2 hr. The products were purified by dissolution in 4 ml $CHCl_3$ and precipitated into ether at -20°C. For PEADC 1:1: Yield 2.50 g. IR (neat) 3550, 2965, 2900, 1740, 1630, 1445, 1260, 1045, 760. NMR ($CDCl_3$) δ 3.11 (S), 3.8 (m-broad), 4.15(s), 4.4 (m-broad). Density 1.406, MW 1510. For PEADC 1:2: Yield 3.00 g. IR (neat) 3550, 2965, 2900, 1740, 1450, 1260, 1045, 760. NMR ($CDCl_3$) δ 3.05(S), 3.7 (m-broad), 4.10 (s), 4.3 (m-broad). Density 1.365. MW 1370.

Poly(ethylene phthalate), PEPh, was prepared by reacting 3.00 g phthalic anhydride (recrystallized) with 1.26 g ethylene glycol catalyzed by 0.04g PTSA in 6 ml diglyme (distilled) with 2 ml toluene (for azeotroping water byproduct) at 160-170°C for 5.5 hr. The temperature was then raised to 190-200°C, solvents distilled and vacuum applied for 3 hr. The product was purified by dissolution in 4 ml $CHCl_3$ and precipitation into 100 ml ether. Yield 1.79 g. IR (neat) 3080, 2965, 2890, 1733, 1280, 1130, 1070, 745. NMR ($CDCl_3$) δ 4.50 (s-broad, 4H), 7.58 (m, 2H), 7.70 (m, 2H). Density 1.325. MW 1540.

Poly(ethylene methylmaleate, PEMM, was prepared by reacting 2.00 g methylmaleic anhydride (distilled) with 1.11 g ethylene glycol catalyzed by .025 ml titanium tetra-n-propoxide (distilled) in 6 ml diglyme (distilled) with 2 ml benzene (for azeotroping water byproduct) at 140-150°C for 22 hr. followed by 2 hr. at 160-170°C. The product was purified by dissolution in 10 ml $CHCl_3$ and precipitation into 300 ml ether. Yield 1.50 g. IR (neat) 2975, 1740, 1655, 1450, 1385, 1270, 1180, 1060, 970, 885, 775. NMR ($CDCl_3$) δ 2.08 (S, 3H), 4.4 (m-broad, 4H), 5.9 and 6.3 (S, vinyl H, 1H). Density 1.297. MW 1770.

Poly(ethylene dimethylmaleate), PEDMM, was prepared by reacting 2.00 g dimethylmaleic anhydride (recrystallized) with 1.00 g ethylene glycol catalyzed by 0.02 g PTSA at 130-140°C for 2 hr. One ml toluene was added to wash by reflux some of the dimethylmaleic anhydride, which had sublimed into the flask neck, back into the reaction mixture. The temperature was increased to 140-150°C for 24 hr. Vacuum was then applied for 3 hr. Approximately 1.5 g dimethylmaleic anhydride sublimed into the trap. The residue product was dissolved in 2 ml $CHCl_3$ and precipitated into 100 ml ether. Yield 0.30 g. IR 2960, 2880, 1725, 1650, 1270, 1100, 765, NMR ($CDCl_3$) δ 1.95 (S, 3H), 3.6 (M, 2H), 4.2 (m, 2H). Density 1.264. MW 1100.

Poly(ethylene dichloromaleate), PEDCM, was prepared by reacting 4.89 g dichloromaleic anhydride (recrystallized) with 1.82 g ethylene glycol catalyzed by 0.04 g PTSA in 4 ml chloro-

benzene (distilled) with 1 ml toluene (for azeotroping water byproduct) at 150-155°C for 2 days. The product was purified by dissolution in 5 ml $CHCl_3$ and precipitation into 250 ml ether. Second and third reprecipitations into CH_3OH and ether was necessary to remove residual dichloromaleic anhydride. Yield 2.60 g. IR (neat) 2970, 1751, 1600, 1250, 1040, 765, 680. NMR ($CDCl_3$) δ 4.50 (S). Density 1.568. MW 8090.

Poly(ethylene adipiated), PEA, was obtained from Aldrich Chemical Company. Density 1.183. MW 1890.

Poly(propylene maleate), PPM, was prepared by reacting 3.079 g maleic anhydride (recrystallized) with 2.412 g 1,3-propanediol catalyzed by .045 ml titanium tetra-n-propoxide (distilled) in 6 ml diglyme (distilled) with 2 ml xylene (for azeotroping water byproduct) at 145°C for 13 hr. The temperature was then raised to 160°C for 2 hr. at which time formation of a gel was observed. (Previous attempts at higher reaction temperature resulted in extensive gel formation.) The reaction mixture was cooled, disbursed in 20 ml $CHCl_3$, filtered through silk screen to remove gel, and purified by dropwise precipitation into 300 ml of ether at -20°C. Yield 2.1 g. IR (neat) 3070, 2980, 2920, 1747, 1650, 1415, 1220, 1180, 1050, 825. NMR ($CDCl_3$) δ 2.05 (quintet, 1H), 4.3 (t, 2H), 6.3 (S, 2H). Density 1.225. MW 2050.

RESULTS AND DISCUSSION

The issue of interest in this study is the peculiar features of the PEM structure that imparts a high absorption sensitivity for DMMP. The structure of PEM may be viewed as a

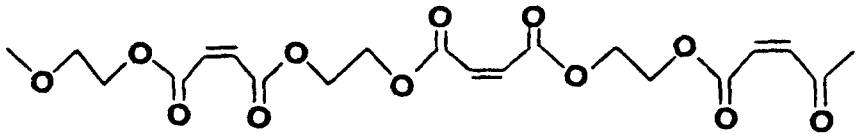

grouping of polymer-chain-connected maleate groups (which are highly polarized dieneophiles) or as subgroupings of ester groups and olefin linkages. Systematic variations on this PEM structure involve: 1) substitutions on the olefin linkage (PEADC, PEPh, PEMM, PEDMM, PEDCM), 2) saturation of the olefin linkage (PES) with a progressive shortening (PEMo, PEOX) and lengthening (PEA) of the spacing between ester carbonyl units and, 3) increasing the spacing between maleate groups (PPM). It must be realized that these changes in composition and structure have effects on the morphology (crystallinity) and thermal properties (T_g and T_m) which in turn affect the vapor absorption sensitivity. Differential scanning calorimetry and solubility interaction data are jointly considered when interpreting the DMMP-SAW response data.

The polyesters of Table 1 were synthesized by the acid catalyzed esterification of the cyclic anhydride monomer with ethylene glycol or the transisterification of the methyl esters of oxalic, malonic and acetylenedicarboxylic acids with ethylene glycol. The details are described in the experimental section. Three general observations are noteworthy. As the maleic anhydride monomer becomes more substituted (methyl, dimethyl, dichloro), the esterification reactivity drops. This is reflected by more severe reaction conditions and lower yields. In the case of PEOX, the synthesis is complicated by a cyclic dimer-linear polymer equilibrium[9]. The equilibrium

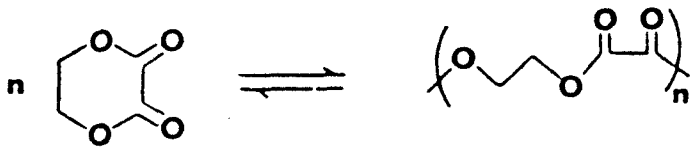

is much more rapidly approached from the cyclic dimer, which undegoes a 25°C solid-state polymerization to its equilibrium point in two weeks while the polymer has indefinite stability at room temperature[7]. This polymer purification involves a tedious series of acetonitrile extractions. The transesterification of dimethylacetylene dicarboxylate is complicated by a competing reaction involving addition of the hydroxyl group across the triple bond. As a model compound reaction, we observed methanol to add across the triple bond of dimethylacetylene dicarboxylate and isolated the 1:1 and 2:1 adducts.

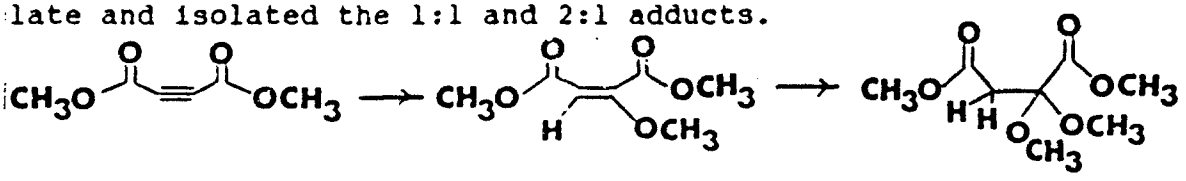

We presume that similar chemistry occurs for ethylene glycol in the polymerization system and that a polymer structure with varying degrees of the two reactions can represent the coating. Physically, this coating is a chloroform-soluble hard gum which is very desirable for the SAW coating application. Considering it structurally related to a substituted PEM with pendant hydroxyl groups, two coatings with diol:dimethyl ester stoichiometry ratios of 1:1 and 2:1 were prepared and included in the study.

Morphology information was obtained from DSC measurements. Four of the polymers had sufficient crystallinity for T_m measurement although the endotherm for PEDCM was very weak indicating a low level of crystallinity. PEM partially isomerizes to the fumarate ester structure during polymerization (2), which, by extrapolation, would contribute to the amorphous character of the maleic anhydride derived polymers. The T_g values are all below room temperature, and generally follow the dependence on intermolecular forces and chain flexibility.

As a measure for solubility interaction, the Hildebrand solubility parameter is a simple and useful index although limited to the regular solution model. Values for the polymers of this study are presented in Table 1. They are measures of solvent-solvent interactions and follow the polarity of the structures. An attempt was made to measure the hydrogen bond basicity of these coatings by ^{19}F NMR[10]. However, the polymers are not soluble in carbon tetrachloride, and use of chloroform with a correction factor was not workable since the shift caused by chloroform masked any effect caused by the polymer.

SAW vapor sensitivity measurements for DMMP were made with 112[5] and 52[6] MHz devices. The 112 MHz measurement included 3 points in a concentration range of 6 to 30 ppm, and the sensitivity is reported as the slope of the frequency change vs. vapor concentration plot normalized to the mass of the coating. The 52 MHz measurement involved a single measurement with DMMP vapor generated from a 0°C bubbler (470 ppm), and this measurement is reported as the mass of absorbed vapor normalized to the mass of the coating. For the purpose of comparison, these measurements are presented relative to the value for the PEM coating in Table 1.

The agreement in relative responses in some cases is good (PEMM, PEDCM) while in other cases is poor (PPM, PEDCA 1:1). While it is possible some crossover in relative DMMP sensitivity may occur between the two concentration ranges, this has not yet been experimentally studied. It is possible to extract some correlations and trends from the data. PEM and PPM are the most sensitive coatings although all of the coatings are within one order of magnitude in sensitivity. The coatings in Table 1 are listed in order of decreasing solubility parameter with the exceptions of PPM, which is not derived from ethylene glycol, and PEDCA's, which do not have well-defined structures. A solubility parameter match between DMMP (δ = 10.6 $(cal/cm^3)^{.5}$ $mole^{-1}$) and the polymer coatings does not appear to correlate with sensitivity. PEDMM, which has the largest solubility parameter difference, is significantly more sensitive than PEMo, which has the closest solubility parameter match. With respect to morphology, those polymers which are crystalline (PEOX, PES, PEA and PEDCM) have lower sensitivity as might be expected since crystalline regions should be less vapor penetrable. In general, it appears that polyesters have a high sensitivity toward DMMP but that more accuracy in the SAW measurement or perhaps determination of the total adsorption isotherm is necessary to discriminate the effects of small structural changes within this class of polymers. It is noteworthy that all are soluble in chloroform except PEOX.

TABLE 1

Polyester Characterization and DMMP Vapor Response Data

Polymer	Structure	Xn	Tg	Tm	δ	SAW Measurement 112 MHz	52 MHz
PEOX	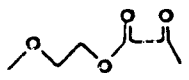	17	68	150	11.4	.03	.54
PEMo	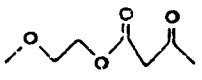	8	-27		10.8	.23	.32
PES	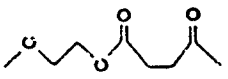	30	19	97	10.4	.61	.28
PEM	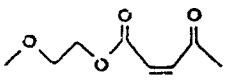	32	-10		10.1	1.00	1.00
PEPh	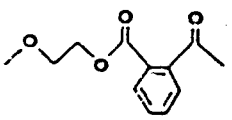	16	3		10.1	.35	.75
PEA	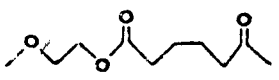	22	-50	47	9.3	.56	.13
PEMM	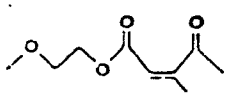	23	-30		8.9	.83	.99
PEDCM	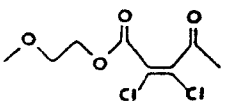	77	12	60	8.9	.58	.68
PEDMM	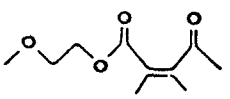	13	-39		8.1	.56	.93
PPM	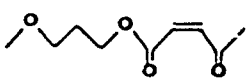	26	-16		9.3	2.00	.81
PEDCA 1:1	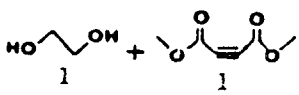	22	7			.28	.93
PEDCA 2:1	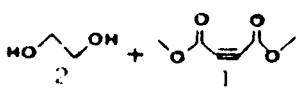	20	-8			.49	1.07

CONCLUSION

Eleven polyesters, which are structurally related to PEM, were synthesized, characterized, and evaluated for relative sensitivity to DMMP vapor. Characterization included IR and NMR spectroscopies, differential scanning calorimetry, molecular weight measurement and solubility parameter. SAW vapor response measurements were conducted at low concentration (6-30 ppm) with 112 MHz devices and at high concentration (470 ppm) with 52 MHz devices. All coatings displayed sensitivity at the low DMMP concentration, and the response variation between coatings was within one order of magnitude. PEM and PPM were the most sensitive coatings. Crystalline polymers had lower sensitivity than amorphous polymers. A correlation of solubility parameter match between DMMP and the coating for ranking of sensitivity was not effective.

REFERENCES

1. Chemistry Division, Naval Research Laboratory, Washington, DC 20375-5000.

2. A.W. Snow, H. Wohltjen, and N.L. Jarvis, 1982 Scientific Conference on Chemical Defense Research, AR-CSL-SP-83030, Aberdeen Proving Grounds, MD, 1983, pp. 251-257.

3. N.L. Jarvis, J. Lint, A.W. Snow and H. Wohltjen, 1983 Scientific Conference on Chemical Defense Research, CRDC-SP-84014, Aberdeen Proving Ground, MD, 1984, pp. 45-54.

4. A.W. Snow, H. Wohltjen, J. Lint and N.L. Jarvis, 1984 Scientific Conference on Chemical Defense Research, CRDC-SP-85006, Aberdeen Proving Grounds, MD, 1985, pp. 301-307.

5. D.S. Ballantine and A.W. Snow, companion paper, this proceedings.

6. A.W. Snow, W.R. Barger, M. Klusty, H. Wohltjen, and N.L. Jarvis, Langmuir 2, 513 (1986).

7. W.H. Carothers, J.A. Arvin and G.L. Dorough, J. Am. Chem. Soc. 52, 3292 (1930).

8. C. Moureu and J.C. Bongrand, Ann. Chim. 14, 5 (1920).

9. W.H. Carothers, G.L. Dorough and F.J. Van Natta, J. Am. Chem. Soc. 54, 761 (1932).

10. (a) M.J. Kamlet and R.W. Taft, J. Am. Chem. Soc. 98, 377 (1976); (b) D. Gurka and R.W. Taft, J. Am. Chem. Soc. 91, 4794 (1969).

P. PERFORMANCE LIMITS OF CHEMICAL MICROSENSOR TECHNOLOGY

James Murday*, Steve Caras* and Hank Wohltjen**

ABSTRACT

Four chemical microsensor technologies are reviewed with special attention to their physical performance limits for CBWD detection. The sensors include Surface Acoustic Wave (SAW) devices, Chemiresistors, CHEMFETs, and Optical Waveguides.

INTRODUCTION

A number of microfabricated, solid state devices are being investigated for their potential as chemical sensing devices.[1-4] Several of these devices are particularly attractive for the difficult problem of detecting/monitoring chemical warfare agents. Over the last five years, we have investigated a variety of sensors for their potential in this application. These sensors include Surface Acoustic Wave (SAW) devices, Chemiresistors, Optical Waveguides, and CHEMFETs. Work on device design has been important to improvements in sensitivity and selectivity; however the major controlling feature lies in the coatings which are used to transduce the presence of a chemical moiety into a property detected by the device. The operative principle behind the four sensor concepts are summarized in Table 1. The enormous variety of coating materials and operating configurations that are possible with these devices makes it very difficult to predict their ultimate capabilities. Nevertheless, a more detailed knowledge of the physical principles by which these coated devices function is emerging. By carefully analyzing the coated device physics it is possible to predict some of the major advantages and disadvantages of the various approaches to chemical microsensor technology.

TABLE 1
CHEMICAL MICROSENSOR CONCEPT

Probe	Sensitive Property	Selective Property
Surface Acoustic Wave	Mass, Modulu.	Solubility
Optical Waveguide	Refractive Index	Solubility + $n^*(\lambda)$
Microelectrode Array	Electrical Conductivity	Solubility + Oxid/Red
CHEMFET	Interfacial Potential	Solubility + Dielectric

The availability of microsensors grouped in arrays will help solve the problems of obtaining adequate chemical selectivity in a complex environment.[5-8] An individual sensor will not be uniquely selected to an individual agent but the array response pattern

* Naval Research Laboratory, Code 6170, Washington, DC 20375-5000
** Microsensor Systems, Inc., P.O. Box 90, Fairfax, VA 22030

will be characteristic of the vapor or combination of vapors to which the array is exposed. Performing quantitative analysis of mixtures is not possible unless the number of components in the mixture is known and the array contains more sensors than unknown vapors. This situation rarely exists in practice. However, for detection and alarm applications, quantitative analysis is not necessary. Rather the sensor instrument pattern recognition software can be trained to respond to patterns that correspond to hazardous conditions. A very significant advantage of an array sensor is that it can easily identify a number of hazardous vapor conditions that is far in excess of the number of sensors in the array. In addition, as new hazards appear, it becomes feasible to make the detector responsive to the hazard by changing the pattern recognition software rather than changing the sensors themselves.

SURFACE ACOUSIC WAVE (SAW) DEVICES

Acoustic wave devices are mechanically resonant piezoelectric structures whose resonance frequency is perturbed by the mass or viscoelastic properties of a thin layer deposited onto the device surface.[9] The most common configuration for a Surface Acoustic Wave (Rayleigh wave) vapor sensor is that of a delay line oscillator in which the device resonates at a frequency determined by the wave velocity and the spacing of electrodes used to excite and detect the wave. If the mass of a chemically selective coating on top of the device is altered, then changes occur in the wave velocity that can be measured as a shift in the oscillator frequency.

The SAW vapor sensor is quite similar to the bulk wave piezoelectric quartz crystal sensor.[10-12] However, SAW devices possess several distinct advantages including substantially higher sensitivity (owing to the much greater device operating frequencies that are possible with SAW), smaller size, greater ease of coating, uniform surface mass sensitivity, and improved ruggedness. Demonstrated SAW vapor sensors currently have active surface areas of a few square millimeters and resonance frequencies in the range of 300 MHz. Modern microlithographic techniques permit the fabrication of SAW devices having a total surface area significantly less than a square millimeter and resonant frequencies in the Gigahertz range. A 300 MHz SAW device having an active area of 8 mm^2 is able to provide resonant frequency shift of about 1500 Hz when perturbed by a surface mass change of 1 nanogram. This level of sensitivity is predicted theoretically, and has been confirmed experimentally by using Langmuir-Blodgett films as calibrated mass loadings on the device.[13] The same device exhibits a typical "noise" of less than 30 Hz RMS over a 1 second measurement interval (i.e. 1 part in 10^7). Thus, the 1 nanogram mass change will provide a signal to noise ratio of almost 50 to 1.

The development of coatings to selectively adsorb chemical agents is proceeding steadily.[8,14-17] Solubility has been found to be a very effective guiding principle in the design of sensitive and selective coatings.[18-19] In this approach, the coating on the SAW device is used as a "solvent" for the vapor to be detected. SAW selectivities in excess of 10000:1 for CW agent/simulants: interferents have been demonstrated by using vapor/coating "solutions".[20] These same devices have also exhibited sensitivites adequate to detect organophosphorus compounds at concentrations below 0.1 mg/m^3. The selectivity of the device is discussed in another paper by Rose et al. in this proceedings.

Based on our present understanding of SAW device operating mechanisms and the rate of progress being made in the development of selective coatings based on solution concepts, it is possible to broadly define the performance available from existing SAW vapor sensors and to make some very conservative predictions about where the state-of-the-art might lie in the year 2000. These conclusions are summarized in Table 2. There are many new applications of acoustic microsensors that are emerging. Recent

	SURFACE ACOUSTIC WAVE		CHEMIRESISTOR		WAVEGUIDE	
	PRESENT	YEAR 2000	PRESENT	YEAR 2000	PRESENT	YEAR 2000
A. UNCOATED DEVICE CHARACTERISTICS (including support electronics)						
Surface Area	10^{-1} cm^2	10^{-4} cm^2	10^{-1} cm^2	10^{-4} cm^2	3 cm^2	10^{-3} cm^2
System Volume	10 cm^3	10^{-1} cm^3	10 cm^3	10^{-2} cm^3	10 cm^3	10^{-1} cm^3
Power Consumption	1 W	10^{-1} W	10^{-2} W	10^{-5} W		
B. COATED SENSOR CHARACTERISTICS						
Detection Limit						
mg/m^3 DMMP in FPOL	0.05	0.001	-	-	-	-
in PtPc	-	-	5	10^{-2}	-	-
in PEM	-	-	-	-	10^{+2}	-
Response Time (sec)	1 - 100	0.01-100	10-1000	1-100	1-100	-
Selectivity						
DMMP vs. H_2O in FPOL	10,000:1	-	-	-	-	-
in PtPc	-	-	1000:1	-	-	-
in PEM	-	-	-	-	100:1	-

developments by Bastiaans, et. al.[21] and Thompson et al.[22] have extended the use of micro-acoustic wave technology to monitoring immunological reactions in solution with very high sensitivity.[21] This approach is being actively investigated for its potential in detecting toxins and other biological agents.

CHEMIRESISTORS

As the name suggests, chemiresistors are chemically sensitive devices whose resistance changes when exposed to a chemical species of interest. They are distinguished from other classical electrochemical devices by virtue of the fact that change in electrical conductivity arises from change in the number of electron rather than ion charge carriers. Recent chemiresistor devices utilize a microfabricated interdigitated electrode array coated with a thin layer of organic semiconductor film[23,24], which is chosen to facilitate diffusion of species into the film (compared with denser inorganic semiconductors such as Si, Ge, GaAs). The noise is determined by the background currents in the system. These currents arise from the intrinsic electronic conductivity of the semiconductor coating; parasitic conduction paths in the "insulating" substrate upon which the electrode is fabricated; and leakage currents (i.e. input bias current) of the supporting amplifier electronics.

Various phthalocyanine coated devices have been demonstrated that can detect a number of electron donor and electron acceptor gases at concentrations below 1 ppm[24,25] With a specially prepared Pt phthalocyanine derivative film, the Naval Research Laboratory has demonstrated the selective detection of DMMP at concentrations below 5 mg/m^3 with response times of about 20 seconds. This same coating showed selectivity between DMMP and water vapor of 1000 to 1. Film deposition was accomplished using the Langmuir-Blodgett method. The phthalocyanines have also been shown to be quite sensitive to chemical warfare agents in other work[23]. There are a large number of other classes of organic semiconductors that may also prove to be useful in vapor detection applications.

The mechanisms by which the conductivity of the organic semiconductors is altered are complex. Generally speaking, the apparent conductivity of the device will be altered if there is a change in the number or mobility of electronic charge carriers. Vapors donating or accepting electrons from the semiconductor will produce conductivity changes that depend on the efficiency of the charge transfer process. A typical chemiresistor using a phthalocyanine exhibits a background current in the 10^{-13} to 10^{-10} amp range. Thus, the number of charge carriers necessary to generate a signal above the background current fluctuation level will be in the range of 10^6 to 10^9. If the charge transfer efficiency between the vapor and semiconductor is high and the intrinsic carrier concentration low, then the chemiresistor is theoretically able to respond to incredibly small concentrations of vapor. One million molecules of a vapor like DMMP has a mass of about 2×10^{-16} grams, 3 to 4 orders of magnitude better than anything believed to be possible using a resonant piezoelectric device such as the SAW sensor. Based on our understanding (albeit limited) of the behavior of microelectrodes and organic semiconductor films it is possible to make some estimates of the performance capabilities of chemiresistor devices. These estimates are summarized in Table 2.

OPTICAL WAVEGUIDE

The use of optical schemes to detect gas phase chemical species has a number of advantages: the impact of electromagnetic interference can be reduced, physical contact with the environment may be avoided (emission spectroscopy), wavelength selectivity may introduce an additional degree of freedom and fiber optics can facilitate remote detection where the electronics package is located in a centralized, secure site. The optical approach has a number of generic disadvantages including susceptibility to stray light interference, possible photodegradation of organic and polymeric materials and somewhat limited dynamic range. Seitz[26] has published a general review of fiber optic approaches to chemical sensors; several other reviews have been published which focus on optical detectors for immunoassays in liquids.[27-29]

There are five conceptual approaches to optical chemical sensors discussed in the literature: absorption, scattering, refractometry, emission, interferometry. Of these five, only two (refractometry and interferometry) have been used to probe low concentrations of gas phase species. Absorption spectroscopy, based on variations in the imaginary part of the dielectric constant, is a powerful approach to the identification of molecules; it is a bad approach to trace analysis as one must look for small changes in a large signal. Emission, the inverse process to absorption, is recognized as a technique for trace analysis; fluorescence emission has been exploited by a number of researchers for detection in fluids.[30-31] This approach has the desired characteristic of increasing signal for increasing concentration, but only if the species fluoresces or reacts with a fluorescent coating. This restriction limits the breadth of this approach.

Photorefractometry dates back to the 1950's when it was used to sensitively measure the complex index of refraction n^* of liquids.[31] Photorefractometry makes use of the critical angle for light reflection when proceeding from a higher index of refraction media into a lower index media. Light incident on the interface with angles below the critical angle (i.e. closer to normal incidence) tends to be transmitted; above the critical angle it is reflected. In a waveguide this corresponds to light leaving the guide (radiative modes) and remaining in the guide, respectively. Designed carefully, a photorefractometer has been shown to measure changes in n^* of 1 part in 10^6. Tiefenthaler et al.[32-33] have designed a single mode waveguide approach to photorefractometry which has shown sensitive detection of gas phase chemical species (H_2O, ethanol, and acetone). With demonstrated sensitivity to ~0.1 ng H_2O this technique is promising, but it needs more research to define its full potential for gas phase sensing; high sensitivity may be at the expense of dynamic range. The approach is amenable to integrated optics fabrication; however, constraints on the grating coupler will keep the device size to millimeter dimensions, at least for visible light. Giuliani et al.[34-35] have demonstrated the detection of gas phase chemical species using a cylindrical multimode waveguide; their work reports signal versus concentration data for several species, including G-agent simulants. Detection of species at the parts per million level in the gas phase has been shown, as has some selectivity based on polymer coatings on the waveguide surface. That work has not been modeled sufficiently well to project ultimate sensitivities; however, the results are promising in that simple, inexpensive components made up the system.

When a clad optical fiber is coated with a material which changes size under the influence of an external field (temperature, electric, magnetic, etc), the small change in optical path causes a phase shift in the light propagating in that waveguide which can be detected by watching the interference fringe pattern set up by mixing the light from an uncoated waveguide.[36] Butler[37] has shown that this concept will work for gas phase chemical detection; he demonstrated sensitivity of 1 to 10^4 ppm H_2 via its reaction with

a Pt coating. He estimates that more careful design will result in at least an order of magnitude better sensitivity for H_2 and that polymer coatings may be able to extend the range of detectable species. This approach is inherently very sensitive, but its utility will be governed by as yet unknown coatings.

The work on optical waveguide detectors is still too rudimentary to project device limits; some information is presented in Table 2.

CHEMFET

The CHEMFET measures the gate electrode potential at a insulator-coating interface through the silicon-insulator field effect, i.e. changes in the concentration of holes or electrons just below the silicon-insulator interface. The Suspended Gate CHEMFET is discussed here as an example; this device has a gap between the gate electrode and the silicon insulator interface[9,41]. A selective coating can be deposited in this gap. A potential applied to the gate electrode is dropped across both the coating and the insulator, the relative amounts determined by their impedance characteristics. The sensitivity of the CHEMFET depends on the transconductance g_m of the device, and the altered potential resulting from a change in the coating impedance. Suspended Gate CHEMFETs have been used for chemical vapor detection.[39-40] Josowitz[40] electropolymerized polypyrrole on a Suspended Gate CHEMFET; changes in work function were measured in response to various gas phase dipolar solvents. In principle, a chemiresistive coating could be applied to a Suspended Gate CHEMFET (or to an interdigitized array in series with the gate of a MOSFET).

CONCLUSIONS

The SAW sensor concept is the best developed at this time. However, the chemiresistor and optical waveguide approaches have the theoretical capability for equivalent or better performance. Whether they ultimately achieve that performance depends mostly on coating development and to a lessor extent on device improvements. The CHEMFET approach is still further behind and struggling with microfabrication and passivation problems. The impetus for further development of the three trailing technologies lies in two observations. First, each has its own set of advantages/disadvantages which may influence its choice for a particular situation. For instance, the optical waveguide is insensitive to EMI/EMP and might be preferred in systems with large amounts of interference. Second, when presented with an unknown compound, an analytical chemist will choose a suite of analytical tools to measure several physical properties. In this way, a more definitive identification can be made. The same will inevitably be true for chemical microsensors.

ACKNOWLEDGEMENTS

The authors are grateful to ONR, ONT, CRDEC, and AMD for supporting the research underlying this work.

REFERENCES

1. J. Zemel, and P. Bergveld (eds.), Chemically Sensitive Electronic Devices - Principles and Applications, Elsevier Sequoia S.A., Lausanne, 1981.

2. T. Seiyama, K. Fueki, J. Shiokawa, and S. Suzuki (eds.), Analytical Symposia Series, Vol. 17, Chemical Sensors, Elsevier Science Publishers, Amsterdam, 1983.

3. H. Wohltjen, "Chemical Microsensors and Microinstrumentation", Anal. Chem. 56(1), 87A-103A (1984).

4. J. Janata and R.J. Huber (eds.), Sold State Chemical Sensors, Academic Press, New York, 1985.

5. A. Ikegami, M. Kaneyasu, "Olfactory Detection Using Integrated Sensor", Digest of Technical Papers for the 1985 International Conference on Solid State Sensors and Actuators, Philadelphia, IEEE Cat. No. 85CH2127-9, pp. 136-139.

6. W.P. Carey, K.R. Beebe, B.R. Kowalski, D.L. Illman, T. Hirschfeld, "Selection of Adsorbates for Chemical Sensor Arrays by Pattern Recognition", Analytical Chemistry 58, 149-152 (1986).

7. J.R. Stetter, P.C. Jurs, and S.L. Rose, "Detection of Hazardous Gases and Vapors: Pattern Recognition Analysis of Data from an Electrochemical Sensor Array", Analytical Chemistry 58, 860-866 (1986).

8. D. Ballantine, J.W. Grate, H. Wohltjen and A. Snow, "Response Characteristics of Twelve Coatings on a Dual 112 MHz SAW Device to Selected Simulants and Interferents", Proceedings of the U.S. Army Scientific Conference on Chemical Defense Research, Edgewood, MD, November 1985, pp. 107-112.

9. H. Wohltjen, "Mechanism of Operation and Design Considerations for Surface Acoustic Wave Device Vapor Sensors", Sensors and Actuators 5, 307-325 (1984).

10. J.F. Alder and J.J. McCallum, "Piezoelectric Crystals for Mass and Chemical Measurements", The Analyst 108, 1169-1189 (1983).

11. J. Hlavay and G.G. Guilbault, "Applications of the Piezoelectric Crystal Detector in Analytical Chemistry", Anal. Chem. 49(13), 1890-1898 (1977).

12. W.H. King, "Piezoelectric Sorption Detector", Anal. Chem. 36, 1735-1739 (1964).

13. H. Wohltjen, A.W. Snow, W.R. Barger and D.S. Ballantine, "Trace Chemical Vapor Detection Using SAW Delay Line Oscillators", accepted by IEEE Transactions on Ultrasonics, Ferroelectrics, and Frequency Control, March 1987.

14. H. Wohltjen, A. Snow, J. Lint, and N.L. Jarvis, "An Investigation of Some Coating Materials for SAW Vapor Sensors", Proceedings of the U.S. Army Scientific Conference on Chemical Defense Research, Edgewood, MD, November 1983.

15. D. Ballantine, S.A. Rose, J.W. Grate, and H. Wohltjen, "Correlation of SAW Coating Responses with Solubility Properties and Chemical Structure Using Pattern Recognition", Naval Research Laboratory Memorandum Report 5813, August 1986.

16. D.U. Olness, T.B. Hirschfeld, J.E. Lane, R.J. Steinhaus, "Portable Field Sorption Detector for the Detection and Recogniton of Chemical Agents", U.S. Army CRDEC Technical Report CRDEC-TR-86073, August 1986.

17. W.P. Carey, K.R. Beebe, B.R. Kowalski, D.L. Ulman, T. Hirschfeld, "Selection of Adsorbates for Chemical Sensor Arrays by Pattern Recognition", Analytical Chemistry 58, 149-152 (1986).

18. M.J. Kamlet, R.M. Doherty, M.W. Abraham, and R.W. Taft, "Applications of Linear Solvation Energy Relationships to Chemical Defense Problems", Proceedings of the U.S. Army Scientific Conference on Chemical Defense Research, Edgewood, MD, November 1984, pp 601-606.

19. J. Grate, et. al., to be published.

20. D. Ballantine, A. Snow, M. Klusty, G. Chingas, and H. Wohltjen, "USAF/NRL Surface Acoustic Wave Vapor Sensor Program", Naval Research Laboratory Memorandum Report 5865, October 1986.

21. J.E. Roederer and G.J. Bastiaans, "Microgravimetric Immunoassay with Piezoelectric Crystals", Analytical Chemistry 55, 2333-2336 (1983).

22. M. Thompson, C.L. Arthur and D.K. Dhaliwal, Anal. chem. 58, 1206 (1986); M. Thompson, C.L. Arthur, D.K. Dhaliwal and G.S. Calabresse, IEEE Trans. Ultrasonics Ferroelect. Freq. Contr., in press.

23. A.W. Barendsz, C.A. van Beest, P.P.M.M. Wittgen, "Detection of CW Agents with Organic Semiconductors", Proceedings of the U.S. Army Scientific Conference on Chemical Defense Research. Edgewood, MD, November 1981, pp 35-41.

24. H. Wohltjen, W.R. Barger, A.W. Snow, and N.L. Jarvis, "A Vapor Sensitive Chemiresistor Fabricated with Planar Microelectrodes and a Langmuir-Blodgett Organic Semiconductor Film", IEEE Trans. Elect. Dev., ED-32(7), 1170-1174 (1985).

25. A.W. Snow, W.R. Barger, M. Klusty, H. Wohltjen and N.L. Jarvis, "Simultaneous Electrical Conductivity and Piezoelectric Mass Measurements on Iodine Doped Phthalocyanines", Langmuir 2, 513-519 (1986).

26. W.R. Seitz, "Chemical Sensors Based on Fiber Optics", Anal. Chem. 56(1), 16A-34A (1984).

27. J.F. Place, R.M. Sutherland and D. Dahne, Biosensors 1, 321 (1985).

28. J.R. North, Trends in Biotechnology 3, 180 (1985).

29. J.D. Andrade, R.A. Vanwagenen, D.E. Gregonis, N. Newby and J.N. Lin, IEEE Trans. on Electron Devices ED-32, 1175 (1985).

30. K. Newby, J.D. Andrade, R.E. Benner and W.M. Reichert, "Remote Sensing of Protein Adsorption Using a Single Optical Fiber", J. Coll. and Interface Sci. 111, 280-282 (1986).

31. N.S. Kapany and D.A. Pontarelli, Applied Optics 2(4), 425 (1963).

2. M. Seifert, K. Tiefenthaler, K. Henberger, W. Lukosz and K. Mosbach, Anal. Lett. 19 205 (1986).

3. K. Tiefenthaler and W. Lukosz, Thin Solid Films 126, 205 (1985).

34. J.F. Giuliani, N.L. Jarvis and A.W. Snow in Fundamentals and Applications of Chemical Sensors, ACS Symposium Series 309, D. Schuetzle and R. Hammerle, Eds. (American Chemical Society, Washington, DC, 1986) p 320.

35. J.F. Giuliani, H. Wohltjen and N.L. Jarvis, "General Theory and Design Considerations for Optical Waveguide Chemical Vapor Sensors", Naval Research Laboratory Memorandum Report 5457, Dec. 7, 1984.

36. T.G. Giallorenzi, J.A. Bucaro, A. Dandridge, G.H. Sigel, J.H. Cole, S.C. Rushleigh and R. Priest, J. Quantum Electron 18, 626 (1982).

37. M.A. Butler, "Optical Fiber Hydrogen Sensor", Appl. Phys. Lett., 45 (10), 1007-1009 (1984).

38. J. Janata and R.J. Huber, in Ion Selective Electrodes in Analytical Chemistry, Plenum Press, New York, NY, 1980, Vol. 2, Chapter 3.

39. J. Cassidy, S. Pons and J. Janata, "Hydrogen Response of Palladium Coated Suspended Gate Field Effect Transistor", Anal. Chem. 58, 1757-1761 (1986).

40. M. Josowicz, and J. Janata, Submitted for publication.

C. CHEMIRESISTOR VAPOR SENSOR COATINGS: STRUCTURE AND PROPERTIES

W. R. Barger, A. W. Snow, J. L. Dote, R. Price and
M. A. Klusty[1] and H. Wohltjen[2]

ABSTRACT

Practical vapor detectors using chemiresistor microsensors that change their electrical resistance when exposed to vapors require an inventory of suitable sensor coatings. Structure and properties of metal-free tetrakis (cumylphenoxy) phthalocyanine were studied as representative of the class of phthalocyanine derivatives successfully used in experimental sensors. Electron microscopy revealed that these coatings consist of layers built up from a two-dimensional microemulsion. The thermal stability of coatings could be tailored by the choice of transfer promoter used in the Langmuir-Blodgett deposition technique. Kinetic studies showed that absorption and desorption of vapors by the coatings followed a second order rate law.

If individual vapor sensors are made very small, clusters of these sensors can be combined in a vapor detector that gives a response pattern characteristic of the detected vapor. Chemiresistor vapor sensors have the potential for use in this manner. Chemiresistors can be made by positing thin coatings of organic compounds over planar interdigital electrodes microfabricated on small quartz substrates. A coating is required which changes its electrical resistance on exposure to the vapor to be sensed. The fact that phthalocyanine compounds exhibit changes in conductivity on exposure to vapors has been known for many years[3], and a gas sensor using vapor-deposited phthalocyanines was described by Japanese workers in 1978[4]. Chemiresistors made by sublimation of different metal phthalocyanines onto interdigital electrodes were examined, but it was found that at room temperature, reversibility was poor[5]. Very thin coatings would be expected to give rapid responses to vapors because of reduced diffusion times. One

method of preparing reproducible coatings of precisely controlled thicknesses is the Langmuir-Blodgett (LB) deposition technique. In the classical LB technique, single-molecule-thick layers of oriented polar organic compounds are formed on a water surface and then transferred, one monomolecular layer at a time, to a solid substrate by repeated passing of the substrate through the air/water interface. Organic derivatives of phthalocyanine suitable for deposition by the LB technique were synthesized in our laboratory[6]. Chemiresistors were prepared from the phthalocyanine derivatives and were found to be more sensitive and more reversible than the sensors using sublimed compounds[7]. A series of tetrakis (cumylphenoxy) phthalocyanines containing H_2, Co, Ni, Pd, Pt, Cu, Zn, and Pb were used to make chemiresistors which were exposed to ammonia, DMMP, and sulfur dioxide[8]. This experiment showed that an array of small chemiresistor sensors could produce patterns of response when exposed to low concentrations of vapors. Reversibility, selectivity, and sensitivity in the low ppm range were demonstrated.

Relationships between chemical structure, morphology, and properties of these materials are being investigated so that films with improved vapor-sensing characteristics may be produced. Details about the preparation of monolayer films of the tetrakis (cumylphenoxy) phthalocyanines and mixed monolayers containing octadecanol have been reported elsewhere[9]. Studies of the the LB films of these compounds by Resonance Raman Spectroscopy have also been reported[10]. New information to be presented in this paper includes results of examination of the LB films by Transmission Electron Microscopy, results of experiments to control the melting point of mixed films, and kinetics of absorption and desorption by films exposed to concentrated vapors.

Transmission Electron Microscopy

Experiment. To prepare a 1:1 mole ratio chloroform solution of metal-free tetrakis (cumylphenoxy) phthalocyanine ($H_2Pc(Cp)_4$) with octadecanol, 5 ml of a 4×10^{-4} M solution of the phthalocyanine was mixed with 1 ml of 2×10^{-3} M solution of octadecanol. A micropipet was used to spread 0.25 ml of this solution on the Langmuir trough. To prepare a single layer sample for examination by Transmission Electron Microscopy (TEM), a 25 mm x 50 mm fused silica microscope slide was withdrawn vertically from beneath the water surface while the film pressure was maintained at 20 mN/M. The resulting film-covered slide was platinum shadowed at a 45 degree angle to make a replica of the film. The replica was floated off the surface of the silica with a dilute solution of hydrofluoric acid. Figure 1 is a photograph of the TEM image.

Discussion. The film has a previously unsuspected nodular structure that looks like a two-dimensional microemulsion. However, the particles are not spherical, but more like pancakes, with width to height ratios on the order of 10 or more

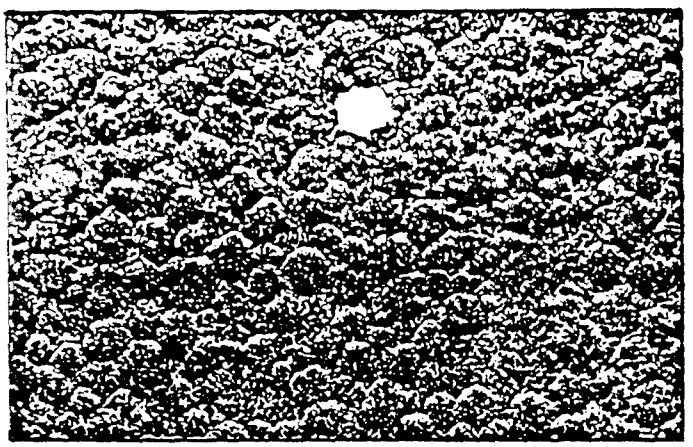

Figure 1. TEM image of a 45° Pt-shadowed LB film of 1:1 metal-free tetrakis (cumylphenoxy) phthalocyanine and octadecanol. Nodule diameters range approximately from 500 to 800 Angstroms. Their heights are estimated at approximately 50 Angstroms.

to 1. Contact angle measurements indicate that the top side of the film is hydrophobic. However, not enough octadecanol is present to cover the entire top surface of the film with a close-packed monolayer such as would be found in a true emulsion or micelle. The bottoms of the pancake structures may be hydrophilic, which would be consistent with the apparent behavior of this complicated structure as a classical LB film. Stacks of phthalocyanine molecules with the bottom molecule of the stack flat on the substrate would be consistent with the Resonance Raman Spectroscopic data[10]. The area per molecule determined by film pressure vs. area measurements[9] is too small for monomers alone to be adsorbed at the surface. The X-ray powder diffraction spectrum[6] showing a 3.3 Angstrom spacing suggests some cofacial stacking. Electron Paramagnetic Resonance data for mixed LB films containing Cu indicate some anisotropy and may lead to a calculation of an approximate average angle of orientation of the stacks. All of this information leads to a complex model of aggregated phthalocyanine with a hydrocarbon-like top surface and containing some oriented stacks of the tetrakis (cumylphenoxy) phthalocyanine. All stacks need not be perfectly aligned like in a crystal. Since the nodules are formed by evaporation of the chloroform from a 1:1 mole ratio mixture with octadecanol, some octadecanol is likely to be trapped inside the nodules. A monolayer of pure octadecanol probably occupies the voids between nodules on the silica surface.

Influence of Transfer Promoter on Thermal Stability

Experiment. Differential Scanning Calorimetry (DSC) was used to compare the thermal stability of several LB films and

corresponding bulk transfer promoters. Using solutions prepared as described earlier, LB films of over a hundred layers thickness were deposited onto small aluminum disks approximately 6 mm in diameter. Six disks were stacked in the DSC sample pan for each run and contained a total of approximately 0.2 mg of film[11]. Temperature was raised at a constant rate in the range of 25 to 150° C, and the heat absorbed or released was observed. The transfer promoters stearyl alcohol, stearyl amide, and stearyl amideoxime were studied as bulk pure compounds, as LB films, and as LB films mixed with $H_2Pc(Cp)_4$. Results are in Table 1.

Table 1. Melting Points by DSC

Transfer Promoter	Mixed LB Film w/$H_2Pc(Cp)_4$	LB Film	Bulk (meas.)	Bulk (lit.)
Stearyl Alcohol	56.3-57.9	58.5	---	58.5
Stearyl Amide	107.0	108.7,109.2	108.7	109
Stearyl Amideoxime	not obs.	--	106.8	--

Discussion. The melting point of the mixed films is determined by the transfer promoter. In the case of stearyl alcohol (octadecanol), there is evidence of irreversible change near 52° during the first rising temperature run. Successive heating and cooling cycles show a different DSC thermogram shape. Morphology changes may have occurred during the first run. In the stearyl amide case multiple runs are identical, and a two-phase system appears to be present with some of the amide present in its pure form. In the stearyl amideoxime case the DSC thermogram is a straight line between 25 and 150° C. The amideoxime is either intimately mixed with the phthalocyanine or the mixture melts above or below the temperature range of the test. The general result of these experiments is that mixed films with melting points above 100° C can readily be made.

Kinetics of Film Interaction with Concentrated Vapors

Experiment. Rapid preliminary investigations of the properties of candidate coatings for both chemiresistor and surface acoustic wave (SAW) microsensors were conducted using a dual 52 MHz SAW delay line oscillator with one side used as a chemiresistor[11]. Frequencies were measured with a Systron-Donner Frequency Counter, and resistances were measured with a Keithley 617 Programmable Electrometer. Both instruments were connected to a microcomputer with an IEEE-488 interface to give a simultaneous reading of frequency shift and resistance change as a function of time while the coated sensor was exposed to a test vapor. The frequency shift of the SAW sensor is directly proportional to the mass of vapor absorbed into the coating[12]. Vapors were generated by bubbling nitrogen at 20 ml/min through a sintered glass tube submerged in the pure liquid. During a run, 5 min of baseline data was recorded with pure nitrogen

flowing, then saturated vapor was switched into the sample stream for 40 min. At the 45-min mark the pure nitrogen stream was switched in place of the vapor, and desorption of vapor from the coating continued for the remainder of the 120-min test period. Test vapors of iodine, dimethyl-methylphosphonate, and ethyl-chloroethyl sulfide were used with LB films for chemiresistors and sprayed polymer films for SAW sensors.

Discussion. Both absorption and desorption of the saturated test vapors by all the coatings followed a second order rate law.

$$\frac{dC}{dt} = kC^2$$

C = Mass of vapor absorbed
Co = Mass of vapor when saturated
k = Rate constant
t = Time

OUTGASSING

$$\frac{1}{C} - \frac{1}{Co} = kt$$

ABSORPTION

$$C = Co - \frac{1}{1/Co + kt}$$

By the method of least squares the best straight line through a plot of 1/frequency change vs time was fitted to obtain values for Co and k. The relationship between C values and frequency shifts could be obtained by calibration of the SAW device with LB films[11]. An absolute calibration was unnecessary when only the relative quantity of vapor absorbed per quantity of coating was desired. Since the frequency shift due to application of the coating was measured, and the additional limiting frequency shift at saturation could be computed when SAW frequency shifts due to vapor uptake were used for the C values in the above equations, the ratio of the limiting frequency shift to the shift due to the pure coating material was obtained. Table 2 reports the results for DMMP absorption into several classes of coatings.

Table 2. DMMP Vapor Absorbed into Microsensor Coatings

Coating Type	Maximum Mass of Vapor Absorbed per Mass of Coating (g/g)
Polymers for Saw Sensors[a]	0.43-0.96
LB Film Overcoated with Polymer[b]	0.39
LB Mixed Films for Chemiresistor Sensors[c]	0.05-0.13
LB Transfer Promoters[c]	0.01-0.03

a) polyethylene succinate, polyethylene dichloromaleate, polypropylene maleate, and polyethylene maleate.
b) $H_2Pc(Cp)_4$/stearyl alcohol coated with polyethylene maleate.
c) as listed in Table 1 with the addition of stearic acid.

CONCLUSIONS

Transmission Electron Microscopy coupled with other observations indicates that chemiresistor coatings made from

mixed multilayer films containing phthalocyanine derivatives are much more complex than classical Langmuir-Blodgett films. The thermal stability of these coatings is determined by the melting point of the transfer promoter. Films with melting points above 100° C can be made. Interaction of the coatings with concentrated vapors follows a second order rate law. Therefore, the limiting amount of vapor absorbed can be computed. Coatings can be ranked according to their ability to absorb vapors. Mixed LB coatings can increase their mass 5-13% by absorbing vapors. An overcoat of polymer can increase this vapor absorbing capacity, and the overcoat may act as a selective membrane.

ACKNOWLEDGEMENTS

We are grateful to Wanda Carter-Peters for providing the DSC measurements and to Philip Berg for preparing many of the LB films. Sponsors contributing to the support of this work were the Naval Research Laboratory, the Office of Naval Technology, and the Chemical Research, Development and Engineering Center.

REFERENCES

1. Naval Research Laboratory, Chemistry Division, Washington, D. C. 20375. Dr. Dote is an NRC Postdoctoral Fellow at NRL.
2. Microsensor Systems, Inc., P. O. Box 90, Fairfax, VA 22030.
3. A. B. P. Lever, in H. Emeleus and A. G. Sharpe (eds.), Advances in Inorganic Chemistry and Radiochemistry, Vol. 7, Academic Press, New York, 1965, pp. 27-114.
4. Y. Sadaoka, N. Yamazoe and T. Seiyama, Denki Kagaku Oyobi Kogyo Butsuri Kagaku, 46 (1978) 597.
5. W. R. Barger, H. Wohltjen, A. W. Snow, J. Lint and N. L. Jarvis, in D. Schuetzle and R. Hammerle (eds.), Fundamentals and Applications of Chemical Sensors, ACS Symposium Series No. 309, American Chemical Soc., Wash. D. C., 1986, pp. 155-165.
6. A. W. Snow and N. L. Jarvis, J. Am. Chem. Soc. 106 (1984) 4706.
7. H. Wohltjen, W. Barger, A. Snow, and N. L. Jarvis, IEEE Trans. Electron Devices, 32 (7) (1985) 1170.
8. W. R. Barger, H. Wohltjen and A. W. Snow, in Transducers '85, IEEE, New York, 1985; IEEE No. 85CH2127-9, pp. 414-417.
9. W. R. Barger, A. W. Snow, H. Wohltjen, and N. L. Jarvis, Thin Solid Films 133 (1985) 197-206.
10. D. P. DiLella, W. R. Barger, A. W. Snow, and R.. R. Smardzewski, Thin Solid Films 133 (1985) 207.
11. A. W. Snow, W. R. Barger, M, Klusty, H. Wohltjen, and N. L. Jarvis, Langmuir 2 (1986) 513-519.
12. H. Wohltjen, A. Snow, and D. Ballantine, in Transducers '85, IEEE, New York, 1985; IEEE No. 85CH2127-9, pp. 66-70.

N. SORPTION KINETICS MEASURED BY SURFACE ACOUSTIC WAVE SHIFTS

David L. Bartley[1],
Dawn D. Dominguez, William R. Barger, Arthur W. Snow[2] and
Hank Wohltjen[3]

ABSTRACT

Vapor sorption vs. time is measured by monitoring the surface acoustic wave (SAW) frequency of a quartz substrate under a polymer film. Uniform spin-coatings are developed. T-dependent effects in SAW support electronics and mounting are minimized and characterized. Kinetics of diffusion of vapors into polymer films are measured in terms of concentration and polymer history. Preliminary data modelling is carried out. Aside from application in characterizing mass transfer into and out of protective equipment (for example), results of this research may find use in development of a diffusive sampling (i.e., pumpless) constant-baseline vapor microsensor.

INTRODUCTION

Gas or vapor transfer within polymers represents a central focus of active investigation from a number of angles. From a chemical or physical point of view, dynamic information on polymer response provides a useful probe into structure and its deformation. Of mathematical interest is the qualitative shift from dispersive to wave character in solutions of the diffusion equation as nonlinearities and polymer history become significant. Practical applications are immediate: Lingering of hazardous gases following exposure is of importance both in military and industrial applications. Alternatively, mass transfer is a dominant phenomenon determining the efficacy of protective equipment such as gloves or goggles. Related is the effectiveness of polymers for use in packaging or as protective paints.

Characterization of a polymer-penetrant pair requires measurement of uptake and loss vs. time. In the case of slowly relaxing glassy polymers in which the diffusion rate sometimes depends on recent exposure history, a succession of such measurements is necessary. So as to make such experimentation feasible, the approach adopted in the present paper is to employ thin polymeric films so as to cut experimentation time by many orders of magnitude from that required in characterizing samples of the order of mm thicknesses.

Specifically, a polymer film is deposited on a quartz substrate provided with interdigital electrodes for the transmission and detection of surface acoustic waves (SAW). Upon exposure to soluble gas or vapor, mass or elasticity changes in the film may be measured by monitoring shifts in SAW characteristics. With the extremely rapid SAW detector response instantaneous traces in time can be determined.

EXPERIMENTAL

film deposition

The films used in the present series of experiments were composed of polycarbonate, a glassy polymer at room temperature, and were deposited onto the quartz substrate as follows. Polymer dissolved in suitable solvent is placed upon the quartz which is then immediately spun with rapid angular acceleration about an axis perpendicular to its surface. All but a boundary layer of solution is thereby thrown off, leaving behind a polymeric film after evaporation of the solvent. Film thickness is measured thereafter by combining measured film weight (and area) with interference fringe shifts. Crystals with films are kept in a dessicator until used, since humidity effects were found to be excessive.

Suitability of the solvent was determined by trial and error. Films deposited from chloroform solutions proved to be plagued by enormous waves in the polymer. Interestingly, the wave crests ran radially out from the spin center and bifurcated regularly so that a constant wavelength was maintained. Measurement of the waves by interferometry indicated that the wave amplitudes were of the order of the film thickness itself and therefore could lead to 100 percent errors in transfer rate measurements.

This problem of film nonuniformity was solved through the use of a more viscous and less volatile solvent. Specifically, polycarbonate films spun from chlorobenzene were found to be entirely wave-free. Perhaps, the smoothness was obtained as a result of reducing boundary layer turbulence by Reynolds number reduction through kinematic viscosity increase.

apparatus

The results given below were obtained using a 52 MHz oscillator with SAW crystal in a delay line as described elsewhere.[4] The temperature dependence of the electronics/crystal was found to be excessive at times. Therefore, in order to minimize any temperature-sensitivity, the entire oscillator was confined to an enclosure with temperature controlled by heater and fan to within ±0.1° C of 31.0° C.

Saturated toluene vapor (the penetrant in the experiments described below) was produced by bubbling purified nitrogen and was then diluted to the desired concentration. So as to keep the dead volume delay time to a minimum, a large flow rate equal to 200 mL/min was selected. With the system dead volume estimated at 5 mL, 200 mL/min corresponds to a delay equal to about 1 sec. A constant flow system was implemented so as to maintain the instrumental time lag at a constant value (experiment indicated no flow or pressure sensitivity of the SAW crystal outside the temperature dependency mentioned above). The result was a flow system with the capability of switching quickly between pure nitrogen and a mixture of nitrogen and toluene.

experimental results

The following experiments were conducted using the equipment described above. Four toluene sorption/desorption pair runs were carried out at each of 5, 10, 25, 50 and 100 percent saturated toluene in nitrogen in a 2800 Angstrom polycarbonate film spun from chlorobenzene.

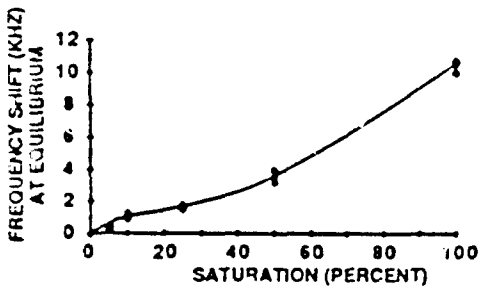

Figure 1. Sorption isotherm.

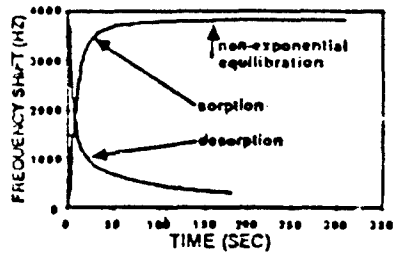

Figure 2. Kinetics at 50% saturation.

In Figure 1 is shown the sorption isotherm obtained from the collective data of these experiments. Given is the equilibrium SAW frequency shift in terms of toluene concentration. Note that at a toluene concentration equal to about 20 percent saturation, the curvature in the sorption isotherm changes sign. Perhaps the structure observed in the curve is a result of the combination of surface adsorption together with bulk absorption by the polymer film.

Also important is the approach to equilibrium (see Figure 2). At both 50 and 100 percent saturation, sorption equilibrium is achieved in a finite time interval, rather than via exponential decay. Such behavior may indicate motion of a sharp sorption front through the polymer as seen optically by some and hypothesized by many researchers.(5-6)

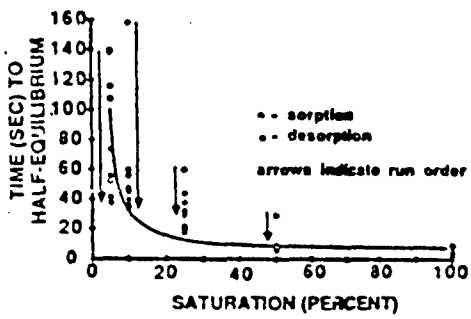

Figure 3. Time to half-equilibrium.

A summary of other nonequilibrium features of the toluene-polycarbonate system is presented in Figure 3. Shown is the time $t_{1/2}$ required for the system to achieve half of the equilibrium frequency shift for each of the concentrations. Were the diffusion rate D independent of concentration then such a relaxation time indicator would be given by

$$t_{1/2} = (\pi/16)\cdot(\delta^2/D), \qquad (1)$$

where δ is the film thickness. Even though the diffusion rate is actually strongly concentration dependent and, with glassy polymers, history dependent, the time $t_{1/2}$ is indicative of relaxation times relevant during sorption and desorption and is therefore used in this paper for a rough interpretation of data.

The following general observations can be made concerning the data of Figure 3:

(1) Desorption and sorption times $t_{1/2}$ at each fixed concentration generally decrease during the course of the experiments as the polymer ages and diffusion rates increase.

(2) The times $t_{1/2}$ may approach a limiting value which as mentioned above is strongly concentration dependent and is given approximately by

$$t_{1/2} = 4 \text{ sec/S}, \qquad (2)$$

where S is the concentration measured as fractional saturation (continuous curve in Figure 3).

(3) Only at concentrations less than 20 percent is sorption quicker than desorption (possibly related to the curvature shift in the sorption isotherm of Figure 1).

In short, an interesting variety of qualitative features are present in the data, and therefore inadequate theory should straightforwardly find itself selected out.

THEORETICAL

Modelling of the above data is as yet far from complete because of the nontrivial nature of the theory and numerical approximations required. Nevertheless, several interesting results have been uncovered and therefore are reported here. Our findings are relevant both to the understanding of diffusion in polymers and a class of nonlinear partial differential equations, as well as to numerical methods of solution.

theoretical model

Diffusion of a substance with concentration C is governed by the diffusion equation,

$$\partial C/\partial t = [\partial/\partial z D \partial/\partial z]C, \tag{3}$$

where D is the diffusion rate and z is a spatial coordinate which here is taken to be fixed (i.e., stretches) with respect to the polymer. At equilibrium, D is assumed to approach a purely concentration dependent function $D_{eq}(C)$. In this paper $D_{eq}(C)$ is modelled as

$$D_{eq}(C) = D_o + D_1 C, \tag{4}$$

where D_o and D_1 are unknown constants. Equation 4 is consistent with Equation 2 over a limited range of concentration values C.

The least certain part of the diffusion theory concerns the polymer relaxation following changes in the concentration, in other words, how the instantaneous diffusion rate D approaches D_{eq}. Perhaps the simplest assumption is that a single relaxation time τ is dominant; i.e., the rate of change of D is proportional to its distance from D_{eq}:

$$\partial D/\partial t = \tau^{-1}(D_{eq} - D). \tag{5}$$

Equation 5 is actually part of a theory to be found in the literature containing yet further models to be sorted out by experiment.[5-6]

numerical methods

Numerical solution of Equations 3-5 and their like is beset by such problems as stability, accuracy, convergence and computation time requirements.[7] This paper adopts a heuristic approach which touches on others' methods developed from alternative viewpoints. The result is an

extension specifically applicable to the solution of the diffusion equation with non-constant diffusion rate.

Inaccuracy in finite difference solutions of Equation 3 is dramatically evident in approximations of the analogous Schrodinger equation (Equation 3 with constant, complex D). In this case inaccuracy takes the form of the gradual disappearance of particles---an unacceptable divergence to zero in a particle conserving system. The way out of this difficulty is to revamp the approximation scheme so that particles are conserved exactly at the finite difference level---not only in the limit of infinitessimal grid spacing. This is accomplished by approximating the argument of the laplacian by a two-time average.

In the language of Equation 3, the concentration value C_{RHS} to be used in the right hand side of the equation is approximated as

$$C_{RHS} = (C_t + C_{t+\delta t})/2, \tag{6}$$

where δt represents the temporal resolution of the approximation. This expression (at constant diffusion rate) may be recognized as identical to the Crank-Nicolson approximation,[6] which infinitely extends the range of stability of diffusion equation finite difference solutions. The diffusion equation analogue of particle conservation can also be carried over from quantum mechanics for the case in which the diffusion rate D is not constant spatially. The (unpublished) result is again Equation 6 together with the following approximation for the differential operator on the right hand side of Equation 3:

$$2\cdot\partial/\partial z(D\partial/\partial z) \sim \delta_- D_{z+\delta z}\delta_+ + \delta_+ D_{z-\delta z}\delta_-, \tag{7}$$

where $\delta_\pm$ are forward/backward spatial differences over a grid with resolution δz. At this point the model and its numerical approximation are so defined that solution on present-day personal computers is possible by exact solution of the tridiagonal linear equations which result using Equations 6-7.

numerical results

No attempt at fitting the data presented above has been made as yet. Nevertheless, preliminary calculations indicate the possibility of sharp concentration front motion for some ranges of model parameters (consistent with the above data). For the case in which the concentration at the polymer surface is raised suddenly from zero to a constant value C_o, there are only two independent parameters which define all the model solutions (aside from scaling in space or time):

$$\mu_1 = D_1 C_o/D_o \tag{8}$$

$$\mu_2 = \tau_o/\tau, \tag{9}$$

where τ_o ($= \delta^2/D_o$) is (proportional to) the relaxation time were the diffusion rate constant and equal to D_o. Therefore, μ_1 measures the departure of the diffusion rate from constancy, and μ_2 specifies the polymer relaxation time τ. In the regime, μ_1 and μ_2 small in comparison to unity, concentration profiles have a "Fickian"

shape with curvature always positive. However, if both parameters are large relative to unity, the profiles take on the shape of a sharp (aside from a heavily damped advance Fickian component) wave front moving through the polymer at constant velocity. An example of such a front at a specific time following polymer exposure is shown in Figure 4.

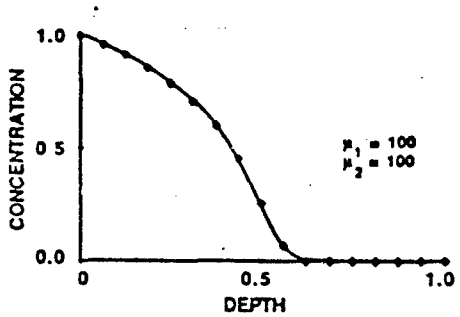

Figure 4. Concentration front profile.

CONCLUSIONS

Results presented in this paper demonstrate the potential of using surface acoustic waves (SAW) to monitor the uptake and loss of gases or vapors by polymers. The advantage lies in the film thinness which makes extensive experimentation feasible and, in fact, permits characterization of polymer history effects. In this regard, a simplest polymer relaxation model and its approximation are capable of depicting sorption wave fronts which are evident in the SAW data collected.

Future research in this area must broaden the scope of the polymer/penetrant systems examined and their model descriptions. In a separate vein, the relationship between surface and bulk sorption phenomena must be determined---by sorting out surface from volume effects and by determining the effect of the specific film deposition techniques employed. The results of this type of research could lead to a comprehensive understanding of gas and vapor diffusion in polymers.

ACKNOWLEDGEMENT

This research was carried out in part under U.S. Navy Contract No. NR677-003.

REFERENCES

1. National Institute for Occupational Safety and Health, 4676 Columbia Parkway, Cincinnati, Ohio 45226

2. Naval Research Laboratory, Code 6170, Washington, D.C. 20375

3. Microsensor Systems, Inc., P.O. Box 90, Fairfax, Virginia 22030

4. H. Wohltjen, Sensors and Actuators 5:307-325 (1984).

5. J. Comyn, ed., Polymer Permeability. Elsevier Applied Science Publishers, London (1985).

6. J. Crank, The Mathematics of Diffusion. Clarendon Press, Oxford (1976).

7. G. Smith, Numerical Solution. Clarendon Press, Oxford (1978).

CRDEC '87

CORRELATION OF SAW VAPOR SENSOR RESPONSES WITH PARTITION COEFFICIENTS

Jay W. Grate*, Arthur Snow*, David S. Ballantine, Jr.**,
Hank Wohltjen***, Michael H. Abraham****,
R. Andrew McGill****, and Pnina Sasson****.

*Chemistry Division, Naval Research Laboratory,
Washington, DC 20375-5000 USA,
**Geo-Centers, Inc., 10903 Indian Head Highway, Suite 502
Ft. Washington, 20744 USA,
***Microsensor Systems, Inc.,
P.O. Box 90, Fairfax, VA 22030, USA,
****Department of Chemistry,
University of Surrey, Guildford Surrey GU2 5XH, United Kingdom

ABSTRACT

Many gas sensors operate by detecting the gas molecules which are absorbed and concentrated by a thin film. The equilibrium distribution of the gas between the gas phase and the thin film (or stationary phase) can be quantified by the partition coefficient. Polymer/gas partition coefficients have been calculated from the responses of polymer-coated surface acoustic wave (SAW) vapor sensors, and these values are in agreement with values determined independently by gas-liquid chromatography. Quantification of the gas-polymer interaction facilitates the interpretation and prediction of SAW sensor behavior, and is relevant to any gas sensor employing a thin absorbent film.

INTRODUCTION

A key component of many gas sensors is the chemical coating material which absorbs and concentrates the gas to be detected. Absorption of the gas can be modeled as a solute-solvent interaction, where the gas is the solute and the sensor coating is the solvent. This model has been very useful in understanding the behavior of surface acoustic wave (SAW) vapor sensors, which detect the mass of vapor absorbed into a soft polymeric stationary phase coating. (Further details on SAW vapor sensor operation can be found in reference 1.)

The solute hydrogen bonding properties, in particular, have been indicated as an important factor in determining the sensitivity and selectivity of SAW vapor sensors. Using pattern recognition techniques, the data from a variety of coating materials on SAW devices exposed to vapors with a full range of solubility properties were examined. Heiarchical cluster analysis demonstrated that vapors which could accept or donate hydrogen bonds were distinguished from non-hydrogen bonding vapors.[2]

A better understanding of the factors influencing the sorption of gases and vapors into sensor coating materials would facilitate the development of gas sensors for specific applications. Indeed, one of the attractive features of sensors employing thin absorbent films is their potential to be adapted to a wide variety of gas phase analytical problems by strategic design or selection of the coating material. However, full realization of this potential will require methods to quantify, understand, and ultimately, to predict, the vapor/coating interactions responsible for vapor sorption.

Quantification of the equilibrium distribution of vapor between the gas phase and a sensor coating (stationary phase) can be achieved using a partition coefficient, K, which gives the ratio of the concentration of the vapor in the stationary phase, C_s, to the concentration of the vapor in the gas phase, C_v (equation [1]).

$$K = C_s/C_v \qquad [1]$$

This concept is illustrated in Figure 1.

Partition coefficients are a particularly useful concept for thinking about SAW sensor responses because the sensors response, a frequency shift, can be directly related to the partition coefficient by equation [2].

$$\Delta f_v = \Delta f_s \, C_v \, K \, / \, \rho \qquad [2]$$

In this equation, Δf_v is the frequency shift caused by vapor absorbed into the coating, Δf_s is the frequency shift caused by the application of the coating to a bare device (and provides a measure of the amount of coating applied), C_v is the concentration of the vapor in the gas phase, K is the partition coefficient, and ρ is the coating material density. With this simple equation, partition coefficients can be calculated from SAW sensor data. Alternatively, if K is known from GLC measurements or solvatochromic correlation equations, then these values can be used to estimate SAW sensor responses using equation [2].

The relationship between partition coefficients and SAW sensor responses was experimentally tested using the coating material 'fluoropolyol', which has proven in repeated testing to be a very well behaved and reproducible sensor coating. The structure of the repeat unit of fluoropolyol is shown in Figure 2. Polymer/gas partition coefficients calculated from sensor responses were compared with the same partition coefficients determined independently by GLC measurements, using fluoropolyol as the column stationary phase. The results are in good agreement, confirming the solubility model above. This work is presented briefly below; additional details can be found in references 3-5.

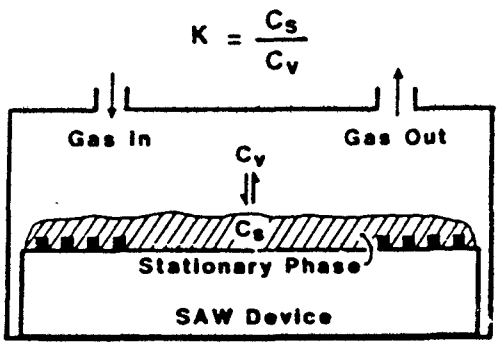

Figure 1. The partition coefficient.

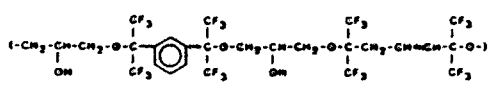

Figure 2. Fluoropolyol.

SAW PARTITION COEFFICIENTS

SAW vapor sensors were prepared by spray coating one delay line of a dual delay line SAW device with a dilute solution of fluoropolyol, as has been described previously.[2,4] These sensors were tested against vapors by alternately exposing them to clean air or a calibrated vapor stream using an automated vapor-generation instrument described in reference 6. The change in the frequency observed when the gas over the sensor was changed from clean air to vapor gives Δf_v. For reliable measurements of K, this frequency shift must be determined only after the sensor has reached a stable, equilibrium response level.

In this study, we report data for two 158 MHz SAW vapor sensors labelled "A" and "B". Sensor "A" had 223 kHz of fluoropolyol coating, and was tested against vapors in three separate testing sequences over a two month period. It was tested a fourth time several months later. Sensor "B" had 221 kHz of fluoropolyol coating, and was tested twice. These tests were conducted at 35 $\pm$ 2°C. These data provide comparisons of reproducibility from one sensor to another, as well as the reproducibility of a single sensor tested repeatedly over several months. Data sets of vapor exposures were collected by exposing the sensors to each of nine vapors, each vapor at four concentrations, each concentration repeated four times. In addition, dimethyl methylphosphonate (DMMP) was repeated throughout the dataset and its reproducibility was very good.

The SAW frequency shifts for each vapor exposure were used to calculate partition coefficients, denoted K_{SAW}, according to equation [10]. These were converted to logarithms and the sixteen values for each vapor (or ca. one hundred for DMMP) were averaged and their standard deviation determined. These log K_{SAW} values are reported in Table I. The standard deviations of these values were typically 0.02 to 0.10 log units.

The average log K_{SAW} values for each vapor are generally consistent over the six datasets collected. For six of the nine vapors, the difference between the highest and lowest values is 0.15 log units or less. A variation of +/- 0.075 log units in log K_{SAW} corresponds to +/- 18% in the SAW Δf_v values. For comparison, the uncertainty in the vapor concentrations is up to +/- 15%, depending on the particular concentration generated.[6] These results demonstrate that fluoropolyol-coated SAW sensors can be fabricated and tested reproducibly, and that the responses do not change over a period of months. Previous results with fluoropolyol on 112 MHZ dual delay line SAW devices have shown that sensor responses are similar from one day to two months after coating, and that annealing the fluoropolyol film at 110°C for one hour did not influence its performance.[4] The vapor/coating interactions are therefore consistent and reproducible, and fit the model of simple, reversible sorption.

For most of the vapors the calculated K_{SAW} values were constant over the concentration range reported. This corresponds to a linear sorption isotherm, as illustrated for 1-butanol in Figure 3. The number next to each data point is the corresponding K_{SAW} value. A linear sorption isotherm represents ideal solution behavior. The sorption isotherms of dimethyl methylphosphonate (DMMP), and N, N-dimethylacetamide deviated significantly from linearity, with K_{SAW} values decreasing with increasing concentration. These results are illustrated for DMMP in Figure 3 and suggest specific, preferential vapor/oligomer interaction at low concentrations. This interaction is likely to be hydrogen bond formation between hydrogen bond donating (HBD) hydroxyl groups on the fluoropolyol and hydrogen bond accepting (HBA) oxygen atoms on the vapor.

The influence of temperature on SAW sensor responses was investigated by measuring the sorption of DMMP at 20 μg/L at six temperatures between 35 and 80°C. Sensor response and vapor sorption decrease exponentially with increasing temperature. Thus, log K decreases linearly, from ca. 6.5 at 35°C to ca. 5.0 at 80°C.

TABLE I. Log K_{SAW} Values for Fluoropolyol

	Typical Concentration Range µg L^{-1}	Sensor, Data Set					
		A,1	A,2	A,3	B,1	B,2	A,4
DMMP	29 - 137	6.33	6.21	6.22	6.30	6.28	6.28
N,N-Dimethylacetamide	11 - 81	6.37	6.21	6.08	6.18	6.11	6.13
1-Butanol	1310 - 7820	3.82	3.86	3.85	3.92	3.86	3.94
2-Butanone	16400 - 95400	3.60	3.54	3.53	3.61	3.58	3.64
Water	893 - 5320	3.49	3.31	3.10	3.13	3.43	3.54
Diethyl sulfide	9030 - 53500	3.19	3.11	3.08	3.23	3.14	3.23
Toluene	7080 - 42000	3.03	2.96	2.94	3.09	3.03	3.04
1,2-Dichloroethane	20600 - 120000	2.69	2.63	2.57	2.70	2.57	2.61
Isooctane	15000 - 88500	2.31	2.29	2.20	2.41	2.25	2.27

TABLE II. Comparison of Log K_{SAW} and Log K_{GLC} Values

VAPOR	Log K_{SAW}	Log K_{GLC}
DMMP	6.52	7.53
N,N-Dimethylacetamide	6.33	7.29
1-Butanol	3.88	3.66
2-Butanone	3.58	3.48
Water	3.33	2.89
Diethyl sulfide	3.16	2.54
Toluene	3.02	2.64
1,2-Dichloroethane	2.63	1.94
Isooctane	2.29	1.22

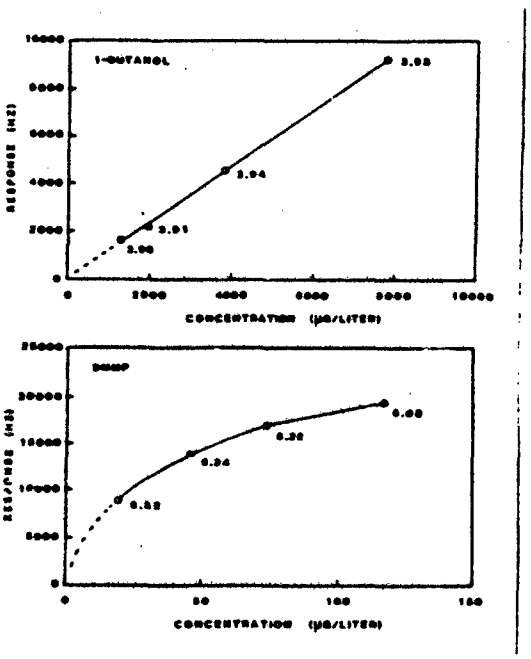

Figure 3. Sorption isotherms.

GLC PARTITION COEFFICIENTS

Partition coefficients for a wide variety of solute vapors were determined by gas-liquid chromatography using fluoropolyol as the stationary phase. Partition coefficients as defined in equation [1] are actually identical to the Oswald solubility coefficients usually denoted as L. We will continue to use the symbol K, and refer to GLC partition coefficients as K_{GLC}.

Absolute values of K_{GLC} were obtained essentially as described previously in reference 7, using glass columns 1.5 m long containing a 4% loading of fluoropolyol on acid-washed, silanized chromosorb G, with helium as the carrier gas and a thermal conductivity detector. Corrections for the pressure drop across the column and for gas imperfections were carried out. Two series of measurements were made, at 25°C and 60°C using alcohols as standard solutes. Additional solutes were then examined at 25°C and/or 60°C using a flame ionization detector. Relative values of K were converted to absolute values using the known absolute values of the standard solutes, as described before.[7]

GLC peaks on fluoropolyol were sometimes broad, especially at 25°C. Therefore, 26 K_{GLC} values were determined at both 25°C and 60°C and the following correlation was found to hold:

$$\log K_{GLC}\,(25^{\circ}C) = 0.728 + 1.470 \log K_{GLC}\,(60^{\circ}C) \qquad [3]$$
$$n = 26,\ sd = 0.156,\ r = 0.986$$

When retention times were too long to measure at 25°C, equation [3] and the measured value of K_{GLC} at 60°C were used to estimate the value of K_{GLC} at 25°C.

Log K_{GLC} and log K_{SAW} values for nine solute vapors are compared in Table 2, with the vapors in order of decreasing log K_{SAW}. All of the GLC values refer to 25°C. In one case, diethyl sulfide, the log K_{GLC} values was estimated from various correlations we have constructed using solvatochromic parameters. Log K_{GLC} values refer to the vapor concentration at infinite dilution. The log K_{SAW} values refer to 35°C and finite vapor concentrations. Except for DMMP, and N,N-dimethylacetamide, the values reported are averages of those in Table I. The two exceptions showed significant increase in K with decreasing concentration, and the values in Table 2 are for the lowest concentrations measured.

DISCUSSION

The log K_{SAW} values correlate qualitatively with the log K_{GLC} values in Table II. With the exception of the estimated value of log K_{GLC} for diethyl sulfide, the order of decreasing log K is identical for the SAW and GLC measurements. The log K values for specific vapors are not always identical. However, the experimental conditions for measuring partition coefficients with a SAW device are somewhat different than those for GLC measurements. SAW measurements, for instance, are carried out at finite vapor concentrations while the GLC measurement refers to infinite dilution. In addition, the SAW measurements reported here were conducted at 35°C, while the GLC measurements were rigorously thermostatted to 25°C. Finally, the calculation of K_{SAW} assumes that the vapor causes the sensor to respond based on mass effects alone; if mechanical effects become significant for a particular vapor/coating interaction, then the calculated K_{SAW} will be inaccurate. One or more of the above factors may be responsible for differences in the precise values of log K_{SAW} and log K_{GLC} shown in Table II.

For example, for DMMP, the log K_{GLC} was 1 log unit higher than log K_{SAW}. The DMMP sorption isotherm in Figure 3 shows that log K_{SAW} will increase as DMMP concentration approaches zero, thus more closely approximating the log K_{GLC} value. Temperature effects also show that if the K_{SAW} measurement were at 25°C instead of 35°C, then log K_{SAW} would be closer to the log K_{GLC} value.

The temperature effects observed are worth examining for practical reasons. The results demonstrate that precise thermostatting of a SAW sensor to fractions of a degree is clearly not critical, but variations of ten degrees may influence sensor response and reproducibility. The form of equation [3] shows that temperature effects will be largest for the most strongly sorbed vapors. For example, DMMP sorption with log K_{GLC} of 7.5 at 25°C, is predicted to be 7.0 at 35°C, a difference of 0.5 log units. By comparison, a log K value of 3.0 at 25°C becomes 2.9 at 35°C, a difference of only 0.1 log unit. Therefore increasing temperature reduces selectivity in addition to the sensitivity.

The temperature effect and the overall correlation in the order of K_{SAW} and K_{GLC} values are consistent with the sorption model. Accordingly, partition coefficients are a useful concept for interpreting SAW sensor behavior,[8,9] and a more detailed consideration of the factors responsible for sorption is warranted. Since partitioning represents dissolution of a solute vapor into the solvent stationary phase, solubility interactions must be relevant in determining sensor responses.

A simple examination of the order of the partition coefficients determined in this study illustrates the importance of solubility properties. The lowest K values are those of isooctane, a solute which is not dipolar or polarizable, and which cannot accept or donate hydrogen bonds. Solutes which are more polarizable, such a dichloroethane, toluene, and diethyl sulfide have greater K values than isooctane. However, these solutes are still incapable of hydrogen bonding. The top of the list contains exclusively those solutes which can accept and/or donate hydrogen bonds. Vapor sorption is also influenced by the saturation vapor pressure, P^o_v, of the solute vapor,[8] with lower P^o_v giving larger partition coefficients. For example, both DMMP and 2-butanone are hydrogen bond acceptors. But DMMP has a much lower P^o_v and is more strongly sorbed.

Solubility interactions can be placed on a more quantitative scale by the use of solvatochromic parameters, which describe the dipolar and hydrogen bonding properties of the solute vapors.[10-13] Such parameters are available for a wide range of vapors, but similar parameters are not yet available for very many coating materials. In order to better understand vapor/coating interactions, it will be necessary to also characterize the solubility properties of the stationary phase coatings. In addition, it would be desirable to be able to predict partition coefficients for any vapor with any characterized phase. Methodologies to accomplish this are being developed using equations of the general form shown in equation [4].[14]

$$\log K = \text{constant} + s\pi^* + a\alpha + b\beta + l \log L^{16} \qquad [4]$$

In this equation, the parameters π^*, α, β, and log L^{16} characterize the solute vapor. π^* measures the ability of a compound to stabilize a neighboring charge or dipole. For non-protonic, aliphatic solutes with a single dominant dipole, * values are approximately proportional to molecular dipole moments. α and β measure solute hydrogen bond donor acidity and hydrogen bond acceptor basicity, respectively. L^{16} is the Ostwald solubility coefficient (partition coefficient) of the solute vapor on hexadecane at 25°C, and provides a measure for dispersion interactions. The coefficients s, a, b, and l are determined by multiple regression analysis and characterize the stationary phase. For example, b, as the coefficient for solute hydrogen bond acceptor basicity, provides a measure of the stationary phase hydrogen bond donor acidity. For any particular stationary phase/vapor interaction, evaluation of the individual terms (such as $b\beta$) and comparison of their magnitudes allows the relative strengths of various solubility interactions to be sorted out and examined.

The structure of fluoropolyol by itself does not allow precise predictions of which interactions will be most important in determining the sorption of a particular vapor. Full characterization of fluoropolyol by GLC measurements and equations of the form

in [4] is in progress. In addition, various other polymeric stationary phases which have been useful as SAW sensor coatings are being examined. Once a regression equation has been determined for a given phase, partition coefficients can be predicted for any vapor whose solvatochromic parameters are known.

CONCLUSIONS

An equation has been derived which relates SAW vapor sensor frequency shifts directly to partition coefficients. This equation has been validated by a comparison and correlation of partition coefficients determined independently by SAW vapor sensor responses and GLC measurements. This correlation also confirms reversible sorption as the mechanism of vapor/coating interaction. Solubility properties such as dipolarity and hydrogen bonding are indicated as important factors in determining the extent of vapor sorption. The saturation vapor pressure of the solute vapor also influences sorption. The direct relationship between SAW sensor response and partition coefficients provides an avenue for estimating SAW sensor response from measured GLC partition coefficients. Partition coefficients predicted from solute vapor solvatochromic parameters and correlation equations characterizing the solvent stationary phase are also expected to be useful for estimating SAW sensor responses.

ACKNOWLEDGMENT

The authors acknowledge M.J. Kamlet for many useful discussions on solubility interactions. This work was supported by the U.S. Army, CRDEC, Aberdeen Proving Ground, MD; and the U.S. Naval Surface Weapons Center, Dahlgren, VA; and the Office of Naval Technology.

REFERENCES

1. Wohltjen, H. Sens. Actuators, 1984, 2, 307-325.
2. Ballantine, D.S.; Rose, S.L.; Grate, J.W.; Wohltjen, H., Anal. Chem., 1986, 58, 3058-3066.
3. Grate, J.W.; Snow, A.W.; Ballantine, D.S., Jr.; Wohltjen, H.; Abraham, M.H.; McGill, R.A.; Sasson, P., Proc. of the 4th Int. Conf. on Solid-State Sensors and Actuators-Transducers '87, Tokyo, Japan, June 2-5, 1987, pp. 579-582.
4. Grate, .W.; Snow, A.; Ballantine, D.S.; Wohltjen, H.; Abraham, M.H.; McGill, R.A.; Sasson, P., NRL Memorandum Report 6024, 1987; NTIS ADA 183694.
5. Grate, J.W.; Snow, A.; Ballantine, D.S.; Wohltjen, H.; Abraham, M.H.; McGill, R.A.; Sasson, P., submitted to Anal. Chem.
6. Grate, J.W.; Ballantine, D.S., Jr.; Wohltjen, H., Sens. Actuators, 1987, 11, 173-188.
7. Abraham, M.H.; Grellier, P.L.; McGill, R.A., J. Chem. Soc. Perkin Trans. 1, 1987, 797- 803.
8. Snow, A.; Wohltjen, H. Anal. Chem., 1984, 56, 1411-1416.
9. Wohltjen, H.; Snow, A.; Ballantine, D., Proc. of the 3rd Int. Conf. on Solid State Sensors and Actuators - Transducers '85, Philadelphia, PA, June 11-14, 1985, IEEE Cat. No. CH2127-9/85/0000-0066, pp 66-70.
10. Kamlet, M.J.; Doherty, R.M.; Abboud, J.-L.M.; Abraham, M.H.; Taft, R.W., CHEMTECH, 1986, 16, 566-576.
11. Abraham, M.H.; Doherty, R.M.; Kamlet, M.J.; Taft, R.W., Chemistry in Britain, 1986, 22, 551-554.
12. Kamlet, M.J.; Taft, R.W., Acta Chem. Scand., Ser. B, 1985, B39, 611.
13. Kamlet, M.J.; Abboud, J.M.; Abraham, M.H.; Taft, R.W., J. Org. Chem., 1983, 48, 2877.
14. Abraham, M.H.; Grellier, P.L.; McGill, R.A.; Doherty, R.M.; Kamlet, M.J.; Hall, T.M.; Taft, R.W.; Carr, P.W.; Koros, W.J., Polymer, 1987, 28, 1363-1369.

SYNTHESIS AND EVALUATION OF HEXAFLUORODIMETHYLCARBINOL FUNCTIONALIZED POLYMERS AS SAW MICROSENSOR COATINGS

L. G. Sprague, A. W. Snow[1], R. L. Soulen, John Lint, H. Wohltjen, D. S. Ballantine and J. W. Grate

ABSTRACT

Polystyrenes, polyacrylates and poly(3,4-isoprenes) incorporating the hexafluorodimethylcarbinol functionality have been synthesized, characterized and tested for dimethylmethylphosphonate, DMMP, vapor absorption sensitivity. The syntheses involve monomer functionalization and polymerization or hexafluoroacetone reaction with preformed polymer. SAW microsensor testing (158 MHz) over a large DMMP vapor concentration range demonstrated exceptional DMMP sensitivity (up to 40% by weight absorption at P/P_o of 0.80) when compared with polystyrene and polyacrylate control polymers. IR spectroscopic investigation of DMMP vapor absorption indicates conversion of free hydroxyl groups to hydrogen bonded groups, and the order of sensitivity increased with quantity of free hydroxyl relative to hydrogen bonded hydroxyl in the fluoroalcohol polymer. Acylation of the hydroxyl group and retesting further confirmed the effectiveness of the hydrogen bonded interaction on DMMP absorption sensitivity.

INTRODUCTION

Coatings for chemical microsensors with highly sensitive, reversible and selective absorptions for particular vapors are necessary for the successful development of electronic chemical microsensors. In this work, coatings which have a specific interaction with g-agent simulants are being investigated using a surface acoustic wave (SAW) device. The SAW device detects extremely small gravimetric changes in a coating (i.e., vapor absorption and desorption) by a shift in resonant frequency of the piezoelectric substrate. Approaches to the design of coating chemical structure involve selection and incorporation of an appropriate functional group to serve as a vapor receptor site and the thermodynamic considerations of solubility interactions. Previous work from this laboratory has followed the functional group approach with a model reactive polymer-vapor poly(ethylene maleate)-cylopentadiene system[2], a series of amidoxime functionalized poly(butadiene-co-acrylonitrile) coatings[3] and a comparative study of N-vinylimidazole and 4(5)-

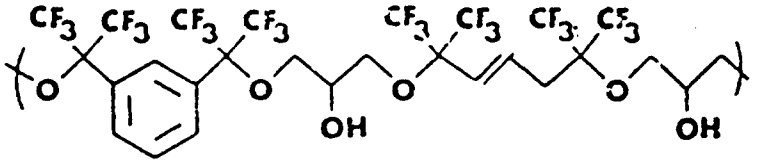

FPOL

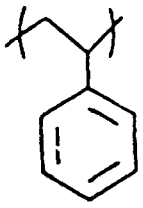

PS

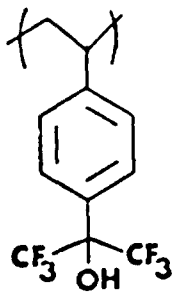

PSpFA

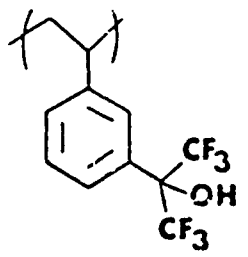

PSmFA

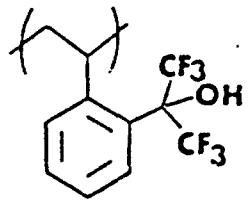

PSoFA

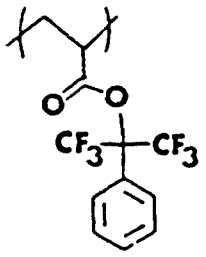

PA

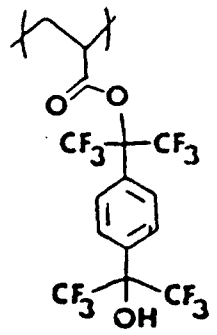

PAFA

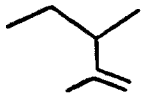

PIP

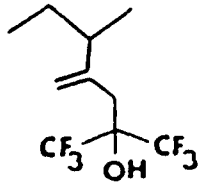

PIPFA2

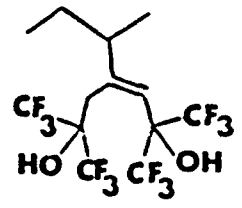

PIPFA1

Figure 1. Structures of Fluoroalcohol and Control Polymers.

vinylimidazole homopolymer coatings[4] while the solubility interaction approach was studies with a series of poly(ethylene maleate) variant structures[5]. The current work is directed at synthesis of fluoroalcohol polymer coatings and evaluation of hydrogen bonding promoted absorption of phosphonate esters.

The hexafluorodimethylcarbinol functionality was first incorporated into copolymers to utilize the hydrogen bonding capability for preparation of polymer blends by Pearce[6]. Barlow extended this concept to microsensor coatings using a styrene-4-vinylhexafluorocumyl alcohol copolymer on a piezoelectric crystal for sensing DMMP[7]. To more closely examine the structure-property relationship of fluoroalcohol polymers' absorption of DMMP vapor, we have synthesized, characterized and tested a variety of homo and copolymers incorporating the hexafluorodimethylcarbinol functionality as presented in Figure 1. The hydroxyl groups of two of the fluoroalcohol polymers have been acylated to demonstrate the hydrogen bonding effect of the hydroxyl group.

EXPERIMENTAL

All reagents and solvents were of reagent grade quality, purchased commercially and used without further purification unless otherwise noted. Elemental analysis was performed by Schwartzkopf Microanalytical Laboratory. DMMP absorption isotherms were determined by frequency response measurements of 158 MHz SAW devices coated with a 250 KHz fluoroalcohol polymer film exposed to varying concentrations of DMMP. Measurements were conducted at Microsensor Systems, Inc. using a VG 7000 automated vapor delivery system with DMMP source bubbler maintained at 15°C and SAW device at 25°C.

NRL Flucropolyol, FPOL. This material is a fluoroepoxy prepolymer synthesized from hexafluoroacetone, benzene, propene and epicholorohydrin some years ago at NRL for coating applications[8].

Poly(4-vinylhexafluorocumyl alcohol), PSpfA. 4-Bromostyrene (2.0 g, 0.011 mole) was dissolved in 2 ml THF and added to magnesium (1.0 g, 0.04 g-atom) with stirring. Upon initiation of the Grignard reagent, magnesium (5.0 g, 0.21 g-atom) was added followed by 4-chlorostyrene (33.1 g, 0.231 mole) and 48 ml THF. The resultant dark green solution was stirred at room temperature for 1 hr. Hexafluoroacetone (42.8 g, 0.258 mole) was introduced, and the solution stirred for 1 hr followed by pouring into 100 ml 3N HCl to produce a yellow oil. The oil was separated, combined with two 80 ml $CHCl_3$ extracts, rotary evaporated, dissolved in 200 ml 10% w/v NaOH, rotary evaporated, acidified with 200 ml 6N HCl, separated, dried over Na_2SO_4 and distilled in vacuo to yield 39.9 g (59%) with 99% GC purity. The monomer (5.01 g, 0.019 mole) was polymerized with AIBN initiator (0.131 g, 0.008 mole) in 125 ml benzene at 60°C to yield 4.08 g (80%) polymer.

Poly(3-vinylhexafluorocumyl alcohol), PSmFA. This monomer was prepared in a similar manner from 3-bromostyrene (5.11 g, 0.028 mole), Mg (0.7 g, 0.029 g-atom) and 30 ml THF. Yield 3.90 g (52%). The monomer (3.44 g, 0.013 mole) was polymerized with AIBN initiator (0.021 g, 0.0008 mole) in 10 ml benzene at 60°C to yield 2.23 g (65%) of filtered polymer.

Poly(2-vinylhexafluorocumyl alcohol), PSoFA. This monomer was prepared in a similar manner from 2-bromostyrene (1.55 g, 0.0009 mole), Mg (0.22 g, 0.009 g-atom) and 8.5 ml THF. Yield 0.99 g (43%). The monomer (0.96 g, 0.0036 mole) was polymerized with AIBN initiator (0.0032 g, 0.0003 mole) in 3.0 ml benzene at 60°C to yield 0.24 g (25%) product.

Poly(2-phenyl-1,1,1,3,3,3-hexafluoro-2-propyl acrylate), PA. The corresponding monomer was prepared by reacting 61.0 g 2-hydroxy-2-phenyl-1,1,1,3,3,3-hexafluoropropane with 27.15 g acryloyl chloride catalyzed by triethyl amine in 100 ml freon 113 at 5 to 15°C under nitrogen. After aqueous acid and base extraction workup, the monomer was isolated by vacuum distillation (50-57°C/0.2mm) followed by alumina column chromatography (freon 113 elution) and vacuum distillation (55 to 57°C/0.2mm) to yield 34.8g of 99.8% (GC) pure monomer. A 1.15 g quantity of monomer in 8 ml THF was polymerized in the presence of 0.0024 g AIBN initiator at 60°C. The polymer was isolated by precipitation in 500 ml 60/40 methanol/water and vacuum dried.

Poly[4-(1,1,1,3,3,3-hexafluoro-2-hydroxy-2-propyl)phenylene-1,1,1,3,3,3-hexafluoro-2-propyl acrylate], PAFA. The corresponding monomer was prepared by reacting 5.00 g 1,4-bis(2-hydroxyhexafluoro-2-propyl)benzene with 0.99 g acryloyl chloride catalyzed by 3.70 g triethyl amine in 120 ml ether at 2 to 4°C. The reaction was worked up by extracting with HCl and $NaHCO_3$ and analyzed by GC to contain 45.2% diol, 37.7% monoacrylate and 19.9% diacrylate. The diol was separated by sublimation (60°C/0.15 mm). The diacrylate and monoacrylate were separated by silica column chromatography with chloroform elution and the monoacrylate sublimed (90°C/0.1 mm). A second silica column and sublimation purification yielded monoacrylate monomer >99% pure by GC. A 0.28 g quantity of this monomer in 2 ml THF was polymerized in the presence of 0.00048, AIBN initiator at 60°C. The polymer was isolated by precipitation in water and vacuum dried to yield 0.1558 g.

Poly(3,4-isoprene) functionalized fluoroalcohols, PIPFA1 and PIPFA2. The precursor polymer, poly(3,4-isoprene) was prepared by Ziegler-Nata polymerization by a modified procedure of Natta[10]. The catalyst was prepared by inert atmosphere addition of 0.25 ml titanium tetrapropoxide followed by 0.75 ml triethyl aluminum to 50 ml toluene. After aging for 15 min, 15 ml freshly distilled isoprene was added, and the polymerization

conducted at 23°C for 10 hr. The polymer was isolated by precipitation into 300 ml methanol acidified with 0.5 ml HCl and vacuum dried to yield 1.32 g. PIPFA1 was prepared by reacting 0.50 g PIP with 7.73 g hexafluoroacetone in 3 ml benzene in a small Fisher-Porter tube at 120°C for 12 hr. On cooling the polymer precipitated from solution and was purified by dissolution in methanol and precipitation in ether followed by vacuum drying to yield 0.93 g. Analysis: found C,44.32; H,3.93; calc. for $C_5H_8(C_3F_6O)_{0.80}$ C,44.22; H,3.98. PIPFA2 was prepared by reacting 0.25 g PIP with 0.36 g hexafluoroacetone in 3 ml benzene in a small Fisher-Porter tube at 100°C for 12 hr. The reaction mixture was evaporated to dryness, product dissolved in methanol, precipitated into water and vacuum dried to yield 0.39 g. Analysis: found C,53.45; H,5.48; calc. for $C_5H_8(C_3F_6O)_{0.46}$ C,53.04; H,5.54.

Acylation of FPOL and PSpFA. A 0.65 g quantity of FPOL was reacted with 0.57 g acetylchloride catalyzed by 0.73 g triethyl amine in 10 ml chloroform at 20°C for 1 hr. The reaction mixture was extracted with 5% HCl and water, dried over Na_2SO_4, filtered, evaporated to dryness and vacuum dried to yield 0.67 g. A 0.32 g quantity of PSpFA was reacted with 0.47 g acetylchloride catalyzed by 0.60 g triethyl amine in 10 ml THF at 20°C for 3 hr. The reaction was worked up by filtering drying over Na_2SO_4. An IR spectrum indicated only a partial acylation had been accomplished, and the product was cycled through the acylation reaction two more times to yield 0.22 g product with a greater than 90% acylation.

RESULTS AND DISCUSSION

The initial report of a fluoroalcohol polymer as a highly sensitive phosphonate ester vapor absorbing coating was that of Barlow in 1984[7]. In that particular copolymer of styrene and 4-vinyl hexafluorocumyl alcohol, the trifluoromethyl groups would be expected to enhance the hydroxyl hydrogen bond acidity and phosphonate ester absorption. At that time and inspired by that report, we tested a fluoroepoxy prepolymer which was available at NRL from previous aircraft coatings work[8]. Although this material does not have trifluoromethyl groups positioned alpha to the hydroxyl sites (see Figure 1), it possesses exceptional phosphonate ester sensitivity and good coating mechanical properties. This polymer is referred to as FPOL and has been studied as a SAW vapor sensor coating[12].

A recent Workshop on Coatings for Microsensors recommended that the homopolymer of styrene with a hexafluorodimethylcarbinol group in the para position, PSpFA, be synthesized with the objective of having adequate quantity of this structurally well-defined coating available for extensive characterization, testing and cooperative work with other laboratories. For comparative purposes, synthesis of the meta, PSmFA, and ortho, PSoFA, substituted isomers was also undertaken. PSpFA was prepared from the monomer which was synthesized from p-chloro-

styrene by a method similar to that reported by Pearce[9]. PSmFA and PSoFA were analogously prepared by reaction of the corresponding Grignard reagents and hexafluoroacetone followed by radical polymerization. In our hands the ortho isomer polymerized poorly and only a trivial amount of polymer was available for study.

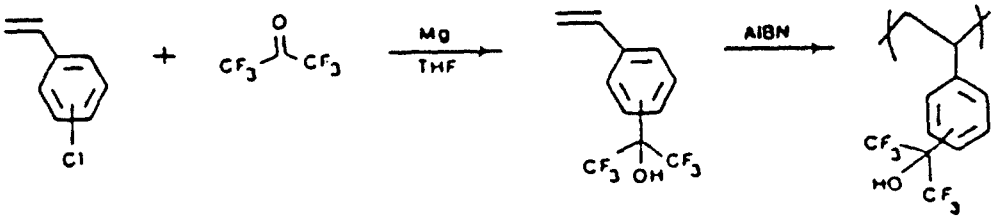

A polyacrylate fluoroalcohol, PAFA, and polyacrylate control, PA, were synthesized as comparative analogues with the polystyrene series. The issue of interest here is the effect of a basic carbonyl site incorporated into the polymer structure. PA and PAFA were synthesized by the following reactions.

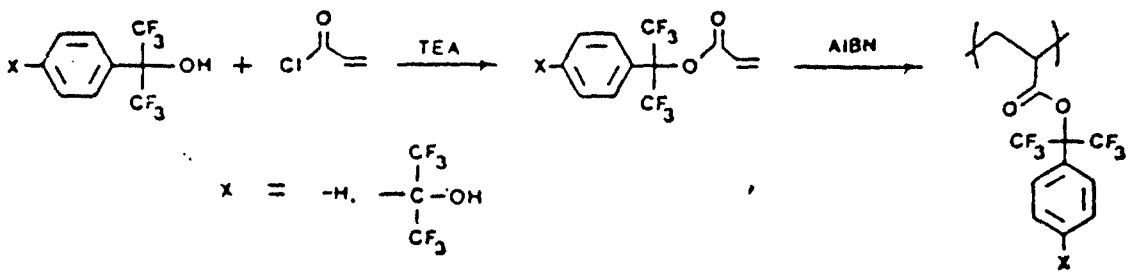

A third approach is directed at incorporation of the hexafluorodimethylcarbinol group into an isoprene rubber which complements previous observations that rubbery coatings have higher absorption capacity for vapors. The poly(3,4-isoprene fluoroalcohols), PIPFA1 and PIPFA2, were synthesized by reacting poly(3,4-isoprene) with hexafluoroacetone presuming similar chemistry to occur as reported by Urry[11] for the reaction of perfluoroketones with terminal olefins. Multiple addition of hexafluoroacetone to the 3,4-isoprene repeat unit is possible.

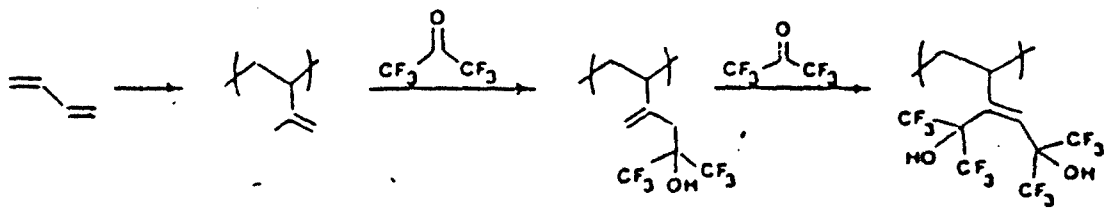

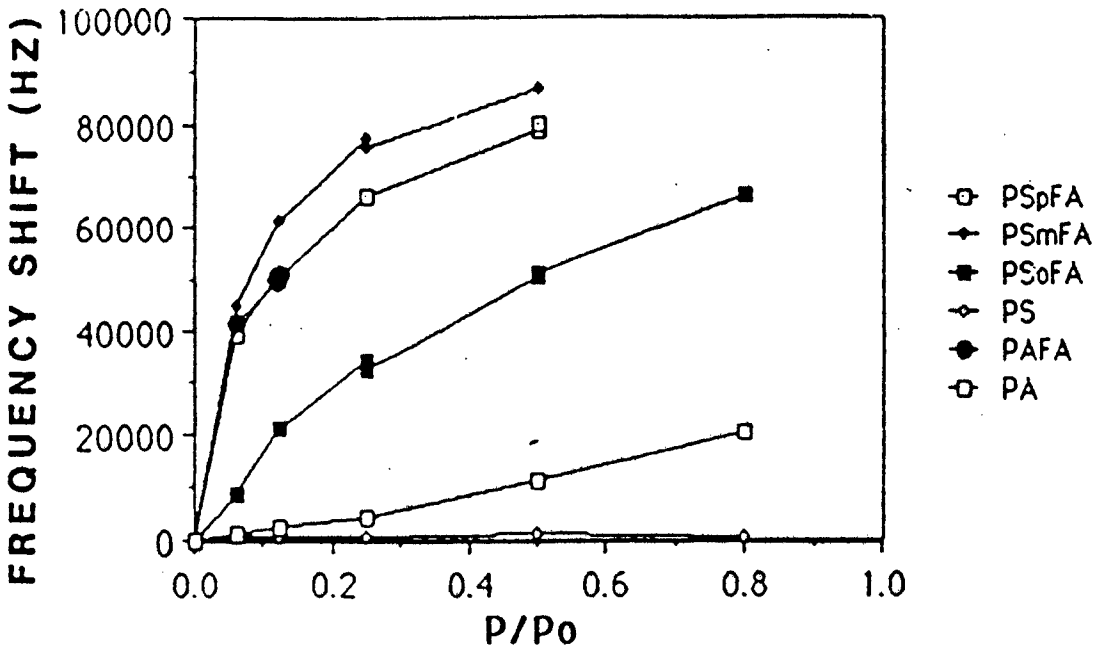

Figure 2. DMMP Absorption Isotherms for Polystyrene and Polyacrylate Fluoroalcohol and Control Coatings.

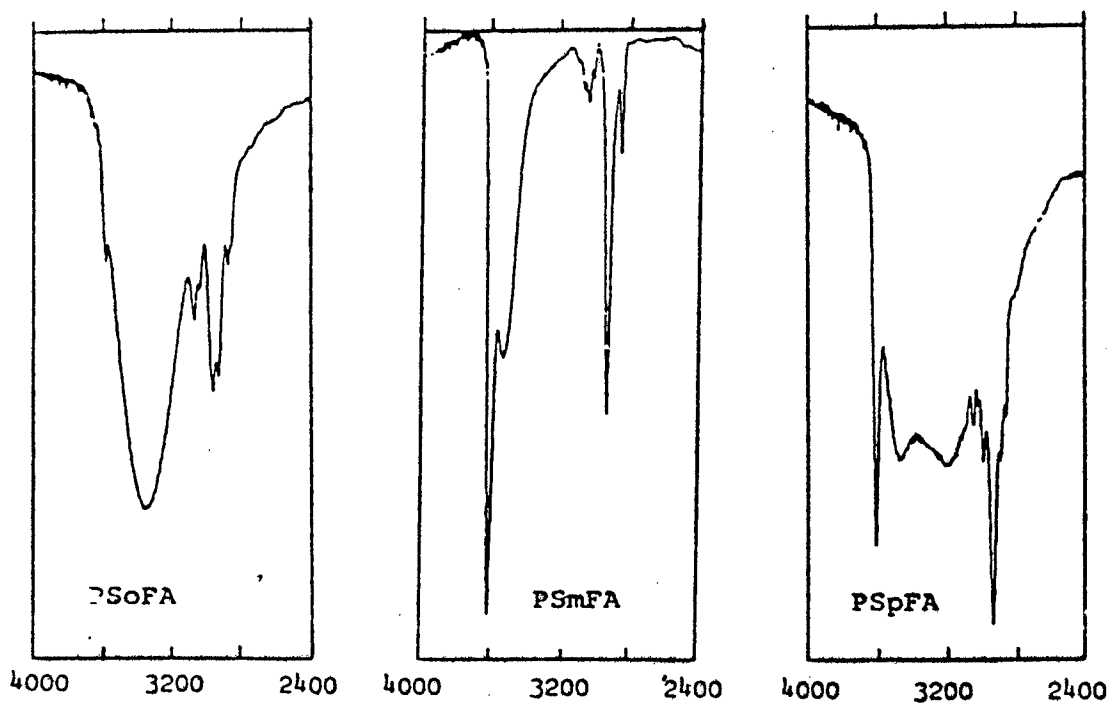

Figure 3. Infrared Spectra of Hydroxyl Region of Poly(styrene) Fluoroalcohols.

Two polymers were prepared: one with a high ratio of hexafluoroacetone to isoprene, PIPFA1, and one with a low ratio, PIPFA2.

DMMP vapor absorption isotherms were determined by depositing a thin film of polymer on a 158 MHz SAW device and measuring the frequency shift with varying DMMP vapor concentration up to 80% saturation at 25°C. This data for the polystyrene and polyacrylate series is presented in Figure 2. The SAW frequency shift may also be expressed as a weight percent of absorbed DMMP by dividing by the frequency shift caused by the film deposition mass. Typically, for strong 100 KHz DMMP shifts the corresponding weight percent of absorbed DMMP is 40%. The large enhancement resulting from incorporating the hexafluorodimethylcarbinol group in the polymer matrices is observed by comparison of the PS and PA controls with the corresponding fluoroalcohol polymers. For the polystyrene series, the order of DMMP sensitivity (meta > para > ortho) is paralleled by the intensity of free hydroxyl IR band at 3600 cm^{-1} (Figure 3). This observation indicates that a free hydroxyl is a stronger DMMP receptor site than one hydrogen bonded within the polymer matrix. Data for the polyisoprene fluoroalcohols is comparable in sensitivity to the polystyrene and polyacrylate fluoroalcohols but displays an isotherm crossover (Figure 4).

To further illustrate the effect of the fluoroalcohol group on DMMP absorption, FPOL and PSpFA were acylated and retested for DMMP absorption. The SAW isotherm data is presented in Figure 5. The effect of converting the hydroxyl to an acetate group is a marked lowering of the DMMP absorption particularly at the low concentration end of the isotherm as illustrated by the enormous difference in slopes. This is very important for detection applications directed at high sensitivities. The higher sensitivity of PSpFA may be an effect of a higher hydroxyl group density and stronger acidity although PSpFA is glassy while FPOL is rubbery.

The infrared spectra of FPOL and PSpFA, their acylated adducts and their DMMP vapor absorption provides additional molecular insight (Figures 6 and 7). As might be expected from steric considerations, the free hydroxyl content as indicated by the 3600 cm^{-1} band is substantially greater for PSpFA than for FPOL. However, the acylation reaction was nearly quantitative for FPOL and only approached 90% after 3 acylation cycles for PSpFA as indicated by the residual hyudroxyl band at 3400 cm^{-1}. The 1760 cm^{-1} carbonyl band of the acyl group is also prominent. When DMMP vapor is absorbed by FPOL or PSpFA, the free hydroxyl disappears and the hydrogen bonded hydroxyl band shifts from 3390 to 3370 cm^{-1} and from two bands at 3430 and 3200 to one at 3110 cm^{-1}, respectively. The most prominent DMMP band is at 1040 cm^{-1} as indicated by an arrow. When the

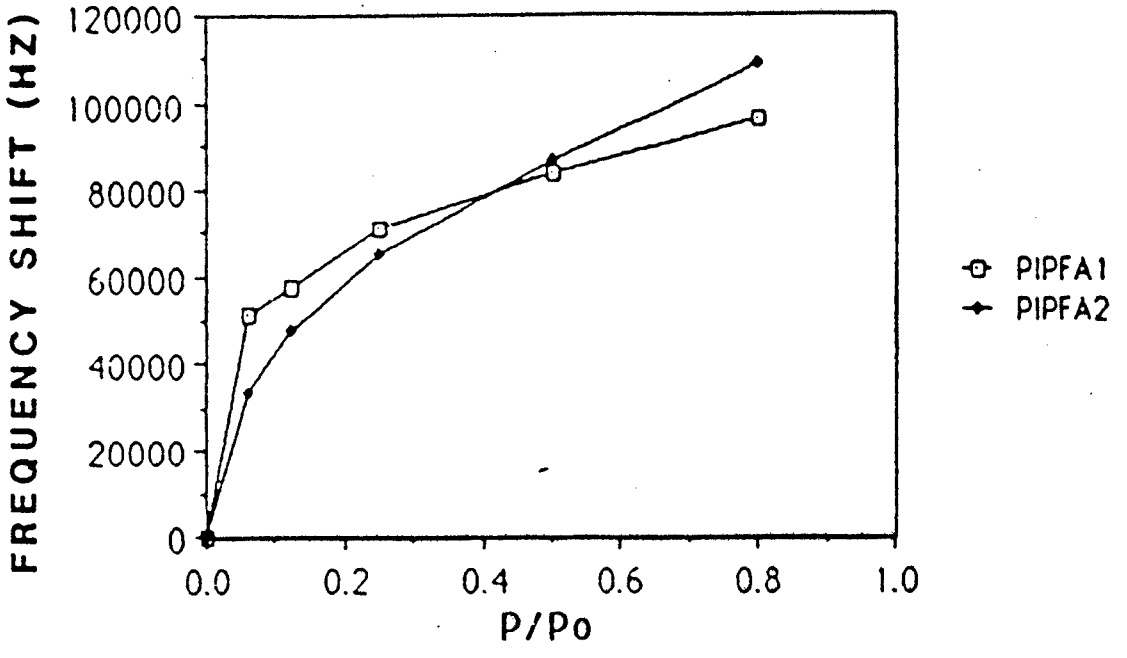

Figure 4. DMMP Absorption Isotherms for PIPFA1 and PIPFA2.

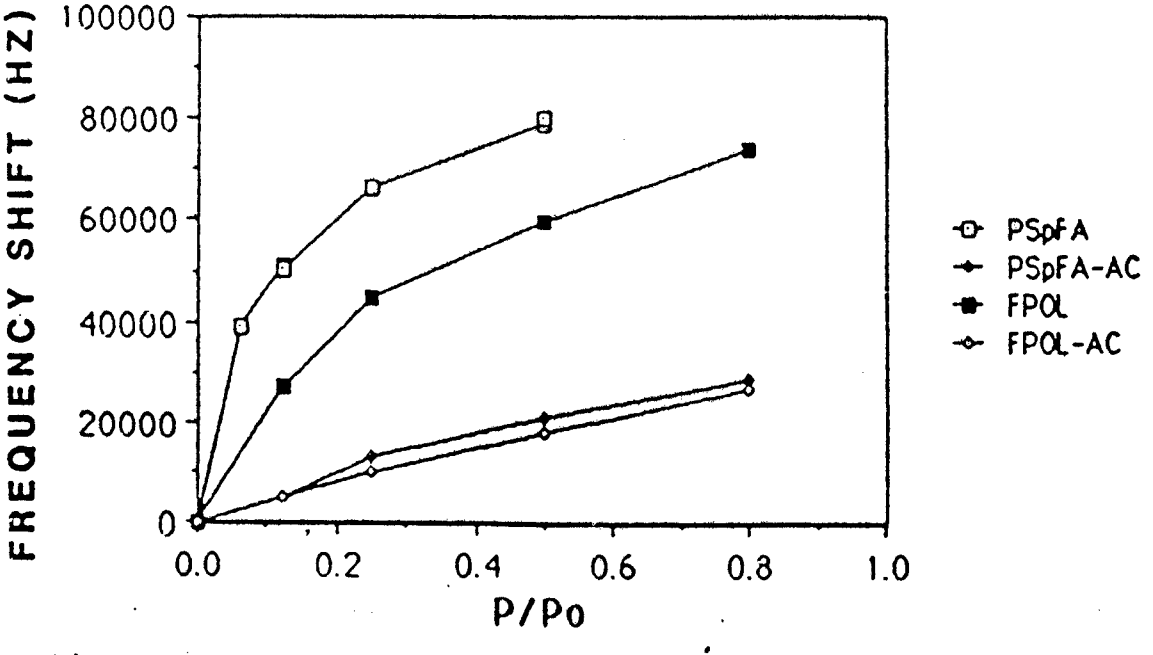

Figure 5. DMMP Absorption Isotherms for FPOL and PSpFA and their Respective Acylated Analogues.

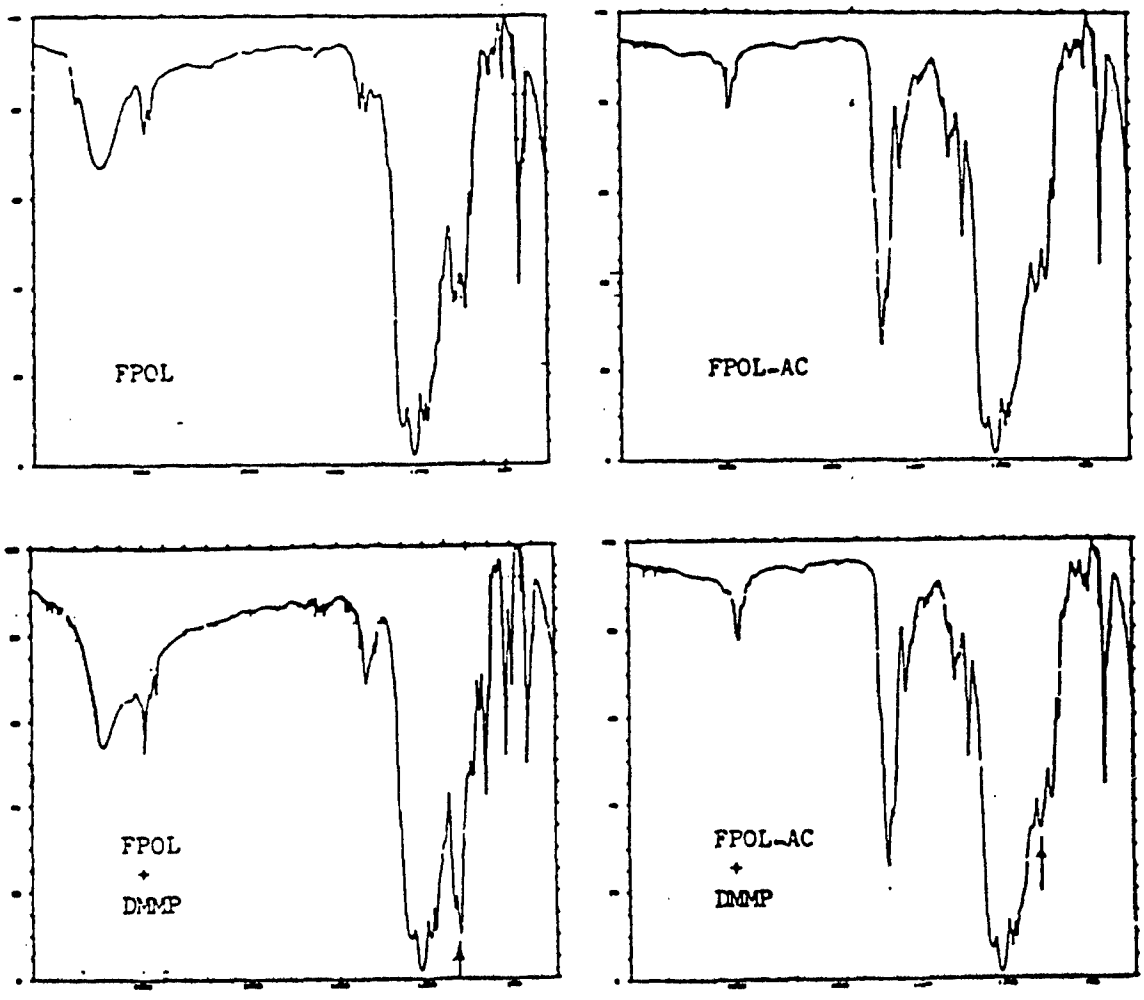

Figure 6. Infrared Spectra of FPOL, Acylated FPOL (FPOL-AC) and their Respective Absorption of DMMP Vapor.

acylated analogues are exposed to DMMP vapor, absorption is less as indicated by the intensity of the 1040 cm^{-1} band which is consistent with the SAW result above.

CONCLUSION

The hexafluorodimethylcarbinol group is a potent receptor site for DMMP. The polymer matrix to which it is attached does not strongly affect the DMMP absorption sensitivity as demonstrated by the polystyrene, polyacrylate and polyisoprene fluoroalcohol series. However, the free hydroxyl content should be maximized for highest sensitivity.

REFERENCES

1. Code 6120, Naval Research Laboratory, Washington, DC 20375-5000.

2. A. W. Snow, H. Wohltjen and N. L. Jarvis, 1982 Scientific Conference on Chemical Defense Research, AR-CSL-SP-83030, Aberdeen Proving Ground, MD, 1983, pp. 251-257.

3. N. L. Jarvis, J. Lint, A. W. Snow and H. Wohltjen, 1983 Scientific Conference on Chemical Defense Research, CRDC-SP-84014, Aberdeen Proving Ground, MD, 1984, pp. 45-54.

4. A. W. Snow, H. Wohltjen, J. Lint and N. L. Jarvis, 1984 Scientific Conference on Chemical Defense Research, CRDC-SP-85006, Aberdeen Proving Ground, MD, 1985, pp. 301-307.

5. A. W. Snow, D. S. Ballantine, T. Whitney, W. R. Barger, M. Klusty, H. Wohltjen, J.Gate and D. Chaput, 1986 Scientific Conference on Chemical Defense Research, CRDEC-SP-87008, Aberdeen Proving Ground, MD, 1987, pp. 695-703.

6. S. P. Ting, E. M. Pearce and T. K. Kwei, J. Poly. Sci. Poly. Lett. Ed. 18, 201 (1980).

7. J. W. Barlow, T. Wilmanns, D. R. Lloyd and P. E. Cassidy, 1984 Scientific Conference on Chemical Defence Research, CRDC-SP-85006, Aberdeen Proving Ground, MD, 1985, pp. 123-128.

8. D. E. Field, J. Paint Technology 48, 43 (1976).

9. E. M. Pearce, T. K. Kwei and B. Y. Min, J. Macromol. Sci. Chem. A21, 1181 (1984).

10. G. Natta, L. Porri and A. Carbanaro, Makromol. Chem. 77, 126 (1964).

11. W. H. Urry, J.H.Y. Niu and L. G. Lundstead, J. Org. Chem. 33, 2302 (1967).

12. H. Wohltjen, A. W. Snow, W. R. Barger and D. S. Ballantine, IEEE Translations on Ultrasonics, Ferroelectrics and Frequency Control, Vol. UFFC-34, No. 2, 172 (1987).

13. N. L. Jarvis and A. R. Katritzky, Final Report on Microsensors Workshop, March 6-7, University of Florida. Available from CRDEC, Aberdeen Proving Ground, MD.

Reprinted from Analytical Chemistry, 1986, 58, 2883.

Optical Waveguide Humidity Detector

David S. Ballantine*

Geo-Centers, Inc., Suitland, Maryland 20746

Hank Wohltjen

Microsensor Systems, Inc., P.O. Box 90, Fairfax, Virginia 22030

The relative humidity of ambient air can have a significant impact on many physical and chemical processes of industrial interest (*1–5*). As a result, research toward the development of sensitive and reliable humidity sensors has increased. Current developments have centered around either electronic devices (e.g., moisture-sensitive resistors, capacitors, or conductive cells), or colorimetric devices. The electronic sensors exhibit sensitivity to temperature as well as humidity, whereas colorimetric reagents, such as metal salts of Co^{2+}, Cu^{2+}, or V^{5+}, are highly selective for moisture with little or no temperature dependence. These colorimetric reagents are usually suspended in gels or in adsorbent paper. The extent of hydration is determined by visual inspections, which are highly subjective and nonquantitative.

The use of colorimetric reagents coated on an optical waveguide has been demonstrated (*6*). Such devices have the advantage of higher sensitivity and quantitative precision compared to visual methods. The use of an optical fiber sensor for humidity measurements has been described by Russell and Fletcher (*7*). They employed a cobalt chloride/gelatin film on a silica optical fiber as the humidity probe. These probes were attached to an optical system consisting of a visible light monochromator and a photodetector. While this system was useful in demonstrating the applicability of optical devices as humidity sensors, it is not practical for field applications.

In this work we describe an optical waveguide humidity sensor that also uses a cobalt chloride/polymer film. It utilizes small, inexpensive optical components that enhance the practical nature of the device for use in the field, or for other applications requiring a portable detector. Experimental results and response characteristics are presented, and possible improvements of the devices are discussed.

THEORY

The optical waveguide is related to internal reflection spectroscopy, which has been described in detail by Harrick (*8*). It takes advantage of the fact that light will propagate through a medium (i.e., a glass rod or optical fiber) by internal reflection. The lightwave can interact with a second material which is in contact with the reflecting surface of this medium. The degree of interaction is related to the angle and wavelength of the incident light and the refractive indexes of the two media.

If the refractive indexes of the waveguide and the coating material are nearly equal, then the lightwave is not reflected at the glass/film interface, but travels unimpeded into the film (see Figure 1). The lightwave would then be reflected at the film/air interface. If light is absorbed as it passes through the film, then the waveguide can be used for spectroscopic analyses. The more reflections that occur, the greater the degree of interaction of the lightwave with the film. The sensitivity of the device is thus a function of the length and thickness of the waveguide.

EXPERIMENTAL SECTION

A. Device Components. The waveguide humidity detector consists of an optical waveguide coated with a reagent/polymer film, a light source, a photodetector, and an associated electronics package.

The light sources used in this study were light emitting diodes (LEDs). They are relatively inexpensive, and commercially available in four spectral ranges (red, orange, yellow, green). Phototransistors were used as photodetectors. Like the LEDs, they are suitable for use in a small device, are relatively inexpensive, and commercially available. The spectral response of the phototransistors used in this study drops off dramatically below 600 nm, so only the red (660 nm) and orange (635 nm) LEDs were used as light sources.

The waveguide consisted of a thin-walled glass capillary tube (~1.0 mm o.d. × 90 mm long; 0.2 mm thick wall). One end of these capillary tubes was rounded off, which aided in focusing the transmitted light onto the phototransistor. Clear plastic rods were used to manufacture optical couplers that were bored to accommodate the individual components (see Figure 2). These couplers held the optical components in a rigid, reproducible geometry which eliminated the need to strictly control the wavelength or angle of incident light. In addition, these couplers enhanced the transmission of light from the LED to the waveguide, and from the waveguide to the phototransistor. Cells to hold the waveguide were fashioned out of plastic rods that were

0003-2700/86/0358-2883$01.50/0

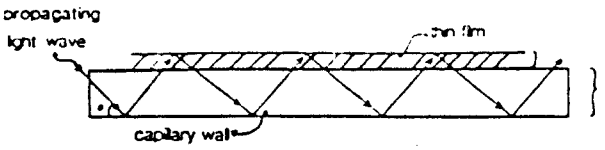

Figure 1. Diagram illustrating the interaction of an internally reflected lightwave with a thin film coated on the surface of a glass capillary waveguide.

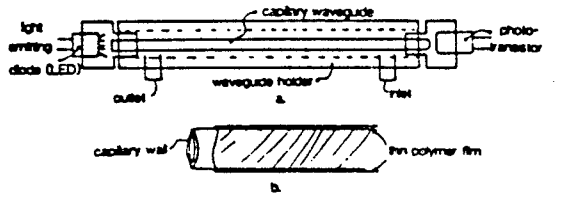

Figure 2. Diagram of the components comprising the optical waveguide detector.

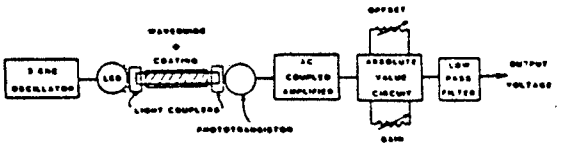

Figure 3. System diagram for the optical waveguide humidity detector.

bored to hold the optical components. These cells have a very small dead volume and were painted black to prevent the introduction of stray light.

The electronics package (Figure 3) consists of a modulated LED power source and signal processor which amplifies, demodulates and filters the phototransistor voltage. A 3-Hz RC timed, astable multivibrator circuit is used to pulse modulate the LED. Modulation of the light source is essential for reducing the effects of temperature drift in the phototransistor dark current. Without modulation, small variations in phototransistor temperature would produce unacceptable variations in the base line signal. The phototransistor signal was amplified by using an ac coupled op-amp and fed into an absolute value circuit and low pass filter which provided a dc voltage level proportional to the intensity of light striking the phototransistor. Small variations in light intensity produced by changes in the waveguide coating characteristics produced very easily measured changes in the output voltage of the electronics system. The system also was equipped with offset and gain controls to permit output signal adjustment to 0% and 100% transmittance conditions.

B. Reagent Films. The colorimetric reagent selected for testing with this device was $CoCl_2 \cdot 6H_2O$. The anhydrous salt ($CoCl_2$) is blue and exhibits a strong absorption peak between 600 and 750 nm. When hydrated, the absorption peak shifts to 500 nm, characteristic of the $CoCl_2 \cdot 6H_2O$ complex. This behavior is completely reversible and is well suited for probing with LEDs that produce 635–660 nm wavelengths of light.

Since the anhydrous cobalt chloride is a crystalline salt that does not readily adhere to the surface of the waveguide, it was suspended and immobilized in a poly(vinylpyrrolidone) (PVP) film. The PVP film has a refractive index of 1.53 (9), which is slightly greater than that of the soda lime glass waveguide (n_D = 1.49). Under these conditions, light would travel unimpeded through the glass/film interface and be reflected at the film/air interface. In addition, PVP is optically transparent in the wavelength region used for this study.

We were interested in determining the effect of various film parameters on the device response. For this reason, solutions were prepared in acetone/H_2O that contained varying concentrations of $CoCl_2 \cdot 6H_2O$ (from 30 mg/mL to 230 mg/mL). Known weights of poly(vinylpyrrolidone) (PVP) were then added to these solutions to produce solutions containing 0.75–3.0% (w/w) of PVP. In addition, solutions of just $CoCl_2 \cdot 6H_2O$ and just PVP were prepared to examine the effect of each component on the overall response.

Prior to coating with reagent/polymer films, the waveguides were etched for 5 min in a buffered, dilute HF solution. Reagent films were then applied using one of two different methods.

Table I. Film Reagent Concentrations and Reponse Characteristics

film label	$[CoCl_2 \cdot 6H_2O]$, mg/mL	% PVP (w/w)	100% T, mV	response time, s
AB 1	133	2.0	1900	57
AB 2	161	1.5	1200	51
AB 4	168	0.75	850	47
AB 5	67	1.0	825	49
AB 6	230	0.86	1210	70
AB 10	100	1.0	1250	52
AB 12	100	1.0	1720	47
AB 17	200[a]	1.5	3560	170
AB 18	200[b]	1.5	2450	88
DIP 1	30	1.0	2430	66
DIP 10	100	1.0	1710	52

[a]Thick. [b]Thin.

The first method involved dip-coating the waveguides by immersing them in a solution and slowly withdrawing them. As the solvent was evaporated with a heat gun, a light blue film of $CoCl_2$/PVP was deposited on the surface of the waveguides. The second method involved using an air brush to spray a light mist of reagent/solvent on the waveguide surface, which was then dried using a heat gun. The films produced by dip coating were thicker, and contained areas of high $CoCl_2$ concentrations, indicated by spots of darker blue color. Air brush films were generally thinner and more evenly distributed. Waveguides coated with these films were exposed to varying concentrations of water vapor at 22 °C. The introduction of water vapor to the cell, and the acquisition of response data were controlled by the computer system described below.

C. Analytical System. A gas handling system was designed and constructed to control the introduction of vapor and/or diluting air to the sensor. Flow rates of water-saturated air and dry air were controlled with variable rotameters. Introduction of clean, dry air or water-saturated air to the sensor was controlled by solenoid valves which had been interfaced to an Apple IIe microcomputer via the I/O game-controller. The percent relative humidity of water-saturated air was assumed to be ~95% when calculating the relative humidity of diluted vapor streams.

Voltage data from the phototransistor were collected by the Apple II via an A/D converter card. Voltage vs. time data were plotted by using our own data acquisition program.

Before data were collected, a waveguide was inserted into the holder assembly, the LED was turned off, and the zero adjustments were made. The LED was then turned on, and the null adjustment was used to produce an output voltage just greater than 0 V. The device was then ready for testing.

RESULTS AND DISCUSSION

Response characteristics and film properties are listed in Table I. Individual films are identified as air-brushed films (AB) or dipped films (DIP). Examples of typical humidity reponse curves are given in Figure 4. In general, the response follows an S-shaped curve, with percent transmission increasing rapidly in the range of 60–85% relative humidity (RH), and then gradually leveling off as 100% RH is approached. This behavior holds true for all $CoCl_2$/PVP films.

Films of PVP alone exhibited no significant response to water vapor. It appears that the polymer film serves two purposes; first, it acts as a binder to ensure long life and good contact between the reagent film and the waveguide surfaces, and second, it acts as a protective, semipermeable membrane to regulate the introduction of water vapor to reagent. Films containing $CoCl_2$ alone exhibited poor adherence to the waveguide surface. Signal losses were noted, which may be the result of light scattering off $CoCl_2$ crystals.

To determine the effect of film variables on response, response times were determined for each film and are summarized in Table I. These response times represent the time required for the device response to level off at a maximum

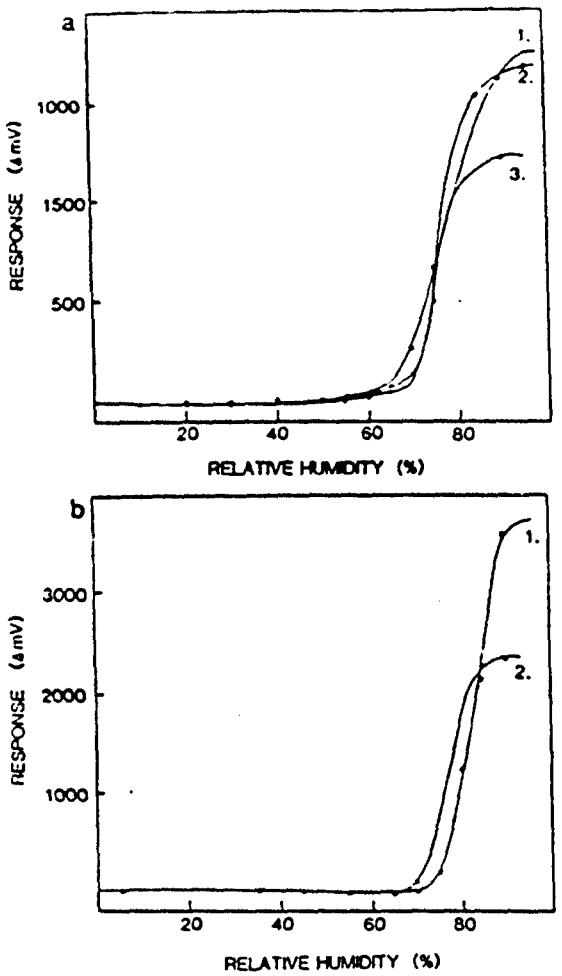

Figure 4. These S-shaped curves are typical of the waveguide device response (ΔmV) vs. percent relative humidity (% RH). (a) Films prepared from solutions of 100 mg/mL $CoCl_2$ and 1.0% PVP. Curves are for the following films: (1) DIP 10; (2) AB 12; (3) AB 10. (b) Films prepared from solutions of 200 mg/mL $CoCl_2$ and 1.5% PVP. Curves are for the following films: (1) AB 17; (2) AB 18.

value upon exposure to an air stream of 95% RH. The two variables examined were film thickness and cobalt chloride concentration.

To determine the effects of film thickness, response times for films prepared from the same solution were compared. Figure 4a shows response curves for three (3) films prepared from a solution 100 mg/mL of cobalt chloride and 1.0% (w/w) of PVP. Figure 4b shows response curves for two films prepared from a solution of 200 mg/mL cobalt chloride and 1.5% PVP. It is worth noting that while the maximum signals vary, the relative shapes of these curves are very similar.

Since the films in each case were prepared from the same respective solutions, any difference in response times should be due to difference in film thickness. A qualitative assessment of relative film thicknesses can be made by comparing maximum signals (100% T); thicker film containing more $CoCl_2$ would exhibit a larger difference between 0% and 100% T.

For the three films represented in Figure 4a, no appreciable difference in response times is observed, even though the maximum signals differ by 30%. For the films represented in Figure 4b, however, there is an obvious increase in response time with film thickness. The data also indicate some dependence of response time on $CoCl_2$ concentration for some films but this effect is not as strongly indicated as the effect of film thickness.

The dependence of response time on film thickness is readily explained, in that it takes longer for a thick film to become saturated and reach equilibrium with water vapor than for a thin film. For films with high concentrations of cobalt chloride, it is possible that microcrystals of the metal salt have formed within the film. Such microcrystals may be responsible for the increased response times observed for some films containing high concentrations of $CoCl_2$.

CONCLUSIONS

The waveguide humidity sensor presented here exhibits very good sensitivity in the range of 60–95% RH. The general response data follow an S-shaped curve, and are comparable to the results obtained by Russell and Fletcher. Our results indicate that the portable, inexpensive device described here can be used to obtain reliable humidity measurements.

Before the device can be utilized as a throw-away device, better agreement between individual waveguides is necessary. This involves applying uniform, reproducible films on individual capillary waveguides. The device could then be developed as is for use in specific cases where the desired humidity levels are within the range of good response.

Further development of the reagent/polymer film may extend the region of reliable response of the present device. Such film development could include the use of polymer/copolymer films of different hygroscopicity (e.g., poly(vinyl alcohol) (PVA) or poly(styrenesulfonic acid) (PSSA), or combinations of different metal salts as reagents.

In addition, some form of temperature monitoring or control would be desirable to facilitate conversions from parts per million (H_2O) to percent relative humidity and vice versa.

ACKNOWLEDGMENT

Work was performed in the Chemistry Division, Code 6170, Naval Research Laboratory, Washington, DC 20375-5000.

Registry No. $CoCl_2$, 7646-79-9.

LITERATURE CITED

(1) Meade, K. E.; Auerbeck, I; and Erickson, R. H. *Org. Coat. Plast. Chem.* **1981**, *44*, 336–342.
(2) Allred, R. E.; Reylance, D. K. *J. Mater. Sci.* **1983**, *18*, 852–856.
(3) McMurray, P. M.; Wilson, J. C. *J. Geophys. Res.* **1983**, *88*, 5101–5108.
(4) Ferron, G. A. *J. Aerosol Sci.* **1977**, *8*, 251–267.
(5) Tanto, J.; Ambrus, A; and Visi, E. *Pestic. Chem.: Hum. Welfare Environ., Proc. Int. Congr. Pestic. Chem., 5th, 1982* **1983**, *4*, 129–134.
(6) Giuliani, J. F.; Wehlburg, H.; Jarvis, N. L. *Opt. Lett.* **1983**, *8*, 54–56.
(7) Russell, A. P.; Fletcher, K. S. *Anal. Chim. Acta* **1985**, *170*, 209–216.
(8) Harrick, N. J. *Internal Reflection Spectroscopy*; Interscience: New York, 1967.
(9) *Polymer Handbook*; Bandrup, J., Immergut, E. H., Eds.; Wiley: New York, 1974; pp 111–243.

RECEIVED for review August 27, 1985. Resubmitted May 30, 1986. Accepted June 10, 1986. This research was supported in part by USAFSAM, San Antonio, TX 78235.

Reprinted from LANGMUIR, 1986, 2, 513.

Simultaneous Electrical Conductivity and Piezoelectric Mass Measurements on Iodine-Doped Phthalocyanine Langmuir–Blodgett Films

Arthur W. Snow,* William R. Barger, and Mark Klusty

Naval Research Laboratory, Washington, D.C. 20375

Hank Wohltjen

Microsensor Systems Inc., Fairfax, Virginia 22030

N. Lynn Jarvis

Chemical Research and Development Center, Aberdeen Proving Ground, Maryland 21005

Received January 14, 1986. In Final Form: March 18, 1986

Mixed mono- and multilayer L–B films of tetrakis(cumylphenoxy)phthalocyanine compounds and stearyl alcohol were transferred to a dual 52-MHz surface acoustic wave (SAW) device for simultaneous measurement of the electrical conductivity and mass changes caused by doping with iodine vapor. The conductivity increased by 4 orders in magnitude, and a complex formation stoichiometry of two to four iodine atoms per phthalocyanine ring was measured. Variation of the complexed central metal ion, which included cobalt, nickel, copper, zinc, palladium, and platinum as well as hydrogen, had very little effect on either the magnitude of the conductivity increase or the complex stoichiometry. The measured conductivity increased with increasing film thickness but approached a constant value when the film became thicker than the planar interdigital microelectrode. The quantity of iodine a phthalocyanine film may absorb is dependent on the film morphology, while the magnitude of the conductivity increase is nearly independent of the morphology.

Introduction

Thin films of phthalocyanine compounds, in general, and those prepared by the Langmuir–Blodgett (L–B) method, in particular, display novel electrical properties.[1] The L–B technique for depositing mono- and multilayer coatings with well-controlled thickness and morphology offers excellent compatibility with microelectronic technology. Such films have recently been reviewed for their potential applications.[2] The combination of L–B supramolecular films with small dimensionally comparable microelectronic substrates affords new opportunities for generation of fundamental chemical property information and evaluation of new organic thin film semiconductors as microelectronic components. In this work an interdigital microelectrode array and surface acoustic wave (SAW) device are used in combination to obtain electrical conductivity and piezoelectric mass measurements on the iodine doping of metal-substituted and metal-free phthalocyanine–stearyl al-

(1) Baker, S. *Proceedings of International Syumposium on Future Electron Devices*; Bioelectronic and Molecular Electronic Devices, Tokyo, Nov, 1985; pp 53–58.

(2) Roberts, G. G. *Sens. Actuators* **1983**, *4*, 131.

0743-7463/86/2402-0513$01.50/0

cohol mixed mono- and multilayer L–B films. The phthalocyanine–iodine doping combination represents a model system for studying the electrical response of thin-film organic semiconductors to vapors since this system has been intensively studied by using bulk polycrystalline and single-crystal samples.[3] The phthalocyanine–iodine complex formation is accompanied by a large increase in electrical conductivity. The issues of interest in the current experimental work involving exposure of a L–B film composed of a peripherally substituted phthalocyanine compound to iodine vapor are (1) magnitude of the conductivity change, (2) phthalocyanine ring/iodine stoichiometry, (3) capability of making both the conductivity and mass measurements simultaneously on the same film, (4) dependence of measured responses on the complexed central metal ion, (5) dependence of measured responses on L–B film thickness (number of monolayers) and comparison with the planar interdigital electrode thickness, and (6) effect of morphological variation by comparison of the L–B film with a fused L–B film and a "sprayed on" film.

Previous work has shown that the tetrakis(cumylphenoxy)-substituted phthalocyanine compounds used in this work (see Figure 1) exist as oligomeric cofacially oriented aggregates in solution and form L–B films with the aggregate size and force–area curves that depended on the phthalocyanine-complexed metal ion.[4] As mixed monolayers with stearyl alcohol, multilayer L–B films of these compounds have been transferred to interdigital microelectrodes and investigated as a chemiresistor system for parts per million level detection of trace concentrations of ammonia.[5] The morphology of these films has been studied by using resonance Raman,[6] copper ESR anisotropy,[7] and force–area solvent dependence[8] characterization. At other laboratories, L–B films of phthalocyanine compounds with different peripheral substituents have been reported with interest directed at both film morphology[9] and device applications.[2,10]

Experimental Section

Metal-free, copper, zinc, platinum, palladium, cobalt, and nickel tetrakis(cumylphenoxy)phthalocyanines were synthesized and purified as described previously.[4] Stearyl alcohol, (1-octadecanol, 99.5%, LaChat) and chloroform (reagent grade, Fisher) were used as received. Monolayer spreading solutions with a 1:1 molar ratio of phthalocyanine/stearyl alcohol were prepared at a concentration 4×10^{-4} M in chloroform.

Film pressure vs. area isotherm measurements and film depositions on electrodes were carried out in a constant temperature (25 °C) room using a computer-controlled thermostated Langmuir trough designed and constructed in our laboratory. The 14 cm wide × 82.5 cm long × 3 mm deep paraffin-coated trough with a 6.0 cm diameter, 7.5 cm deep well near one end was interfaced to an Apple II-E microcomputer which read surface tension from a Gould UC-2 strain gauge carrying a 1.7 cm wide platinum foil Wilhelmy plate. Motors for controlling the bar to put pressure on the film and for dipping the device being coated were controlled by the microcomputer. A simplified illustration of this apparatus using a trough of slightly different dimensions is described in ref 5, and more detail on the present configuration trough is reported in ref 8. Water, triply distilled with the last two distillations from an all-quartz still, was used as the subphase. Film-transfer operations began with the substrate submerged. The device being coated was allowed to dry in air for 5 min after each down–up cycle. The dipping velocity was 4.2×10^{-4} m/s.

The device used to perform the measurements reported in this study is a dual 52-MHz surface acoustic wave device (Microsensor Systems, Inc.). This device consists of a piezoelectric quartz (ST cut) slab measuring 1.5 × 2.5 cm on which four interdigital microelectrodes have been fabricated by using optical lithography (see Figure 3). The electrodes were fabricated from gold deposited on a thin layer of titanium to provide adhesion to the quartz. Each electrode consists of 50 finger pairs with the following dimensions: spacing, 15 μm; finger width, 15 μm; overlap length 4800 μm; center-to-center spacing of transmitter–receiver electrode pair, 1 cm; electrode thickness, 760 Å (measured by Nomarski phase contrast microscopy). After removing the residual photoresist by washing with acetone, the device was dipped in a chromic acid cleaning solution for 2 min and rinsed with distilled water, acetone, and chloroform. Immediately before transfer of the films, the devices were cleaned by Soxhlet extraction with chloroform.

After it was coated with a multilayer film, the device was mounted in a machined Delrin housing in which provision had been made for metal pressure clip connection to the electrodes as well as for passage of regulated quantities of iodine vapor through entrance and exhaust ports directly above the device (see Figure 4). The SAW frequency measurement was performed by connecting a pair of interdigital transducers on one side of the device to a wide-band rf amplifier. The resulting circuit oscillated at a resonant frequency determined by the interdigital electrode spacing and the Rayleigh wave velocity. The resonant frequency was monitored by using a digital frequency counter (Fluke Model 1910A). See ref 11 for additional SAW frequency measurement detail. The conductivity measurement was made by application of a 1-V bias to either of the two remaining electrodes and measurement of the current using a precision current to voltage converter consisting of an operational amplifier (Analog Devices #515) and a switch selectable feedback resistor.

The mechanism of the SAW frequency measurement and its porportionality to mass on the substrate surface have been discussed elsewhere.[11] Briefly described, a radio-frequency (rf) voltage is applied to the transmitter electrode of the transmitter–receiver interdigital electrode pair to generate a mechanical Rayleigh surface wave on the piezoelectric quartz substrate. This wave propagates across the surface to the receiver electrode and is converted back into an rf voltage. Connection of this electrode pair through a rf amplifier makes the device oscillate at a resonant frequency determined by the interdigital electrode spacing and the Rayleigh wave velocity. Coating the device with a thin film causes a substantial reduction of the Rayleigh wave velocity and a corresponding decrease in the resonant frequency of the device. Vapor absorption further alters the mass and mechanical properties of the coating thereby producing easily measured frequency shifts. For most organic films, the modulus is small, and the mechanical property contribution to the frequency shift is negligible, leaving the frequency shift proportional to the mass change. This measurement assumes the conductivity of the film is too low to electrically short the electrodes or couple with the electric field of the propagating Rayleigh wave.

The conductivity measurement has been described more extensively elsewhere.[5] The important features are an ohmic contact with the film and an electrode spacing and a geometry to facilitate measurement of very low conductances. The gold electrode material satisfies the ohmic contact requirement. Current–voltage plots for the phthalocyanine L–B films of this study were linear over a ±1-V range analogous to that reported previously for a copper (cumylphenoxy)phthalocyanine/stearyl alcohol 45-layer film.[5] The sensitivity of the conductivity measurement is en-

(3) Marks, T. J.; Kalina, D. W. In *Extended Linear Chain Compounds*; Miller, J. S., Ed.; Plenum Press: New York, 1982; Vol. 1, pp 197–331.
(4) Snow, A. W.; Jarvis, N. L. *J. Am. Chem. Soc.* 1984, *106*, 4706.
(5) Wohltjen, H.; Barger, W. R.; Snow, A. W.; Jarvis, N. L. *IEEE Trans. Electron Devices* 1985, *ED-32*, 1170.
(6) DiLella, D. P.; Barger, W. R.; Snow, A. W.; Smardzewski, R. R. *Second International Conference on Langmuir–Blodgett Films*; Schenectady, NY, 1985; *Thin Solid Films* 1986, *133*, 207.
(7) Pace, M. D.; Snow, A. W.; Barger, W. R. *27th Rocky Mountain Conference, 8th, Int. EPR Symposium*, Denver, July, 1985.
(8) Barger, W. R.; Snow, A. W.; Wohltjen, H.; Jarvis, N. L. *Second International Conference on Langmuir–Blodgett Films*, Schenectady, NY, 1985; *Thin Solid Films* 1986, *133*, 197.
(9) (a) Kovacs, G. J.; Vincett, P. S.; Sharp, J. H. *Can. J. Phys.* 1985, *63*, 346. (b) Fryer, J. R.; Hann, R. A.; Eyres, B. L. *Nature (London)* 1985, *313*, 382. (c) Baker, S.; Petty, M. C.; Roberts, G. G.; Twigg, M. V. *Thin Solid Films* 1983, *99*, 53.
(10) (a) Baker, S.; Roberts, G. G.; Petty, M. C. *Proc. IEEE* 1983, *130*, 260. (b) Batey, G.; Petty, M. C.; Roberts, G. G.; Wight, D. R. *Electron. Lett.* 1984, *20*, 489.

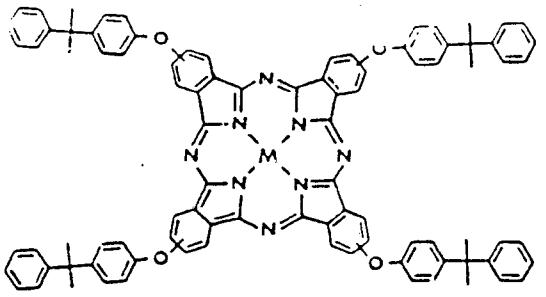

M = H_2, Co, Ni, Cu, Zn, Pd, Pt

Figure 1. Molecular structure of tetrakis(cumyulphenoxy)-phthalocyanine compounds. The cumyulphenoxy substitution is at either the 2- or 3-position of each bingo ring in the phthalocyanine compound.

hanced by the interdigital electrode's large perimeter and small electrode spacing. To normalize the measured conductance to a bulk conductivity, the conductance is divided by the ratio of the cross-sectional area (determined by the number of electrode "fingers", the overlap length and either the electrode thickness or the L–B film thickness whichever is smaller) to the electrode separation distance.

A simple iodine-generating apparatus was constructed from a 1-L flask (in which iodine crystals saturated the atmosphere), nitrogen source, flow meter, and regulating needle valve (see Figure 4). The nitrogen flow rate was set at 20 mL/min. The rate of iodine delivery under these conditions was 0.3 mg/200 s as measured colorimetrically (λ_{max} = 516 nm, log ϵ = 2.96) by trapping the iodine vapor in carbon tetrachloride for several 200-s intervals. An iodine exposure experiment consisted of initially bypassing the iodine reservoir flask for the first 100 s to establish conductivity and SAW frequency measurement base lines. This was followed by diversion of the nitrogen flow through the iodine reservoir for 2400 s to obtain exposure data followed by a second bypassing of the iodine reservoir to obtain desorption data. Conductivity and SAW frequency measurements were simultaneously recorded at either 50- or 100-s intervals depending on the rate of change. The iodine desorption was allowed to continue overnight. The SAW frequency change attributable to the L–B film was then measured by removing the top of the device housing, recording the frequency, and, then, very carefully removing the L–B film from the active area of the SAW device (area including and between transmitter and receiver electrode pair) with a chloroform wetted cotton-tipped swab until a constant value was obtained.

The differential scanning calorimetry thermograms were obtained using a Perkin-Elmer 7 Series thermal analysis system. Samples were prepared by transferring a metal-free phthalocyanine/stearyl alcohol film (183 layers) onto six covers of aluminum DSC sample pans (6.5-mm diameter) which corresponds to a total transferred mass of about 0.2 mg. The six coated covers were stacked in a sample pan and run against an uncoated blank over a temperature range 25–100 °C in a nitrogen atmosphere at a heating rate of 10 °C/min.

A "sprayed on" metal-free phthalocyanine–stearyl alcohol film was applied to a 52-MHz, dual SAW device using a Badger air brush (Model 200) and an phthalocyanine–stearyl alcohol (1:1 mol ratio) solution in chloroform. The device was positioned about 8 in. from the air brush nozzle, and the film was sprayed on using the finest spray setting with 1-s passes until a film of comparable appearance to the 45-layer L–B film was obtained.

Results and Discussion

Preparation and Transfer of Phthalocyanine L–B Films. Synthesis and purification of the phthalocyanine compounds (see Figure 1 for structures) and their monolayer formation have been reported elsewhere.[4] As pure one-component monolayers, films of these compounds do not transfer with good uniformity or deposition ratios.

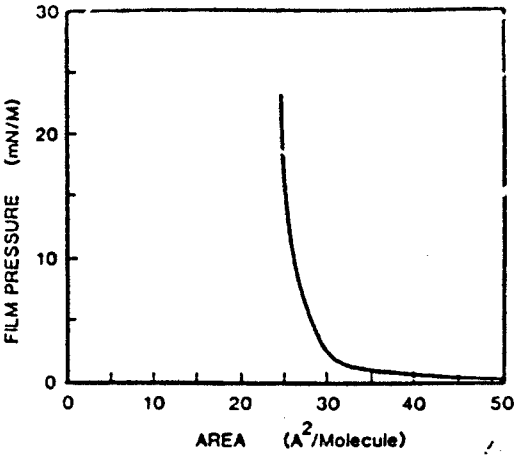

Figure 2. Force–area diagram of a 1:1 copper tetrakiscumylphenoxy)chthalocyanine/stearyl alcohol mixed monolayer.

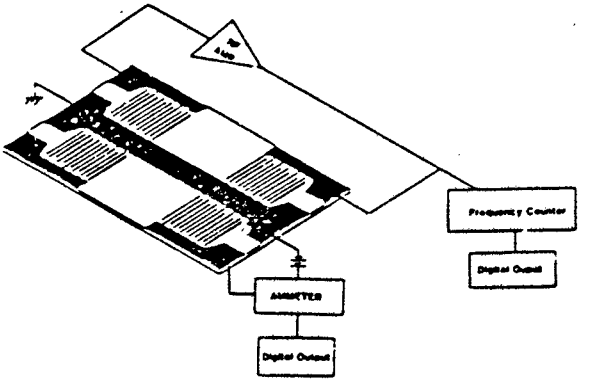

Figure 3. Dual 52-MHz SAW device used for simultaneous mass and conductivity measurements on L–B films.

Subsequent work has shown that addition of stearyl alcohol improves the transfer characteristics without adversely affecting the electrical properties.[5,8]

In this work films were prepared as 1/1 molar mixtures of phthalocyanine/stearyl alcohol and transferred at film pressures of 20 mN/m to quartz (with gold interdigital electrodes deposited for conductivity and SAW measurements) and aluminum substrates (for differential scanning calorimetry (DSC) measurements) with good deposition ratios (e.g., between 0.8 and 1). The force–area diagram of a copper phthalocyanine–stearyl alcohol mixed monolayer is presented in Figure 2 as a typical example. The analysis of the force–area diagrams has been presented elsewhere.[8] In contrast to a facile transfer of the mixed phthalocyanine–stearyl alcohol films, attempts to transfer pure stearyl alcohol films for control experiments were frustrated by poor deposition ratios (e.g., 0.3). Varying the film-transfer pressure or making the subphase strongly alkaline (pH of 11) did not improve this deposition ratio. Consequently, the quality of the transferred pure stearyl alcohol films is not equivalent to that of the mixed films. This difference in behavior is not understood at this time.

Dual Conductivity and SAW Frequency Measurements. Simultaneous measurements of phthalocyanine L–B film conductivity and mass changes during iodine doping were made using a dual 52-MHz SAW device. This device consists of two pairs of interdigital microelectrodes deposited on a piezoelectric quartz surface (see Figure 3). One pair of the electrodes is used for the SAW frequency (L–B film mass) measurement, and either of the remaining two is used for the conductivity measurements. Use of a SAW device to measure coating mass and changes in

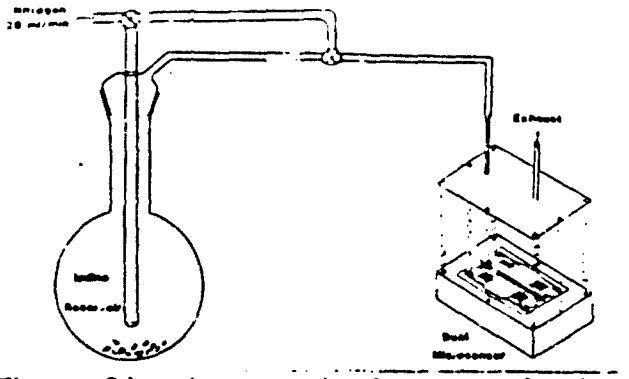

Figure 4. Schematic representation of apparatus used for the iodine-doping experiment.

coating mass has been discussed in detail elsewhere[11] and is briefly summarized in the Experimental Section. The important feature is the proportionality between the SAW frequency shift and coating mass. In this work, this relationship is demonstrated by the linear dependence of the SAW frequency shift on the number of monolayers in the L-B coating film (see Figure 7). The microelectrode conductivity measurement has been described more extensively elsewhere[5] but is also briefly summarized in the Experimental Section. Its important features are an ohmic contact with the film and an electrode spacing and geometry to facilitate measurement of very low conductances at low (1 V) bias voltages.

Combination of the conductivity and SAW frequency measurements into a single device for simultaneous measurements on the same coating is a new sensing technique. Further, SAW frequency measurements on L-B films have not been previously reported. The phthalocyanine L-B film–iodine vapor doping system is a particularly good system for testing the measurement technique in that the chemistry of closely related phthalocyanine–iodine bulk systems is being intensively investigated,[3] and the magnitude of signals, i.e., a large conductivity change due to iodine doping (as extrapolated from bulk phthalocyanine–iodine systems[3]) and a large SAW frequency shift due to the high molecular weight of iodine, should be easily measured.

The iodine-doping experiment was conducted using the apparatus schematically represented in Figure 4. A saturated atmosphere of iodine in nitrogen could be switched on and off for delivery to a small dead-volume chamber which housed the L-B film coated device and the electrical contacts. Absorption and desorption of iodine with consequent conductivity and mass changes of the film were monitored over a 4500-s period by measuring current and SAW frequency shifts. A typical example of these data are presented in Figure 5 for a 45-layer copper phthalocyanine film. The iodine reservoir was bypassed during the initial 100 s to establish a base line, and then the iodine flow was switched on for 2400 s. During this time all of the films tested reached a saturated or maximum conductivity level. Over the 2500–4500-s interval the iodine reservoir was again bypassed, and the iodine desorption was monitored.

It is readily apparent that the iodine vapor absorption continues after the conductivity has reached its saturation maximum. The charge-transfer interaction of iodine involves transfer of an electron from the phthalocyanine ring and formation of the triiodide anion (eq 1). The absorption is complicated in that the charge-transfer reaction is not quantitative,[3] and additional iodine may be absorbed as molecular iodine or in formation of the pentaiodide anion (eq 2).

$$2Pc + 3I_2 \rightleftharpoons 2Pc^+I_3^- \quad (1)$$

$$I_2 + I_3^- \rightleftharpoons I_5^- \quad (2)$$

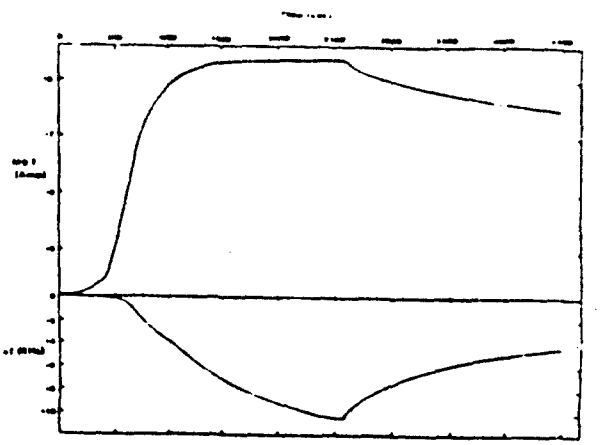

Figure 5. Measurement of current and SAW frequency changes as a function of time caused by iodine doping of a 45-multilayer cooper phthalocyanine–stearyl alcohol L-B film supported on a dual 52-MHz SAW device.

The experimental measurements of interest from the data are Δf_0, the SAW frequency shift attributable to the L-B film, I_0, the initial current passing through the film in a nitrogen atmosphere, I_{max}, the maximum current passing through the film after iodine doping, and Δf_I, the frequency shift caused by absorbed iodine where the current value approaches that of I_{max}.

Since the current and frequency measurements are being made simultaneously on the same film, the current change may be related directly to the iodine content. The bulk conductivity of the film, σ, may be calculated from the microelectrode's geometry and dimensions and the bias voltage:

$$\sigma = \frac{J}{E} = \frac{I/A}{V/d} = \frac{I}{V}\frac{d}{(2n-1)lh}$$

where J is the current density, E is the electric field, I is the measured current, V is the bias voltage, A is the cross-sectional area between electrodes, and d is the electrode spacing. If the L-B film is thick enough to fill the channel between the electrode "fingers", then A may be calculated as the product of the number of channels between the electrode "fingers", $2n - 1$ (n is the number of electrode "finger pairs"), the overlap length of the electrode "fingers", l, and the electrode thickness or height, h. It is also possible to calculate a ratio of moles of absorbed iodine to moles of phthalocyanine ring, X in $(MPcCP)I_x$, by using the proportionality between SAW frequency shift and film mass and the relative concentration of the phthalocyanine and stearyl alcohol film components:

$$X = \frac{\Delta f_I / M_I}{W_{Pc}(\Delta f_0 / M_{Pc})}$$

where Δf_I is the SAW frequency shift attributable to absorbed iodine, Δf_0 is the SAW frequency shift attributable

(11) (a) Wohltjen, H. "Mechanism of Operation and Design Considerations for Surface Acoustic Wave Device Vapor Sensors"; NRL Memorandum Report 5314; Naval Research Laboratory: Washington, DC, 1984; ADA 141537. (b) Wohltjen, H. *Sens. Actuators* 1984, *5*, 307.

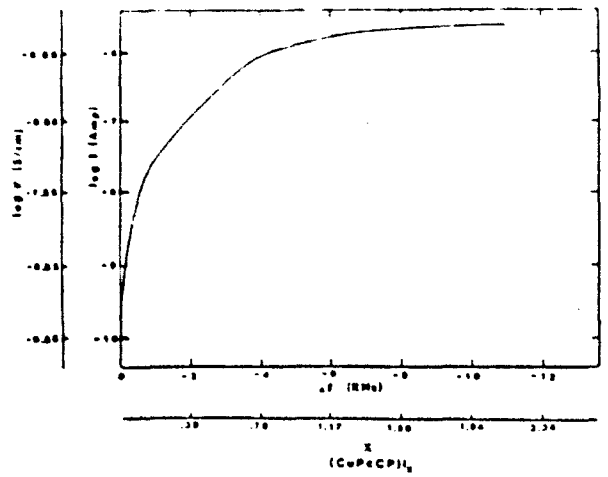

Figure 6. Dependence of conductivity on quantity of absorbed iodine for a 45-layer L–B film of mixed copper phthalocyanine–stearyl alcohol (1:1 mole ratio).

to the L–B film, W_{Pc} is the weight fraction of the phthalocyanine component, M_I is the atomic weight of iodine, and M_{Pc} is the molecular weight of the phthalocyanine component in the film. As presented in Figure 6 for the 45-layer copper phthalocyanine example, the experimental quantities of current and SAW frequency shift or the calculated quantities of conductivity and stochiometric iodine content may be plotted as is traditionally found for phthalocyanine-doping experiments. Typically, the conductivity increases by 4 orders in magnitude from 10^{-10} to 10^{-6} S/cm as a stoichiometric ratio of 2:1 iodine/phthalocyanine is approached. While this conductivity change is significant, it is not nearly as large as the 10 orders of magnitude reported for pressed-pellet samples of pure unsubstituted phthalocyanine compounds with comparable iodine doping. Considering the relatively large size of the cumylphenoxy substituent groups, the mixed-isomer nature of the tetrakis(cumylphenoxy)phthalocyanine compounds, and the inclusion of stearyl alcohol in the L–B film, such a comparison is not very meaningful although methyl substitution at the phthalocyanine ring periphery is reported to reduce the pressed-pellet conductivity by 2–3 orders of magnitude for comparable iodine-doped samples.[3]

Complexed Metal Ion Dependence. The effect of the metal ion is of particular interest. Previous work has shown that the metal ion has a distinctive influence on the degree of phthalocyanine aggregation in solution as well as the force–area curves when monolayers are formed.[4] For sensing applications, weakly interacting vapors (e.g., ammonia, sulfur dioxide, water, etc.) exhibit a variety of responses depending on the metal ion.[12]

The results of iodine-doping experiments using 45-layer L–B films of metal-free, copper, zinc, platinum, palladium, cobalt, and nickel phthalocyanine–stearyl alcohol are tabulated in Table I. All of the films display approximately a 4 order of magnitude conductivity increase after iodine doping with very little dependence on metal ion substitution although they have been listed in the order of decreasing iodine-doped conductivity. Regarding the contrast between metal-free and nickel phthalocyanine films, a similar difference has been noted for the case of single-crystal measurements on the parent compounds.[13] For iodine vapor, the charge-transfer interaction is strong, involving the phthalocyanine ring with the metal ion having only a weak effect.

Table I. $(MPcCP)I_x/C_{18}OH$ L–B Film Conductivity and Pc/I Stoichiometry

Pc compd	X	σ, S/cm	I, A	Δf_o, kHz	Δf_I, kHz
H_2PcCP		2×10^{-9}	6×10^{-10}	−69 ± 3	
$(H_2PcCP)I_x$	2.2	6×10^{-6}	2×10^{-6}		−11.8 ± 0.2
CuPcCP		6×10^{-10}	2×10^{-10}	−69 ± 1	
$(CuPcCP)I_x$	2.2	6×10^{-6}	2×10^{-6}		−11.3 ± 0.7
ZnPcCP		2×10^{-10}	8×10^{-11}	−79	
$(ZnPcCP)I_x$	2.0	3×10^{-6}	1×10^{-6}		−12.1
PtPcCP		2×10^{-11}	6×10^{-12}	−75 ± 2	
$(PtPcCP)I_x$	2.5	3×10^{-6}	1×10^{-6}		−13.1 ± 0.3
PdPcCP		3×10^{-10}	1×10^{-10}	−50	
$(PdPcCP)I_x$	3.9	1×10^{-6}	5×10^{-7}		−14.4
CoPcCP		8×10^{-10}	3×10^{-10}	−77	
$(CoPcCP)I_x$	2.6	1×10^{-6}	4×10^{-7}		−15.1
NiPcCP		8×10^{-11}	3×10^{-11}	−68 ± 3	
$(NiPcCP)I_x$	2.8	3×10^{-7}	1×10^{-7}		−14.4 ± 0.3
H_2PcCP (sprayed)		8×10^{-10}	3×10^{-10}	−45	
$(H_2PcCP)I_x$ (sprayed)	>9.4	8×10^{-6}	3×10^{-6}		>−33

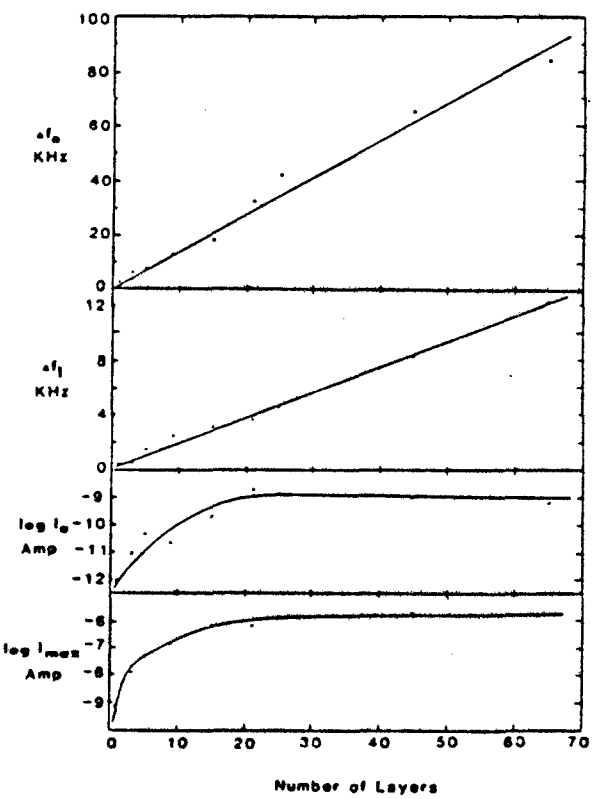

Figure 7. Dependence of SAW frequency shift of the undoped L–B film (Δf_o), SAW frequency shift caused by absorbed iodine where conductivity approaches a maximum (Δf_I), current passing through the undoped film in a nitrogen atmosphere (I_o), and maxim current passing through the film after iodine doping (I_{max}) on number of layers in the L–B multilayer film of metal-free phthalocyanine–stearyl alcohol (1:1 mol ratio).

Film Thickness Dependence. The relationship between L–B film thickness and microelectrode thickness is an important issue when either chemical properties of the film are being measured or the film is being evaluated as a microelectric component. To investigate this relationship for an iodine-doping experiment as well as to examine the

(12) Barger, W.; Wohltjen, H.; Snow, A. W. "Chemiresistor Transducers Coated with Phthalocyanine Derivatives by the Langmuir–Blodgett Technique"; *Transducers '85*; IEEE: New York; 1985; IEEE No. 85CH2127-9, pp 414–417.

(13) Marks, T. J. *Science (Washington, D.C.)* 1985, 227, 881.

sensitivity of the conductivity and SAW frequency measurements for very thin films. Substrates were coated with films ranging from 1 to 65 layers, and values for Δf_0, Δf_1, I_0, and I_{max} were measured. These data are plotted as a function of number of layers in Figure 7. The dependence of Δf_0 and Δf_1 on the number of transferred layers is linear as would be expected from the linear dependence of SAW frequency shift on coating mass. The values of both I_0 and I_{max} level off with increasing film thickness at about 20 layers. If this thickness is considered to be the stage where the gap between the planar electrodes is filled, a value of 35–40 Å per layer may be calculated from the 760-Å thickness of the electrodes. This value is reasonable although somewhat high when compared with the stearyl alcohol chain length of about 25 Å. Theoretical calculations based on SAW frequency shifts also predict a film thickness of about 40 Å.[11] These experiments also indicate that the conductivity measurement is more sensitive than the SAW frequency measurement. For one- or three-layer films, the conductivity changes by 2.5–3 orders in magnitude while the SAW frequency change is on the order of 100–200 Hz. Control experiments with an uncoated device or a stearyl alcohol coated device after iodine exposure display conductivity changes of approximately 1 order in magnitude (e.g., from $\log I_0 = -12.4$ to $\log I_{max} = -11.2$) and frequency shifts of about 100–200 Hz. These control experiments were repeated several times, and the largest responses to iodine vapor are reported here. Experimental difficulties with the control experiments are poor transfer characteristics with the pure stearyl alcohol monolayers as mentioned earlier, extremely low levels of conductivity to be measured, the SAW device's sensitivity to pressure on the mounting clips and temperature variation, and trace iodine contamination in the apparatus between runs. Closer electrode spacing and higher frequency devices may enhance sensitivity in future work.

Morphology Variations. In addition to being a good technique for reproducibly coating thin films onto electronic devices, the L–B procedure may confer a unique morphology (multilayered structure with vertical regularity and specific in-plane orientation and packing of constituent molecules) to the coatings by nature of hydrophobic and hydrophilic interactions between the molecules within the film and the surface of the water or the substrate during application of the film. Resonance Raman and ESR studies have produced evidence of phthalocyanine anisotropy in these films.[6,7] To determine whether the conductivity and iodine vapor absorption are strongly influenced by the L–B film multilayer morphology, films of similar thickness but different morphologies were deposited on the dual 52-MHz SAW substrate.

In one case, a film was deposited by a spraying technique which involved air brushing a fine mist of the phthalocyanine–stearyl alcohol–chloroform solution until the film color intensity appearance was comparable to that of the 45-layer L–B film. The Δf_0 value for the "sprayed on" film was −45 KHz which is slightly less than the −69 KHz of the 45-layer LB film. The iodine exposure data for the "sprayed on" film and L–B film are presented in Figure 8. The conductivity response of these two films is not significantly different, but the SAW frequency data are markedly different. The "sprayed on" film absorbs 4 times as much iodine over a 1900-s exposure time, and it would be even larger for a longer exposure time. An explanation for the higher capacity of the "sprayed on" film to absorb iodine would be that it has a much looser packing and higher porosity hence a larger surface area and void volume to accommodate more iodine absorption than the L–B film.

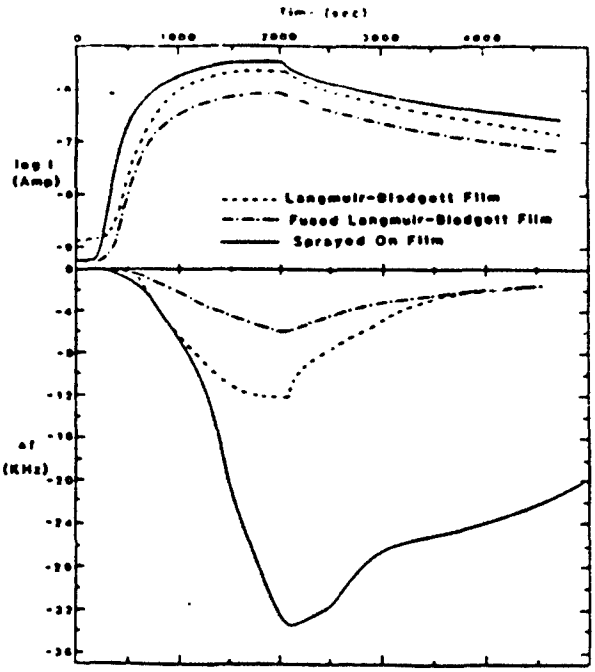

Figure 8. Comparison of a 45-layer L–B film with a fused 45-layer L–B film and a "sprayed on" film of metal-free phthalocyanine-stearyl alcohol (1:1 mol ratio) in an iodine-doping experiment.

This could facilitate absorption of iodine in excess of that engaged in the charge-transfer interaction with phthalocyanine (eq 1), possibly as molecular iodine or as in the formation of the pentaiodide ion (eq 2).

In the second case, a fused L–B film was prepared by heat treating a 45-layer L–B film for 10 min at 100 °C which causes melting of the stearyl alcohol component. The iodine exposure data for the fused film compared with the normal L–B film are presented in Figure 8. In this case, both the conductivity response to a small extent and, more significantly, the SAW frequency shift are less than for the "as-prepared" L–B film. A probable explanation is that the coating morphology is changed. Fusion of the coating followed by ambient cooling may result in loss of vertical regularity of the layered structure and consequent phase separation to a stearyl alcohol overcoating on a phthalocyanine precipitate. In a small test tube experiment, fusion and cooling of the two components results in visually observable precipitation of the phthalocyanine to the bottom of the tube from an initially uniform melt. A stearyl alcohol overcoating would have little affinity to absorb iodine as indicated by the stearyl alcohol coating control experiment and could retard iodine diffusion to the active phthalocyanine phase.

A special differential scanning calorimetry (DSC) experiment was performed to obtain information about the fusion-induced L–B film morphology change. A sample was prepared by L–B transfer of 183 layers onto six aluminum disk substrates which were stacked into a single DSC sample pan and had a calculated total transferred film mass of 0.2 mg. The DSC thermograms for the freshly prepared phthalocyanine–stearyl alcohol film, one recycle, and a pure stearyl alcohol control film are presented in Figure 9. The phthalocyanine mixed L–B film displayed several overlapping transitions on the first scan with two broad peaks at 57.9 and 56.3 °C. The recycle scan displayed a narrower more intense peak at 57.7 °C. The stearyl alcohol control film displayed a thermogram similar in shape to that of the recycle but with a transition peak

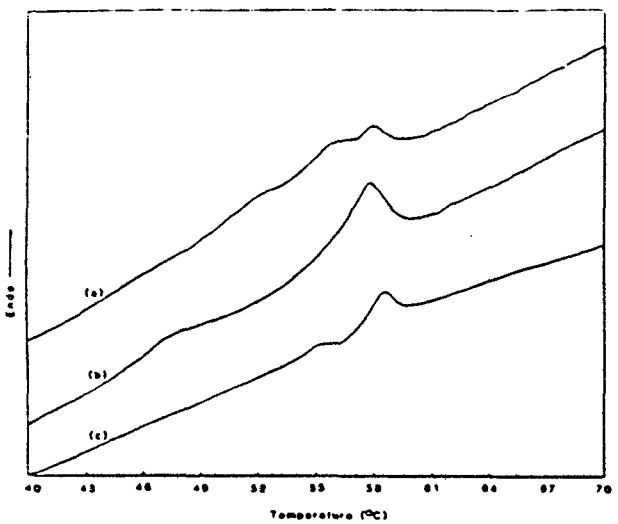

Figure 9. DSC thermograms of (a) a freshly prepared metal-free phthalocyanine–stearyl alcohol (1:1 mol ratio) 183-layer L–B film, (b) a fused (recycled scan) L–B film, and (c) a pure stearyl alcohol L–B film.

at 58.5 °C. These thermograms indicated that the morphology of the L–B film is more complicated than a simple fused mixture and is irreversibly altered by the 100 °C thermal treatment.

Summary

L–B films of tetrakis(cumylphenoxy)phthalocyanine–stearyl alcohol mixed monolayers strongly interact with iodine vapor, and it is possible to simultaneously measure the conductivity and gravimetric changes in the film by a novel planar microelectrode surface acoustic wave measurement technique. The conductivity increased by 4 orders of magnitude and a complex formation stoichiometry of two to four iodine atoms per phthalocyanine ring was measured. The identity of the complexed central metal ion has very little effect on either the magnitude of the conductivity increase or the complex stoichiometry. The conductivity measurement is dependent on the multilayer film thickness unless the film is thicker than the planar microelectrode. The quantity of iodine a phthalocyanine film may absorb is dependent on the film morphology while the magnitude of the conductivity increase is nearly independent of the morphology.

Acknowledgment. We thank Phillip Berg and Russell Jeffries for making the electrode thickness measurement by interferometry and Wanda Carter for obtaining the DSC data.

Registry No. CuPcCP, 93530-47-3; ZnPcCP, 93530-48-4; PtPcCP, 93530-49-5; PdPcCP, 93530-50-8; CoPcCP, 93530-45-1; NiPcCP, 93530-46-2; H_2PcCP, 93530-40-6; I_2, 7553-56-2.

Hard Copy

PROCEEDINGS OF THE SYMPOSIUM ON

SENSOR SCIENCE AND TECHNOLOGY

April 6-8, 1987
Electronics Design Center
Case Western Reserve University
Cleveland, Ohio 44106

Proceedings Editors
B. Schumm, Jr., C. C. Liu, R. A. Powers, and E. B. Yeager

Sponsored by
Cleveland Local Section of The Electrochemical Society
The Edison Sensor Technology Center
Resource for Biomedical Sensor Technology
Case Center for Electrochemical Sciences

Proceedings Volume 87-15

THE ELECTROCHEMICAL SOCIETY, INC., 10 South Main St., Pennington, NJ 08534-2896

SURFACE ACOUSTIC WAVE SENSORS, CHEMIRESISTOR SENSORS AND HYBRIDS USING BOTH TECHNIQUES SIMULTANEOUSLY TO DETECT VAPORS

W. R. Barger, M. A. Klusty, A. W. Snow, J. W. Grate,
D. S. Ballantine[1] and H. Wohltjen[2]
Chemistry Division, Naval Research Laboratory
Washington, D. C. 20375

Two new types of vapor sensors can be fabricated by depositing chemically-selective thin organic films over the microfabricated interdigital electrodes of chemiresistor devices or surface acoustic wave (SAW) delay-line oscillators. Sensitivity and selectivity depend on the interaction of vapors with the coatings. Chemiresistors can measure vapor-induced changes in the coating's electrical resistance while SAW devices can measure increases in the coating's mass due to vapor absorption. Hybrid devices can measure both effects simultaneously. Research to obtain suitable coatings and to develop practical vapor sensors is discussed.

INTRODUCTION

Research on chemical vapor sensors that use microfabricated interdigital electrodes has been underway in a number of laboratories for several years. A broad review of chemical microsensors including surface acoustic wave delay line oscillators (SAW) and chemiresistors used as vapor detectors was prepared by Wohltjen in 1984 [1]. The fact that coatings such as phthalocyanines respond to vapors by changing their electrical resistance has been known for decades [2], and Japanese workers [3] described chemiresistor vapor sensors using phthalocyanine compounds deposited on interdigital electrodes in 1978.

Other groups pursuing work closely related to the topics discussed here are located at the University of Maine [4,5] and Sandia National Laboratory [6,7]. Research and development involving SAW chemical sensors are also being conducted in several industrial laboratories, including Bendix, TRW, and Microsensor Systems, Inc. Abroad, there has been active research on vapor detection using both the SAW and chemiresistor devices in the Netherlands [8] and in the United Kingdom [9,10]. Work on a closely related (but not microfabricated) detector, the quartz crystal oscillator which also depends on the absorption of vapor by a coating film, has been conducted by researchers at several laboratories [11,12]. Earlier work on the quartz crystal detector has been reviewed by Alder and McCallum [13].

The research program on microsensor vapor detectors being pursued in our laboratory has several closely interrelated parts. The following topics are being actively investigated:

1) Basic research on SAW sensor and Chemiresistor device design. This work is conducted in collaboration with Dr. Webb from the Electronics Technology Division of our laboratory and with Dr. Wohltjen of Microsensor Systems, Inc.

2) Development of suitable instrumentation to make use of the microfabricated sensors as practical vapor detectors [14,15,16]. Again collaboration is with H. Wohltjen.

3) Development of guidelines for synthesis of novel organic compounds or for selection of commercially-available compounds suitable for use as vapor-sensitive coatings on SAW, chemiresistor and hybrid vapor sensors [17]. A strong organic synthesis effort has been carried out by Dr. A. Snow from the very beginning of this research, and more recently a collabortive effort has begun with investigators at the University of Florida.

4) Development of methods of applying the coatings to the surface of the microsensor and methods of controlling the morphology of the coating films. Techniques used in our laboratory have included sublimation, spin-coating, and application of films by the Langmuir-Blodgett technique [18-20].

5) Testing of coated devices configured as small vapor-detecting instruments against a series of low-concentration simulants for toxic vapors and realistic concentrations of potential interferent vapors (such as water vapor) [20,21]. Dr. D. Ballantine of Geo-Centers, Inc. has conducted the majority of recent coating tests in our laboratory with vapors of controlled, known concentrations.

6) Application of modern data interpretation techniques which make use of advances in capabilities of microcomputers [21]. Using pattern-recognition techniques not only enables identification of the toxic vapor of interest, but also aids in the design of coating materials for an array sensor which, of necessity, will have a limited number of individual microsensors in order to reduce size, power consumption, and cost. This work is done in collaboration with Ms. S. Rose-Pehrsson of the Chemical Diagnostics Branch of our Division.

DEVICE TYPES

The engineering aspects of the vapor detectors being studied will be only briefly reviewed here, since more detailed descriptions have been published elsewhere [14,15,19]. Results of pattern-recognition studies done in our laboratory using 112-MHz SAW sensors have been recently reported by Ballantine, et al. [21], so they will not be discussed. This paper emphasizes some of the recent information that we have learned about coating films and describes how it was obtained.

---

1. Employed by Geo-Centers, Inc. at the Naval Research Laboratory.
2. Microsensor Systems, Inc., Fairfax, Virginia.

The similarities in the fundamental designs of devices being studied are illustrated in Figure 1, which shows a single surface acoustic wave delay line oscillator (SAW), a dual SAW, and a substrate for a chemiresistor. A SAW device has a characteristic resonant frequency when it is placed in an oscillator circuit. The devices in Figure 1 become vapor sensors when selective coating films are deposited on their surfaces. When the coating increases in mass by absorbing the vapor, the resonant frequency of the SAW vapor sensor shifts. A chemiresistor requires a coating that changes its resistance upon absorbing a vapor. If coated with an appropriate film, a dual SAW can be wired to act as a hybrid vapor sensor which uses one side as a SAW sensor and the other as a chemiresistor to simultaneously measure changes in mass and in electrical resistance of the coating due to vapor absorption.

All of the devices discussed in this paper were fabricated by depositing gold interdigital fingers on ST-cut quartz. SAW delay line oscillators and resonators can, of course, be fabricated from other materials, such as lithium niobate, and the interdigital electrodes can be made from other metals, such as aluminum. Gold fingers were chosen to avoid device damage by corrosive vapors, such as iodine. SAW vapor sensors require only that the coating which is applied to the device act as a sorbent for the vapor of interest. The signal results from an increase in the mass of the coating. In order to sense only the vapor of interest, the coating must be selective. It must preferentially absorb the vapor to be detected. In practice, perfect selectivity cannot be achieved. Therefore, an array of sensors with different coatings is used which gives a characteristic response pattern upon exposure to the unknown mixture containing the toxic vapor. In an array-type detector, not only must coatings with high sensitivity to the trace toxic vapor be used, but also coatings which are sensitive to interferents (such as water vapor), so that corrections can be made for the influence of the interferents. A detector containing a sensor array of this type must rely on built-in microcomputing capability.

SAW SENSOR EVALUATION

Typical data for the performance of a SAW sensor coated with a polymer and tested against a vapor of known concentration is shown in Figure 2. In this case a 290 MHz dual SAW was coated with the polymer "fluoropolyol" and exposed to successive doses of 7.1 ppm (by volume in dry air) of dimethyl acetamide vapor.

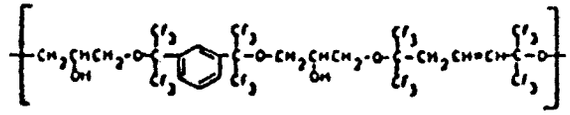

"Fluoropolyol"

The normal testing procedure is to record a baseline while passing dry air over the coated sensor which is housed in a closed Delrin, Teflon, or metal chamber with an inlet and outlet port for the vapor. Then, dry air containing a known concentration of the test vapor is switched in place of the pure carrier. After a fixed period of time, the dry air is switched back in place of the test stream in order to observe the diffusion of the vapor out of the coating. A second dose follows the first to check reproducibility. Only reversible coatings are studied in our testing program. This test sequence is carried out with many vapors, each at several concentrations. Table I lists typical vapors and representative concentrations that have been used for testing SAW and Chemiresistor sensors.

Table I. A Typical Series of Test Vapor Concentrations

Vapor	ppm	Vapor	ppm
Sulfur dioxide	1.9	Water	11,500
Dimethyl methylphosphonate	7.6	Diethyl sulfide	17,000
Dimethyl acetamide	16.5	Toluene	17,700
Ammonia	76.4	Iso-octane	29,900
Tributyl phosphate	105	Dichloroethane	46,700
1-Butanol	4,110	2-Butanone	50,700

Relationship of Frequency Shift to Mass Loading

In general, for SAW sensor coatings we have used polymers that were above their glass transition temperatures. For these compounds the relationship between the shift in resonant frequency of a SAW sensor and the mass loading on its surface can be closely approximated by the following simplified expression [14,16]:

$$f = kf^2hp \qquad \text{(Eq. 1)}$$

where f is the change in resonant frequency, f is the resonant frequency of the bare SAW device, h is the film thickness, p is the film density, and k is a constant. The product hp is the mass loading per unit area on the surface. Therefore, the frequency shift is proportional to the mass of the film, and that mass can change when vapor is absorbed.

One method to verify this approximation is to apply films to the surface in a manner such that the mass per unit area is accurately known and then determine the corresponding frequency shifts. The ratio of the frequency shift to the mass per unit area should be directly

proportional to the square of the frequency for a series of bare devices with different fundamental resonant frequencies. This has been demonstrated using several different SAW oscillators (31, 52, and 112 MHz) which were coated by the Langmuir-Blodgett technique. Results are shown in Figure 3. Within the precision of experimental results obtained for devices up to 290 MHz, the simple relationship of Eq. 1 appears to be valid.

Langmuir-Blodgett Film Deposition

The Langmuir-Blodgett technique of applying films requires a material that will form a monolayer film on water. Such films change the surface tension of water and can be monitored by measuring surface tension [22]. Film pressure is defined as the change in surface tension of the water caused by the film, and these films can be compressed to higher pressures with a moving barrier. A film pressure vs. area curve is analogous to a pressure vs. volume diagram for a gas. When a known quantity of monolayer is spread onto a known area of water surface from a solution of known concentration, a film for which the mass per unit area is accurately known has been made. If the film is maintained at a fixed pressure while the device to be coated is passed repeatedly through the air/water interface, a single layer is transferred to the device on each pass. A plot of film pressure vs. surface density is shown in Figure 4. The use of a computer-controlled feedback system to maintain the pressure at a constant value of 20 mN/M during the transfer of the film results in a film of precisely known mass per unit area on the SAW surface. A film that gives a 1:1 transfer ratio from the water to the SAW surface must, of course, be used. Detailed information on this technique, the films used, and chemiresistor sensors fabricated in this manner have been previously reported [15,17,18].

CHEMIRESISTOR SENSORS

The substrates (Fig. 1) and electronics for chemiresistor sensors are much less sophisticated than for SAW sensors, but the requirements for coatings are more stringent, since the coatings must change resistance on exposure to vapors in addition to acting as selective sorbents. Presently, a Keithley Model 617 programmable electrometer which is interfaced to a microcomputer through an IEEE-488 interface is used to measure current passing through the coatings while a bias of 1 volt is maintained across the interdigital electrodes. This instrument can also measure very high resistances directly. A companion multimeter can be used to read signals from an array of chemiresistor sensors mounted in a gas-tight chamber with an inlet and outlet for vapors.

The mechanism of resistance change in the coatings exposed to vapors is not sufficiently well understood to easily choose new

compounds for synthesis. Some of the current ideas about conducting organic compounds have been summarized by Marks [23] and by Cowan and Wiygul [24]. As noted in the introduction, phthalocyanines are well known for their response to vapors. We originally examined several phthalocyanine films that were applied by sublimation to the interdigital electrodes, however, reversibility was poor when the sensors were operated near room temperature [20]. Workers using these coatings at higher temperatures have seen much better performance [8,9,10]. Our recent work has concentrated on organic derivatives of the phthalocyanines, and most heavily on the tetrakis (cumylphenoxy) phthalocyanines. A series of these compounds that contain different transition metals in the center of the macrocyclic ring have been evaluated [19]. Two properties of these compounds have been of interest: 1) they are suitable for deposition by the Langmuir-Blodgett technique [18], and 2) sensors made by that technique exhibit good reversibility at room temperature [19]. For example, results at room temperature for a chemiresistor coated with a Langmuir-Blodgett multilayer film containing nickel tetrakis (cumylphenoxy) phthalocyanine, one of the better materials for detection of ammonia, are shown in Figure 5.

Many of the compounds which were chosen for investigation with the possibility of being compatible with Langmuir-Blodgett deposition are illustrated in Figure 6. In most cases, although these compounds can form films on water, it has been necessary to resort to the use of a mixture with a second, more classical, monolayer-forming film in order to get high-quality multilayer films to transfer to the surface of the gas sensor. These "transfer promoters" limit the temperature to which the mixed films can be heated. Therefore, some experimental work has been done to select a transfer promoter with a high melting point. In the case of the tetrakis(cumylphenoxy) phthalocyanines, the mixed film is a two-phase system. Melting points are very close to the melting points of the pure transfer promoters, as shown in Table II for a 1:1 mole ratio mixed film.

Table II. Melting Points (°C)

Transfer Promoter:	Stearyl Alcohol	Stearyl Amide
Bulk transfer promoter:	58.5	108.7
L-B film of transfer promoter:	58.5	108.7,109.2
Mixed L-B film with $H_2Pc(Cp)_4$	56.3,57.9	107.0

HYBRID SENSORS

Given the general similarities of design of chemiresistors and SAW sensors as seen in Figure 1, it should not be surprising that it is

possible to design devices that can serve both purposes simultaneously. The use of the interdigital electrodes can be determined by the external circuitry. We have used a dual 52 MHz SAW substrate to make both sensor types and a hybrid. The simultaneous measurement of viscosity and mass changes in a coating film increases the ability of the sensor to discriminate between two vapors because two conditions must be met to identify a vapor. Highly sensitive and selective vapor detectors based on this principle may be possible, but our primary use of these hybrid sensors has been more modest.

The hybrid sensor can be used as a powerful tool to either evaluate coating materials that are candidates for use on chemiresistor sensors or simply to study gas/coating interactions. Typical results obtained from a hybrid system when saturated iodine vapor in dry nitrogen is passed over the sensor are seen in Figure 7. The coating in this case was metal-free tetrakis(cumylphenoxy) phthalocyanine deposited on a 52-MHz dual SAW was coated by the Langmuir-Blodgett technique with 45 layers of a mixed film containing a 1:1 mole ratio of octacosyl alcohol and the phthalocyanine. Like the earlier experiments described for SAW and chemiresistor sensors, pure nitrogen purged the sensing chamber for 5 min, then dry nitrogen saturated with iodine vapor was flowed through for 40 min. The pure nitrogen stream was then switched back on, and the vapor diffused out of the film.

Much information is gained in an experiment of this type. First, when the SAW device is coated by the Langmuir-Blodgett technique, the mass sensitivity can be determined by a simple measurement of the difference between the resonant frequency of the device before and after the application of the film. Since the surface density in g/cm^2 is known for the film, the shift in frequency in KHz/ng/cm^2 for the film can be obtained for that particular device. When an additional shift in frequency occurs due to vapor absorption, the mass of the vapor (ng/cm^2) can be determined. One can either let the experiment run for a long time, or fit a curve through the frequency shift vs. time data to obtain the limiting mass of vapor (Ce) that will enter the film when it is in final equilibrium with a vapor of given concentration. Since the mass of coating per unit area is known, the ratio of vapor mass to the initial film mass (C/Cf) can be determined, and from this the mole ratio if the molecular weights are known. This information can be directly correlated with data on resistance change obtained from the chemiresistor side of the sensor. One knows directly how many molecules of vapor are required per molecule of coating film to produce a resistance of a certain value, since calculations are done with the concentration of vapor actually inside the film, and not with vapor concentrations in the space above the film.

Figure 8 shows an example of the information needed for the calibration of a conductive film. The most sensitive chemiresistor devices have the steepest slope of microamperes per frequency change (KHz), so that the frequency change scale could be converted to units of molecules of iodine per molecule of phthalocyanine

by multiplying by a constant factor, since the device has been calibrated. When this conversion is made, it is found that the maximum current flows when there are approximately 2 iodine atoms present per phthalocyanine molecule. As this ratio increases beyond 2:1 the conductivity decreases. (In the figure, the iodine vapor remains on until the point indicated by the arrow.)

An alternative method of film application is to spray the coating onto the surface of the SAW device with an artist's air brush. Polymers used as SAW sensor coatings are routinely applied by this method after they have been dissolved in a volatile solvent. To make reproducible coatings, the top is removed from the gas-tight sensor chamber, the frequency of the clean device is recorded, and then spraying proceeds while the uncovered device is oscillating. By watching the frequency counter during the spraying, a reproducible quantity (expressed in KHz of coating) can be applied to many different devices. Typically, enough polymer is sprayed onto a 52 MHz device to produce a 50 KHz decrease in frequency. Then when the vapor is delivered to the coating, the ratio, C/Cf, of frequency shift by the vapor, to frequency shift due to the coating alone is determined. This ratio is equivalent to the mass of vapor per mass of coating when equation 1 is obeyed. Again, the value when the coating is in equilibrium with the test vapor can be determined by curve fitting.

It has been found that a mathematical expression such as for a second order chemical reaction can describe the data for absorption into and diffusion out of films for many film-vapor pairs. A few are illustrated in Figure 8. Values for k and Ce in the equations below can be determined by fitting a straight line to data for 1/frequency change vs. time by the method of least squares.

$$\frac{dC}{dt} = kC^2 \qquad \text{(Eq. 3)}$$

C = Mass of vapor absorbed
Ce = Mass of vapor when saturated
k = Rate constant
t = Time

$$\frac{1}{C} - \frac{1}{Ce} = kt$$

OUTGASSING (Eq. 3)

$$C = Ce - \frac{1}{1/Ce + kt}$$

ABSORPTION (Eq. 4)

Using the Ce values, a series of coatings exposed to the same fixed concentration of test vapor can be ranked by their ability to absorb that vapor. Table III lists such a ranking of coatings that were exposed to saturated vapor of dimethyl methyl-phosphonate (DMMP) at

room temperature. The ratio of frequency shift due to the film at equilibrium with the test vapor to frequency shift due to the amount of film sprayed on the device is listed. In the case of the first entry in the table, for example, it is seen that polyethylene maleate can absorb up to 96% of its own weight of DMMP from saturated vapor at room temperature. The table reveals that coatings chosen for SAW sensors are clearly better absorbers than typical conductive film mixtures used on our chemiresistors or their transfer promoters.

Table III. DMMP Vapor Absorbed into Sensor Coatings

COATING TYPE	Max. Mass of Vapor Absorbed per Mass of Coating (g/g)
POLYMERS FOR SAW SENSORS	
Polyethylene maleate (PEM)	0.96
Polypropylene maleate (PPM)	0.85
Polyethylene dichloromaleate (PEDCM)	0.44
Polyethylene succinate (PES)	0.43
LB FILM OVERCOATED WITH POLYMER	
$H_2Pc(Cp)_4$/SA + PEM	0.39
LB MIXED FILMS FOR CHEMIRESISTOR SENSORS	
$H_2Pc(Cp)_4$/SAM	0.13
$H_2Pc(Cp)_4$/SA	0.11
$H_2Pc(Cp)_4$/SAMX	0.07
$H_2Pc(Cp)_4$/SAC	0.05
LB TRANSFER PROMOTERS	
Stearyl amide (SAM)	0.01
Stearyl alcohol (SA)	0.01
Stearyl amideoxime (SAMX)	0.01
Stearic acid (SAC)	0.01

A series of compounds similar to polyethylene maleate were synthesized and examined by this method to try to better understand the influence of chemical structure on ability to absorb certain vapors. Results are shown in Figure 9. This experiment was conducted using DMMP vapor generated by bubbling dry nitrogen through the pure liquid held at 0 °C, so that the vapor reaching the sensor was held at a reproducible concentration less subject to condensation on surfaces than the DMMP generated at room temperature. The structural effects are evident in the figure.

SUMMARY AND CONCLUSIONS

This overview of research being conducted on vapor sensors that depend on sensitive, selective organic coatings applied over microfabricated interdigital electrodes has shown that SAW sensors, chemiresistors, and hybrids can be successfully used for vapor sensing. The success of the detectors described in this paper is greatly dependent on the choice and the method of application of the organic coating. Progress in the area of coating research has been slow, because chemists working outside of multidisciplinary organizations have been handicapped by the fact that much of the test instrumentation has not been available commercially [25]. Generally, collaboration with electrical engineers has been necessary to design and assemble apparatus for testing coatings. Results from our laboratory and other laboratories mentioned earlier that are engaged in this work have been very encouraging, but much more work needs to be done, especially in understanding the mechanisms of interaction between the vapors and coatings so that better guidelines for the selection or synthesis of new, improved coating materials can be established.

ACKNOWLEDGEMENTS

We are grateful to Philip Berg for help in preparation of numerous Langmuir-Blodgett films. Portions of this work were sponsored by the U. S. Army Chemical Research, Development, and Engineering Center, the Office of Naval Technology and NSWC Dahlgren, Va., along with the U. S. Air Force, Brooks AFB.

REFERENCES

1. M. Wohltjen, Anal. Chem. 56, 87A (1984).
2. A. B. P. Lever, in "Advances in Inorganic Chemistry and Radiochemistry", J. Emeleus and A. G. Sharpe, Eds., Vol. 7, pp. 27-114, Academic Press, New York (1965).
3. Y. Sadaoka, M. Yamazoe, and T. Seiyama, Denki Kagaku Oyobi Kogo Butsuri Kagaku 46, 597 (1978).
4. A. Bryant, D. L. Lee, and J. F. Vetelino, Proc. 1981 IEEE Ultrasonics Symp. pp. 171-174 (1981).
5. A. Bryant, M. Poirer, G. Riley, D. L. Lee and J. F. Vetelino, Sensors and Actuators 4, 105 (1983).
6. A. J. Ricco, S. J. Martin, and T. E. Zipperian, Sensors and Actuators 8, 319 (1985).
7. S. J. Martin, K. S. Schweizer, S. S. Schwartz, and R. L. Gunshor, Proc. 1984 IEEE Ultrasonics Symp., pp. 207-211 (1984).
8. A. W. Barendsz, J. C. Vis, M. S. Nieuwenhuizen, E. Nieuwkoop, M. J. Vellekoop, W. J. Ghijsen, and A. Venema, Proc. 1985 IEEE Ultrasonics Symp. pp 586-590 (1985).
9. B. Bott and T. A. Jones, Sensors and Actuators 5, 43 (1984).

10. T. A. Jones and B. Bott, in "Transducers '85", PP. 414-417, IEEE, New York (1985), IEEE Cat. No. 85CH2127-9.
11. M. P. Carey, K. R. Beebe, B. R. Kowalski, D. L. Illman, and T. Hirschfeld, Anal. Chem. 58, 149 (1986).
12. J. F. Alder and J. J. McCallum, The Analyst 108, 1169 (1983).
14. H. Wohltjen, A. Snow, and D. Ballantine, in "Transducers '85" PP. 66-70, IEEE, New York (1985).
15. H. Wohltjen, W. R. Barger, A. W. Snow, and N. L. Jarvis, IEEE Trans. Electron Devices ED-32, 1170 (1985).
16. H. Wohltjen, A. W. Snow, W. R. Barger, and D. S. Ballantine, IEEE Trans. Ultrasonics, Ferroelectrics, and Frequency Control UFFC-34, 172-178 (1987).
17. A. W. Snow, W. R. Barger, M. Klusty, H. Wohltjen, and N. L. Jarvis, Langmuir 2, 513 (1986).
18. W. R. Barger, A. W. Snow, H. Wohltjen, and N. L. Jarvis, Thin Solid Films 133, 197 (1985).
19. W. R. Barger, H. Wohltjen, and A. Snow, in "Transducers '85" PP. 410-413, IEEE, New York (1985).
20. W. R. Barger, H. Wohltjen, A. W. Snow, J. Lint, and N. L. Jarvis, in "Fundamentals and Applications of Chemical Sensors", D. Schuetzle and R. Hammerle, Eds., PP. 155-165, ACS Symposium Series No. 309, American Chemical Society, Washington, D. C. (1986).
21. D. S. Ballantine, S. L. Rose, J. W. Grate, and H. Wohltjen, Anal. Chem. 58, 3058 (1986).
22. G. L. Gaines, "Insoluble Monolayers at Liquid-Gas Interfaces", Interscience Publishers, New York (1966).
23. T. J. Marks, Science 227, 881 (1985).
24. D. O. Cowan and F. M. Wiygul, "The Organic Solid State", Chem. & Eng. News, July 21, 1986, PP. 28-45.
25. Most of the microfabricated interdigital electrode devices mentioned here can be obtained from Microsensor Systems, Inc., P. O. Box 90, Fairfax, Va. 22030.

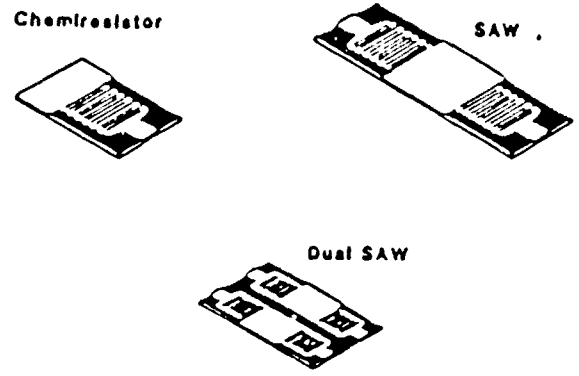

Fig. 1. Planar microsensors. Surface acoustic wave (SAW) delay line oscillators, chemiresistors, and hybrid devices can be similar in design.

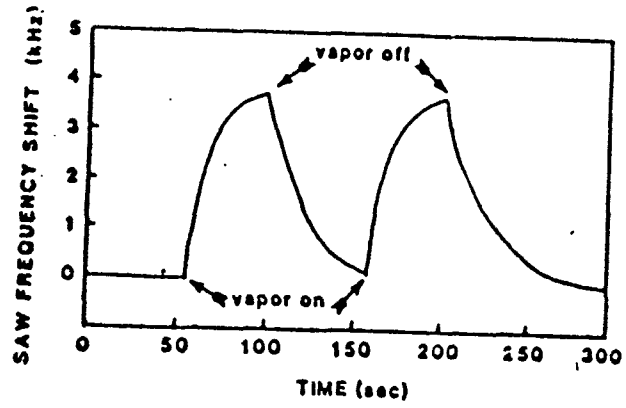

Fig. 2. Dose-response results for exposures of a 290-MHz SAW sensor coated with fluoropolyol to 7.3 ppm of dimethyl acetamide in dry air.

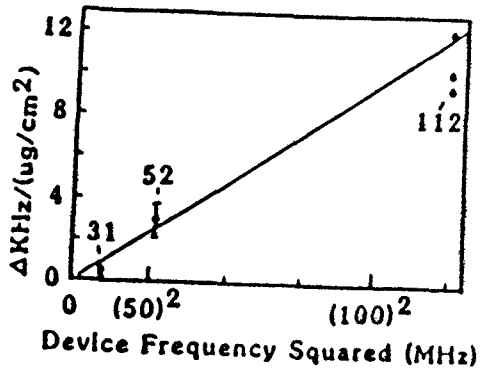

Fig. 3. The sensitivity of SAW vapor sensors coated with Langmuir-Blodgett multilayers is proportional to the square of the fundamental operating frequency for the 31-, 52-, and 112- MHz delay line oscillators studied.

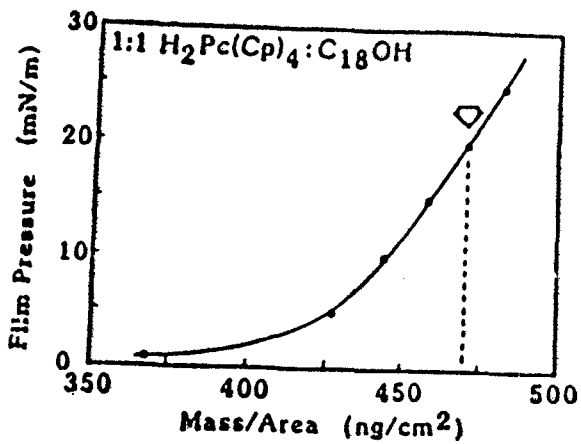

Fig. 4. Pressure of a Langmuir film on water is a function of surface concentration. Data for a monolayer of a mixed film containing equal numbers of molecules of stearyl alcohol and metal-free tetrakis (cumylphenoxy) phthalocyanine are shown. Transfers are usually made at a pressure of 20 mN/M.

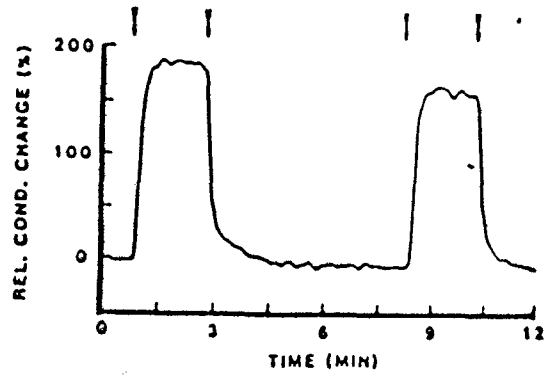

Fig. 5. Dose-response results for a chemiresistor coated with a mixed 45-layer film containing Ni tetrakis (cumylphenoxy) phthalocyanine which was exposed to 2 ug/L of ammonia in dry air. The arrows indicate when the gas stream was switched.

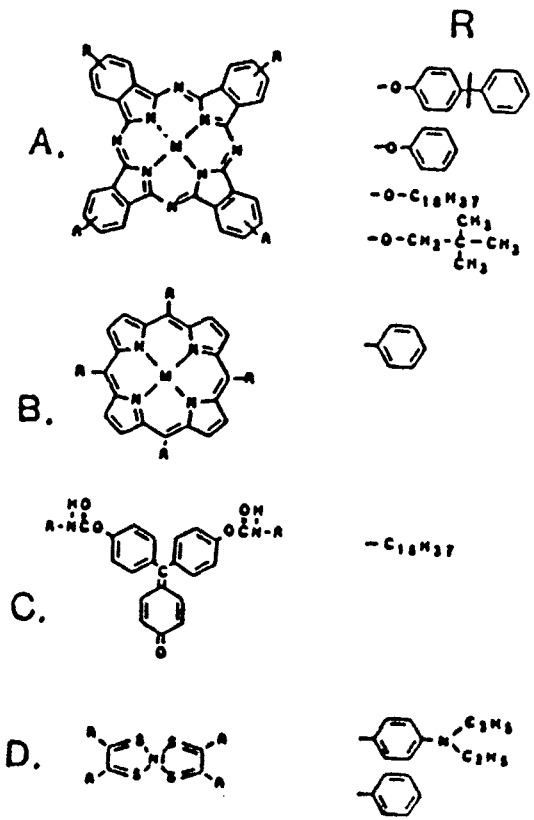

Fig. 6. Structures of several of the compounds that have been examined as candidate chemiresistor coatings. Compounds showing the most promise have been the derivatives of phthalocyanine (a) and the nickel dithienes (d).

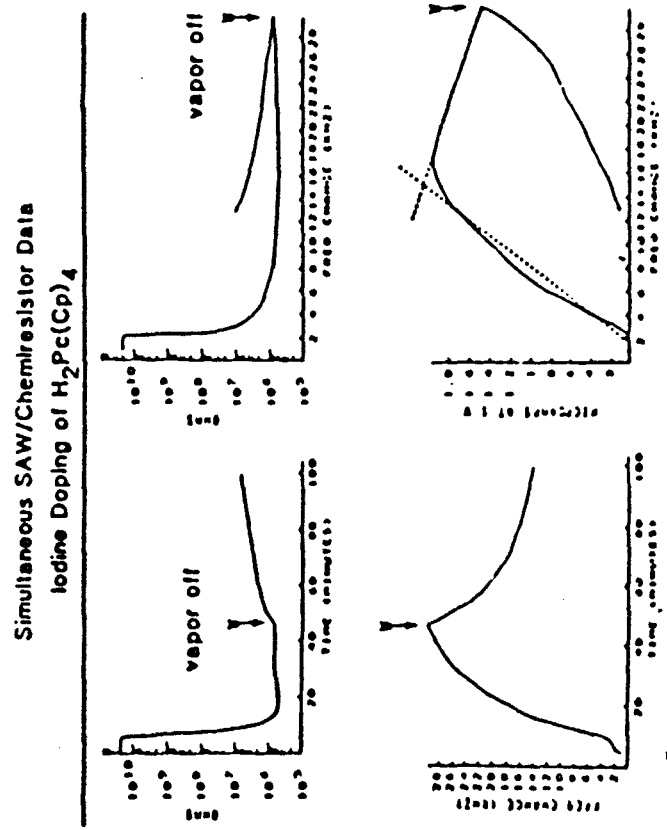

Fig. 7. Dose-response results from exposure of iodine vapor in dry nitrogen to a hybrid vapor sensor coated with 45 layers of a mixed film containing metal-free tetrakis (cumylphenoxy) phthalocyanine and stearyl alcohol. The vapor stream is switched in place of the nitrogen at 5 minutes and off again at 45 minutes (indicated by the arrows).

Fig. 8. Examples of vapor/coating pairs for which a second order equation can be used to represent the change in frequency with time. Solid lines are the fitted curves. DMMP = dimethyl methylphosphonate) M/2 = chloroethyl, ethyl sulfide.

COMPOUND	Ce/Cf
PEM	0.81±.03
PEMM	0.80±.06
PEPM	0.75±.06
PEPh	0.61±.09
PEDCM	0.55
PEOX	0.61±.26
PEMO	0.32
PES	0.23±.03
PEA	0.11

Fig. 9. Compounds with variations on the structure of polyethylene malonate are ranked by the quantity of DMMP vapor they can absorb. Ce/Cf is equivalent to the mass of vapor per mass of coating. Equilibration was with saturated vapor in nitrogen made from liquid at 0 °C.

DISCUSSION

Question #1. S. Hettiarachchi, SRI Intl

Did you measure the surface conductivity of the phthalocyanines?
Answer - We can provide figures for the whole structure where we measure pico amps in 20 micron spaced fingers. One can also compute some other parameters.

Question. Has a four point method been tried?
Answer - No.

Question. Has polyphthalocyanine been used?
Answer - No, but another group is working on these.

Question #2. J.G. Brace, Johnson Controls, Inc.

Are all the devices on cuts?
Answer - They are on ST cut quartz with gold fingers. There are some temperature problems but the electronics also require temperature compensation.

Question #3. W. Schramm, U. of Michigan

Can you predict which substrate will work best for particular material detection?
Answer - No, but others are measuring partition coefficients, e.g. M. Abraham at the Univ. of Surrey, England on solvato-chromatic parameters.

Question #4. C. Scortichini, Dow Chemical Co.

Do the vapors to be detected form a physical or a chemical bond?
Answer - The rapid absorption-desorption suggests only physical absorption. The devices are very sensitive.

Question #5. T. Mezza, Signal Research Center

What is the advantage of the SAW device versus a coated quartz device?
Answer - The SAW sensor is an extension of coated quartz technology. But the coating substitutes for the requirement for thinner and thinner quartz and is simpler to make.

Question #6. J. Cutting, CWRU

What is the AC resistance versus the DC resistance? and how do you separate electrode resistance from the film resistance?
Answer - We have only measured DC resistance and do not separate the electrode resistance from the film resistance.

Question #7. A.M. Yacynych, Rutgers Univ.

How do you deal with baseline shift?
Answer - By careful choice of coating.

Question #8. A.M. Yacynych

Do yo have any more complex devices? What happens to mechanical problems? and Aren't there irquency shifts?
Answers - All of our recent devices are dual devices. Mechanical and frequency shift problems are minor compared to other things.

Question #9. B. Simic-Glavaski, CWRU

Are there interferences from CO or O_2?
Answer - We don't fully know yet.

Question #10. A.M. Yacynych, Rutgers Univ.

Are there adaptations to restore baseline performance?
Answer - Perhaps we will be able to use a chosen vapor.

Question #11. D.L. Wise, Cambridge Scientific, Inc.

Have you looked at biological vapor detection?
Answer - Not yet, but we may have a program soon.

Question #12. J.L. Kenty, General Motors Research Labs.

Are the devices any more sensitive to CO than others?
Answer - No, but this is a good area for study as would NO_x be also.

Comment - B. Simic-Glavaski, CWRU - One can make phthalocyanines more or less sensitive to CO or NO_x.

Reprinted from Analytical Chemistry, 1986, 58, 3058.

Correlation of Surface Acoustic Wave Device Coating Responses with Solubility Properties and Chemical Structure Using Pattern Recognition

David S. Ballantine, Jr.

Geo-Centers, Inc., 4710 Auth Place, Suitland, Maryland 20746

Susan L. Rose and Jay W. Grate*

Chemistry Division, Naval Research Laboratory, Washington, D.C. 20375-5000

Hank Wohltjen

Microsensor Systems, Inc., P.O. Box 90, Fairfax, Virginia 22030

Twelve surface acoustic wave device coatings were exposed to 11 chemical vapors and responses were correlated with solubility properties and coating structure to determine possible vapor/coating interaction mechanisms. Hydrogen bonding ability is implicated as a significant vapor/coating interaction mechanism. Pattern recognition schemes applied to the preliminary data aided in solubility property/response correlations. Principal component analysis demonstrated good separation of different classes of chemical vapors tested. Hierarchical clustering provided additional evidence of the correlations between solubility properties and the observed clustering. In addition, pattern recognition methods were used to determine potential selectivity of an array detector using these coatings. Learning techniques show that one-fourth of the sensor can adequately separate compounds of interest from chemically similar interferences.

Surface acoustic wave (SAW) devices exhibit great potential as small, very sensitive chemical sensors. The principles of operation have been described in detail (*1*), but they are essentially mass-sensitive detectors. They consist of a set of interdigital transducers that have been microfabricated onto the surface of a piezoelectric crystals. When placed in an oscillator circuit, an acoustic Rayliegh wave is generated on the surface of the crystal. The characteristic resonant frequency of the device is dependent on transducer geometry and the Raleigh wave velocity. Small mass changes or elastic modulus changes on the surface perturb the wave velocity and are readily observed as shifts in this resonant frequency. The extreme sensitivity of these devices makes them attractive as potential gas sensors. The 112-MHz dual SAW devices routinely used in our laboratory, for example, have a theoretical sensitivity of >17 Hz/(ng/cm^2). Considering that the active area of the device covers 0.17 cm^2 and assuming a signal to noise ratio of 3, this sensitivity results in a minimum detectability of about 0.2 ng (*1*).

The ultimate performance of a SAW device as a chemical sensor is critically dependent on the sensitivity and selectivity of the adsorbent coating applied to the surface of the piezoelectric crystal. However, no systematic investigation of

0003-2700/86/0358-3058$01.50/0

adsorbent coatings on SAW devices has yet been reported, and references to responses of specific SAW coatings to specific vapor are few in number (2–5). The most closely related sensor technology is the bulk piezoelectric crystal sensor, which has been reviewed (6). Coatings exhibiting selectivity to specific vapors have been identified in some cases, but many coatings have been of ill-defined composition and, until recently, selection has been largely empirical (6–11). It is therefore essential to identify coatings for SAW devices which respond to vapors of interest and to develop a rationale for the selection or design of such coatings.

The development of adsorbent coatings alone may not be sufficient for some applications of these devices. It is unlikely that any given material possesses sufficient selectivity to permit accurate detection and identification of a single chemical vapor of interest in the presence of multiple, unknown interferences. A promising approach to this type of analytical problem is the use of pattern recognition techniques in conjunction with an array of sensors of varying selectivity. This approach has been applied to vapor response data from electrochemical sensors (12) and to the selection of coatings for piezoelectric crystal sensors (7).

Pattern recognition techniques, as applied to sensor data, can be described as follows. The sensors encode chemical information about the vapor in numerical form. Each sensor defines an axis in a multidimensional space. Vapors can be represented as points positioned in this space according to sensor responses. Vapors that produce similar responses from the set of coatings will tend to cluster near one another in space. Pattern recognition uses multivariate statistics and numerical analysis to investigate such clustering and to elucidate relationships in multidimensional data sets without human bias. In addition, the method can reduce interference effects and improve selectivity in analytical measurements.

In this study, we have generated a large data base consisting of the responses of 12 SAW coatings to 11 vapors at various concentrations, and we have analyzed these data by using pattern recognition techniques. Our objectives were 2-fold. First, we wished to gather sufficient data to investigate and possibly identify the types of vapor/coating interactions responsible for the observed SAW devices responses. Pattern recognition techniques assisted in this effort by clustering vapors with similar response patterns and by identifying similarities between coatings based on responses to vapors. Secondly, we wished to determine the ability of pattern recognition techniques in conjunction with SAW sensors to discriminate between vapors of interest and chemically similar interferences. Such discrimination is necessary for an array detector to be practical and effective.

EXPERIMENTAL SECTION

Materials. Solvents for vapor stream generation were commercial materials of 99.99% purity, except diethyl sulfide (98%, Aldrich) and dimethyl methylphosphonate (97%, Aldrich). These materials are listed in Table I.

The following coating materials were obtained from Aldrich: abietic acid, octadecyl vinyl ether/maleic anhydride copolymer, poly(epichlorohydrin), *cis*-poly(isoprene), and acrylonitrile/butadiene copolymer (0.45/0.55). Poly(vinylpyrrolidone) and OV210 were purchased from Alltech. The two polyphosphazines are proprietary materials and were obtained courtesy of Ethyl Corp. Poly(ethylene maleate) was prepared as described by Snow and Wohltjen (2). Poly(amidoxime) was prepared by reaction of the acrylonitrile/butadiene copolymer (Aldrich) with hydroxylamine. Subsequent IR analysis indicated a nitrile to amidoxime ratio of 0.38/0.07 (13). Fluoropolyol was prepared using methods described by O'Rear et al. (14). These materials and their structures are given in Table II.

Analytical System. The 112-MHz dual SAW delay lines used in this study were fabricated photolithographically on polished S-T Quartz substrates (1 cm × 1 cm × 0.08 cm thick). The electrodes were made of gold (100 Å thick) deposited onto titanium (about 200 Å thick) to provide adhesion. Each electrode array consisted of 50 "finger" pairs with each electrode 7 μm wide and spaced 7 μm from the next finger. The electrode arrays had an aperture of 0.226 cm. The devices were clamped into a Teflon holder using small pressure clips and screws. A lid attached to this holder was fitted with inlet and outlet tubes to provide a vapor flow path. The two delay lines used in this system were connected as shown in Figure 1.

Table I. Test Vapors and Solubility Parameters

	π^*	β	α
Permeation Tubes, Class 1			
methanesulfonyl fluoride (MSF)			
N,N-dimethylacetamide (DMAC)	0.88	0.76	0.0
dimethyl methylphosphonate (DMMP)[a]		(0.81)	(0)
Bubblers, Class 2			
1,2-dichloroethane (DCE)	0.81	0.00	0.0
water	1.09	0.18	1.17
isooctane (ISO)[a]	(0.0)	(0.0)	(0.0)
toluene (TOL)	0.54	0.11	0.0
diethyl sulfide (DES)[a]	0.36	0.28	0.0
tributyl phosphate (TBP)[a]	0.65	0.77	0.0
2-butanone (BTN)	0.67	0.48	0.0
1-butanol (BTL)	0.47	0.88	0.79

[a] These values are unpublished data from Abraham (25). Values in table for DMMP are taken from a similar compound, DEP; values for isooctane are taken from 2,4-dimethylpentane.

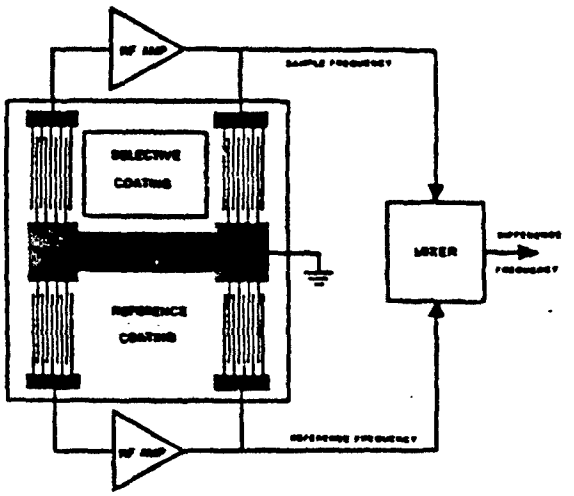

Figure 1. 112-MHz SAW device and associated electronic circuit diagram.

Dilute solutions of the coating materials were prepared in volatile solvents, usually chloroform, tetrahydrofuran, or a methanol/chloroform mixture. To make chemical sensors, one delay line was coated with the material under investigation using an airbrush. Coating deposition produced frequency shifts of 75–200 kHz, which were recorded and used as a measure of film thickness for normalization and comparison of data (1).

The uncoated delay line acted as a reference oscillator to provide compensation for ambient temperature and pressure fluctuations. Each delay line was connected to a TRW 2820 wide band rf amplifier to provide the amplification required for oscillation to occur. The frequencies obtained from each oscillator were mixed in a double balance mixer (Mini Circuits Labs SRA-1) to provide the low-frequency difference signal which was measured. Frequency measurements were made with a Systron-Donner frequency counter, Model 6042A. The frequency counter was interfaced to an Apple IIe microcomputer via an IEEE 488 bus and interface card.

Vapor Generation System. Vapor streams were generated with an automated gas handler system interface with an Apple IIe microcomputer. Plumbing connections were made by using

Table II. Coating Materials and Structures

COATING	STRUCTURES	HYDROGEN BOND ACCEPTOR–DONOR (% OF TOTAL)
POLY (ETHYLENE MALEATE) (PEM)	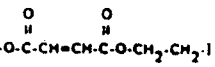	CARBONYL (HBA)-20% O-LINKAGE (wHBA)-11%
OCTADECYL VINYL ETHER/ MALEIC ANHYDRIDE COPOLYMER (OVEMAC)	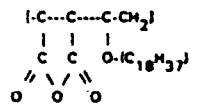	CARBONYL (HBA)-14% O-LINKAGE (wHBA)-8%
POLYVINYLPYRROLIDONE (PVP)	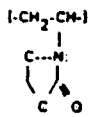	CARBONYL (HBA)-25% N: (HBA)-13%
ACRYLONITRILE/ BUTADIENE COPOLYMER (PBAN)	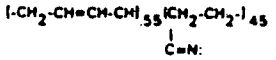	NITRILE (HBA)-22%
POLY (AMIDOXIME) (PAOX)	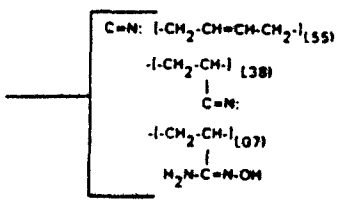	NITRILE (HBA)-19% AMIDOXIME (HBA-DI)-3%
POLY (EPICHLOROHYDRIN) (PECH)	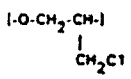	O-LINKAGE (wHBA)-17%
ABIETIC ACID (ABACD)	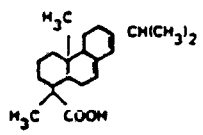	CARBOXYL (HBA-DI-15%
OV210	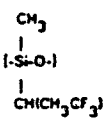	O-LINKAGE (wHBA)-10%
FLUOROPOLYOL (FPOL)	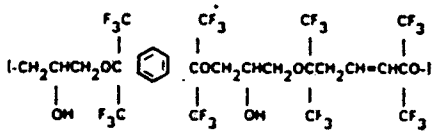	HYDROXYL (HBA-DI-4%
POLY (ISOPRENE) (PIP)	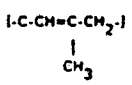	NONE (NHB)
POLYPHOSPHAZINES (PPZN1, PPZN2)	----	----

$^1/_8$-in. stainless steel or nickel tubing. The carrier gas was compressed air that was dried by passage through Drierite. Flow rates were controlled with mass flow controllers (Tylan).

Individual vapor streams were generated from one of up to eight bubblers, or one of up to four permeation tubes. Air flow to bubblers was maintained at 39 mL/min, while flow rates to permeation tubes varied from 39 to 200 mL/min, depending on the desired concentration. Additional air for dilution could be added downstream, up to a total volumetric flow of 1200 mL/min. Based on the accuracy of the mass flow controllers, the uncer-

tainties in the total volumetric flow rates were 1.7%. A constant system output of 39 mL/min to the sensor was maintained by a piezoelectric precision gas leak valve. This system will be described in more detail elsewhere (*15*).

The bubblers consisted of stainless steel vessels containing approximately 100 mL of solvent, with inlet and outlet tubes of $^1/_8$-in. stainless steel tubing. Vapor mass flow rates were determined by adsorbing the vapor output onto clean, dried charcoal traps. The traps were weighed after 15–20 min collection periods, and mass flows were determined. Two traps in series were periodically used to check for breakthrough. Multiple successive determinations resulted in calculated mass flow (in mg/min) with errors of less than 6%.

A calibrated permeation tube containing methanesulfonyl fluoride was purchased from G.C. Industries (Chatsworth, CA). Permeation tubes containing 1–3 mL of dimethyl methylphosphonate or *N,N*-dimethylacetamide were prepared using 1–$1^1/_2$ in. lengths of Teflon heatshrink tubing ($^3/_8$ in. i.d., Cole-Parmer) capped at both ends with Teflon rods. These tubes were stored in a desiccator for 1–3 weeks and then calibrated at operational temperatures (DMMP, 50 °C; DMAC, 25 °C). The tubes were weighed every 2–3 days until constant permeation rates (in μg/min) were obtained. Permeation rates had errors of less than 10%.

Data Collection and Analysis. During coating testing, the difference frequency output of the sensor was recorded every 2 s at 1 Hz resolution. In a typical experiment, the sensor was exposed to air for 1 min to establish a base line response. This was followed by repeated exposures of vapor/air/vapor/air, with each exposure of 2-min duration.

Each of the 12 coatings was exposed to 11 chemical vapors. Each vapor was run at four different concentrations, with two experiments (four vapor exposures) at each concentration. Frequency shifts caused by these vapor exposures were determined by integrating the area under the signal peak and averaging over the number of data points collected. An equilibration time of 20 min was scheduled at the beginning of each new vapor to allow the vapor stream to achieve equilibrium. At the completion of the experiments for a given vapor, the gas handler system was flushed with clean air for 10 min.

Pattern Recognition. Since dividing the sensor responses by concentration is not possible for a field instrument measuring unknowns, it is important for each sensor to be exposed to the same concentrations, and to apply a closure method (such as pattern normalization) to the results. The data were collected on individual sensors rather than an array. As a result, the sensor data for a given vapor were not always collected at the same concentration for each sensor. To get the same concentrations for each vapor across a pattern vector, responses for some sensors were interpolated from the calibration curves. For most of the 11 vapors, average frequency shifts were determined for two experiments at each of three concentrations. Only two concentrations resulted in satisfactory responses for MSF, while all four concentrations of DMMP were consistent for all of the sensors tested. These response values, or descriptors, for the 11 vapors formed a 66 × 12 data matrix. Each row in the matrix is a pattern vector, representing responses of the 12 coatings to a given vapor/concentration experiment.

These data were then analyzed on a VAX 11-750 using pattern recognition routines included in ADAPT (*16*). The pattern vectors were normalized using pattern normalization methods described previously (*12*). The normalization procedure removes the effects of concentration and the sensitivity of one vapor relative to another. This is necessary to obtain the maximum amount of chemical information from vapors that give only weak responses. Each descriptor for a given coating was then autoscaled to a mean of zero and a standard deviation of unity. Although autoscaling alters the actual values of the sensor responses, it does not alter the number of features or the basic geometry of the clustering (*16*).

Multiple linear regression was used to investigate the uniqueness of each sensor while testing for collinearities which could cause numerical instabilities in the analysis. After the set of sensor responses was checked for collinearities, pattern recognition techniques for display and mapping, clustering, and classification were implemented.

Because it is impossible to imagine the data points clustering in *n*-dimensional space, a display method was used to transform the data into two-dimensional space for easier visualization. The Karhunen–Loeve transformation finds the axes in the data space that account for the major portion of the variance while maintaining the least amount of error. A correlation matrix for the stored data set is computed and the eigenvalues and eigenvectors are then extracted. The two-principal-component plot presents the plane that best represents the data (*17*). For display purposes, a nonlinear mapping routine is used to separate vapors that overlap when projected onto this plane but are separated in the multidimensional space. The nonlinear mapping routine transforms a set of points from *n*-space to two-space by maintaining the similarities between the points. It does this by minimizing an error function (*18*).

Clustering techniques, which are unsupervised learning techniques because the routines are given only the data and not the class membership of the points, group compounds together according to some criterion. By examination of the different clustering results, a clearer insight is gained into the actual clustering in *n*-space (*17*). ADAPT includes a variety of agglomerative hierarchial clustering routines which group the data by progressively fusing them into subsets, two at a time, until the entire group of patterns is a single set. The routines maintain a particular within-group homogeneity, depending on the criterion and the fusing strategy used. Three dissimilarity metrics were used: (a) Euclidean distance squared, (b) Euclidean distance, and (c) Canberra distance. The fusing strategies investigated were (a) nearest neighbor, (b) median, (c) average, and (d) flexible fusion. Resulting data are displayed in dendrograms (*19*).

Classification methods, which are also considered supervised learning techniques because they are given both the data and the correct classification results, generate mathematical functions to described the clustering. There are two basic modes of operation for classification methods: (a) parametric, and (b) nonparametric. Parametric techniques use statistical information based on the underlying data to define the boundaries of the clusters. Their performance is based on the assumption made concerning the statistical characteristics of the data. The nonparametric techniques use mathematics to define the area between the clusters. The primary parametric programs used in these studies are Bayes linear and quadratic (*17*), while the nonparametric routines were the perceptron (*17*) and adaptive least-squares (ALS) (*20*).

To achieve the best classification results, each sensor response is multiplied by a constant so that the contribution of each sensor is weighted. The vector that is generated is called a weight vector. The routine iteratively updates the weight vector, and a decision surface can be located between the classes. The weight vector for a linear decision surface can be generated by one classifier, stored, and then used subsequently in another classifier. Weight vectors can be improved by passing them between classifiers.

Learning techniques are used to train the algorithm on the correct classification results. A discriminant function is found that separates one class from another. The width of the function is a measure of the separation. Feature selection is used to reduce the number of sensors to the smallest set while maintaining good classification results (*14*). One feature selection method randomly removes vapors from the data set for each analysis in multiple applications of the perceptron algorithm. As each vapor is removed, the variance in the weight vector is determined. If the observed variance is large, then the information from the corresponding sensor does not contribute significantly to the observed separation of classes.

RESULTS

Vapors used during this study are given in Table I. These vapors were chosen to represent a variety of structural and functional groups. In addition, we were specifically interested in coatings that would be sensitive to toxic organophosphorus compounds. The set of vapors contains three vapors selected as simulants of these materials. Methanesulfonyl fluoride is an irreversible enzyme inhibitor and, as such, exhibits biological activity similar to the organophosphorus insecticides (*21*). Dimethylacetamide has solubility properties that are similar to these materials, as indicated by the solubility pa-

Table III. Normalized Vapor Responses (10^{-3} Hz/(ppm/kHz))

	coatings											
vapors	PEM	OVEMAC	PVP	PBAN	PAOX	PECH	ABACD	FPOL	PIP	OV210	PPZN1	PPZN2
MSF	240	78	44	160	130	0.0	96	390	21	0.0	30	37
DMAC	650	60	0.0	38	290	210	39	1360	15.6	6.4	19	130
DMMP	6500	460	40	450	830	550	590	15600	230	204	340	990
DCE	4.2	0.9	2.0	3.4	4.2	3.0	3.3	2.4	2.5	0.4	0.5	0.9
water	2.8	1.3	4.8	0.3	0.4	0.6	0.4	0.2	0.09	0.2	0.2	0.7
ISO	0.7	0.6	0.13	0.4	0.4	0.4	1.9	0.4	1.7	0.3	0.0	0.4
TOL	3.8	1.3	0.7	3.9	4.8	3.9	9.4	0.12	3.7	0.6	0.5	1.4
DES	4.4	1.3	0.4	3.4	4.0	4.1	8.7	3.0	3.7	0.6	0.4	1.7
TBP	24	3.6	3.0	6.4	17	7.2	13.8	13	0.08	29	3.7	
BTN	3.6	0.5	0.5	1.8	1.9	2.0	2.2	3.0	0.54	0.3	1.3	1.9
BTL	11	2.7	11	3.4	8.9	2.6	18	8.0	1.0	0.7	0.9	1.1

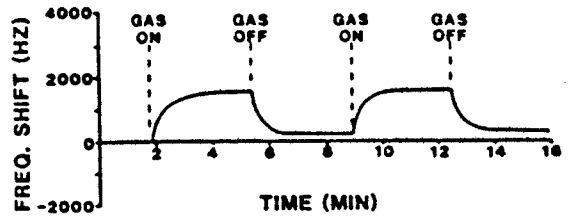

Figure 2. Typical SAW device reversible response.

rameter values in Table I. Dimethyl methylphosphonate (DMMP) is structurally similar to many of the organophosphorus pesticides. These three vapors are grouped together and labeled class 1 vapors. The remaining vapors are called class 2 and represent a very general set of potential interferences. Note that tributyl phosphate is also an organophosphorus compound. It has been included in class 2 specifically to test the ability of the coatings and pattern recognition techniques to distinguish between chemically similar compounds. Included in the table are solvatochromic parameters, which are a scale for comparing the solubility properties of these vapors (22, 23). These parameters are a measure of the dipolarity/polarizability (π^*), hydrogen bond donor acidity (α), and hydrogen bond acceptor basicity (β). The ranges of values in the tables are evidence of the generality of the set of selected vapors. No data are available directly for DMMP or isooctane. Values in the table for DMMP are based on values for a similar compound, dimethyl ethylphosphonate (DMEP). Values for isooctane are based on values for 2,4-dimethylpentane. These parameters will be correlated with observed response behavior in the discussion section.

Adsorbent coatings exhibited good response times, usually reaching 90% of total response within 1 min. At high vapor concentrations, the response time was more a function of the system dead volume than of the coating response behavior. At lower concentrations, however, responses may have been affected by longer equilibration time between vapor and coating, or by adsorption of vapor onto tubing walls. Upon removal of the vapor stream, a rapid return to stable baseline was usually observed. A typical response is shown in Figure 2. Reversible responses were observed for all vapor/coating pairs given in Table III. Frequency shift data were used to generate calibration curves. The slopes of these curves in Hz/ppm (vapor), were then normalized by dividing by the film thickness (in kHz). Normalized responses are presented in Table III.

Coating materials and their structures are given in Table II. Because we were interested in detecting organophosphorus compounds, coatings were selected based on preliminary tests that indicated a sensitivity to DMMP. Coating sensitivities to other vapors in this study were not known, and extreme selectivities to DMMP and other class 1 vapors were not

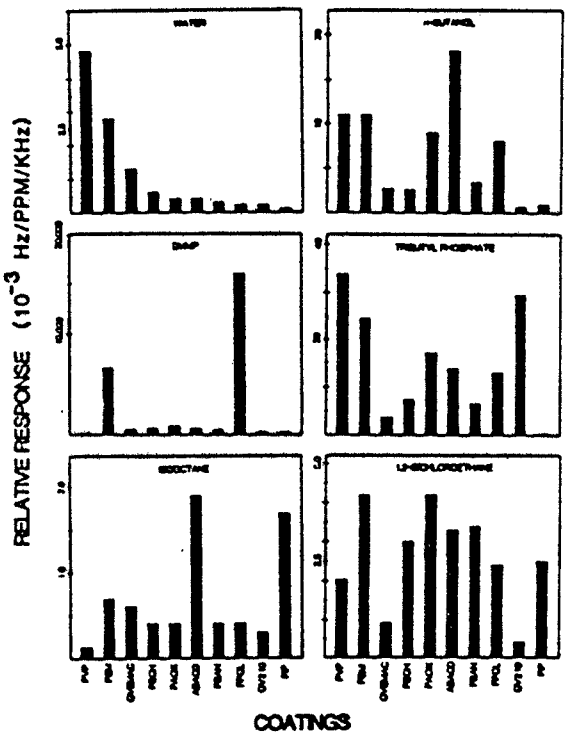

Figure 3. Bar graphs showing relative response patterns of 10 coatings to specific vapors.

suspected. In general, most of the coatings were more sensitive to class 1 than to class 2 vapors and exhibited particularly good sensitivity to DMMP. Poly(ethylene maleate) and fluoropolyol were the most sensitive coatings for detecting DMMP and other class 1 vapors. The response of fluoropolyol to DMMP was the response of greatest magnitude in the entire data set and was at least 2000 times greater than its response to any class 2 vapor. The coating that was least sensitive to DMMP was poly(vinylpyrrolidone). While it was the most sensitive coating for water, its response to water was still 10 times less than its response to DMMP.

Noise levels of 10–15 Hz are associated with the SAW devices. Assuming a S/N ratio of 3, the minimum detected signal is 45 Hz. For a 100-kHz film of fluoropolyol, for example, this translates into detection limits of 0.03 ppm for DMMP and <2000 ppm for water. For a 100-kHz film of poly(vinylpyrrolidone), these detection limits are 11 ppm and 100 ppm, respectively.

Individual bar graphs showing the relative responses of the 12 coatings to six of the vapors are shown in Figure 3. For display, responses are normalized to the coating with the greatest responses, while the scale of actual response (in

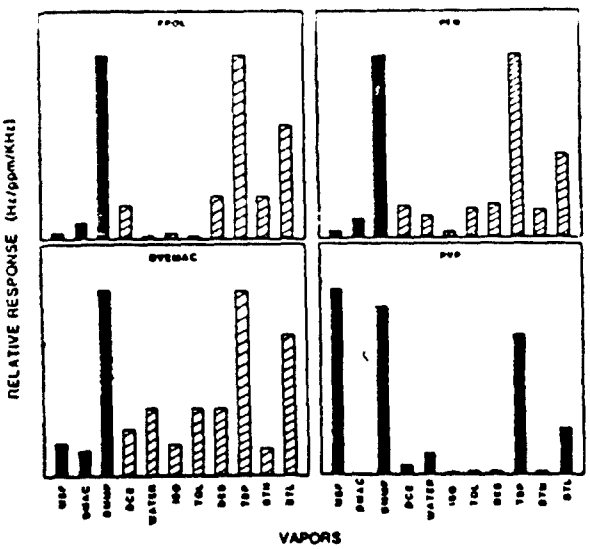

Figure 4. Bar graphs showing relative response patterns of four coatings normalized to class 1 vapors (solid bars) and class 2 vapors (parallel striped bars).

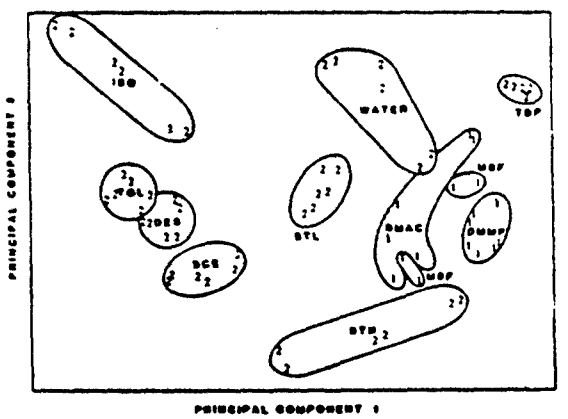

Figure 5. Principal component plot using results from all 12 coatings.

Hz/(ppm/kHz) is given on the y axis. Similarly, bar graphs showing the responses of four of the coatings to all 11 vapors are shown in Figure 4. The solid bars shown are all normalized to the vapor eliciting the highest response. In most cases, the class 2 vapors elicited much lower responses than class 1 vapors. For this reason, the response patterns for these vapors are not easily seen when plotted on the same scale as the class 1 vapors. To display the relative responses of the class 2 vapors on the same graph, the class 2 vapors were normalized to the highest class 2 response. Bars have been superimposed in Figure 4 to show the response pattern of the normalized class 2 vapors.

Pattern Recognition. The multiple linear regression results indicate that the correlation between sensors is not strong, so individual coatings could not be eliminated on the basis of redundancy. According to eigenanalysis, ten sensors account for 99% of the variance, indicating that at least two of the sensors can be removed without reducing the separation between compounds. The first two principal components from the Karhunen–Loeve transformation were used to initialized the nonlinear mapping routine. The resulting plot is shown in Figure 5. Class 1 and class 2 compounds are labeled on the plot with a 1 or a 2, respectively. It is clear that responses for individual vapors tend to cluster in discreet sectors of space with well-defined boundaries. In addition, class 1 vapors tend to cluster near one other. Vapors cluster in n-space based on similarities in response patterns. These clusters may indicate

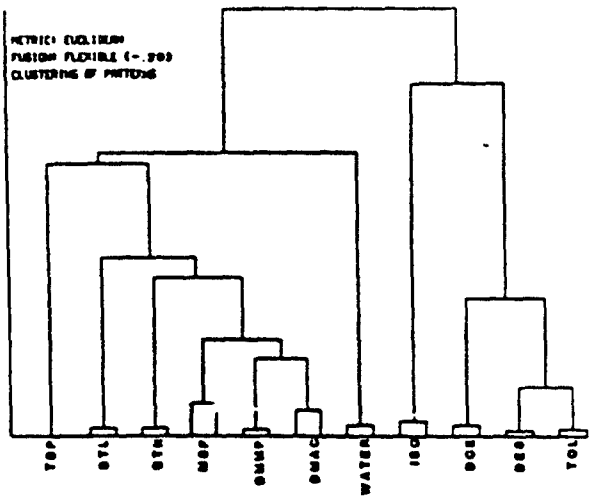

Figure 6. Typically hierarchical cluster results of all the vapors based on all 12 coatings (Euclidean distance metric with flexible fusion).

Table IV. Weight Vector Components for Four Best Coatings

coating	weight vector value	no. wrong		% recognition
		class 1	class 2	
		0	0	100
OVEMAC	-0.06783	3	1	93.9
PEM	0.11633	2	8	84.9
PVP	-0.80966	18	0	72.7
FPOL	0.20978	14	6	69.7

similarities in vapor/coating interaction mechanisms for these vapors.

Hierarchical cluster analysis produce similar results for each metric. The fusion methods, however, produced different groupings. Flexible fusion was selected for display because it is space conserving and does not change the relationships between the groups of data (*24*). The dendrogram resulting from hierarchical cluster analysis on one third of the data set is shown in Figure 6. The original matrix was reduced to simplify visualization. Results from the second experiment of the two highest concentrations were selected. The y axis of the dendrogram is a measure of the dissimilarity of response patterns for given vapors. Thus, diethyl sulfide and toluene exhibit very similar response patterns, and the lines representing the response patterns for these vapors converge very low on the y axis of the dendrogram. Conversely, the lines for water and isooctane do not converge, indicating very dissimilar response patterns.

Similarities and dissimilarities in the coating were examined by applying cluster analysis on the transpose of the 66 × 12 matrix. Since no structural information was available for the polyphosphazine coatings, information derived from these coatings is of limited value. Disregarding the response data for these coatings, cluster analysis was also applied to the transpose of the resulting 66 × 10 matrix. These results are displayed in Figure 7.

By use of classification routines and feature selection to reduce the sensors with the most variance, four coatings were found that could separate class 1 from class 2 vapors. These were poly(ethylene maleate), fluoropolyol, octadecyl vinyl ether/maleic anhydride copolymer, and poly(vinylpyrrolidone). The hyperplane between the two classes can be given a dead zone (or a width of 1000 times the normal width produced by the routines), which indicates that the classes are well separated. With all four coatings, 100%

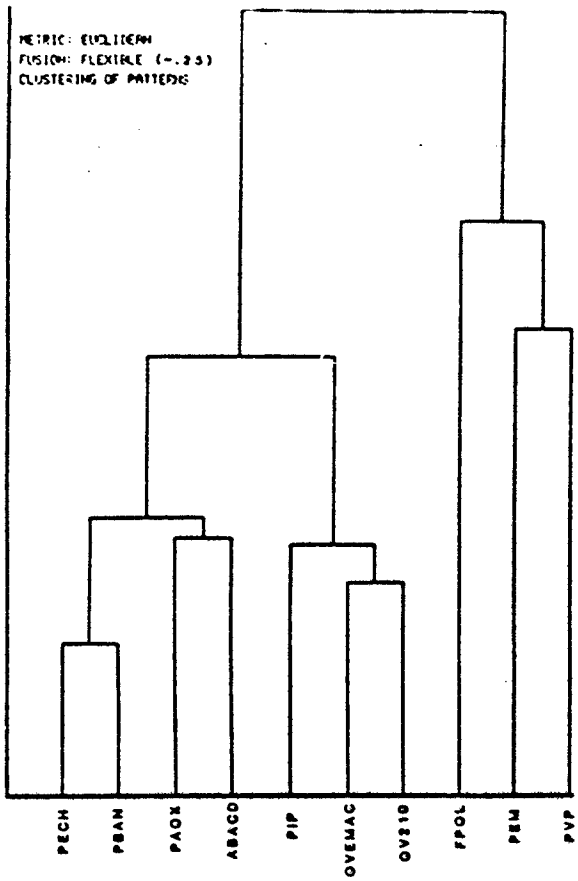

Figure 7. Typical hierarchical cluster results of coatings based on responses to 11 vapors (Euclidean distance metric with flexible fusion).

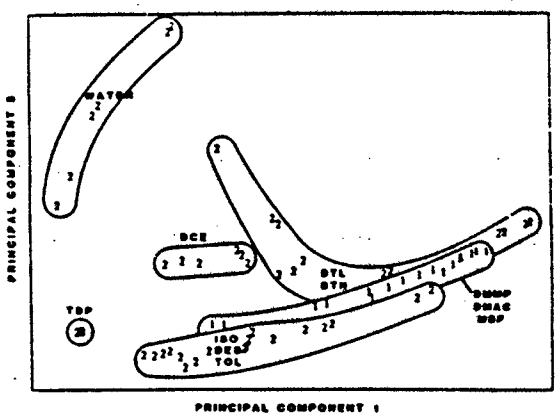

Figure 8. Principal component plot using results from the four best coatings: PEM, FPOL, PVP, OVEMAC.

recognition of vapors as class 1 or class 2 is possible. Eliminating octadecyl vinyl ether/maleic anhydride copolymer decreases this to 94%, which still represents reasonably good discrimination. The weight vectors for these coating are given in Table IV. Of these coatings, fluoropolylol and poly(vinylpyrrolidone) are most important for the correct classification of class 1 vapors, while poly(ethylene maleate) is important for class 2 vapors.

The nonlinear mapping plot from the two principal components using these four coatings is shown in Figure 8. While the cluster spaces for some of the vapors appear to overlap, the boundary for class 1 compounds is still well defined. The dendrogram produced by Euclidean metrics and flexible fusion for these coatings is given in Figure 9. Class 1 compounds

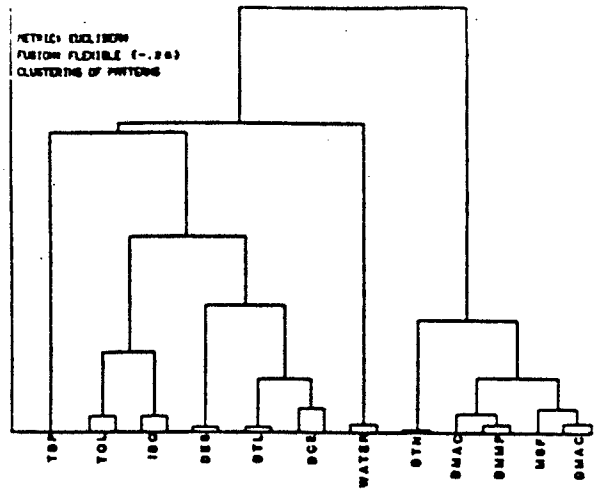

Figure 9. Typical hierarchical cluster results of the vapors for the best four coatings (Euclidean distance metric with flexible fusion).

are clustered very closely, and except for butanone, are well separated from the interference vapors.

DISCUSSION

In the course of discussing these results we will attempt to develop a rationale to be used in future coating design and/or selection. The solvatochromic parameters in Table I represent a relative scale for comparing solubility properties of the vapors. The values in the table are for bulk solutions and do not describe all possible solubility interactions. For the purposes of the discussion they represent a reasonable first approximation of the solubility properties of these materials. By correlating observed responses with these parameters, we hope to identify the vapor/coating interaction mechanisms that are responsible for our results.

Since no quantitative scale is available to characterize the solubility properties of the coating materials, qualitative estimates of relative hydrogen bond acceptor (HBA) and hydrogen bond donor (HBD) strengths were made based on the weight percentages of HBA and HBD functional groups in their structure. These percentages are reported in Table II. Materials lacking any hydrogen bonding functional groups were labeled non hydrogen bonding (NHB). All these materials are polymers with the exception of abietic acid, which is a crystalline organic material. Since no structural information was available for the polyphosphazines, results for these coatings will not be included in the discussions of structure/response correlations.

The vapor/coating interaction could be modeled as the dissolution of a solute vapor in a solvent coating. It is reasonable to model the coatings as a solvent phase since all the polymers were employed above their glass transition temperatures. The response should be determined by solubility interactions, e.g., dipole–dipole and hydrogen bond interactions. The data set as a whole indicates that the solubility properties represented by the parameters in Table I are important in determining SAW device responses. The six vapors whose response patterns are illustrated by the bar graphs in Figure 3 are representative of various classes of vapors, based on solubility properties. Water is a strong HBD and a weak HBA; 1-butanol is both HBD and HBA; DMMP and tributyl phosphate are HBA but not HBD; isooctane is a NHB vapor with little or no dipolarity/polarizability; and dichloroethane is a NHB vapor with significant dipolarity/polarizability. The bar graphs in Figure 3 show that vapors with different solubility properties elicited different coating response patterns. Vapors with similar solubility properties, such as DMMP, dimethylacetamide, and 2-butanone have more similar re-

sponse patterns (see data in Table III). DMMP and tributyl phosphate, however, have easily distinguishable response patterns but have a similar solubility properties. Closer examination shows that this is primarily due to poly(vinylpyrrolidone), fluoropolyol, and OV210. While the overall response of the remaining coatings is still more sensitive to DMMP, the general response pattern of these coatings is more similar.

The reason for which all the coatings were most sensitive to DMMP is not clear. Examination of the solubility parameters in Table I indicates that DMMP is not exceptional in its hydrogen bonding ability. Therefore, the extremely high response of these coatings to DMMP must be due to some solubility property that has not been characterized in Table I, such as its dipolarity/polarizability, or to a fortuitous combination of solubility properties.

The noted differences observed between DMMP and tributyl phosphate are also likely due to differences in a solubility parameter that is not examined here. Structurally, these vapors differ in size, with tributyl phosphate containing large alkyl groups that may significantly affect its solubility in certain materials.

Hierarchical cluster analysis provides a more systematic determination of the similarity or dissimilarity of the various vapors, as determined by SAW sensor responses. The resulting dendrogram in Figure 6 sorts the vapors in a manner that is consistent with their solubility properties. Starting from the top of the plot and working down (toward increasing similarity), the NHB vapors on the right are separated from the HBA and HBD vapors on the left. Isooctane is separated from the other NHB vapors, a result consistent with the unique character of isooctane as indicated in Table I. It is the only vapor with near zero dipolarity/polarizability. The NHB vapors with significant dipolarity/polarizability (1,2-dichloroethane, toluene, and diethyl sulfide) are more similar to one another than they are to isooctane or the HBA and HBD vapors. In this cluster, dichloroethane stands out in the dendrogram and in Table I as the NHB vapor with the greatest dipolarity/polarizability.

Among the HBA and HBD vapors on the left of the dendrogram, water is the least similar to any other vapors. Accordingly, water is seen in Table I to have extremely highly dipolarity/polarizability. It is also unusual in its relatively high HBD character. The other HBD vapor, 1-butanol, has significantly greater HBA character and less dipolarity/polarizability than water and is shown in the dendrogram to be more similar to the other HBA vapors. In general, the HBA vapors cluster together, with DMMP and dimethylacetamide being the most similar. These results demonstrate that the solubility properties in Table I should be considered as important factors affecting SAW sensor responses.

Exceptions to these general trends must also be considered. For example, methanesulfonyl fluoride clusters with the other HBA vapors, but it is a weak HBA vapor and may be more similar to that of diethyl sulfide, a NHB vapor. Similarly, tributyl phosphate does not cluster as closely to DMMP as might be expected based on the fact that both are organophosphorus compounds with similar HBA strength. Individual comparisons, therefore, emphasize the importance of factors in addition to the solubility properties in Table I.

The roles of coating properties and structures in determining sensor responses cannot be fully determined by these data. Coating responses will be influenced by a mixture of interactions with various structural features such as double bonds, conjugation, aliphatic side chains, and heteroatomic functional groups. The relative importance of these interactions is difficult to determine, and relevant solubility properties for these coatings have not yet been identified.

We can, however, explore the role of hydrogen bonding interactions by using the relative scale of HBA and HBD strengths in Table II. With the exception of poly(isoprene), all of the coatings contain heteroatoms capable of accepting hydrogen bonds. HBA strength should be significant for those coatings containing carbonyls of nitrogen-containing groups. Weaker HBA strength is expected for those coatings containing only ether linkages. Three of the coatings also contain HBD groups (fluoropolyol, poly(amidoxime), and abietic acid). Water and butanol are the only HBD vapors in our data set. Of these, trends in the response to water vapor are most likely due to HBA strength of the coatings because water has stronger HBD than HBA strength and has no aliphatic character. For this reason, coatings were listed on the x axis of Figure 3 in order of decreasing response to water.

The results in Figure 3 show that the relative coating responses to water tend to follow the relative HBA strengths estimated from the weight percentages of the HBA functional groups in the coating structures. This confirms that hydrogen bonding interactions are important and justifies consideration of the simple scale in Table II. While water also has considerable dipolarity/polarizability properties, the data indicate no correlation with polarity. Nonpolar isooctane does not exhibit a trend opposite to that exhibited by water nor does polarizable dichloroethane follow any apparent trend. The other HBD vapor, 1-butanol, exhibits a different response pattern. This may be due to greater HBA strength and more organic character relative to water.

On the low end of this scale, poly(isoprene) is the only NHB vapor coating in this study. It exhibits a much larger response to the NHB vapor isooctane than any other coating, with the exception of abietic acid. In addition, the responses of poly(isoprene) to other NHB vapors (dichloroethane, toluene, and diethyl sulfide) are larger than for the HBA and HBD vapors in class 2. In general, the other coatings exhibit higher responses to class 2 HBA vapors, particularly TBP and butanol, than to the NHB vapors.

The bar graphs in Figure 4 and the data in Table III indicate that all the coatings, except poly(vinylpyrrolidone), have a fundamental similarity. They are more sensitive to class 1 than to class 2 vapors. Cluster analysis helps to more clearly identify similarities and dissimilarties among the coatings. In the dendrogram in Figure 7, fluoropolyol, poly(ethylene maleate), and PVP stand out as being most dissimilar to other coatings and also dissimilar to one another. These results can be related to the data by examining the bar graphs in Figure 3. Relative to the other coatings, fluoropolyol has very strong response to DMMP, a weak response to water, and average responses to tributyl phosphate and isooctane. Poly(ethylene maleate) exhibits strong response to DMMP, water, and tributyl phosphate, and an average response to isooctane. Poly(vinylpyrrolidone) has strong responses to water and tributyl phosphate, but gives the weakest responses to DMMP and isooctane. In relating the dendrogram results to structure, it is worth noting that poly(vinylpyrrolidone) may be the most basic of the coatings in the data set. Poly(ethylene maleate) may be the most polar, since it has polar groups in the backbone and no side chains. Fluoropolyol is distinctive in its combination of structural features, such a fluoroaliphatic, aromatic, ether, and hydroxyl groups.

Similarities among the coatings are shown in the dendrogram by the clustering of poly(isoprene), octadecyl vinyl ether/maleic anhydride copolymer, and OV210. These all have substantial hydrophobic character. The cluster containing poly(epichlorohydrin), abietic acid, acrylonitrile/butadiene copolymer, and poly(amidoxime) is of interest because poly(amidoxime) is a modification of the acrylonitrile/butadiene copolymer. The modification created a small percentage

(0.07) of HBD groups. As a result, poly(amidoxime) clusters slightly closer to abietic acid, which also has HBD groups, than to its parent polymer. A previous study of 27 coating materials on piezoelectric sensors demonstrated that clustering of these materials may be influenced by structural similarities (7). Fewer coatings were used in our data set, and the coatings employed were structurally more diverse. As a result, such clustering is not as evident.

CONCLUSIONS

The solubility properties considered in this paper were systematically demonstrated to be important factors in determining SAW sensor responses. The exceptions noted indicate the limitations of using bulk solution values in describing dilute solutions and also indicate that additional properties not yet considered may also exert some influence. Solubility properties currently provide the best rationale for selecting or designing coatings for specific applications. A more detailed investigation of the relationship between structure and observed solubility properties would also facilitate the selection and design processes.

Pattern recognition techniques were valuable in extracting information regarding vapor/coating interactions from this multidimensional data set. In addition, it is clear that the combination of multiple sensor arrays of coated SAW devices and appropriate pattern recognition software will provide a sensor system that can be selective as well as sensitive for a broad spectrum of compounds.

ACKNOWLEDGMENT

The authors wish to thank the following persons for their efforts: Peter Jurs for his guidance in the pattern recognition work; Arthur Snow and James Griffith of the NRL Polymeric Materials Branch, NRL, for supplying us with much of the coating materials and related structures; and M. J. Kamlet and Michael Abraham for much informative discussion. Research was performed at Naval Research Laboratory, Washington, DC.

Registry No. MSF, 558-25-8; DMAC, 127-19-5; DMMP, 756-79-6; DCE, 107-06-2; ISO, 540-84-1; TOL, 108-88-3; DES, 352-93-2; TBP, 126-73-8; BTN, 78-93-3; BTL, 71-36-3; PEM, 25949-13-7; OVERMAC, 28214-64-4; PVP, 9003-39-8; PBAN, 9003-18-3; PAOX, 103496-60-2; PECH, 24969-06-0; ABACD, 514-10-3; FPOL, 104051-33-4; PIP, 9003-31-0; H_2O, 7732-18-5.

LITERATURE CITED

(1) Wohltjen, H. *Sens. Actuators* **1984**, *5*, 307.
(2) Snow A.; Wohltjen, H. *Anal. Chem.* **1981**, *58*, 1411.
(3) Bryant, A.; Poirier, M.; Riley, G.; Lee, D. L.; Vetelino, J. F. *Sens. Actuators* **1983**, *4*, 105.
(4) D'Amico, A.; Palma, A.; Verona, E. *Sens. Actuators* **1982/1983**, *3*, 31.
(5) Chuang, C. T.; White, R. M.; Bernstein, J. J. *IEEE Electron. Device Lett.* **1982**, *3*(6), 145.
(6) Alder, J. F.; McCallum, J. J. *Analyst (London)* **1983**, *108*, 1169.
(7) Carey, W. P.; Beebe, K. R.; Kowalski, B. R.; Illman, D. L.; Hirschfeld, T. *Anal. Chem.* **1986**, *58*, 149.
(8) Fog, H. M.; Reitz, B. *Anal. Chem.* **1985**, *57*, 2634.
(9) Morrison, R.; Guilbault, G. *Anal. Chem.* **1985**, *57*, 2342.
(10) Guilbault, G.; Kristoff, J.; Owen, D. *Anal. Chem.* **1985**, *57*, 1754.
(11) Kindlund, A.; Sundgren, H.; Lundstrom, I. *Sens. Acuators* **1984**, *6*, 1.
(12) Stetter, J.; Jurs, P. C.; Rose, S. L. *Anal. Chem.* **1986**, *58*, 860.
(13) Jarvis, N. L.; Lint, J.; Snow, A. W.; Wohltjen, H. Proceedings of the 1983 Scientific Conference on Chemical Defense Research; CRDC-SP-84014; Dimmick, R. L.; Reusa, M., Eds. U.S. Army, 1984; pp 45–53; NTIS, ADB-09086L.
(14) O'Rear, J. G.; Griffith, J. R.; Reines, S. A. *J. Paint. Technol.* **1971**, *43*(552), 113.
(15) Grate, J. W.; Ballantine, D. S., Jr.; Wohltjen, H. *Sens. Actuators*, in press.
(16) Stuper, A. J.; Brugger, W. E.; Jurs, P. C. *Computer Assisted Studies of Chemical Structure and Biological Function*; Wiley-Science: New York, 1979.
(17) Tou, J. T.; Gonzalez, R. C. *Pattern Recognition Principles*; Addison-Wesley: Redding, MA, 1974.
(18) Beech, G. *Fortran IV in Chemistry*; Wiley: New York, 1975.
(19) Massart, D. L.; Kaufman, L. *The Interpretation of Analytical Chemical Data by Use of Cluster Analysis*; Wiley: New York, 1983.
(20) Moriguchi, I.; Komatsu, K.; Matsushita, Y. *J. Med. Chem.* **1980**, *23*, 20.
(21) Dalton, A.; Neenan, J. P.; Ash, C. E.; Bette, L.; Finke, J. M.; Garman, J. A.; Rao, M.; Walsh, K.; Williams, R. R. *Biochem. Biophys. Res. Commun.* **1982**, *104*, 597.
(22) Kamlet, M. J.; Taft, R. W. *Acta Chem. Scand., Ser. B* **1985**, *B39*, 611.
(23) Kamlet, M. J.; Abboud, J. M.; Abraham, M. H.; Taft, R. W. *J. Org. Chem.* **1983**, *48*, 2877.
(24) Williams, W. T.; Lance, G. N. In *Statistical Methods for Digital Computers*; Enslein, K., Ralston, A., Wilf, R., Ed.; Wiley-Interscience: New York, 1975.
(25) Abram, M. H., personal communication.

RECEIVED for review April 15, 1986. Accepted June 19, 1986. The authors gratefully acknowledge the support of the coatings testing work by Army/CRDC, Aberdeen Proving Ground, MD (61-1439), and of the pattern recognition work by Brad Rikke, HQ AMD/RDSX, Brooks Air Force Base, TX (MIPR 85-0005).

Reprinted from Analytical Chemistry, 1988, 60, 869.

Determination of Partition Coefficients from Surface Acoustic Wave Vapor Sensor Responses and Correlation with Gas–Liquid Chromatographic Partition Coefficients

Jay W. Grate* and Arthur Snow

Chemistry Division, Naval Research Laboratory, Washington, D.C. 20375-5000

David S. Ballantine, Jr.

GEO-Centers, Inc., 10903 Indian Head Highway, Ft. Washington, Maryland 20744

Hank Wohltjen

Microsensor Systems, Inc., P.O. Box 90, Fairfax, Virginia 22030

Michael H. Abraham, R. Andrew McGill, and Pnina Sasson

Department of Chemistry, University of Surrey, Guildford, Surrey GU2 5XH, United Kingdom

Surface acoustic wave (SAW) devices coated with a thin film of a stationary phase sense chemical vapors in the gas phase by detecting the mass of the vapor that distributes into the stationary phase. This distribution can be described by the partition coefficient. An equation is presented that allows partition coefficients to be calculated from SAW vapor sensor frequency shifts. The experimental responses of fluoropolyol-coated 158-MHz dual delay line SAW vapor sensors are converted to partition coefficients by this method, and these results are compared with partition coefficients determined by gas–liquid chromatography. These two methods rank the vapors in the same order of increasing sorption, but individual partition coefficient values are not always in precise agreement. The influence of temperature and gas-phase vapor concentration on vapor sorption is also examined.

The use of surface acoustic wave (SAW) devices for sensing chemical vapors was first reported in 1979 (*1*) and has since been investigated by several groups (*2–19*). SAW devices function by generating mechanical Rayleigh surface waves on a thin slab of a piezoelectric material (such as quartz) that oscillates at a characteristic resonant frequency when placed in a feedback circuit with a radio frequency (rf) amplifier (*7*). The oscillator frequency is measurably altered by small changes in mass or elastic modulus at the surface of the SAW device. Vapor sensitivity is typically achieved by coating the device surface with a thin film of a stationary phase that will selectively absorb and concentrate the target vapor. Vapor sorption increases the mass of the surface film and a shift in the oscillator frequency is observed. SAW devices offer many advantages as chemical sensors including small size, low cost, ruggedness, and high sensitivity. A further advantage is the potential for these sensors to be adapted to a variety of gas-phase analytical problems by designing or selecting specific coatings for particular applications. Methods to quantify vapor sorption and to understand the solubility interactions responsible for vapor sorption will facilitate coating development.

Equilibrium sorption of ambient vapor into the SAW device coating represents a partitioning of the solute vapor between the gas phase and the stationary phase. This process is illustrated in Figure 1. The distribution can be quantified by a partition coefficient, K, which gives the ratio of the concentration of the vapor in the stationary phase, C_s, to the concentration of the vapor in the vapor phase, C_v

$$K = C_s/C_v \qquad (1)$$

An equation is derived herein that allows K to be calculated directly from observed SAW vapor sensor frequency shifts. This conversion provides a method of normalizing empirical SAW data in a way that provides information about the vapor/coating sorption equilibrium.

As a sorption detector, the SAW sensor is similar to the bulk-wave piezoelectric (BWP) crystal detector first reported by King (*20, 21*). A linear relationship between the BWP crystal frequency shift (Δf) and K was later derived by Janghorbani and Freund (*22*). These authors investigated the use of coated BWP crystals as gas chromatographic detectors and demonstrated that peak areas were linearly related to retention volumes for three *n*-alkanes on squalene. (Retention volumes are directly proportional to K.) Edmonds and West demonstrated that the responses of a tricresyl phosphate coated BWP crystal to five vapors at 30 °C correlated with relative gas–liquid chromatographic (GLC) retention times at 93 °C; these results provided qualitative experimental support for the linear relationship between Δf and K (*23*). Alder et al. have also noted that there is a relationship between Δf and K, and that the slope of response–concentration plots should provide a measure of K (*24*). The relevance of K to SAW vapor sensor responses has also been previously noted (*6, 8*). The frequency shifts of a poly(ethylene maleate) coated device in response to five vapors were compared with relative K values estimated by using solubility parameters (*8*).

None of the previous studies, however, have calculated partition coefficients from sensor responses or compared them with absolute values of K determined by any other method. This is due, in part, to the scarcity of literature data on absolute K values, especially near ambient temperatures. We have therefore begun measuring absolute K values by GLC at 25 °C for a wide variety of vapors on SAW coating materials, with several objectives in mind. First, we wish to use GLC as an independent method of measuring sorption into our coating materials and to compare K values determined by GLC with K values determined from SAW measurements. Partition coefficients provide the best available first approximation for the prediction of SAW sensor responses. Second, the database of GLC K values can be correlated with

0003-2700/88/0360-0869$01.50/0

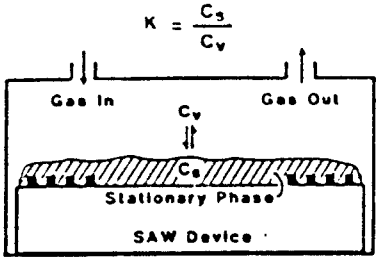

Figure 1. Distribution of vapor between the gas phase and the stationary phase which is quantified by the partition coefficient, K.

vapor solvatochromic parameters which describe vapor solubility properties (*25–28*). These correlations yield regression equations that predict K values for additional, unmeasured vapors whose solvatochromic parameters are known (*29*). Third, the coefficients in these equations provide a method for characterizing the solubility properties of the coating materials (*29*).

In this paper, we develop the equation relating SAW frequency shifts to K values and introduce the methods used to pursue the objectives above. We specifically examine the sorption of nine vapors into a soft oligomeric material referred to as fluoropolyol. This material was chosen on the basis of a prior study where several diverse stationary phases were applied to SAW devices and exposed to a range of chemical vapors (*5*). The fluoropolyol-coated sensor gave some of the highest responses observed. These results prompted us to begin a more extensive investigation of its sorption behavior.

THEORETICAL DEVELOPMENT

The change in oscillator frequency, Δf_s, observed when a bare SAW device is coated with an isotropic, nonpiezoelectric, nonconducting, thin film has been described by

$$\Delta f_s = (k_1 + k_2)F^2h\rho - k_2F^2h\left(\frac{4\mu}{v_R^2}\left(\frac{\lambda + \mu}{\lambda + 2\mu}\right)\right) \quad (2)$$

where k_1 and k_2 are material constants for the piezoelectric substrate, F is the unperturbed resonant frequency of the SAW oscillator, which is determined by the geometry of the interdigital transducers fabricated onto the surface, h is the coating thickness, ρ is the coating density, μ and λ are the shear modulus and Lamé constants of the coating, and v_R is the Rayleigh wave velocity in the piezoelectric substrate (*7*). The second term in this equation depends on the mechanical properties of the film and is often negligible for soft organic materials. If the mechanical properties are neglected, then eq 2 reduces to eq 3, which describes the perturbation in frequency caused by the mass of the applied film (*7*). This

$$\Delta f_s = (k_1 + k_2)F^2h\rho \quad (3)$$

treatment assumes 100% coverage of the device active area. The product of the factors h (film thickness in meters) and ρ (film density in kilograms per cubic meter) in this equation is simply the mass per unit area. Therefore the frequency shift, Δf_s, in hertz, caused by application of the thin film coating onto the bare SAW device can be expressed as

$$\Delta f_s = (k_1 + k_2)F^2m_s/A \quad (4)$$

The variable m_s is the mass of the coating in kilograms and A is the coated area in square meters. The frequency shift, Δf_v, in hertz, caused by absorption of the vapor into the coating can be expressed similarly as

$$\Delta f_v = (k_1 + k_2)F^2m_v/A \quad (5)$$

The variable m_v is the mass of the vapor in the stationary phase coating. Dividing eq 5 by eq 4 and rearranging gives eq 6, which is identical with an equation derived by King for coated BWP crystal detectors (*20*).

$$\Delta f_v = \Delta f_s m_v/m_s \quad (6)$$

The mass of the vapor in the stationary phase coating is the factor of greatest interest. It can be related to the concentration of the vapor in the stationary phase C_s, in grams per liter, by

$$C_s = m_v/V_s(0.001 \text{ kg g}^{-1}) \quad (7)$$

V_s is the volume of the stationary phase in liters. Now, substituting eq 7 into eq 3 and rearranging gives

$$m_v = KC_vV_s(0.001 \text{ kg g}^{-1}) \quad (8)$$

C_v is the concentration of the vapor in the gas phase in grams per liter. Finally, substitution of eq 8 into eq 6 relates Δf_v to K as shown in eq 9.

$$\Delta f_v = \Delta f_sKC_vV_s(0.001 \text{ kg g}^{-1})/m_s \quad (9)$$

This result can be further simplified by noting that V_s/m_s is the reciprocal of the density, ρ, of the stationary phase. If Δf_s is converted from hertz to kilohertz, the 0.001 conversion factor cancels out. The final result is

$$\Delta f_v = \Delta f_sC_vK/\rho \quad (10)$$

where Δf_v is the vapor frequency shift in hertz, Δf_s is the coating frequency shift in kilohertz, ρ is the coating density in kilograms per liter (grams per milliliter), C_v is the vapor concentration in the gas phase in grams per liter, and K is the partition coefficient. Experimentally, Δf_s is determined when the vapor-sensitive coating of density ρ is applied to the bare SAW device. Δf_v is measured when the sensor is exposed to a calibrated vapor stream of concentration C_v. The units of C_v, grams per liter, are appropriate since dynamic vapor streams are typically prepared by diluting a measured mass flow (grams per minute) into a known volumetric flow (liters per minute) of carrier gas (*30, 31*). These units are also easily converted to micrograms per liter, which is equivalent to the international standard of milligrams per cubic meter for gas-phase concentrations. Equation 10 provides a simple relationship for calculating K values from measurable sensor characteristics. The relationship is independent of the specific SAW substrate, having no dependence on SAW device frequency (F) or piezoelectric material constants (k_1, k_2).

The assumptions inherent in eq 10 are that the SAW device functions as a mass sensor (mechanical effects are negligible) and that the observed mass change is due to partitioning of the vapor between the gas phase and the stationary phase coating. In this regard, the equation represents a solubility model, i.e. dissolution of the solute vapor into the solvent stationary phase. One additional assumption is made in the substitution of the reciprocal of the stationary phase density, ρ, for V_s/m_s in eq 9. The variable m_s is the mass of the stationary phase, whereas V_s is actually the volume of the stationary phase when an equilibrium quantity of vapor has been absorbed. This volume is assumed to be equal to the volume of the stationary phase itself. As long as the mass loading of the stationary phase by vapor is low, as it will be for low vapor concentrations or weakly sorbed vapors, this assumption is reasonable.

Equation 10 is related (but not identical) to equations in ref 22–24 which describe the relevance of K to the responses of coated BWP crystal detectors.

EXPERIMENTAL SECTIONS

Materials. Fluoropolyol is a clear, very viscous oligomeric material, whose repeat unit is illustrated in Figure 2. The fluoropolyol used in these studies was provided by Dr. Jim Griffith of the Naval Research Laboratory Polymeric Materials Branch.

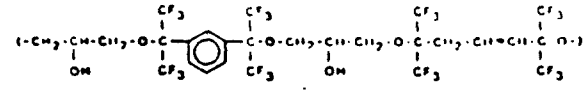

Figure 2. Repeat unit of fluoropolyol.

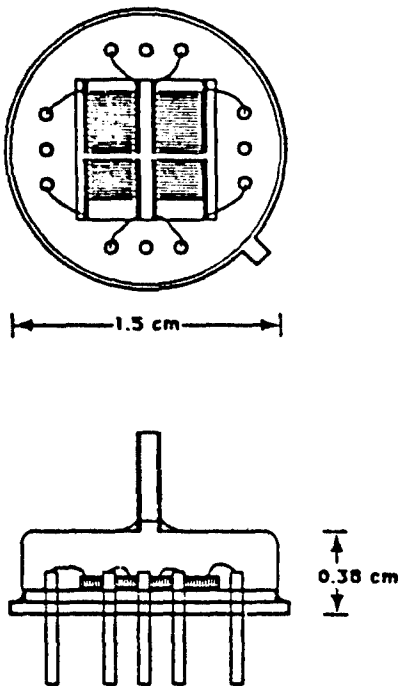

Figure 3. Schematic diagram of a 158-MHz dual SAW delay line mounted on a TO-8 style package with wire-bonded electrical connections.

These types of materials are prepared by methods described by O'Rear et al. (32). The density of fluoropolyol was measured by using a bulb with a calibrated vertical stem. (Fluoropolyol's high viscosity precluded the use of a density bottle or a pycnometer tube.) The bulb was weighed before and after adding fluoropolyol and placed in a thermostated bath. The results at various temperatures are as follows (T (°C), ρ (g mL^{-1}): 25, 1.6530; 40, 1.6322; 60, 1.6044; 90, 1.5629. The glass transition temperature of fluoropolyol is 10 °C, determined by DSC.

The liquid solvents used to generate vapor streams were commercial materials of greater than 99% purity, except diethyl sulfide (98%, Aldrich) and dimethyl methylphosphonate (DMMP) (97%, Aldrich). The solutes used in the GLC measurements were also commercial materials used as received; the GLC method does not require highly purified compounds.

158-MHz SAW Device. The 158-MHz dual SAW devices used in this study, shown in Figure 3 (Microsensor Systems, Inc., SD-158-A) were fabricated on ST cut quartz substrates approximately 0.5 cm square, with Al interdigital fingers. The entire surface was protected with ca. 200 Å of silicon dioxide. The input interdigital transducer for each SAW device consisted of 75 pairs of electrodes with each pair repeated at 20-μm intervals (i.e. an acoustic wavelength of 20 μm). The acoustic aperture was 70 wavelengths (i.e. 0.1400 cm). The output interdigital transducer was spaced 10 wavelengths (i.e. 0.0200 cm) from the input transducer and consisted of 100 pairs of electrodes also having each pair repeated at 20-μm intervals. The edges of the quartz substrate beyond the ends of the delay lines were cut 5° out of parallel with the IDT fingers to send acoustic reflections off-axis. This chip was epoxied onto a conventional gold-plated, 12-pin, TO-8 style integrated circuit package and electrical connections were made from the SAW interdigital electrodes by means of ultrasonically welded 1-mil gold wires. After one delay line was coated with fluoropolyol, the device was covered and sealed by a nickel-plated lid with two $^1/_{16}$-in. stainless steel tubes for vapor flow.

rf Electronics. The SAW sensor packages were plugged into Microsensor Systems, Inc., RFM-158A RF electronics modules. This circuitry operates each delay line of the dual delay line devices as a resonating element in an oscillator circuit. The frequencies of the two oscillators are mixed to provide a low-frequency difference signal. Two experimental systems were employed. The first consisted of four rf electronics modules, a power supply, and plumbing connections for delivering gas to the sensors (Microsensor Systems, Inc., SAS-158A). This system outputs the difference signals of each of the rf modules. The second system contained one rf electronics module, a buffer amplifier, and a power supply (Microsensor Systems, Inc., SPM-158A). This system outputs both the individual delay line frequencies and their difference frequency.

Vapor Sensor Coating. Vapor sensors were prepared by spraying a dilute solution of fluoropolyol in chloroform through a mask onto one delay line of a dual delay line SAW device. The spray was generated with an airbrush and was distributed over the entire surface of the delay line, including the interdigital transducers (IDT). The remaining uncoated delay line served as a reference sensor to provide temperature and pressure compensation. During coating, the oscillator frequencies of both the individual delay lines and their difference frequency were monitored. The change in the frequency of the delay line (Δf_c) provides a measure of the amount of coating applied (7). Two sensors, labeled A and B, were prepared. Sensor A had 228-kHz fluoropolyol on the coated delay line and 5 kHz on the reference line, for an effective coating of 223 kHz when the difference frequency is monitored. Sensor B had 222 kHz on the coated line and 1 kHz on the reference, for an effective coating of 221 kHz. The average thickness of these coatings (e.g. for 222 kHz) calculated according to eq 3 is 40 nm, using values of -8.7×10^{-6} and -3.9×10^{-6} m^2 s kg^{-1} for k_1 and k_2 on ST cut quartz (33). Given that the area of the IDTs and the space between them is 0.052 cm^2, this corresponds to 0.37 μg of material on the active surface.

Vapor Stream Generation. Vapor streams for testing sensors were generated from gravimetrically calibrated permeation tubes or gravimetrically calibrated bubblers using an automated vapor-generation instrument described in ref 31. This instrument generates selected vapor streams, dilutes them, and delivers a programmable flow rate of either clean carrier gas or the diluted vapor stream to the sensor. The instrument is controlled with an Apple IIe computer.

For these studies the carrier gas was dry air delivered to the sensor at ambient pressure. Dimethyl methylphosphonate and *N,N*-dimethylacetamide vapor streams were generated by using permeation tubes and the remaining vapor streams were generated from bubblers. Vapor streams from bubblers were diluted to 4–25% of saturation prior to delivery to the sensors. The flow rate of vapor stream to the sensor was 100 mL/min.

Sensor Response Data Collection. Frequency measurements were made with a Phillips PM6674 frequency counter. The data were transferred over an IEEE-488 bus to an Apple IIe computer. This computer was in communication with the computer controlling the vapor stream flows so that data collection and vapor stream operations were synchronized. The frequency data were collected at a resolution of 1 Hz. The temperature of the sensor was monitored with a YSI Model 44TC Telethermometer with a Type 401 thermister probe placed near the sensor in the rf electronics module. For the temperature-dependence study, the entire four-sensor system was placed inside a mechanical convection oven.

In a typical experiment, 225 data points were collected from each sensor at 6-s intervals. The vapor was switched on at point 45, off at point 75, back on again at point 135, and off again at point 165. The base line was determined by averaging the ten points prior to vapor exposure and ten points well after the exposure (i.e. prior to the next exposure or prior to the end of the experiment). The line through these two averages is the base line. The response was determined from the average of ten points prior to turning the vapor off. Base-line drift was usually negligible but was sometimes significant when monitoring the small frequency shifts observed from the reference delay line. Because of the averaging procedure used above, reference delay line shifts may not be exactly the same as the difference between the difference frequency shift and the coated delay line frequency shift.

Gas–Liquid Chromatography (GLC). Fluoropolyol/gas partition coefficients were determined by GLC using the in-

Table I. log K_{SAW} Values for Fluoropolyol

	typical concn range, μg L^{-1}	sensor, data set						std dev	
		A,1	A,2	A,3	B,1	B,2	A,4	min	max
DMMP	29–137	6.33	6.21	6.22	6.30	6.28	6.28	0.09	0.15
N,N-dimethylacetamide	11–81	6.37	6.21	6.08	6.18	6.11	6.13	0.07	0.15
1-butanol	1460–8730	3.77	3.81	3.80	3.88	3.81	3.89	0.02	0.10
2-butanone	25800–148000	3.40	3.34	3.33	3.41	3.38	3.44	0.04	0.09
water	1210-7180	3.37	3.17	2.97	3.00	3.30	3.41	0.06	0.16
toluene	9680–57300	2.90	2.82	2.80	2.95	2.89	2.90	0.02	0.09
diethyl sulfide	23600–137000	2.77	2.69	2.66	2.81	2.72	2.81	0.02	0.05
1,2-dichloroethane	30500–176000	2.52	2.46	2.40	2.53	2.40	2.44	0.02	0.09
isooctane	22000–129000	2.15	2.12	2.03	2.25	2.08	2.10	0.05	0.22

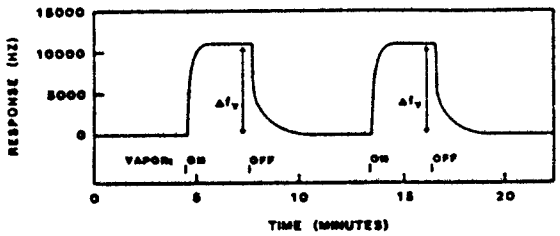

Figure 4. Response curve for two successive exposures of a fluoropolyol-coated SAW sensor to *N,N*-dimethylacetamide at 100 μg L^{-1} gas phase concentration.

strumentation and methodology in ref 34. (In this reference, the Ostwald coefficient, denoted with an L, is identical with the partition coefficient defined here in eq 3.) Fluoropolyol (4% loading) was supported on acid-washed, silanized, Celite Chromosorb G.AW.DMCS (Phase Separations Ltd.) in a 1.5 m long glass column. Absolute K values for a series of alcohols as standard solutes, and for water, were determined at 25 and 60 °C by using He as the carrier gas and a thermal conductivity detector. Corrections were made for pressure drop across the column (see eq 4–6 in ref 34) and for gas imperfections (eq 7 in ref 34). However, the latter were trivial. Three to seven determinations were made on each alcohol, with standard deviations in log K of 0.01 log units or less. Relative K values were then determined for a variety of solutes at 25 and 60 °C, using nitrogen as the carrier gas and a flame ionization detector. Relative K values were converted to absolute K values by using the known absolute K values of the standard solutes, exactly as described in ref 34. A complete listing of K values will appear in a subsequent publication. Values for those vapors also used to test SAW devices are presented below in the results section.

RESULTS

Under a stream of dry air, the delay lines of the dual delay line SAW device oscillate at their base-line values, with the frequency of the coated delay line being lower than that of the reference delay line. Exposure to air containing a vapor which is sorbed by the coating causes the coated delay line frequency to shift to a lower value. Ideally, the reference delay line frequency remains unchanged, and the difference frequency between the two delay lines increases. This increase is taken as the sensor's response, Δf_v, and as a measure of vapor sorption. A typical response curve for two successive vapor exposures is shown in Figure 4.

Datasets of vapor exposures were collected by exposing the sensors to each of nine vapors, each vapor at four concentrations, each concentration repeated four times. In addition, dimethyl methylphosphonate (DMMP) was repeated throughout the dataset and its reproducibility was very good. The SAW frequency shifts for each vapor exposure were used to calculate partition coefficients, denoted K_{SAW}, according to eq 10. These were converted to logarithms and the 16 values for each vapor (or ca. 100 for DMMP) were averaged and their standard deviation determined.

Three datasets for sensor A and two for sensor B were collected over a period of 3 months. A fourth dataset for sensor A was collected another 4 months later. The temperature was 35 ± 2 °C. The sensor responses were determined from the difference frequencies observed, and the resulting log K_{SAW} values are presented in Table I. (A fluoropolyol density of 1.64 g mL^{-1} at 35 °C, interpolated from the data in the Experimental Section, was used for the calculations.) The last two columns in the table give the lowest and highest standard deviations (SD) observed.

The six average log K_{SAW} values for each vapor are generally consistent. For six of the nine vapors, the difference between the highest and lowest values is 0.15 log unit or less. A variation of ±0.075 log unit in log K_{SAW} corresponds to ±18% in the SAW Δf_v values. For comparison, the uncertainty in the vapor concentrations is up to ±15%, depending on the particular concentration generated (*31*). These results demonstrate that fluoropolyol-coated SAW sensors can be fabricated and tested reproducibly and that the responses do not change over a period of months. Previous results with fluoropolyol on 112 MHz dual delay line SAW devices have shown that sensor responses are similar from 1 day to 2 months after coating and that annealing the fluoropolyol film at 110 °C for 1 h did not influence its performance (*3*). The vapor/coating interactions are therefore consistent and reproducible and fit the model of simple, reversible sorption.

As mentioned above, the difference frequency represents sorption into the coating only when the frequency shift of the reference delay line is small in comparison. The reference and coated delay lines of sensor A were monitored individually during dataset 4 (also the difference frequency, as usual). These results are reported in detail in Table II. The frequency shifts are the average of four exposures at each concentration. The log K_{SAW} values determined from the coated delay line are very close to those determined from the difference signal in nearly all cases, in accord with the assumption above. Thus, a ca. 200 Hz shift on the reference delay line is negligible compared to a 10000–20000 Hz shift on the coated delay line in response to low DMMP concentrations. However, the reference delay line is not truly inert, as shown by the shifts in the last column. These shifts become significant when the shift of the coated delay line is small, e.g. 1000 Hz or less, as is observed for water and isooctane. In the case of water, the difference signal does not accurately represent the behavior of the coated delay line. Indeed, the absolute value of the reference delay line signal is greater than the absolute value of the coated delay line signal at low water concentrations.

The reference delay line shifts are not monotonic with vapor concentration, nor are the positive shifts often observed consistent with simple mass loading of the surface. These signals most likely are caused by vapor adsorption onto the glass surface. However, further interpretation is inappropriate because the glass surface has not been carefully characterized and it is slightly contaminated with fluoropolyol. Vapor adsorption onto clean quartz SAW surfaces has been examined in detail by Martin et al. (*13*). The important result here is that while reference delay line effects are usually negligible,

Table II. Detailed Response Data for a Fluoropolyol-Coated SAW Vapor Sensor

		signal monitored				
		difference frequency		coated delay line		ref delay line
vapor	concn, μg/L	av Hz	log K_{SAW}	av Hz	log K_{SAW}	av Hz
DMMP	20	8967	6.52	-8882	6.51	87
	46	13723	6.34	-13589	6.33	134
	74	16826	6.22	-16681	6.21	147
	117	19334	6.08	-19152	6.07	181
N,N-dimethylacetamide	17	5058	6.33	-4971	6.32	102
	40	3094	6.17	-7946	6.16	143
	65	10330	6.07	-10143	6.05	187
	102	12254	5.95	-12027	5.93	218
1-butanol	1460	1623	3.91	-1450	3.85	181
	2200	2189	3.86	-1997	3.81	192
	4300	4542	3.89	-4313	3.86	231
	8730	9159	3.89	-8802	3.86	359
2-butanone	25800	10894	3.49	-10556	3.47	297
	38700	14324	3.45	-14497	3.43	328
	74800	27532	3.43	-26861	3.41	670
	148000	49866	3.39	-47403	3.36	2438
H_2O	1210	591	3.56	ca. 0	-	638
	1820	680	3.44	-45	2.16	638
	3550	1142	3.37	-472	2.98	670
	7180	1882	3.28	-1196	3.07	689
toluene	9680	951	2.86	-997	2.87	-44
	14500	1394	2.85	-1486	2.87	-88
	28400	3173	2.91	-3338	2.93	-178
	57300	7726	2.99	-7261	2.96	466
diethyl sulfide	23600	2053	2.81	-1970	2.78	-63
	35400	2800	2.76	-2801	2.76	-112
	68700	5933	2.80	-5979	2.80	-125
	137000	14376	2.89	-12709	2.82	1675
1,2-dichloroethane	30500	928	2.35	-959	2.35	-27
	45700	1449	2.37	-1521	2.38	-78
	83600	3547	2.48	-3931	2.50	-282
	176000	8800	2.56	-8824	2.56	-74
isooctane	22000	255	1.93	-330	2.03	-77
	33100	379	1.93	-519	2.05	-146
	64300	1163	2.12	-1409	2.20	-247
	129000	4925	2.45	-3356	2.27	1570

they must be considered when the coated delay line signals are small. A truly inert reference would afford some advantages in sensor performance and would simplify the interpretation of vapor sorption.

The data in Table II also illustrate the dependence of log K_{SAW} on gas phase vapor concentration. For most of the vapors the calculated K_{SAW} values were constant over the concentration range reported. This corresponds to a linear sorption isotherm, as illustrated for 1-butanol in Figure 5. The number next to each data point is the corresponding K_{SAW} value. A linear sorption isotherm represents ideal solution behavior and is classified as type I sorption (35). The sorption isotherms of DMMP and *N,N*-dimethylacetamide deviated significanty from linearity, with K_{SAW} values decreasing with increasing concentration. These results are illustrated for DMMP in Figure 5. This plot fits the form of type II sorption (35), indicating specific, preferential vapor/oligomer interaction at low concentrations. This interaction is likely to be hydrogen bond formation between hydrogen bond donating (HBD) hydroxyl groups on the fluoropolyol and hydrogen bond accepting (HBA) oxygen atoms on the vapor.

The influence of temperature on SAW sensor responses and K_{SAW} values was determined by using DMMP as the test vapor. The results at 20 μg L^{-1} DMMP are illustrated in Figure 6. The sensor responses decrease exponentially with increasing temperature; log K_{SAW} values decrease linearly.

Partition coefficients were also determined independently by GLC, which is a versatile and well-established method of making such measurements. These partition coefficients, denoted K_{GLC}, refer to the solute at infinitely dilute concentration. Fluoropolyol was used as the stationary phase at 25 °C. The GLC peaks at this temperature were generally broad and in some cases precise retention volumes (and hence K_{GLC}) were difficult to determine. Therefore 26 K_{GLC} values were

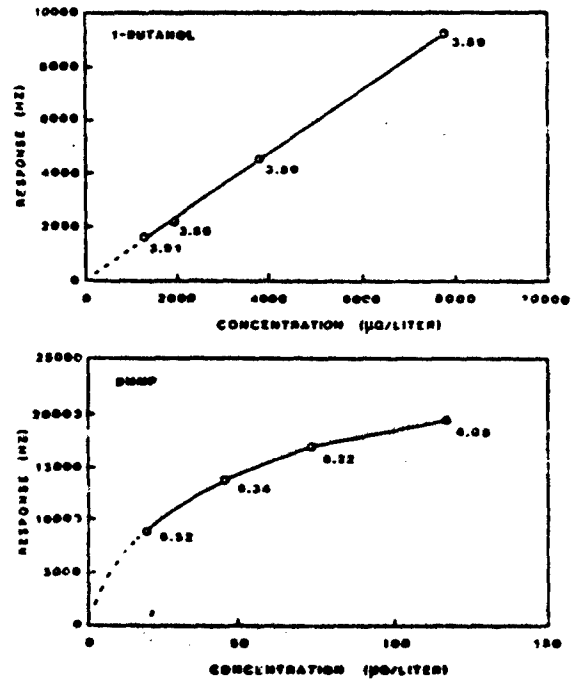

Figure 5. Sorption isotherms for 1-butanol and DMMP on fluoropolyol.

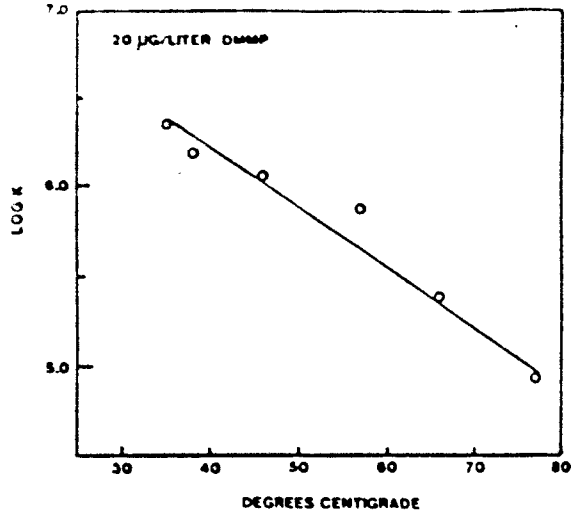

Figure 6. Temperature dependence for DMMP (20 $\mu g\ L^{-1}$) sorption into fluoropolyol.

Table III. Comparison of log K_{SAW} and log K_{GLC} Values

vapor	log K_{SAW}[a,b]	log K_{GLC}[c]
DMMP	6.52	7.53[d]
N,N-dimethylacetamide	6.33	7.29[d]
1-butanol	3.83	3.66
2-butanone	3.38	3.48[d]
water	3.20	2.89
toluene	2.88	2.64[d]
diethyl sulfide	2.74	2.54[e]
1,2-dichloroethane	2.46	1.94[d]
isooctane	2.12	1.22

[a] Values are averages of those in Table I, except the values for DMMP and *N,N*-dimethylacetamide are taken from Table II at the lowest concentrations tested. [b] At 35 °C. [c] At 25 °C. [d] Determined from values measured at 60 °C and corrected to 25 °C with eq 11. [e] Estimated value using a correlation equation.

determined at both 25 and 60 °C, and the following correlation was found to hold:

$$\log K_{GLC}(25\ °C) = -0.728 + 1.470 \log K_{GLC}(60\ °C) \quad (11)$$

$$n = 23, \qquad SD = 0.156, \qquad r = 0.986$$

When retention times were too long to measure at 25 °C, eq 11 and the measured value of K_{GLC} at 60 °C were used to estimate the value of K_{GLC} at 25 °C. In one additional case, diethyl sulfide, the log K_{GLC} was estimated from correlations we have constructed by use of solvatochromic parameters (see below).

The log K_{GLC} values are reported in Table III, along with log K_{SAW} values for comparison. The log K_{SAW} values are averages of those in Table I, except for DMMP and *N,N*-dimethylacetamide. In these two cases, the values reported are for the lowest concentrations examined in order to be more comparable to log K_{GLC} at infinite dilution. The vapors are listed in order of decreasing log K_{SAW}.

DISCUSSION

The order of decreasing log K in Table III is identical for the SAW and GLC measurements. This result demonstrates that relative retention times for various vapors on a GLC column with a given stationary phase should be a reliable indicator of the relative sensitivities of a similarly coated SAW device to these vapors. This requires, of course, that the GLC measurement and SAW sensor operation be at similar temperature.

Beyond this qualitative correlation, the values of log K_{SAW} and log K_{GLC} for individual vapors are not always in precise agreement. The log K_{SAW} values for the most strongly sorbed vapors, DMMP and *N,N*-dimethylacetamide, are 1 log unit less than the log K_{GLC} values, indicating that the frequency shifts that would be predicted by K_{GLC} and eq 10 would be 10 times higher than the SAW frequency shifts actually observed. Nevertheless, the K_{GLC} values are correct in predicting that K_{SAW} values for these two vapors should be very much higher than those for all the other vapors. For the remaining vapors the log K_{SAW} values differ from the log K_{GLC} values by varying amounts. The best agreement is seen for 1-butanol and 2-butanone, where the log K values differ by 0.17 and 0.10 log units, respectively. The poorest agreement is seen for isooctane, where the log K values differ by 1 log unit.

Two experimental factors that are expected to cause K_{SAW} and K_{GLC} values to vary from one another are differences in the gas phase vapor concentration and differences in measurement temperature. A third factor that may cause differences is the assumption in eq 10 that the SAW sensor response is based on mass effects alone; if mechanical effects are significant for a particular vapor/coating interaction, then the calculated log K_{SAW} value will be inaccurate.

Gas phase vapor concentration can cause differences because the GLC measurement refers to conditions of infinite dilution, while the SAW measurement is necessarily carried out at finite vapor concentrations. If the sorption isotherm is linear, as shown for 1-butanol in Figure 5, then K will be independent of concentration and K_{SAW} and K_{GLC} should agree. However, a curved isotherm, as observed for DMMP, will cause K_{SAW} and K_{GLC} to differ. Extrapolation of the DMMP isotherm to lower concentrations shows that K_{SAW} will increase, which would give better agreement with the K_{GLC} measurement.

The influence of increasing temperature is usually to cause partition coefficients to decrease. Therefore K_{SAW} values at 35 °C should be less than K_{GLC} values at 25 °C. While this was observed for DMMP and *N,N*-dimethylacetamide, it was not true for all the remaining vapors and cannot fully account for differences between K_{SAW} and K_{GLC}.

Nevertheless, the temperature effects defined experimentally in Figure 6 and eq 11 are worth examining for practical reasons. The results demonstrate that precise thermostating of a SAW sensor to fractions of a degree is clearly not critical, but variations of ten degrees may influence sensor response and reproducibility. The form of eq 11 demonstrates that temperature effects will be largest for the most strongly sorbed vapors. For example, DMMP sorption with log K_{GLC} of 7.5 at 25 °C is predicted to be 7.0 at 35 °C, a difference of 0.5 log unit. By comparison, a log K value of 3.0 at 25 °C becomes 2.9 at 35 °C, a difference of only 0.1 log unit. Therefore increasing temperature reduces selectivity in addition to the sensitivity.

The temperature effect and the overall correlation in the order of K_{SAW} and K_{GLC} values are consistent with the sorption model. Accordingly, partition coefficients are a useful concept for interpreting SAW sensor behavior (*6*, *8*), and a more detailed consideration of the factors responsible for sorption is warranted. Since partitioning represents dissolution of a solute vapor into the solvent stationary phase, solubility interactions must be relevant in determining sensor responses (*5*).

The order of the partition coefficients in Table II provides a simple illustration of the importance of vapor solubility properties. The lowest K values are those of isooctane, a solute that is not dipolar or polarizable and cannot form hydrogen bonds. Solutes that are more polarizable, such as dichloroethane, toluene, and diethyl sulfide, have greater K values than isooctane. However, these solutes are still incapable of hy-

drogen bonding. The top of the list, from water to DMMP, contains exclusively those solutes that can accept and/or donate hydrogen bonds.

One additional factor influencing vapor sorption is the saturation vapor pressure of the solute vapor. All other things being equal, lower saturation vapor pressure will lead to longer retention times on the GLC, higher K values, and higher SAW sensor responses. In Table III, DMMP, *N,N*-dimethylacetamide, and 2-butanone are all hydrogen bond acceptors. The K values for the lower saturation vapor pressure (ca. 1 Torr) vapors, DMMP and *N,N*-dimethylacetamide, are much higher than those for 2-butanone (saturation vapor pressure ca. 100 Torr).

Solubility interactions can be placed on a more quantitative scale by the use of solvatochromic parameters, which describe the dipolar and hydrogen bonding properties of the solute vapors (*25–28*). Such parameters are available for a wide range of vapors, but similar parameters are not yet available for very many coating materials. In order to better understand vapor/coating interactions, it will be necessary to also characterize the solubility properties of the stationary phase coatings. In addition, it would be desirable to be able to predict partition coefficients for any vapor with any characterized phase. Methodologies to accomplish this are being developed using equations of the general form shown in eq 12 (*29*).

$$\log K = \text{constant} + s\pi^* + a\alpha + b\beta + l \log L^{16} \qquad (12)$$

In this equation, the parameters π^*, α, β, and $\log L^{16}$ characterize the solute vapor. π^* measures the ability of a compound to stabilize a neighboring charge or dipole. For nonprotonic, aliphatic solutes with a single dominant dopole, π^* values are approximately proportional to molecular dipole moments. α and β measure solute hydrogen bond donor acidity and hydrogen bond acceptor basicity, respectively. L^{16} is the Ostwald solubility coefficient (partition coefficient) of the solute vapor on hexadecane at 25 °C and provides a measure for dispersion interactions. The coefficients s, a, b, and l are determined by multiple regression analysis and characterize the stationary phase. For example, b, as the coefficient for solute hydrogen bond acceptor basicity, provides a measure of the stationary phase hydrogen bond donor acidity. For any particular stationary phase/vapor interaction, evaluation of the individual terms (such as $b\beta$) and comparison of their magnitudes allow the relative strengths of various solubility interactions to be sorted out and examined.

The complex structure of fluoropolyol provides an interesting test case for these methods. This material contains a variety of functionalities which provide polarizability, dipolarity, hydrogen bond acceptor sites, and hydrogen bond donor sites. But the structure alone does not allow precise predictions of which interactions will be most important in determining the sorption of a particular vapor. Full characterization of fluoropolyol by GLC measurements and equations of the form in eq 12 is in progress, and we hope to report on this work soon. In addition, various other polymeric stationary phases that have been useful as SAW sensor coatings are being examined. Once a regression equation has been determined for a given phase, partition coefficients can be predicted for any vapor whose solvatochromic parameters are known.

Ultimately, it would be useful to be able to predict SAW vapor sensor responses by using partition coefficients and eq 10. Although this cannot yet be done on a strict quantitive basis, it is clear that the sorption model and partition coefficients provide the best available first approximation for estimating SAW responses. These methods can provide useful guidance in the selection and use of coating materials for specific sensing applications. In addition, an understanding of the factors governing vapor sorption and the interactions occurring between specific vapors and coating aids in the design of useful coating materials.

ACKNOWLEDGMENT

The authors acknowledge M. J. Kamlet for many useful discussions on solubility interactions.

LITERATURE CITED

(1) Wohltjen, H.; Dessy, R. E. *Anal. Chem.* **1979**, *51*, 1458–1475.
(2) Grate, J. W.; Snow, A. W.; Ballantine, D. S., Jr.; Wohltjen, H.; Abraham, M. H.; McGill, R. A.; Sasson, P. *Proc. 4th Int. Conf. Solid-State Sens. Actuators—Transducers '87* **1987**, 579–582.
(3) Grate, J. W.; Snow, A.; Ballantine, D. S.; Wohltjen, H.; Abraham, M. H.; McGill, R. A.; Sasson, P. NRL Memorandum Report 6024, 1987; NTIS ADA 183694.
(4) Wohltjen, H.; Snow, A. W.; Barger, W. R.; Ballantine, D. S. *IEEE Trans. Ultrason., Ferroelectrics. Freq. Contr.* **1987**, *UFFC-34*, 172–178.
(5) Ballantine, D. S.; Rose, S. L.; Grate, J. W.; Wohltjen, H. *Anal. Chem.* **1986**, *58*, 3058–3066.
(6) Wohltjen, H.; Snow, A.; Ballantine, D. *Proc. 3rd Int. Conf. Solid-State Sens. Actuators—Transducers '85* **1985**, IEEE Cat. No. CH2127-9/85/0000-0066, 66–70.
(7) Wohltjen, H. *Sens. Actuators* **1984**, *5*, 307–325.
(8) Snow, A.; Wohltjen, H. *Anal. Chem.* **1984**, *56*, 1411–1416.
(9) Venema, A.; Nieuwkoop, E.; Vellekoop, M. J.; Ghijsen, W. J.; Berendsz, A. N.; Nieuwenhuizen, M. S. *IEEE Trans. Ultrason., Ferroelectrics, Freq. Contr.* **1987**, *UFFC-34*, 148–155.
(10) Nieuwenhuizen, M. S.; Barendsz, A. W. *Sens. Actuators* **1987**, *11*, 45–62.
(11) Nieuwenhuizen, M. S.; Berendsz, A. W.; Nieuwkoop, E.; Vellekoop, M. J.; Venema, A. *Electron Lett.* **1986**, *22*, 184–185.
(12) Venema, A.; Nieuwkoop, E.; Vellekoop, M. J.; Nieuwenhuizen, M. S.; Barendsz, A. W. *Sens. Actuators* **1986**, *10*, 47–64.
(13) Martin, S. J.; Ricco, A. J.; Ginley, D. S.; Zipperian, T. J. *IEEE Trans. Ultrason., Ferroelectrics, Freq. Contr.* **1987**, *UFFC-34*, 142–147.
(14) Ricco, A. J.; Martin, S. J.; Zipperian, T. E. *Sens. Actuators* **1985**, *8*, 319–333.
(15) Martin, S. J.; Schweizer, K. S.; Ricco, A. J.; Zipperian, T. E. *Proc. 3rd Int. Conf. Solid-State Sens. Actuators—Transducers '85* **1985**, IEEE Cat. No. CH2127-9/85/0000-0066, 71–73.
(16) Vetelino, J. F.; Lade, R. K.; Falconer, R. S. *IEEE Trans. Ultrason., Ferroelectrics, Freq. Contr.* **1987**, *UFFC-34*, 156–161.
(17) Bryant, A.; Poirer, M.; Riley, G.; Lee, D. L.; Vetelino, J. F. *Sens. Actuators* **1983**, *4*, 105.
(18) D'Amico, A.; Palma, A.; Verona, E. *Sens. Actuators* **1982/1983**, *3*, 31–39.
(19) Chuang, C. T.; White, R. M.; Bernstein, J. J. *IEEE Electron. Device Lett.* **1982**, *EDL-3*, 145–148.
(20) King, W. H. *Anal. Chem.* **1964**, *36*, 1735–1739.
(21) For a review see Alder, J. F.; McCallum, J. J. *Analyst (London)* **1983**, *108*, 1169–1189.
(22) Janghorbani, M.; Freund, H. *Anal. Chem.* **1973**, *45*, 325–332.
(23) Edmunds, T. E.; West, T. S. *Anal. Chim. Acta* **1980**, *117*, 147–157.
(24) McCallum, J. J.; Fielden, P. R.; Volkan, M.; Alder, J. F. *Anal. Chim. Acta* **1984**, *162*, 75–83.
(25) Kamlet, M. J.; Doherty, R. M.; Abboud, J.-L. M.; Abraham, M. H.; Taft, R. W. *CHEMTECH* **1986**, *16*, 566–576.
(26) Abraham, M. H.; Doherty, R. M.; Kamlet, M. J.; Taft, R. W. *Chem. Br.* **1986**, *22*, 551–554.
(27) Kamlet, M. J.; Taft, R. W. *Acta Chem. Scand., Ser. B* **1985**, *B39*, 611.
(28) Kamlet, M. J.; Abboud, J. M.; Abraham, M. H.; Taft, R. W. *J. Org. Chem.* **1983**, *48*, 2877.
(29) Abraham, M. H.; Grellier, P. L.; McGill, R. A.; Doherty, R. M.; Kamlet, M. J.; Hall, T. M.; Taft, R. W.; Carr, P. W.; Koros, W. J. *Polymer* **1987**, *28*, 1363–1369.
(30) Barrett, R. S. *Analyst (London)* **1981**, *106*, 817–849.
(31) Grate, J. W.; Ballantine, D. S., Jr.; Wohltjen, H. *Sens. Actuators* **1987**, *11*, 173–188.
(32) O'Neal, J. G.; Griffith, J. R.; Reines, S. A. *J. Paint Technol.* **1971**, *43*(552), 113–119.
(33) *Microwave Acoustics Handbook, Vol. 2, Surface Wave Velocities—Numerical Data*; Slobodnik, A. J., Jr., Delmonico, R. T., Conway, E. D., Eds.; Air Force Cambridge Research Laboratory, Report No. AFCRL-TR-74-0536, Oct 1974, p 197.
(34) Abraham, M. H.; Grellier, P. L.; McGill, R. A. *J. Chem. Soc., Perkin Trans. 1* **1987**, 797–803.
(35) Rodgers, C. E. In *Polymer Permeability*; Comyn, J., Ed.; Elsevier: New York, 1985, pp 29–34.

RECEIVED for review April 8, 1987. Accepted November 18, 1987. This work was supported by the U.S. Army, CRDEC, Aberdeen Proving Ground, MD, the U.S. Naval Surface Weapons Center, Dahlgren, VA, and the Office of Naval Technology.

TRANSDUCERS '87

THE USE OF PARTITION COEFFICIENTS AND SOLUBILITY PROPERTIES TO UNDERSTAND AND PREDICT SAW VAPOR SENSOR BEHAVIOR

J.W. Grate and A.W. Snow
U.S. Naval Research Laboratory
Washington, DC 20375-5000, USA

D.S. Ballantine, Jr.
Geo-Centers, Inc.
4710 Auth Place
Suitland, MD 20746, USA

H. Wohltjen
Microsensor Systems, Inc.
P.O. Box 90
Fairfax, VA 22030, USA

M.H. Abraham, R. A. McGill, P. Sasson
Department of Chemistry
University of Surrey
Guildford Surrey GU2 5XH, United Kingdom

ABSTRACT

Surface acoustic wave devices coated with a thin film of a stationary phase sense chemical vapors in the gas phase by detecting the mass of the vapor which distributes into the stationary phase. This distribution can be described by a partition coefficient. An equation is presented which allows partition coefficients to be calculated from SAW vapor sensor frequency shifts, and results are presented for nine vapors into SAW coating "fluoropolyol". Partition coefficients have also been determined independently by GLC and the results are in good agreement. The relationship between SAW frequency shifts and partition coefficients allows SAW sensor responses to be predicted if the partition coefficient has been measured by GLC or if it can be estimated by various correlation methods being developed.

INTRODUCTION

Surface acoustic wave (SAW) devices have been investigated by several groups for sensing chemical vapors in the gas phase[1-10]. The frequency of a SAW device in an oscillator circuit is measurably altered by small changes in mass or elastic modulus at the surface. Vapor sensitivity is typically achieved by coating the device surface with a thin film of a stationary phase which will selectively absorb and concentrate the target vapor. Vapor sorption increases the mass of the surface film and a shift in the oscillator frequency is observed. SAW devices have the potential to be adapted to a variety of gas phase analytical problems by strategic design or selection of coating material. Full realization of this potential will require methods to quantify, understand, and finally to predict the vapor/coating interactions responsible for vapor sorption.

Sorption of ambient vapor into the SAW device coating until equilibrium is reached represents a partitioning of the solute vapor between the gas phase and the stationary phase. This process is illustrated in Figure 1. The distribution can be quantified by a partition coefficient, K, which gives the ratio of the concentration of the vapor in the stationary phase, C_s, to the concentration of the vapor in the vapor phase, C_v (equation 1).

$$K = \frac{C_s}{C_v} \qquad (1)$$

An equation is derived herein which allows K to be calculated directly from observed SAW vapor sensor frequency shifts. This conversion provides a standardized method of normalizing empirical SAW data, and does so in a way that provides information about the vapor/coating equilibrium.

In this investigation, we examine the stationary phase referred to as "fluoropolyol", whose structure is shown in Figure 2. SAW vapor sensors coated with this soft, polymeric material have high sensitivity to certain toxic vapors[2]. Partition coefficients have been determined for nine vapors using SAW sensor frequency shifts. In addition, partition coefficients for the same vapors into fluoropolyol were determined independently by gas-liquid chromatographic (GLC) measurements. The values resulting from these two different techniques are in good agreement.

These results demonstrate that the mechanism of action of a coated SAW device is the same as that of GLC, i.e., reversible absorption of the vapor in the gas phase into the stationary phase. This confirms the solubility model for the interaction of vapors with the SAW coating; i.e., the solute vapor dissolves and distributes into the solvent stationary phase. Finally, the correlation between SAW vapor sensor responses and GLC partition coefficients creates a means for predicting SAW sensor behavior. Thus, if GLC partition coefficients are available from experimental measurement, or can be reliably predicted, then SAW vapor sensor responses can also be predicted.

TRANSDUCERS '87

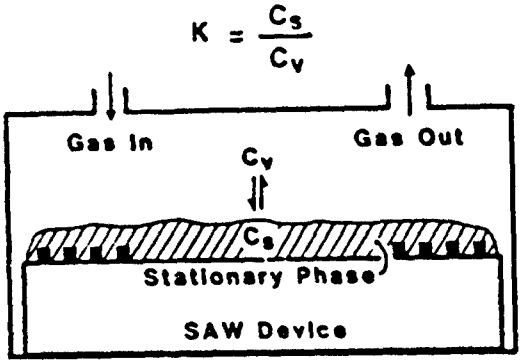

Figure 1. Distribution of vapor between gas phase and stationary phase.

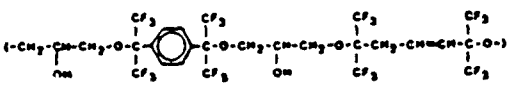

Figure 2. Fluoropolyol structure.

EQUATION RELATING SAW FREQUENCY SHIFT TO THE PARTITION COEFFICIENT

The change in oscillator frequency observed when the mass on the surface of the SAW device increases can be described by equation (2).[6]

$$\Delta f = \frac{(k_1 + k_2)\, f_o^2 m}{A} \qquad (2)$$

Δf is the frequency change; m is the mass increase; k_1 and k_2 are material constants for the piezoelectric substrate; f_o is the unperturbed resonant frequency of the device; and A is the active sensing area. It can be derived that the frequency shift (Δf_v) caused by the mass of vapor absorbed into the stationary phase coated on a SAW device is related to the partition coefficient (K) by equation (3).

$$\Delta f_v = \frac{\Delta f_s\, C_v\, K}{\rho} \qquad (3)$$

Δf_v is obtained in Hz when Δf_s (the frequency shift caused by the mass of the stationary phase applied to the device) is expressed in KHz, C_v (vapor concentration in the gas phase) is in g liter^{-1}, and ρ (stationary phase density) is in g mL^{-1}. The principal assumption inherent in equation (3) is that the SAW device functions as a mass sensor only, mechanical effects being negligible.[6] In addition, it is assumed that mass loading of the coating by vapor is low, since high mass loading would cause the coating density to change.

PARTITION COEFFICIENTS DETERMINED FROM SAW VAPOR SENSOR FREQUENCY SHIFTS

SAW vapor sensors were prepared by spray coating one delay line of a dual delay line SAW device with a dilute solution of fluoropolyol, as has been described previously[2]. The fluoropolyol coating causes the frequency of the device to change by an amount Δf_s, which provides a measure of the amount of coating material applied. These sensors were tested against vapors by alternately exposing them to clean air or a calibrated vapor stream using an automated vapor-generation instrument described in reference [11]. The change in the frequency observed when the gas over the sensor was changed from clean air to vapor gives the frequency shift caused by the vapor. For reliable measurements of K, this shift must be determined only after the sensor has reached a stable, equilibrium response level.

Partition coefficients were calculated from the observed frequency shifts (Δf_v) using equation (3). These values will be referred to as SAW partition coefficients and denoted K_{SAW}. Each sensor was exposed to each vapor at a minimum of two different concentrations (usually four, sometimes seven different concentrations) and at least four exposures at each concentration. A SAW partition coefficient was calculated for each vapor exposure, and these values were converted to logarithms. Then, all the log K_{SAW} values for each vapor on a particular sensor were averaged. Finally, the results from all sensors were averaged and are reported in Table 1. These results represents nearly 900 measurements of SAW frequency shifts.

Table 1. Log K_{SAW} and Log K_{GLC} Values

Vapors	Log K_{SAW}[a]	Log K_{GLC}[b]
DMMP	5.77	7.53[c]
Dimethylacetamide	5.65	7.29[c]
1-Butanol	3.24	3.66
2-Butanone	3.15	3.48[c]
Water	2.88	2.89
Diethyl Sulfide	2.78	2.54[d]
Toluene	2.69	2.64[c]
1,2-Dichloroethane	2.39	1.94[c]
Isooctane	1.97	1.22

a These values are averages from sensors described in the text.
b At 298°K.
c Determined from values measured at 333°K and corrected to 298°K with equation (4).
d Estimated value using a correlation equation.

Three sensors were examined in this study. One 158 MHz SAW device was coated with 207 KHz of fluoropolyol and tested against vapors one week later. Two 112 MHz devices were coated with 106 and 104 KHz, respectively, and were tested both one day and two months after coating. Reproducibility was good and aging appeared to have little effect.

TRANSDUCERS '87

Data from device to device showed some systematic variation, which could be most easily explained by errors in the measurement of the coating material applied. However, the actual source of the variation is not definitely known.

PARTITION COEFFICIENTS MEASURED BY GAS-LIQUID CHROMATOGRAPHY

Partition coefficients for a wide variety of solute vapors were determined by gas-liquid chromatography with fluoropolyol as the stationary phase, using methods described in reference 12. Partition coefficients as defined in equation (1) are actually identical to the Ostwald solubility coefficients usually denoted as L. We will use the symbol K, and refer to GLC partition coefficients as K_{GLC}.

GLC peaks on the fluoropolyol were generally broad, especially at 298°K. Therefore, 26 K_{GLC} values were determined at both 298°K and 333°K and the following correlation was found to hold:

$$\log K_{GLC}(298K) = -0.728 + 1.470 \log K_{GLC}(333K)$$

$$n = 26,\ sd = 0.156,\ r = 0.986 \qquad (4)$$

When retention times were too long to measure at 298°K, equation (4) and the measured value of K_{GLC} at 333°K were used to estimate the value of K_{GLC} at 298°K. Equation (4) shows that thermostatting a SAW sensor to fractions of a degree is not critical. However, changes of 5 to 10 degrees (e.g. due to varying ambient conditions) will become significant, especially for solutes with large K_{GLC}.

Log K_{GLC} and log K_{SAW} values for nine solute vapors are compared in Table 1, with the vapors in order of decreasing log K_{SAW}. All of the GLC values refer to 298°K, either by direct measurement, or via equation (4) as described above. In one additional case, diethyl sulfide, the log K_{GLC} value was estimated from various correlations we have constructed using solvatochromic parameters. With the exception of this estimated value, the order of decreasing log K values is identical for the SAW and GLC measurements. Indeed, there is good agreement between all but the highest Log K values, such that the SAW sensor frequency shifts could be estimated using K_{GLC} values and equation (3).

DISCUSSION

The experimental conditions for measuring partition coefficients with a SAW device are somewhat different than those for GLC measurements. SAW measurements, for instance, are carried out at finite vapor concentrations while the GLC measurement usually refers to infinite dilution. In addition, the SAW measurements reported here were conducted at ambient temperatures, while the GLC measurements were rigorously thermostated. Finally, the calculation of K_{SAW} assumes that the vapor causes the sensor to respond based on mass effects alone; if mechanical effects become significant for a particular vapor/coating interaction, then the calculated K_{SAW} will be altered proportionately. One or more of the above factors may be responsible for differences in the precise values of log K_{SAW} and log K_{GLC} shown in Table 1.

The overall correlation observed clearly shows that partition coefficients are a useful concept for thinking about SAW sensor behavior (see also references 3 and 7). Indeed, the calculation of K_{SAW} values by equation (3) provides a standardized method of normalizing empirical SAW data which also provides information about the magnitude of the vapor/coating interaction. We have previously normalized our data by dividing the sensor response by the ppm of vapor in the gas phase and the KHz of coating. Normalization to yield a partition coefficient, K_{SAW} is very similar, and requires only that the vapor concentration be expressed in g liter^{-1}, and that the density of the stationary phase coating be factored out, according to equation (3).

The experimental correlation between K_{GLC} and K_{SAW} demonstrates that relative retention times for various vapors on a GLC column with a given stationary phase should be a reliable indicator of the relative sensitivity of a similarly coated SAW sensor to these vapors. This requires, of course, that the GLC measurement and SAW device operation be at the same temperature. On a more quantitative level, if absolute K_{GLC} values are determined, then estimates for actual SAW sensor frequency shifts can be made using equation (3). Finally, a clear relationship between SAW sensor responses and K_{GLC} values means that methods developed to predict K_{GLC} values will also be useful in predicting SAW sensor responses.

A simple examination of the order of the partition coefficients determined in this study illustrates the importance of solubility properties (Table 1). The lowest K values are those of isooctane, a solute which is not dipolar or polarizable, and which cannot accept or donate hydrogen bonds. Solutes which are more polarizable, such as dichloroethane, toluene, and diethyl sulfide have greater K values than isooctane. However, these solutes are still incapable of hydrogen bonding. The top of the list contains exclusively those solutes which can accept and/or donate hydrogen bonds. Vapor sorption is also influenced by the saturation vapor pressure, P^o_v, of the solute vapor, with lower P^o_v giving larger partition coefficients (for example, DMMP).

Solubility interactions can be placed on a more quantitative scale by the use of solvatochromic parameters (13). Such parameters are available for a wide range of vapors which may act as solutes in a vapor/coating interaction. Unfortunately, similar parameters are not yet available for a wide range of coating materials. The challenges, therefore, are to develop methods to characterize the solubility properties of stationary phases, and ultimately to be able to predict partition coefficients for any vapor with any characterized phase. This work is in progress, and equations of the general form shown in (5) are being used to predict log K_{GLC} values for fluoropolyol, and for various other stationary phases which have been useful as SAW device coatings[2].

TRANSDUCERS '87

$$\log K_{GLC} = \text{constant} + s\pi^* + a\alpha + b\beta + l \log L^{16} \quad (5)$$

The variables π^*, α, β, and $\log L^{16}$ describe the solubility properties of the vapor. π^* is the dipolarity/polarizability; α is the hydrogen bond donor acidity; β is the hydrogen bond acceptor basicity; $\log L^{16}$ measures the tendency to partition into hexadecane. Coefficients s, a, b, and l describe the stationary phase. For example, b, as the coefficient for vapor β, measures the hydrogen bond donor acidity of the stationary phase. Once the coefficients have been determined for a particular stationary phase, then it will be possible to predict K values for all vapors for which π^*, α, β, and $\log L^{16}$ are known. Then, via equation (3), it will be possible to predict the responses of a SAW vapor sensor to these same vapors.

Finally, specific vapor/coating interactions may sometimes be encountered where mass effects alone do not adequately account for SAW sensor response. Mechanical effects will be implicated in such cases, but have been difficult to estimate thus far. Using equation (3) and a measured (GLC) or predicted (equation (5) K value, it is now possible to calculate the mass only SAW frequency shifts, and to estimate the mechanical frequency shift from the difference between the observed frequency shift and the mass-only frequency shift.

REFERENCES

(1) H. Wohltjen and R.E. Dessy, Analytical Chemistry, 51(9), 1979, pp. 1458-1475.

(2) D.S. Ballantine, Jr., S.L. Rose, J.W. Grate, and H. Wohltjen, Analytical Chemistry, 58, 1986, pp. 3058-3066.

(3) H. Wohltjen, A. Snow, and D. Ballantine, Proc. of the Int. Conf. on Solid State Sensors and Actuators - Transducers '85, Philadelphia, PA, June 11-14, 1985, IEEE Cat. No. CH2127-9/85/0000-0066, pp. 66-70.

(4) A.W. Barendsz, J.c. Vis, M.S. Nieuwenhuizen, E. Nieuwkoop, M.J. Vellekoop, W.J. Ghijsen, and A. Venema, Proc. of the 1985 IEEE Ultrasonics Symp.

(5) S.J. Martin, K.S. Schweizer, S.S. Schwartz, and R.L. Dunshor, Proc. of the 1984 IEEE Ultrasonics Symp.

(6) H. Wohltjen, Sensors and Actuators, 1984, pp. 307-325.

(7) A. Snow, and H. Wohltjen, Analytical Chemistry, 56(8), 1984, pp 1411-1416.

(8) A. Bryant, D.L. Lee, and J.F. Vetelino, Proc. IEEE 1981 Ultrasonics Symposium, pp 171-174.

(9) A. D'Amico, A. Palma and E. Verona, Sensors and Actuators, 1982/1983, pp 31-39.

(10) C.T. Chuang, R.M. White, J.J. Bernstein, IEEE Elect. Dev. Lett., EDL-3(6), 1982, pp 145-148.

(11) J.W. Grate, D.S. Ballantine, Jr., and H. Wohltjen, Sensors and Actuators, 11, 1987, pp 173-188.

(12) M.H. Abraham, P.L. Grellier, and R.A. McGill, J. Chem. Soc. Perkin Trans. I, in press.

(13) M.J. Kamlet and R.W. Taft, Acta. Scand., Ser. B, B39, 1985, pp 611-628, and references therein.

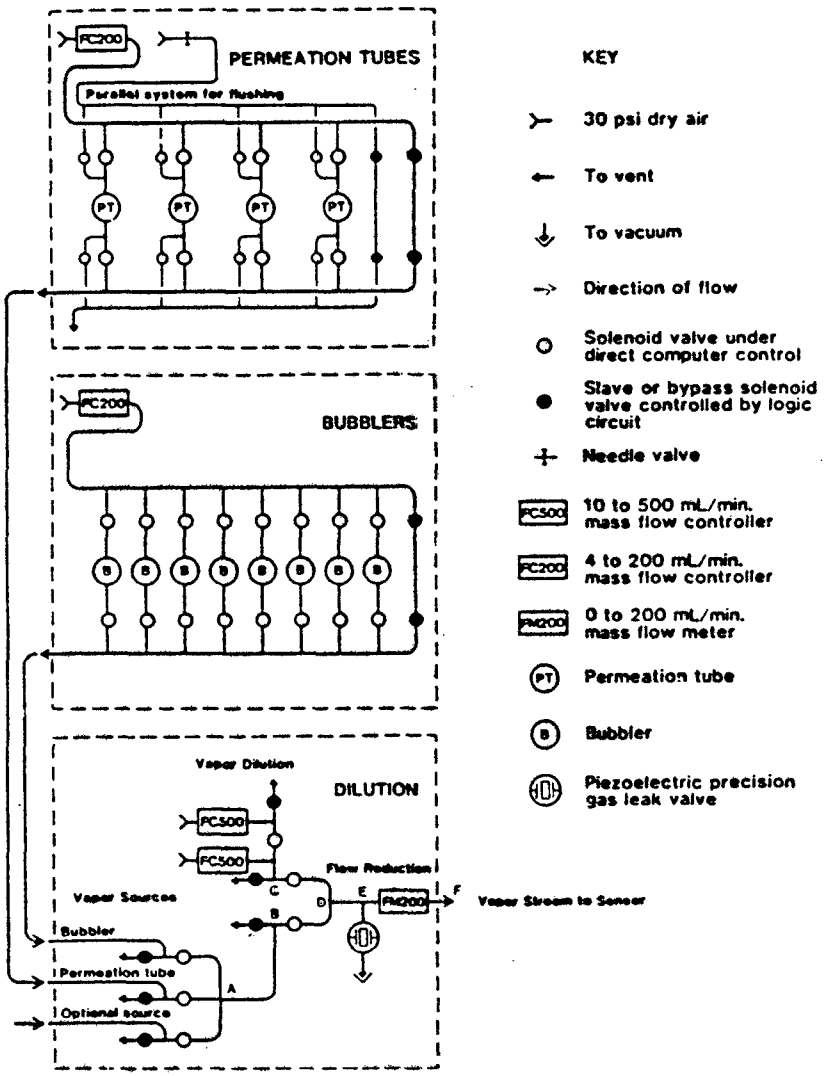

Fig. 2. Vapor stream flow system.

solid circles in Fig. 2 and open to allow flow through the carrier gas loop when none of the bubblers are opened. The flow rate of the carrier gas is regulated by a 4-200 ml/min air mass flow controller (FC200). The bubblers themselves are constructed of 6¾ inch lengths of 2 inch O.D. stainless steel pipe, with 1/8 inch thick stainless steel discs (2 inch diameter) welded to the ends. The top end of each has 1/8 inch stainless steel tubing welded into inlet and outlet holes. The inlet tube extends to 1/2 inch from the bottom and the outlet tube is flush with the inside of the top.

The permeation tube box generates a vapor stream by directing the carrier gas past one of four permeation devices. These devices are closed tubes containing a liquid chemical, which permeates out through a plastic barrier and is swept into the carrier gas [2]. The permeation tubes are contained within chambers constructed of 4 inch hex long nipples (1/2 inch male pipe size) fitted with hex reducing couplings and male connectors on the ends*. Each such assembly is housed in a Dewar flask and maintained at constant temperature by a heating tape and thermocouple.

The flow system within the permeation tube box is similar to that of the bubbler box. Each permeation tube is isolated by a pair of solenoid valves, bypass valves allow flow through the carrier gas loop when no permeation tube is open, and the carrier gas flow is regulated by a 4 - 200 ml/min mass flow controller (FC200). However, a second parallel flow system is also present so that the permeation tube chambers can be flushed to vent when they are not being used to generate a vapor stream for sensor testing. The flushing process assures stable permeation rates by preventing the buildup of high concentrations of vapor within the permeation tube chamber and maintaining a stable concentration gradient across the plastic barrier of the permeation device.

The dilution box contains an arrangement of tubing junctions and solenoid valves, which mixes various gas streams and delivers a gas stream to the sensor at point F in Fig. 2. The output to the sensor can be either clean carrier gas or a vapor stream, and can be switched between the two by opening and closing solenoid valves in carefully planned sequences. Any gas streams not being used as part of the output are vented to a hood.

Clean carrier gas flow within the dilution box is regulated by two 10 - 500 ml/min mass flow controllers. This gas proceeds to the sensor output at F via points C, D and E. Clean carrier gas is used to output clean air, or it is mixed with a vapor stream at point D to output a diluted vapor stream. Initial vapor streams (*i.e.*, prior to their dilution) are supplied by the bubbler and permeation tube boxes and by a third optional input. These can be used singly or mixed, and proceed to the sensor via points A, B, D and E. The configuration of solenoid valves in the dilution box is such that the vapor stream arriving at point B cannot be diluted without sending it to the output at the same time.

The dilution box also contains the flow reduction system, which will be explained separately below. Its function is to maintain the output to the sensor at a constant flow rate, regardless of the total flow of gas required to generate the chosen vapor concentration.

Solenoid valve control

The solenoid valves in the vapor flow system are controlled in two different fashions, depending on their function. Those valves depicted in Fig. 2

*Some commercial permeation tubes come equipped with tube fittings and can be incorporated into the system by means of a simple T junction.

Precise concentrations of individual vapors can be generated by a variety of techniques [1]. Dynamic methods that involve the addition of calibrated amounts of vapor to a flowing stream of carrier gas are generally preferred over static methods, particularly for very dilute vapors. Dynamic methods minimize the effects of wall adsorption on calibration accuracy, and a wide range of concentrations can be prepared by simple manipulation of the gas flow rates.

The instrument reported here is unique in its ability to generate dynamic gas streams of a number of vapors (*i.e.*, 12) from either neat chemical liquid bubblers or calibrated permeation tubes [2]. Moreover, mixtures of low concentration target vapors derived from permeation tubes (typically 1 - 100 mg/m^3) and high concentration interference vapors derived from bubblers (typically 100 - 100 000 mg/m^3) are easily prepared. The gas stream output of the instrument can be switched (under computer control) between the generated vapor stream and clean air so that the zero drift and reversibility of the sensor can be readily observed. Finally, the flow rate of the gas being output to the sensor is regulated to a constant value, regardless of the carrier gas flow rates required to perform the desired dilution. This unusual capability is accomplished using a servo-controlled piezoelectric valve to divert all vapor flow in excess of the amount programmed to be output to the sensor.

Instrument operations are carried out under the control of a microcomputer, and carrier gas flow rates are metered using electronic mass flow regulators. The fully automated character of this instrument affords many advantages including unattended operation during long sequences of tests, reduced operator exposure to toxic chemicals, and improved measurement precision. This system is designed to meet the requirements of a complete chemical vapor sensor research and development program.

2. Description of the instrument

Microcomputer interfacing

The vapor-generation and sensor-evaluation instrument consists of a vapor flow system to generate and deliver vapor streams to the sensor(s), and an Apple IIe microcomputer to control and monitor the vapor flow system. The microcomputer also collects and stores data from the sensor(s)*. The overall system is shown schematically in Fig. 1.

The microcomputer is interfaced with the vapor-generation system and sensors by means of four I/O boards. The IEEE-448 I/O board collects data from a frequency counter, which measures signals from surface acoustic wave (SAW) sensors [3, 4]. This particular I/O board adds great versatility

*Alternatively, sensor data can be collected by a second microcomputer in communication with the first. This configuration is preferred when data must be collected from multiple sensors simultaneously.

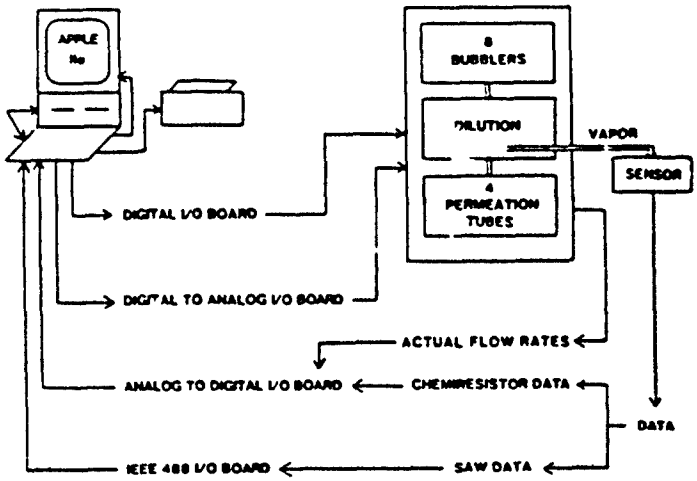

Fig. 1. System interfacing diagram for the vapor-generation instrument.

to the instrument, because other measuring devices such as electrometers can also be interfaced via the IEEE-488 bus. Signals from many types of sensors can therefore be easily monitored. Alternatively, data from any sensor or sensor system whose output is a voltage (*e.g.*, a chemiresistor system [5]) can be collected using the analog to digital I/O board. This board is also used to monitor carrier gas and vapor stream flow rates. Automated control of the vapor flow system is achieved using a digital I/O board, which commands solenoid valves open or closed, and a digital to analog I/O board, which commands mass flow controllers to deliver precise flow rates of carrier gas.

Vapor flow system

The vapor flow system is contained in three boxes: the bubbler box, the permeation tube box and the dilution box. The bubbler and permeation tube boxes are used to generate vapor streams. The dilution box performs several functions: vapor streams are selected from one or more inputs, *e.g.*, from the bubbler and/or permeation tube boxes; the vapor stream or mixture is diluted; either clean carrier gas or diluted vapor stream is output to the sensor. In addition, a flow reduction system within the dilution box regulates the flow rate of gas output to the sensor. The details of the vapor flow system are shown schematically in Fig. 2. The plumbing is constructed using 1/8 inch stainless steel tubing and stainless steel Swagelok fittings.

The bubbler box generates a vapor stream by bubbling a controlled flow rate of carrier gas through a neat chemical liquid. Eight different liquids are contained in separate bubblers, each of which is isolated from the carrier gas loop by a pair of solenoid valves. When a particular bubbler is chosen as the vapor-source, its pair of solenoid valves opens, and all other bubbler valves and the bypass valves remain closed. The bypass valves are depicted as

with open circles are turned on (opened) at the command of signals sent by the digital I/O board in the microcomputer. These valves are used to select vapor sources and gas streams to be sent toward the sensor. They can be individually opened by an operator at the computer keyboard or by statements in the software used to operate the instrument automatically.

Those solenoid valves depicted by solid circles in Fig. 2 cannot be controlled directly by either the computer keyboard or software. Instead, they are controlled by logic circuits in each box, which read the control signals going to the open circle valves in that box and decide on the proper operation of the corresponding solid circle valves. For example, the bubbler box contains a pair of bypass valves depicted by solid circles. The associated logic circuit has eight inputs, one for each bubbler, and functions as an eight-input NOR gate. The output of this gate commands the bypass valves. If any of the bubblers are open, the bypass is closed; if no bubblers are open, the bypass opens. Similar four-input NOR gates control the bypasses in the permeation tube box.

The solenoid valves in the dilution box are arranged in master/slave pairs on T junctions. The master valves are depicted with open circles and the slave valves are depicted with solid circles in Fig. 2. The gas flow coming into a T junction will exit via either the slave valve (to a vent) or the master valve (toward the sensor), depending on which is open. The logic circuit in the dilution box commands the slave valve to be open when the master valve is closed, and vice versa. The circuit functions by inverting each control signal for a master valve and using the inverted signal to control the corresponding slave valve.

Designing the vapor flow system with bypass and slave valves automatically controlled by logic circuits assures that an open flow path from each flow controller to either the sensor or a vent is always maintained. This avoids no-flow conditions in the flow controllers, and continually flushes clean carrier gas through any part of the system not currently being used to generate a vapor stream. Automatic operation of these valves by hardware allows the operator or programmer to be concerned only with those valves leading toward the sensor.

The solenoid valves (Precision Dynamics, New Britain, CT) are normally closed valves with Kalrez seals on the plungers and ethylene propylene rubber (EPR) O-rings*. These valves are powered by 115 VAC, which is switched on and off by optically-coupled solid-state relays. The relays are commanded by the TTL digital signals discussed above.

Mass flow controllers

The carrier gas is supplied to the vapor flow system as dry air at 30 psi. The pressure of this gas is reduced and its flow regulated by means of air mass flow controllers (Tylan, Carson, CA). These devices contain an air mass

*Some vapors cause standard seal and O-ring materials to swell, which can impair valve function.

flow sensor and an electronically actuated needle valve. The mass flow controller is commanded to a particular flow rate by an 0 - 5 V analog signal, which is proportional to the desired flow rate and the range of the flow controller. For example, a 3.0 V control signal to a FC500 commands a 300 ml/min flow rate. Control signals are generated by the digital to analog I/O board in the microcomputer at the command of an operator at the keyboard or by software. The mass flow controllers also generate a 0 - 5 V analog signal proportional to the actual flow rate measured by their air mass flow sensor. These signals are read by the analog to digital I/O board.

Flow reduction system

The flow reduction system is contained in the dilution box and consists consists of a T junction (labeled E in Fig. 2), a precision piezoelectric gas leak valve (Vacuum Accessories Corp., Bohemia, NY), an air mass flow meter (FM200) and an analog control circuit. This system divides the total mixed gas flow arriving at junction E into two paths. The path from point E to F through the flow meter delivers gas to the sensor. The other path leads to the gas leak valve, which bleeds the remaining flow into vacuum. The degree to which the gas leak valve opens is governed by a 0 - 100 V control signal commanded automatically by the analog circuit. This circuit determines the control signal for the gas leak valve by comparing the signal generated by the mass flow meter (FM200) with a 0 - 5 V analog control signal from the microcomputer (via the digital to analog conversion I/O board). If, for instance, the flow rate to the sensor being measured by the flow meter is greater than the flow being commanded by the microcomputer, then the gas leak valve begins to open more. This diverts more gas flow into vacuum, and results in a reduced flow rate though the flow meter. The flow meter output signal starts going down. When it matches the control signal from the microcomputer, the 0 - 100 V command signal to the gas leak valve stops increasing and the gas leak valve opening remains steady at the position that maintains the commanded flow rate through the flow meter.

3. Instrument operation

Automated sensor evaluation

The overall purpose of this instrument is to evaluate sensor behavior under clean air and under various vapor streams. For each vapor, the sensor must first be observed under clean air to determine its baseline drift. Secondly, the sensor is observed under a vapor stream to determine its response. Finally, the sensor is observed under clean air again to determine its recovery. Usually this cycle is repeated to determine reproducibility, and for each vapor it is desirable to observe response under a range of concentrations. The specific solenoid valve operations necessary to switch the instrument between clean air and vapor stream output will be described separately from the overall process of testing sensors.

Sensor testing is normally carried out using two BASIC programs written specifically for this instrument. These programs are outlined in Table 1. Many instrument functions can be accessed directly by commands entered at the computer keyboard, but this is mainly useful for instrument check out. Sensor testing requires keeping track of numerous instrument functions at once, and this is most reliably accomplished with the aid of software.

TABLE 1

Software for sensor testing

Program 1
1. Update vapor source mass flow rates.
2. Calculate menus of concentration choices for each vapor.
3. User selects vapor/concentrations to be generated.
4. Text file stored on disk for each selection.
Program 2
1. Flush flow system, output clean air.
2. Read first text file.
3. Generate and equilibrate vapor stream, output clean air.
4. Test sensor, output clean air, then vapor, then air.
5. Store data on disk.
6. More experiments?
No — Flush flow system, output clean air, end.
Yes — Read next text file.
7. Is the next vapor different?
No — Adjust dilution air, loop to step 4.
Yes — Flush flow system, loop to step 3.

The first BASIC program helps the user to plan the sensor exposure experiments. The mass flow of vapor that each installed vapor source generates is displayed and can be updated. This information is combined with information on the dilution capabilities of the instrument in order to produce menus of possible vapor concentrations. A separate menu is created for each vapor. The user then selects vapors and concentrations in the order that the sensor is to be exposed to them.

Once the user has completed his selections, the program begins storing text files on disk. Each of these text files contains an array of variables that will command the vapor flow system to generate the chosen vapor stream at the chosen concentration. Specifically, the values of these variables dictate which solenoid valves will be opened to generate the chosen vapor stream, and what flow rates the mass flow controllers will set in order to dilute to the chosen concentration. In addition, certain variables indicate which solenoid valves must be opened and shut when the vapor flow system output is switched between clean air and vapor.

After the user has selected vapors and concentrations and stored text files on disk using program 1, sensor testing can proceed using program 2.

This program operates the instrument and performs the experiments (*i.e.*, vapor/concentration) contained in the text files. The program begins operation by opening solenoid valves in a configuration that will flush the entire system (excluding individual bubblers) with clean air. The initial instrument output is also clean air. The first text file is read and the chosen vapor stream is generated and sent to vent. The program does not begin a sensor testing sequence until the vapor stream has equilibrated for twenty minutes. Then sensor data collection begins and the instrument output is switched between clean air and vapor stream at programmed intervals. The results are displayed graphically on the computer monitor. At the completion of the experiment, the test conditions and the sensor response data are stored on disk, the graphics are dumped to the printer, and the next text file is read from disk. If the next vapor is different from that of the previous experiment, the system is flushed with clean air for ten minutes before generating and equilibrating the new vapor stream. If the next vapor is the same but at a different concentration, then the flow rates are adjusted for the new concentration and the experiment proceeds. The cycle of reading the experiment from disk, performing the experiment and saving the data on disk is repeated until all the experiments have been completed. The system is then flushed with clean air until the operator shuts it down.

Clean air and vapor output operations

Following the detailed switching operations of the vapor flow system will require reference to Fig. 2. All solenoid valves depicted by open circles should be assumed to be closed unless indicated otherwise, with the bypass and slave valves operating automatically. The flow controllers are delivering a commanded flow rate of air to their respective carrier gas pathways, and the flow reduction system is automatically maintaining the output of the dilution box at the commanded flow rate.

(1) *Vapor stream generation.* When a particular bubbler contains the chosen vapor, its corresponding pair of solenoid valves is opened. The carrier gas passes through the bubbler and delivers the resulting vapor stream to a T junction in the dilution box. The master solenoid valve on this T junction is opened so that the vapor stream proceeds through junctions at A and B and exits to vent via the slave valve on junction B. This configuration is maintained for at least twenty minutes to equilibrate the vapor source and tubing wall surfaces and achieve a stable, reproducible mass flow of vapor. A vapor stream is generated this way when the first text file is read. The bubbler (or other vapor source) is not closed again until a subsequent text file that requires a different vapor is read.

(2) *Set up dilution and output clean air.* Most of the time the output of this instrument is clean air, which comes from one or both of the FC500s in the dilution box. All of this air proceeds via junctions C and D to E. The flow reduction system then sends the commanded amount to the output at F and diverts the rest via the gas leak valve. When a text file is read, the flow

of air from the FC500 is adjusted to the levels that will be required when the vapor stream is diluted and output.

(3) *Switch to vapor stream output.* The vapor stream is output or 'switched on' by opening the master valve at junction B. This stream proceeds via D and E to the output at F, possibly mixing with dilution air at D. If the vapor stream is not to be diluted at D, then the master valve on junction C is closed at the same time that the master valve on junction B is opened. Switching solenoid valves open and closed at C and D clearly has the potential to change the total volumetric flow rate arriving at junction E in the flow reduction system. Such a change would force the flow reduction system to adjust the opening of the gas leak valve in order to maintain the constant commanded output flow rate. However, such adjustment can be avoided by simultaneously reducing the clean air flow when the vapor stream flow is switched on, as outlined below.

When the vapor stream is to be output in undiluted form, the air used for clean air output comes entirely from the FC500 closest to junction C. (The master solenoid closest to the farther FC500 is closed and its flow exits to a vent.) The flow rate of this air has been set to match the flow rate of the vapor stream arriving at B (and exiting to vent). Clean air output is switched to undiluted vapor stream output by opening the master valve at B and closing the master valve at C. The flow rate arriving at E is unchanged and the flow reduction system makes no adjustments.

If the vapor stream is to be diluted, but with less than 500 ml/min of air, then the FC500 farthest from C is set to match the vapor stream flow rate. The FC500 closest to C is set to provide all the air required to dilute the vapor stream to the chosen concentration. During clean air output the air from both FC500s proceeds from C to E. When the vapor is switched on, the flow from the FC500 farthest from C is switched off (to vent) by closing its master solenoid valve. The flow rate arriving at E is therefore unchanged.

When the vapor stream is diluted with greater than 500 ml/min of air, then the combined flow rate from both the FC500 flow controllers is set to the flow of air needed for the dilution. This flow always proceeds from C via D to E. Clean air is switched to dilute vapor stream by simply opening the master valve at B. The flow reduction system must readjust the gas leak valve in this case because this switching mechanism increases the flow rate arriving at E. However, this flow rate increase is small compared to the amount of dilution air flow already being diverted by the flow reduction system, and the required adjustment in the gas leak valve is minor.

(4) *Switch back to clean air output.* To return the system to clean air output, the solenoid valves are simply returned to their configuration prior to switching the vapor stream on. This requires closing the master solenoid at B and possibly opening another solenoid valve to compensate with more air flow. Note that switching the output between clean air and vapor while a sensor is being tested is accomplished solely by the opening and closing of solenoid valves. The commands to the mass flow controllers are not changed during the course of an experiment.

(5) *Change vapor or concentration for the next experiment.* If the vapor for the next experiment is the same but at a different concentration, then the commanded flow rates to the flow controllers are changed to provide the required dilution. The next experiment can then proceed. If the vapor is to be changed, then the previous vapor source is closed and the system is flushed for ten minutes before opening and equilibrating the next vapor stream.

4. Instrument precision and range

Vapor concentrations

The concentrations of the vapor streams output by the instrument are calculated by dividing the vapor mass flow rate by the total volumetric flow rate of the gas containing the vapor:

$$\text{concentration} = \frac{\text{vapor mass flow rate}}{\text{total volumetric flow rate}} \quad (1)$$

The uncertainty in the vapor concentrations therefore depends on the uncertainties in the vapor mass flow rates and the volumetric flow rates of carrier gas.

The mass flow rate of a permeation tube is dependent on the area, thickness, and material of the permeation barrier, and is independent of the carrier gas flow rate. These devices are conveniently calibrated by determining their mass loss as a function of time at the thermostatted temperature. Successive determinations on Teflon permeation tubes produced in-house gave uncertainties of less than 10%. Commercial permeation tubes purchased already calibrated are rated at 5% uncertainty.

The mass flow rate of a bubbler depends on the vapor pressure of the liquid, the degree to which the carrier gas becomes saturated with the vapor and the flow rate of the carrier gas. The use of electronic mass flow controllers in this instrument assures that the carrier gas flow rate will be constant regardless of changes in downstream flow conditions. The degree of saturation depends on the efficiency of the bubbler and the amount of liquid it contains. These variables can be controlled by good bubbler design and maintenance.

Bubblers were calibrated by passing their effluent into a charcoal filter to trap the vapor quantitatively, and measuring the mass increase of the trap. This procedure was carried out with the bubblers installed in the instrument at ambient temperatures with a carrier gas flow rate of 39 ml/min. Mass flow rates were stable after fifteen minutes of bubbling. Successive determinations resulted in mass flow rates with uncertainties of less than 6%.

It should be noted that simply estimating the mass flow rate of a bubbler from published vapor pressures and the ideal gas law is unreliable. Such estimates can vary from gravimetrically determined values by as much

as 30%. Estimated values were sometimes less than gravimetric values, indicating that the difference between observed and estimated values is not due to a failure to saturate the carrier gas.

The total volumetric flow rate of the gas containing the vapor is equal to the sum of the carrier gas flow rates of those flow controllers contributing to the total flow, plus the volume of the vapor itself. For dilute vapor streams, the volume of the vapor is negligible. The uncertainty in the carrier gas flow rate is then determined by the flow controllers, which are accurate to 1% of full-scale flow, *e.g.*, 5 ml/min for an FC500 (and repeatable to 0.2% of full scale). The percentage uncertainty in total flow of carrier gas is, therefore, the least when the number of flow controllers contributing to the total flow is minimized and when low-flow conditions are avoided through any of those flow controllers (especially FC500s).

Clearly, the uncertainty in the total volumetric flow rate will vary depending on the particular dilution being performed. When a given concentration can be achieved by more than one method of dilution, the most precise method is used. For example, diluting the mass flow from a permeation tube with an increasing amount of volumetric flow from the permeation tube FC200 (up to 200 ml/min) is more precise than diluting 39 ml/min of flow from the permeation tube box with additional volumetric flow from an FC500 in the dilution box.

As noted earlier, vapor/concentration experiments are planned by the user with the help of program 1. This program provides the user with menus of concentration choices for each vapor. Each choice represents a particular procedure for diluting the vapor stream, which was designed to accomplish the dilution in the most precise manner available. One set of procedures was developed for diluting mass flow from permeation tubes, and a different set of procedures was developed for bubblers. For any particular permeation tube, for instance, the mass flow of that permeation tube is divided by the total flow of carrier gas generated by each dilution procedure, and this produces the menu of concentrations. Table 2 provides an example of the dilution information associated with selected menu choices for permeation tubes. An actual menu would include a column of vapor concentrations calculated according to eqn. (1).

Sixteen menu choices are available for permeation tubes, each choice being approximately 80% of the concentration of the choice before it. These range from the concentration of an initial vapor stream, which enters the dilution box and is output to the sensor with no further dilution, to the most dilute stream the instrument can produce. Concentrations relative to that of an initial vapor stream are given in the Fractional concentration column. The instrument can dilute permeation tube vapor streams to 3.3% of their initial concentration. The uncertainty in the total volumetric flow rate is the greatest (5%) for an undiluted vapor stream and least (1%) at maximum dilution. The uncertainty in the output vapor concentration calculated according to eqn. (1) is the sum of the mass flow rate uncertainty (5 - 10%) and the total volumetric flow rate uncertainty (1 - 5%). Permeation tube vapor stream concentrations are therefore known to ±6 to 15%.

TABLE 2

Selected permeation tube dilution menu choices

Menu choice #	Flow controller flow rates (ml/min)			Total volumetric flow rate[a] (ml/min)	Fractional concentration[b]
	FC200[c]	FC500	FC500		
1	39 ± 2	0[d]	0	39 ± 5.1%	1.000
2	48 ± 2	0	0	48 ± 4.1%	0.805
4	77 ± 2	0	0	77 ± 2.6%	0.509
8	195 ± 2	0	0	195 ± 1.0%	0.200
12	200 ± 2	254 ± 5	0	454 ± 1.5%	0.086
16	200 ± 2	500 ± 5	500 ± 5	1200 ± 1.0%	0.033

[a]The sum of the volumetric flow rates from all contributing flow controllers.
[b]Fractional concentration relative to the concentration when the mass flow is carried by 39 ml/min of carrier gas.
[c]FC200 in the permeation tube box. Flow from the FC200 in the bubbler box is not used to dilute permeation tube vapors.
[d]Zeros indicate that this flow controller does not contribute flow or uncertainty to the total flow.

The bubbler menu is set up similarly. However, the maximum dilution for a bubbler is somewhat less, because the carrier gas flow in the bubbler must be constant to deliver a constant mass flow of vapor. Therefore, the FC200 in the bubbler box always contributes 39 ml/min of carrier gas, and all further dilution flow comes from the FC500s. The maximum dilution is into 1039 ml/min of carrier gas, giving a fractional concentration of only 0.038 relative to the concentration of the initial bubbler vapor stream.

The uncertainty in the total volumetric flow rate is 5% for undiluted bubbler vapor stream, and then increases sharply when volumetric flow from an FC500 is added to the 39 ml/min from the FC200. The menu does not allow the user to choose concentrations with high uncertainties. The first diluted choice given is to 40% of the initial vapor stream, with an uncertainty of 7%, the largest uncertainty of any choice on either menu. The uncertainty is below 5% for bubbler dilution choices below 25% of the initial concentration, and is near 1% at maximum dilution. Combining the 6% uncertainty in the bubbler mass flow rates with the 1 - 7% uncertainties in volumetric flow rates gives concentrations (eqn. (1)) known to ±7 to 13%.

However, bubbler vapor streams are not always so dilute that the total volumetric flow rate of gas containing the vapor can be determined simply from the volumetric flow rate of the carrier gas. The volume of the vapor itself must be considered for volatile liquids whose vapor is not diluted by a large volume of carrier gas. For example, isooctane with a gravimetrically-determined mass flow rate of 0.014 g/min will contribute a volumetric flow rate of 3 ml/min at 25 °C and 1 atm, based on an ideal gas law conversion. Addition of 3 ml/min to the 39 ml/min of carrier gas of an undiluted vapor

stream gives a total volumetric flow rate of 42 ml/min. The calculated vapor concentration is 8% too high if the vapor volumetric flow is not added to the carrier gas volumetric flow in the denominator of eqn. (1).

Flow reduction system

The flow reduction system takes the diluted vapor stream and splits the volumetric flow into two paths, one of which goes to the sensor. This process does not change the concentration of the vapor stream or the precision with which it is known. The accuracy of the volumetric flow rate output to the sensor is dependent on a number of factors, including the accuracy of the flow measurement by the mass flow meter (FM200, ±2 ml/min) and minor uncorrected offsets in the analog circuit that controls the system. In practice, actual flow rate output is generally within 5% of the commanded output, 39 ml/min.

The magnitude of the volumetric flow that the flow reduction system can divert via the gas leak valve is dependent on how it is configured. With 1/16 inch stainless steel tubing from the T junction (E on Fig. 2) to the flow meter and a single gas leak valve installed, the flow reduction system can reduce up to 800 ml/min arriving at E to 39 ml/min output at F. With two gas leak valves placed in parallel by having a cross at E instead of a T junction, and 1/8 inch stainless steel tubing from the cross to the flow meter, flow rates in excess of 1200 ml/min arriving at E can be reduced to 39 ml/min output at F.

It was stated in Section 3 that the flow reduction system need not adjust the opening of the gas leak valve when the system output is switched from clean air to vapor, provided that the volumetric flow of air arriving at point E is not changed. This is the case when the vapor stream is either undiluted, or is diluted by less than 500 ml/min of air. Nevertheless, the flow reduction system does sometimes make adjustments under these conditions. This adjustment occurs because the mass flow meter in the flow reduction system is calibrated for dry air, and gives an erroneous reading when high concentrations of a vapor with thermal properties differing from those of air are sent through it. The flow reduction system automatically adjusts the gas leak valve so that the reading from the flow meter will return to the desired value, even though that reading is mis-stating the actual flow. This error becomes negligible when the vapor stream is dilute.

5. Conclusion

The instrument described here has proved to be extremely valuable in conducting chemical sensor research. Sensor coating materials can now be rapidly screened against a range of chemical vapors. The capability of generating mutliple concentrations of a single vapor and maintaining a constant flow rate to the sensor regardless of the dilution required to achieve the desired concentration allows calibration curves to be determined very

conveniently. Extended sequences of tests involving target vapors at low concentrations, potential interferents at high concentrations and mixtures of two vapors can be automaticaaly executed to critically evaluate prototype sensors. Testing sequences requiring days of continuous operation can be routinely conducted. The generation of sensor data sets of sufficient size for the application of pattern recognition techniques is a readily manageable task. A matrix of surface acoustic wave sensor data, which was collected with this instrument and analyzed by pattern recognition techniques, has recently been reported [4]. This type of instrument should be useful to all those who must test and evaluate chemical sensors.

Acknowledgements

The support of the U.S. Army Chemical Research Development and Engineering Center, Aberdeen Proving Grounds, MD, is gratefully acknowledged. The research was performed at the Naval Research Laboratory, Washington, D.C.

References

1 R. S. Barratt, The preparation of standard gas mixtures: a review, *Analyst (London) 105* (1981) 817 - 849.
2 J. Namiesnik, Permeation devices for the preparation of standard gaseous mixtures, *Chromatographia, 17* (1983) 47 - 48, and refs. therein.
3 H. Wohltjen, Mechanism of operation and design considerations for surface acoustic wave device vapor sensors, *Sensors and Actuators, 5* (1984) 307 - 325.
4 D. S. Ballantine, Jr., S. L. Rose, J. W. Grate and H. Wohltjen, Correlation of surface acoustic wave device coating responses with solubility properties and chemical structure using pattern recognition, *Anal. Chem., 58* (1986) 3058 - 3066.
5 H. Wohltjen, W. F. Barger, A. W. Snow and N. L. Jarvis, A vapor-sensitive chemiresistor fabricated with planar microelectrodes and a Langmuir–Blodgett organic semiconductor film, *IEEE Trans. Electron Devices, ED-32* (1985) 1170 - 1174.

Biographies

Jay W. Grate is a Research Chemist at the U.S. Naval Research Laboratory. After completing his undergraduate education (B.A. in chemistry, 1978) at Rollins College, he went on to the University of California, San Diego as a National Science Foundation Pre-doctoral Fellow. His Ph.D. degree (chemistry), which he completed in 1983, was based on studies in organometallic and bio-inorganic chemistry. From 1983 to 1984 he conducted post-doctoral research on the organometallic chemistry of the lanthanides at the University of California, Irvine. Since joining NRL in 1984, his work has addressed several areas of chemical sensor research,

including the use of sorptive materials, semiconductive coatings and Langmuir–Blodgett films for vapor sensing, and the development of automated instrumentation for sensor evaluation.

David S. Ballantine, Jr. was born on Long Island, NY in 1955. He received a B.S. from the College of William and Mary in 1977, and a Ph.D. in analytical chemistry from the University of Maryland, College Park Campus, in 1983. He has been employed by Geo-Centers, Inc. as a research chemist at the NRL facility in Washington, D.C. since 1984. His current research involves investigating vapor/coating interactions using SAW devices, and the testing and development of SAW devices as chemical sensors.

Hank Wohltjen was born in Staten Island, NY on July 20, 1950. He received a B.S. in chemistry in 1972 and a B.S. in engineering science (electrical) in 1974, both from the City University of New York, and a Ph.D. in chemistry from the Virginia Polytechnic Institute, Blacksburg, VA. His dissertation research was in the area of surface acoustic wave chemical sensors. From 1978 to 1980 he was an IBM postdoctoral fellow in the electron beam lithography group at the Thomas J. Watson Research Laboratory, and during this period was also employed in the New Devices group at IBM's research laboratory in Zurich, Switzerland. He joined the U.S. Naval Research Laboratory as a research chemist in 1981 and initiated research in the area of chemical microsensors based on surface acoustic wave devices, organic semiconductors and optical waveguides. In 1985 he founded Microsensor Systems, Inc., an organization dedicated to research and development of chemical microsensor instrumentation.

MICROSENSOR SYSTEMS, INC.

VG-7000

AUTOMATIC VAPOR GENERATION SYSTEM

OPERATING MANUAL

VERSION 2.0
APRIL 1988

TABLE OF CONTENTS

page

I. SYSTEM OVERVIEW
A. Introduction 4

B. VG-7000 System Organization
1. Vapor Generating Module. 7
2. Dilution Module. 8
3. Gas Cylinder Module 9
4. Electronics Module 9

C. System Performance Capabilities and Limitations
1. Vapors 10
2. Concentrations 11

D. Operating Modes
1. System Definition 13
2. Experiment Schedule 15
3. System Check 17
4. System Calibrate 13
5. System Operate 19
6. Immediate Mode 19
7. Exit Vapor Generator 19

II. SYSTEM HARDWARE DESCRIPTIONS
A. Dilution Module
1. Blending Chamber 20
2. Selector Valves 20
3. Mixing Chamber 20
4. Dilution Valves 21
5. Mass Flow Controller 21

B. Vapor Generating Module
1. Transfer Containers 22
2. Temperature Control Block 22
3. Mass Flow Controller 22
4. Bypass Valve 23
5. Check Valve 23
6. Teflon™ Filer 23

C. Gas Cylinder Module
1. Selector Valves 24
2. Mass Flow Controller 24
3. Bypass Valve 24

D. Materials of Construction 25

III. OPERATING SYSTEM SOFTWARE DESCRIPTION
A. System Requirements 26
B. Theory of Operation 27
C. Operating Restrictions 36
D. Starting the System 37
E. Error Messages 38

IV. VG-7000 OPERATION
A. Setting Up the Hardware 39
B. Loading Liquids into the Bubbler Module 40

APPENDIX A. Sample Experiment Schedule

APPENDIX B. Sample System Operation Screens

APPENDIX C. VG-7000 Pneumatic Flow Diagram

APPENDIX D. Connector Cable Pin Assignments

APPENDIX E. Sample Time Log Printout

I. SYSTEM OVERVIEW.

A. Introduction.

The VG-7000 automatic vapor generation system is an advanced instrument for the preparation of test atmospheres for a variety of applications, including chemical vapor sensor performance studies, olfactory investigations and vapor phase reactions. The system employs a novel scheme based on pneumatic pulse width modulation to dilute source vapors with clean carrier gas by dilution factors from 1 (undiluted) to over 1,000,000. Remarkably, the pulse width modulation approach permits this wide range of dilution factors to be realized with no adjustments to the system carrier gas flow rate. This guarantees a constant source vapor flow rate at values ranging from 100 sccm to several liters per minute. At the smaller flow rates there will be a consistently low carrier gas consumption rate. For example, at 700 sccm a compressed zero air cylinder can be used to meet the 20 psi carrier gas requirement for weeks of continuous operation. Noisy pumps and contaminant traps can therefore be eliminated.

Vapors may be obtained from a variety of sources; however, the system was specifically designed for the convenient use of bubblers. Bubblers can be used to generate source vapors from essentially any chemical that is liquid at room temperature. The range of concentrations available from bubblers depends, of course, on the saturated vapor pressures of the liquids of interest, but most often they are typically quite high (e.g.

In the VG-7000, gas flow control and valve timing are managed by a built-in microcomputer system. The system valving is designed fail safe, so that in the event of electronic failure or power loss the system automatically turns off all vapor sources and purges itself with clean carrier gas, thereby eliminating the possibility for undesired vapor mixing or unexpected vapor output. All carrier gas flow rates are regulated by highly precise electronic mass flow controllers.

Operator interactions with the VG-7000 are conducted through an Apple Macintosh™ host computer that communicates with the on-board microcomputer by means of an RS-232C line. System definition, calibration, checks, and operation are all performed by means of a simple-to-use, menu driven operating system that utilizes many of the Macintosh graphics and editing features. Complex experiments may be set up for the VG-7000 that can be carried out completely under computer control for periods up to several days. The only Investigator intervention required would be to assure adequate liquid levels in the bubblers. The experimental schedules are stored on disk and can be recalled and modified or reused.

A programmable solenoid valve is provided at the vapor generator output that can rapidly switch from the vapor stream to clean carrier gas. Thus, sensors under evaluation can easily be re-zeroed to baseline. A TTL compatible signal is provided on the instrument front panel that provides valve status information useful for synchronization of external sensor data acquisition equipment.

B. VG-7000 System Organization.

The VG-7000 was designed as a modular system. It is organized into four component subsystems (or modules) with a computer host. The four component subsystems are: (1) the electronics module; (2) the dilution module; (3) the bubbler module; and (4) the gas cylinder module. A complete system will contain one dilution module, one electronics module, up to three vapor generating modules (either bubbler or gas cylinder modules), and an Apple Macintosh™ computer. The system is normally configured with two bubbler modules and one gas cylinder module. Control of the system is accomplished using a hierarchical multiprocessor computer system. An Apple Macintosh™ serves as the system host and

performs all operator interactions. A Z8 microcontroller imbedded in the vapor generator electronics module is slaved to the Macintosh™ and generates all control signals. Communication is via an RS 232C serial interface. All of these components, except for the Apple Macintosh™ computer, are located in a self-contained enclosure with all necessary external connections supplied either on the front or rear of the chassis. The connections required are discussed in the users manual. A brief description of the function of each module is helpful in understanding the operation of the system and is given below.

1. Vapor Generating Module.

The purpose of the vapor generating module is to produce vapors of the selected materials (liquids) by bubbling a carrier gas through pure samples of the liquids held in Teflon™ transfer containers. This method provides reasonably saturated solutions in a single stage of contact (90% typically). The creation of a fully saturated solution would require the use of several stages in series and is not necerssary for this application. The source vapor is then transported through the process lines to the dilution module. Each Bubbler Module includes Teflon™ transfer containers for four liquids. The four transfer containers are housed in a water cooled aluminum heat sink to maintain the materials at a constant temperature during the evaporation process. The flow of carrier gas to each transfer container is controlled by a series of Teflon™ solenoid valves that direct the carrier gas to the container holding the desired material. The transfer lines which deliver the highly saturated vapor streams are not heated. Thus to prevent vapor condensation in the unheated lines, it is essential that the bubblers be held at constant, sub-ambient temperatures (e.g. 10-20 degrees centigrade). The flow rate for each bubbler module is controlled by an electronic mass flow controller. This flow rate is set to 100 cc/min and is matched with the flow rates used throughout the system.

It is necessary to periodically check the tightness of the fittings and top of the transfer containers. This is done to avoid leaks which can occur with Teflon™ due to cold flow. It is also necessary to check the transfer lines and filters on the bubbler modules to inspect for condensation and liquid accumulation. If liquid is present this indicates a problem with the operation of the bubbler modules and requires further investigation.

3. Gas Cylinder Module.

The gas cylinder module allows for the input of up to four bottled gases to the dilution module. These gases should be calibrated mixtures in clean air rather than pure gases to give accurate flow control. Pure conpressed gases **cannot** be used since the electronic mass flow controllers are calibrated for air. The gas inputs are through bulkhead connectors and are operated using four cylinder selecting valves. This module also contains a mass flow controller that regulates the flow rate of the input gas stream to match that of the carrier gas used in the dilution moduleand the vapor generating (bubbler) modules. The outlet from this module connects to the dilution module. During default conditions or when this module is not selected, pure carrier gas is sent through the process lines to purge any residual vapor which may be present.

4. Electronics Module.

The Electronics Module contains power supplies for the on board microcomputer and the electronic mass flow controllers. The microcomputer communicates with the Macintosh™ host computer over a 9600 baud serial RS-232C communications line (8 data bits, no parity, 2 stop bits). The VG-7000 microcomputer requests information from the Macintosh™ regarding the vapors to be selected, the pulse width modulation duty cycles for each of the three dilution stages of the dilution module, the equilibration period allowed, and the on/off periods for the vapor generator. Each solenoid valve in the system is energized with 115 VAC supplied from an optically isolated solid state relay controlled by the microcomputer. There are only two controls available to the operator. A power switch energizes the entire system, and a microcomputer reset button is used to guarantee that the VG-7000 and Macintosh™ are synchronized. A TTL compatible signal on the front panel of the electronics module provides valve status information useful for synchronization of external sensor data acquisition equipment. This signal is the same as that used to control the final solenoid valve that selects whether the vapor stream or clean carrier gas is being supplied to the sensors. Four identical (except for length) power cables are used to connect the various system modules to the electronics module. These cables carry 115 VAC power supply and return lines for the solenoid valve, chassis ground, and flow controller power (+/- 15 V, ground, signal).

materials into the transfer containers rather than liquid samples. Permeation tubes can be prepared for most materials of interest and are able to produce extremely low concentration vapor streams. The controlled output from the permeation tubes allows for extremely accurate concentration levels below 1.0 mg/m3. This system was designed so that the transfer containers would operate using either liquid samples or permeation tubes.

This system allows for the production of binary and ternary mixtures by using one input from each of the vapor generating modules or from either of the vapor generating modules and the gas cylinder module. The blending valves are used to control the concentrations of the mixtures. Due to the switching time of the blending valves, the concentration range for mixtures is restricted to 5% to 95% by volume of either vapor in the bianry mixture and restricted to 5% To 90% by volume or each vapor for ternary mixtures. The system software program defines the upper and lower concentration limits based on the volume percent as described above. The available concentrations of the mixtures depend on the particular vapors being used.

D. Operating Modes.

There are seven operating modes for this system. Each of these modes can be run separately from each other and in any order desired. The choice of operating mode is done using a screen menu on the Apple Macintosh™. When a mode is selected a new screen appears to either display information or to request inputs from the operator. Each of the operating mode screens contains an option to cancel that mode if it was selected accidentally or if the operator does not wish to use that mode. The first two modes of operation involve only the Macintosh™, the next four modes require interaction between the Macintosh and the system hardware, and the last mode is used to exit the VG-7000 program. These seven modes are described below.

1. System Definition Mode.

The system definition mode is used to allow the user to define the parameters neccessary to operate the vapor generating system. This mode is used during the initial system configuration and at later times when changes have been made to the hardware or vapors. Selection of this mode of operation is done from the screen menu. Once this selection is done, a screen appears which displays each of the system parameters. These parameters include such items as number of vapor transfer containers in the system, number of external gas cylinders hooked up for use, the vapors provided by each transfer container and gas cylinder and their volumetric flowrate, carrrier gas flow rate, system temperature, and default parameters for the experiments. Each of these parameters is described in more detail below.

- **Number of vapor transfer containers.** This system is designed to accept input from a total of 12 input channels divided into three groups of four sources each. The groups of four inputs are contained on either a bubbler moduie or a gas cylinder module. Therefore, the number of vapor transfer containers available is either 4, 8, or 12 for the use of 1, 2, or 3 bubbler modules respectively. The value input into the computer is determined by the equipment configuration. Note that the value input for the number of containers must be the actual number of vapors available.

Each vapor input is labeled with a number recognized by the computer for a specific location and set of operating valves. It is important to refer to the correct transfer container or gas cylinder location when identifying the material placed in that location. This requirement is necessary so that the Z-8 microcontroller can operate the correct valves when selecting a specific vapor. Not all of the vapor inputs need to be used in order for the system to operate. It may be necessary or desirable at times to use only a portion of the available inputs. In these instances, the name of material and calibrated mass flow rate for the empty input channel are left blank.

- **External gas cylinders.** As mentioned above, the system was designed for up to 12 input channels. This allows for a maximum of 12 external gas cylinder hookups if no bubbler modules are used. The number of gas cylinders available is either 0, 4, 8, or 12 for 0, 1, 2, or 3 gas cylinder modules respectively. Note that pure compressed gases **cannot** be used as a vapor source since the electronic mass flow controllers are calibrated for air. Calibrated gas sources containing low concentrations (e.g. less than 1000 ppm) of a gas in air can be used as a vapor source however.

- **Calibrated mass flow rate.** The mass flow rate for each material must be determined for each carrier gas flow rate and system temperature used. When new materials are introduced or different system conditions are used the vapor mass flow rates must be re-calibrated in order to specify this parameter. A calibration mode is available with the vapor generation system specifically for this purpose. The value for mass flow rate must be input in units of mg/m^3. The system display shows concentration in mg/m^3.

- **Carrier gas flow rate.** The carrier gas flow rate is the value which will be set using the mass flow controllers. This flow rate is generally set at 100 cc/min. The system performance is optimized at this value. The blending and mixing chambers were designed and sized to operate most efficiently in the this range of flow throughput. The total carrier gas flow requirement is approximately seven times the flow rate of each mass flow

controller. If this value is set to 100 cc/min the total requirement for the system is 700 cc/min.

• **System temperature.** The value for system temperature refers to the temperature of the transfer containers on the bubbler modules. This is the temperature at which the materials being evaporated are exposed to. This is not adjustable unless an external (user supplied) refrigeration unit is used to circulate cooling fluid through the transfer container heat sink.

Changes to the values displayed during this mode are done only as needed through the use of the Apple Macintosh mouse and keyboard. Once changes have been completed to the system definition these values will remain in a data file until further changes are required.

• **Equilibrium Period.** The equilibrium period is the time specified for the system to produce the desired vapor concentrations prior to output from the instrument. This is done to allow the system to sweep out all traces of previous vapors and carrier gas and reach equilibrium between the vapor being produced and the system.

• **On Period.** The on period is the time during which the VG-7000 outputs vapor to be used.

• **Off Period.** The off period is the time during which the VG-7000 outputs carrier gas. This is done to re-zero the output stream.

2. Experiment Schedule Mode.

A separate mode is used to enter the operating parameters for the experiment schedule. During this mode, the information which defines the experiment schedule is input to the Macintosh™ for computation. In this mode, the operator can either create a new experiment schedule or edit an existing experiment schedule. The created schedules are saved on the "VGDATADISK". Additional data disks can be used if needed to save numerous experiment schedules. The information needed to define the scheduling includes the component(s) of each vapor; the concentration(s) for each vapor; and the number of runs to be performed, equilibration

period, cycle time, and number of cycles at each concentration. Each of these variables is described in further detail below.

- **Vapor components.** For the mixtures being used, there are either two or three components to each vapor and these must be specified. For single component vapors, only one material must be input. For binary mixtures it is required that each of the two components be from separate vapor generating modules. For ternary mixtures there must be one vapor specified from each of the three possible vapor modules. The input of the vapor components allows the Z-8 microcontroller to select the correct valves to generate the desired vapors.

- **Equilibrium period.** Prior to the first vapor output from the system an equilibrium period is necessary to allow a stable vapor concentration to develop. The operator is able to select the time period best suited to the vapors being tested. The input for this parameter is in a number of ten second cycles between 1 and 999. The recommended system requirement is for a minimum of thirty minutes (180 cycles) before each exposure. This time is required because of the methods used to produce the vapor concentrations. The process lines, the blending chamber, and the mixing chambers need to have all of the dead volume swept out as well as reach temperature and flow rate stability. In addition, the production of the vapor stream involves alternating between clean carrier gas and concentrated vapor. This vapor then passes through the mixing chambers to average out the concentration level. This process involves a finite time interval which depends on the mixing chamber volume and the vapor flow rate. The requirement of thirty minutes will allow for the necessary concentration equilibrium period. Any further time period selected by the operator will improve the system performance and is recommended when high boiling vapors are generated.

- **Cycle time.** The exposure cycle time can be broken into two parts, an exposure period and a baseline period. These two parts are referred to as the on period and the off period. The exposure period (on period) is the time during which a vapor stream of set concentration is output from the

vapor generating system. The baseline period (off period) is the time interval when clean carrier gas is output from the vapor generating system. Adding the two time intervals defines the cycle time. The purpose of the baseline period is to allow the operator to generate a reference state for the sensor being evaluated. Both of these time periods are defined by a number of ten second intervals. For example an exposure period of 6 would last for 60 seconds (1 minute) and a baseline period of 3 would last for 30 seconds.

- **Number of cycles.** The number of times the system goes through a cycle (exposure period plus baseline period) can be set to any value between 1 and 999. This number will determine the length of the total exposure time for each concentration.

- **Vapor concentration.** The desired concentration(s) for the single component, binary and ternary mixtures must be specified to the computer. The Macintosh™ calculates the upper and lower concentration limits for each material based on the calibrated mass flow rate data provided to the system definition, and available dilution ratios. These limits are displayed on the computer screen and the concentration value input by the operator must be within these limits. If not, the computer will not accept the input value and request a new value. The actual target concentration generated by the system may be slightly different from that requested by the operator due to round off approximations required by the pulse modulation scheme. For mixtures, there are two sets of concentration ranges, one for each component. Once the concentration is selected for one component, the values available for the second component are limited due to the available mixture ratio. For ternary mixtures there are three sets of concentration ranges, one for each component. These values are also restricted by the available combiantions of vapors selected.

3. System Check Mode.

The system check mode is used to verify the operation of the solenoid valves and the relays in the system. When this mode is selected a screen appears on the Macintosh™ which contains a "button" corresponding to each of the vaives or valve pair. When one of these buttons is selected using

the mouse, the corresponding valve is activated on the VG-7000. Carrier gas **must be off** when this mode is being used. This is done to prevent any dangerous mixtures or situations within the VG-7000 due to improper valve combinations being selected. By selecting the valves individually the operator can then diagnose whether or not all of the valves and relays are functioning correctly before starting a series of experiments. A check for each valve is done by both looking for the indicator light to turn on and listening for the valve to "click" as it switches on and off. The display screen for this mode shows the operation of each valve as it is tested. If any of these indicators is not detected, then the valve(s) in question must be checked further. See appendix B for an example of the system check screen.

4. System Calibrate Mode.

A separate mode of operation is used to calibrate the vapor generating system for use with the desired vapors. To begin this mode, the operator must specify the vapor being tested and the duration of the sampling cycle. The system is automatically operated to produce a 50% dilution of the nearly saturated vapor stream as output to the sensing equipment. A 50% dilution is performed in order to prevent the possibility of vapor condensation in the flow path which could degrade the accuracy of calibration. This vapor stream is then analyzed to determine the concentration in milligrams per meter cubed (mg/m^3). There is a set of instructions shown on the Macintosh™ screen detailing the steps needed for gravimetric analysis. The operator inputs data for the starting weight of the sorbent tube and the final weight of the sorbent tube and vapor trapped. Once this information is obtained, the value for the saturated solution is calculated by the computer. This physical property data is put into the system memory for use by the system definition mode described earlier. This is done when the operator selects the save option. Vapor mass flow rate information is used by the computer software to determine the vapor concentrations produced. If another flowrate is used or the system temperature is changed since the initial calibrations were performed, then all of the calibration data must be redone and entered into the computer memory for these conditions.

Gravimetric analysis of the vapor stream is easily accomplished by passing the vapor output stream through an activated charcoal/molecular sieve 13X trap for a specific period of time and then recording the mass change of the trap. With a flow rate of 100cc/min, a ten minute cycle time would allow 1 liter of vapor to pass through the filter. When the weights are input to the computer the calculation of the vapor mass flow rate is performed and displayed. If the information appears correct then the value can be saved and automatically placed in the system definition.

5. System Operate Mode.

When this mode of operation is selected, the only computer input required is to select which experiment schedule input is the one to be used. The latest schedule is indicated by the date of its entry. The experiment schedule to be used is selected by using the mouse of the Apple Macintosh™. During the operate mode, a time log feature can be selected which will produce a printout that indicates which vapors and concentrations were produced as well as the times when system warm-up, exposure and baseline occured.

6. Immediate Mode

The immediate mode will be available with later versions of the system software. This mode will allow the user to imput data quickly for one single experiment, either a single, binary or ternary mixture at one concentrations. This input is much faster than creating an entire experiment schedule, but is limited to only one vapor.

7. Exit Vapor Generator

This option is selected to exit the vapor generator program.

II. SYSTEM HARDWARE DESCRIPTIONS.

This section of the document describes the four modules of the system and the function of each. These four modulas are the dilution module, vapor generating module, gas cylinder module, and electronics module.

A. Dilution Module.

The dilution module performs the function of generating the concentration of vapors specified in the experiment schedule mode. This is accomplished by mixing the nearly saturated vapor stream or bottled gas with carrier gas in the ratios needed to produce the desired vapor concentrations.

1. Blending Chamber.

The blending chamber is included as a means to effectively mix the components of binary or ternary gas mixtures which are specified during the system initialization. The gas mixtures are combined using vapors from either the vapor generating modules or the gas cylinder module. This chamber is located downstream from the selector valves and combines the vapor streams entering from the vapor generating modules. The blending chamber is constructed of teflon and is carefully designed to effectively smooth the transient vapor pulses into a steady average concentration.

2. Selector Valves.

The selector valves control the process of mixing two or three vapors produced by the vapor generating modules. Responding to the mixture concentrations specified during the system initialization, these valves alternate the selection of vapor paths to create the proper ratio of gas mixtures.

3. Mixing Chamber.

The mixing chambers are located downstream of the blending chamber and are used to dilute the concentration of the initial vapor stream from the blending chamber. There are a total of three mixing chambers in series. Each chamber is capable of a dilution ratio of 1 to 100 therefore allowing a total dillution ratio of 1 to 1,000,000. However, the recommended dilution ratio is 1 to 50 for each chamber and 1 to 125,000 for the system

in order to maintain high levels of accuracy. The mixing chambers are identical to the blending chamber described above.

4. Dilution Valves.

The dilution valves are responsible for switching the vapor and carrier gas flow paths. The mixing of the vapor stream and carrier gas produces the required dilution ratio. This is accomplished by the dilution valves which operate as a pair and alternate between gas streams entering the mixing chamber. When the vapor or carrier gas stream is not directed to the mixing chamber it is sent to the vent lines in order to maintain a constant flow of gas through the system lines.

5. Mass Flow Controller.

Electronic mass flow controllers are used on the dilution level of the system to produce an accurate and repeatable gas flow rate. The sensing element is a small tube with resistance thermometers wound on the outside. The gas passing through the tube is heated a few degrees and the temperature measured before and after heating. Temperature difference is related to mass flow and to gas thermal conductivity. The controller has an observed repeatability of about $\pm$ 0.5% and can control flow rates from 6.0 to 300.0 sccm with an accuracy of $\pm$ 1% of full scale. There are a total of 4 mass flow controllers on the dilution level of this system to match and control the flowrates of each of the gas streams. The close control of the gas stream flowrates is used to eliminate as much error as possible in the production of the low level vapor concentrations. The electronic mass flow controllers are calibrated for pure air. If another gas is used as the major component of the gas stream then the absolute accuracy of the flowrate will change. The output from each of the flow controllers will continue to be matched with the other controllers as long as the same gas is used with each controller.

B. Bubbler Module.

The bubbler module is used to produce the highly saturated vapors required by this system. Two of these modules are included in the automatic vapor generating system described here.

1. Transfer Containers.

The materials used with this system to produce vapors are stored in transfer containers made of Teflon™ to reduce the possibiliy of reaction after long exposure to liquid chemicals. Following each transfer container is a 20 micron Teflon™ filter system to prevent the carryover of aerosols into the system piping which could cause contamination with the other vapors being produced. Periodically inspect the transfer containers for tightness to prevent leakage due to cold flow of the Teflon™. Teflon™ tape is used to help maintain a good seal on the transfer containers. When filling or changing the material in the transfer containers beware of reactive or hazardous materials which may be present in the containers.

2. Temperature Control Block.

A temperature control block is used on the vapor generating module to maintain the temperature of the transfer containers. As liquid is evaporated from the containers the remaining material is cooled slightly due to the heat of evaporation. It is important to maintain the temperature of the transfer containers so that the source vapor concentration is constant. Cooling fluid supplied from a user supplied constant temperature bath can be used to stabilize the system temperature. A sub-ambient temperature in the range of 10 - 20 degrees centigrade is recommended. Connections for the cooling fluid are on the rear of each vapor generating (bubbler) module.

3. Mass Flow Controller.

The vapor generating modules each contain an electronic mass flow controller which maintains a constant flow rate through the bubblers. The flow rate is matched to the slow rate of the dilution and gas cylinder modules to keep all of the system flow rates the same.

4. Bypass Valve.

The bubbler modules contain a bypass valve which is normally open and closes when any of the transfer containers is selected. This allows carrier gas to sweep out the dead volume of the bubbler module when no vapor is selected.

5. Check Valve.

A check valve is located at the inlet to each bubbler module. This is done to prevent reverse flow through the bubbler module in case of overpressure in the vent lines or unusual conditions due to incorrect operation. If flow is allowed to reverse direction in the bubbler module then liquid will be carried back into the system. The check valve is used to prevent this.

6. Teflon™ Filters.

Each transfer container is followed by a 20 micron Teflon™ filter to prevent aerosols from being carried to the dilution module. If liquid is present outside of the temperature controlled transfer containers it will evaporate at a different temperature and this will cause error in the mass flow rate calculations.

C. Gas Cylinder Module.

The bottled gas level is used to take input from up to four external gas cylinders and supply these gases to the dilution level of the automatic vapor generating system. This feature allows the use of calibrated gases or standard compressed gases for use with vapor testing. The bottled gases are attached to labeled bulkhead connectors on the front panel of this module and require only that a regulator be attached to the cylinder to decrease the pressure to within the range of 10 to 30 psig with an optimum of 20 psig. The lower pressure is required to prevent damage to the mass flow controller and the selector valves located downstream from the connectors.

1. Selector Valves.

There are four selector valves located on this level of the vapor generating system. Each valve in used to select one of the four bottled gas inputs and allows this gas to flow to the mass flow controller. The default condition of the valves is in the closed condition so that there is no leakage to the system from the gas cylinders as long as the pressure does not exceed 30 psig. This allows the gas cylinders to be left open permanently if desired without loss of contents as long as the pressure is within the limits stated above.

2. Mass Flow Controller.

There is one electronic mass flow controller used on the bottled gas level of this system. The purpose of this controller is to match the flow rate of the bottled gas input with the flowrates of the other gas streams in the system. This allows for more accurate production of the vapor concentrations specified.

3. Bypass Valve.

There is a bypass valve in the gas cylinder module to allow carrier gas to flush out the dead volume when no gas cylinder hookup is selected.

D. Materials Of Construction.

Teflon.

Teflon is used for the piping and components of the entire vapor generating system. In the vapor generating modules especially there are high concentrations of vapors present at all times and teflon is used because of its high degree of inertness with the materials expected to be used in this system.

III. OPERATING SYSTEM SOFTWARE.

1. SYSTEM REQUIREMENTS

HARDWARE:

The following pieces of hardware are required to operate the VG-7000 automatic vapor generating system.

1. A Macintosh™ computer with 2 disk drives and at least 512K of memory. (with keyboard and mouse available)

2. A cable for the RS232C serial port of the Macintosh™ to connect to the VG-7000 electronics module.

(Optional: An Imagewriter™ printer with appropriate cables to connect to the Macintosh™ computer.)

SOFTWARE:

The only software required to operate the VG-7000 system is a current version of the VG-7000 system disk and a data disk to store the experiment schedules. Both of these disks are supplied with the VG-7000 system. The system disk contains all of the files which are necessary to operate the program. The program was written in Microsoft® Basic version 3.0 (scientific version) and compiled on Microsoft® Basic Compiler V1.0.

2. THEORY OF OPERATION

The Macintosh™ computer and the VG-7000 system software provide a user friendly interface to the VG-7000 hardware. The system software makes extensive use of windows, buttons, and the mouse to preserve the Macintosh™ "environment" when operating the vapor generating system. The program is responsible for keeping track of the system configuration, the sequence of vapors produced, their concentrations, the vapor equilibration periods and the on/off cycle periods. The program takes input from the operator regarding the vapors desired and determines the correct instrument settings to produce these concentrations as near to the desired value as possible. The software provides the means to edit and create experiment schedules as well as check for errors in the information entered by the operator which would cause invalid vapor concentrations to be produced. The program handles all communication with the VG-7000 minicontroller allowing "hands-off" operation of the equipment. All that is required is to connect the output stream from the VG-7000 to the testing equipment.

a) System Definition Mode

OVERVIEW

The VG-7000 has the capability of producing vapors from twelve vapor sources in three banks, consisting of bubbler modules, gas cylinder modules, or a combination of the two. Each of the transfer containers can hold a liquid material which will be turned into a vapor by circulating the carrier gas through the transfer container.

In defining the system configuration, you have th option of assinging 4, 8 or 12 vapor sources. Any materials that you wish to be mixed must reside in defferent bubbler or cylinder banks. Refer to Appendix B for a sample of the screen display.

OPERATION:

The System Definition Mode is strictly data-entry. with no calculations being done by the program. The program will accept almost any data, with the exception of those exceeding system limitations.

There are six groups of data that must be entered in this mode.
They are:

1) "# of Transfer Containers", with a value of 0, 4, 8, or 12
2) "# of Gas Cylinders", same as above, with combined total not to exceede 12.
3) "Carrier Gas Flow Rate", obtained by measuring flow rate at 'Vapor Output' point.
4) "System Temperature.", this temperature corresponds to the temperature of the temperature control block(s) on the bubbler module.
5) "System Defaults". These are the default values the System will use in experiments if not over-ruled by the Experiment Schedule. They are as follows:
   a) Equilibration Period.
   b) Exposure Period
   c) Off Period
   d) Number of Exposure Cycles [For limits and explanations see **Experiment Schedule Mode**]

6) "Material Descriptions." Can be any Alpha-Numeric word or words that will fit in the edit field.
7) "Material Concentrations." Saturated Concentration Values of the materials in mg/m^3, should be determined by running the System Calibration mode.

All data is entered by means of edit fields. (For information on how to use the edit fields, see Macntosh Users Manual.)

To save any changes made to the System Definition Table, press the **[ACCEPT]** button. A window will then ask for confermation, and if acknowleged will save the new Table as the data file 'SDVap'. Warning, any experiment schedules that predate changes to the System Definition should be re-calculated if changes were made in materials or mass flow rate.

To print out a hard copy of the System Definition Table, press the **[PRINT]** button, making sure that the printer is on line.

To leave the System Definition Mode without saving the changes, press the **[CANCEL]** button. This will keep the existing Table unchanged.

COMMENTS:

1) When setting the number of transfer containers and gas cylinders, the total number must be 4, 8, or 12. Any defined container or cylinder that is not used should have "EMPTY" entered in the description edit for that material.

b) Experiment Schedule Mode

OBJECTIVE:

The objective of the Experiment Schedule Mode is to allow the operator of the VG-7000 automatic vapor generating system to create a schedule of vapor exposures and to run the system in a continuous mode. The experiment schedules created are stored so that the same schedule(s) can be used at a later date without the need to redefine the desired vapors and concentrations. Refer to Appendix B for a sample of the screen display.

OVERVIEW:

This Mode allows you to create and edit Experiment Schedules of Vapors consisting of one or two materials at differing concentrations and exposure periods. Each experiment Schedule can have up to sixty different vapors for twelve materials being used or a lesser amount for fewer materials, with each vapor having up to ninty-nine different concentrations. Experiment Schedules should be saved on a seperate disk from the VG7000 program and Macintosh™ Operating System, due to disk size limitations. Experiment Schedules are named as follows:

'Disk Name':Exp'YY-MM-DD"Vol #'.VG2

example: **VGDATADISK:Exp87-02-01A.VG2**

The volume numbers run from 'A' to 'Z', allowing 26 different Experiment Schedules to be created on a single day. More can be created if different data disks are used.

As well as acting as a data entry mode, the program also calculates valve duty cycles for the VG-7000 and mixture ratios for the vapors so there is some delay experienced when entering values.

OPERATION:

The first thing the Experiment Schedule Mode will ask is whether to create a new Schedule or edit an existing one.

If you press the **[Create New Exp. File]** button, you will be prompted for the Disk Name, with the Default being 'VGData'. If you wish to store the Experiment Schedule under a different name, enter the new name. You will then go directly into the Data Entry Mode.

If you press the **[Edit Existing Exp. File]** button, a window will display the Experiment Schedules currently on File on the disk in drive 1. Since this drive should contain no Experiment Schedules, press the **[CHANGE DRIVE]** button to access drive 2. If you need to change disks in the drive, press the **[EJECT]** button and insert the new disk. All the Experiment Schedules on the disk will be displayed.

To select an Experiment Schedule to edit, click the Mouse twice on the file name or Click the Mouse once on the name to select it and press the **[SELECT]** button. If there are more files on the disk than can be displayed at once, use the arrows on the window to scroll up and down the list. If you decide not to edit an existing file, press the **[CANCEL]** button. When you have selected a file, you will then go to the data entry screen.

There are four types of data needed for the Experiment Schedule. They are:

1) "Mixture." Three buttons used to determine if the vapor is a Single, Binary or Ternary mixture. The mixture in effect for the current vapor has a 'radio light' dot to the left of the button lit.
2) "Exposure Values." These are the exposure conditions for the single vapor being defined. They are:
   i) "Equilbrium Period" Time for the VG-7000 to attain a consistant concentration. Can be a value between 1 and 999 ten second intervals. A value of at least 30 minutes or 180 intervals is adequete.
   ii) "Exposure Period" Time that the output stream from the VG-700 will contain the vapor. Ranges from 1 to 999 ten second intervals.
   iii) "Off Period" Time that the vapor is routed to the vent with the output stream being pure carrier gas. Also rangesfrom 1 to 999 ten second intervals.
   iv) "Number of Exposure Cycles" Number of times the program will

cycle between the exposure and off periods. Can be a value between 1 and 999.

Pressing [return] while in the Exposure Value section will allow entry of the next value, until the 'Exp.Cycles' value is entered, where entry will jump to the 'vapor #1' edit field. Pressing [TAB] or the [OK] button will also jump to the 'vapor #1' edit field. If zero (0) is entered for any of these values, the system will use the System Default values set in the System Definition Mode and displayed to the right of the edit fields. If the System Default values are changed after the experiment schedule has been saved, when the experiment schedule is run in the System Operate mode, the new System Default values will be used.

3) "Vapor #." The number of the Gas Source (taken from the System Definition) is entered here. When <RETURN> is pressed, the program displays the name of the Material. If the number entered is not a defined material, exceedes the range, or if two gas numbers are in the same source bank, the computer will beep and will expect a new number to be entered.

4) "Concentration." This is the concentration in mg/m^3 of the selected material desired. The value must be in the range calculated from the Saturated Concentration value for the material entered in the System Definition. If there is a mixture of materials, the concentration range of the second gas is determined by the concentration of the first gas and if present the concentration range of the third gas is determined by the first and sencond gases. When the values are entered, the program will calculate and display the actual concentrations that will be produced.

Once all Exposure, Vapor and Concentration Data has been entered. You can view the different Vapors by using the **[PREVIOUS]** and **[NEXT]** buttons to flip through the vapors. If you wish to edit a Vapor, press the **[EDIT]** button, then re-enter the new values.

If you press the **[INSERT]** button in the Vapor Parameter Section, a space for the new vapor will open, with the vapor that was being displayed being renamed. (ie Vapor 2 will become Vapor 3, 3 to 4, 4 to 5, ect.) If the

Experiment Schedule is large, this may take some time to happen. The new vapor will initially have the same parameters as the last vapor displayed.

If you press the **[DELETE]** button, the vapor shown will be deleted, with all vapors after renamed. (ie Vapor 3 to 2, 4 to 3, 5 to 4, ect.)

To add vapors to the end of the Experiment Schedule, press the **[ADD]** button.

To save the Experiment Schedule, press the **[ACCEPT]** button.

To print a Hard Copy of the Experiment Schedule, press the **[PRINT]** button, making sure the printer is on-line.

To quit the Experiment Schedule Mode without saving the Schedule, press the **[CANCEL]** button.

c) System Check Mode

OBJECTIVE:
This mode is a self diagnosis to check for mechanical problems with the VG-7000 hardware. The program will display a simulation of the display panel of the equipment chassis. Each of the lights displayed on the screen is a button that when pressed will switch the corresponding light and valve on the VG-7000.

OPERATION:
When entering the System Check mode, window will ask you to press the reset button on the vapor generator. If there is no change when the reset button is pressed, check that the power on the VG-7000 is on and the connections between the Macintosh™ and the VG-7000.

When using the System Check mode, be sure that the carrier gas is off or disconnected to avoid the possiblity of generation unknown vapor mixtures.

To leave the System Check Mode, press the **[RETURN]** button.

d) System Calibration Mode

OBJECTIVE:
This mode will allow you to obtain a saturated concentration value for the Materials in the Transfer Containers and the Gas Cylinders.
Refer to Appendix B for a sample of the screen display.

OPERATION:
There are four data values needed for the System Calibration. They are:

1) "Gas Number." a value from 1 to 12, corresponding the maerials defined in the System Definition. When the value is entered, the Material Description is displayed. If the value is invalid, the computer will beep.
2) "Sampling Period." Time of Exposure Period. A 1 to 999 ten second interval.
3) "Sorbent Tube Beginning Weight (mg.)." The pre-exposure sorbent tube weight is entered here.
4) "Sorbent Tube End Weight (mg.)." The final, post-exposure sorbent tube wieght is entered here. After [RETURN] is pressed, the MASS FLOW RATE is calculated based on:

$$\frac{\Delta \text{ wt.}}{\text{Cal.Tm} \times \text{CFR}} \times \frac{1}{\text{Dil.}} = \text{MFR}$$

With Δ wt. - change in Weight(mg.) of Sorbent Tube
Cal.Tm - Calibration Time (min.)
CFR - Carrier Gas Flow Rate (liters/min.)
Dil. - Dilution Factor (50%)
MFR - Mass Flow Rate (mg./m3)

After the new MFR is calculated, it is displayed and can be saved in the System Definition Table by pressing the **[SAVE]** button.

After the Gas Number and Sampling Period values have been entered, to start the Calibration, press the **[CALIBRATE]** button.
A window will then ask you to press the reset button on the vapor generator. If there is no change when the reset button is pressed, check that the power on the VG-7000 is on and the connections between the

Macintosh™ and the VG-7000. Weigh the sorbent tube prior to vapor calibration and input this information into the appropriate blank.

The VG-7000 will then begin a warm up cycle. The time of the warm up cycle will be the same value that is placed in the system definition table. Then it will execute the Sampling Period, which will take the time specified. After the sampling period, weigh the sorbent tube and input this information into the appropriate blank. The program will automatically determine the vapor mass flow rate. If this value is correct press the **[SAVE]** button to save the information.

To halt the System Calibration, press the **[RESET]** button.

To leave the System Calibration Mode, press the **[CANCEL]** button.

e) SYSTEM OPERATE MODE

OBJECTIVE:
The system Operate Mode allows the selection and running of a previously created Experiment Schedule. It displays each Vapor Concentration as it is run, showing time until completion.
Refer to Appendix B for a sample of the screen display.

OPERATION:
When you enter the System Operate Mode, a window will display the Experiment Schedules currently on File on the disk in drive 1. Since this drive should contain no Experiment Schedules, press the **[CHANGE DRIVE]** button to access drive 2. If you need to change disks in the drive, press the **[EJECT]** button and insert the new disk. All the Experiment Schedules on the disk will be displayed. To select an Experiment Schedule to execute, click the Mouse twice on the file name or Click the Mouse once on the name to select it and press the **[SELECT]** button. If there are more files on the disk than can be displayed at once, use the arrows on the window to scroll up and down the list. If you decide not to execute an existing file, press the **[CANCEL]** button. When you have selected a file, you will then go to the System Operate Mode screen.

To start the Experiment, press the **[START]** button. A window will then ask you to press the reset button on the vapor generator. If there is no

change when the reset button is pressed, check that the power on the VG-7000 is on and the connections between the Macintosh™ and the VG-7000.

The program will then send the data for vapor number1 to the VG-7000. After the data is sent, the program will display a count-down timer showing time left for the System Warm Up and System Running period.

If you wish to Pause between Concentration runs, press the **[PAUSE]** button. A window will then appear with saying "Communication will Pause at the End of the Next Concentration." When the concentration run ends, The window will display "Communications Paused." To continue the experiment, press the **[CONTINUE]** button.

If you wish to stop the experiment, press the **[RESET]** button. A window will then tell you to "Press Reset Button on VapGen". Whe you have done this, press the **[CONTINUE]** button.

If you press the **[CANCEL]** button, any experiment running will immediatly stop and you will return to the Main Menu.

4. STARTING THE SYSTEM

To start the system all that is required is to turn on the Macintosh™ computer, and insert the two disks included with the computer startup disks. The two disks necessary to operate the VG-7000 system are (1) VG-7000 SYSTEM DISK "VG7000" and (2) VG-7000 DATA DISK "VGDATADISK". Once the disks are inserted to computer automatically loads the system operating program and associated files. The screen will display the system operating menu when initialization is complete.

5. ERROR MESSAGES

For all error messages, refer to the Microsoft® Basis Interpreter manual, Appendix B.

IV. VG-7000 OPERATION

1. Setting Up the Hardware

The following steps are required before applying power to the VG-7000 system:

1. Set up the Macintosh computer system in accordance with the Apple documentation. Verify that the Macintosh is functioning properly.

2. Check the VG-7000 tubing connectors on the rear panels of all modules to verify that they are tight. Check that the power cable from each module is connected to the correct receptacle on the rear of the electronics module.

3. Connect the RS-232C cable from the VG-7000 to the Macintosh communications port.

4. Connect a supply of 20 PSI clean air carrier gas to the "CARRIER INLET" fitting on the dilution module front panel. Check that the carrier gas air is connected to the correct fitting.

*5. Connect some tubing from the "VENT" fitting on the dilution module to an appropriate chemical fume hood. The pressure drop of the line from the vent to the hood should be kept small. Use the shortest length (e.g. less than 10 ft.) of the largest diameter (e.g. 1/4" I.D.) tubing practical.

***(VERY IMPORTANT NOTE: Each vapor used in the system is present at both the vent and the vapor outlet when that vapor is selected. Use great care in discharging the vent gases if toxic materials are used in this vapor generator.)

6. Connect the VG-7000 Power cord to a grounded receptacle supplying 115 Volts AC at 60 Hz. (The system requires less than 3 amps)

2. Loading Liquids into the Bubbler Module

The transfer containers require periodic inspection and removal from the temperature control block. In most cases it is not necessary to disconnect the tubing from the top of the containers. For inspection, all that is required is to disconnect the teflon tubing on the rear of the bubbler module, disconnect the control cable from the rear of the module, slide the module out of the rack on its rails, and raise the container of interest out of the temperature control block and check that the liquid level if at least 1-2" above the bottom of the container. This is necessary to insure that the carrier gas stream will come into contact with the liquid. The higher the liquid level is above the bottom of the container, the greater the degree of gas/liquid contact will be during operation and the more saturated the vapor produced. The frequency of inspection of the transfer container liquid level depends of the volatility of the material present and the frequency which it is used. Initially, it is recommended that the liquid level be checked at least weekly and after several weeks this inspection schedule can be adjusted as appropriate for each container.

1. Disconnect the teflon tubing at the connectors at the rear of the bubbler module. Also disconnect the module power cable.
2. Slide the bubbler module out of the rack on its rails.
3. Grasp the edges of the transfer container to be inspected.
4. Pull upward on the lid to raise the transfer container out of the temperature control block.

   Do Not Pull On the Teflon Transfer Lines
5. Inspect the liquid level to insure that adequete material is present.
6. If liquid level is adequete skip to step 9.
7. Remove cover to transfer container by turning in a counterclockwise direction.
8. Replace teflon tape on threaded portion of container if necessary.
9. Fill container with material desired to between 1/2 to 2/3 full.
10. Replace cover carefully to avoid spilling material. Tighten cover.

    Do Not Allow Liquid to Enter The Transfer Lines
11. Place container back into temperature control block and slowly push down until the container rests on the bottom.
12. Position container until teflon transfer tubing appears to be without

tension and kinks.

13. Push the module back into the rack.
14. Reconnect the stainless tubing and electrical power connector.

APPENDIX A.

Sample Experiment Schedule

EXPERIMENT SCHEDULE : VGDATADISK:Exp88-04-25A.VG2
DATE CREATED : 04-26-1988 Todays Date : 04-26-1988
LAST UPDATE : 04-26-1988 Time : 14:06:19

Number of Vapors : 4
Approximate Experiment Duration : 8.7

VAPOR NUMBER : 1
GAS 1 : 1 : AMMONIA
Equilibrium Pd. : 180
Exposure Pd. : 30 - System Default
Off Pd. : 30 - System Default
No. Exposure Cycles : 10 - System Default

Concentration Gas 1 : 1.31E+01
Duty Cycles -- MIXTURE : 100 0 0
DILUTION : 98 100 100

VAPOR NUMBER : 2
GAS 1 : 2 : GAS 2
GAS 2 : 6 : GAS 6
Equilibrium Pd. : 180
Exposure Pd. : 30 - System Default
Off Pd. : 30 - System Default
No. Exposure Cycles : 10 - System Default

Concentration Gas 1 : 5.00E-02
Concentration Gas 2 : 5.00E-02
Duty Cycles -- MIXTURE : 50 50 0
DILUTION : 10 10 10

VAPOR NUMBER : 3
GAS 1 : 3 : GAS 3
GAS 2 : 11 : GAS 11
Equilibrium Pd. : 180
Exposure Pd. : 30 - System Default
Off Pd. : 30 - System Default
No. Exposure Cycles : 10 - System Default

Concentration Gas 1 : 1.48E-03
Concentration Gas 2 : 1.46E-03
Duty Cycles -- MIXTURE : 55 0 45
DILUTION : 3 3 3

VAPOR NUMBER : 4

Concentration Gas 1 : 1.39E-02
Concentration Gas 2 : 1.36E-02
Duty Cycles -- MIXTURE : 55 0 45
DILUTION : 7 6 6

APPENDIX B.

Sample System Operation Screens

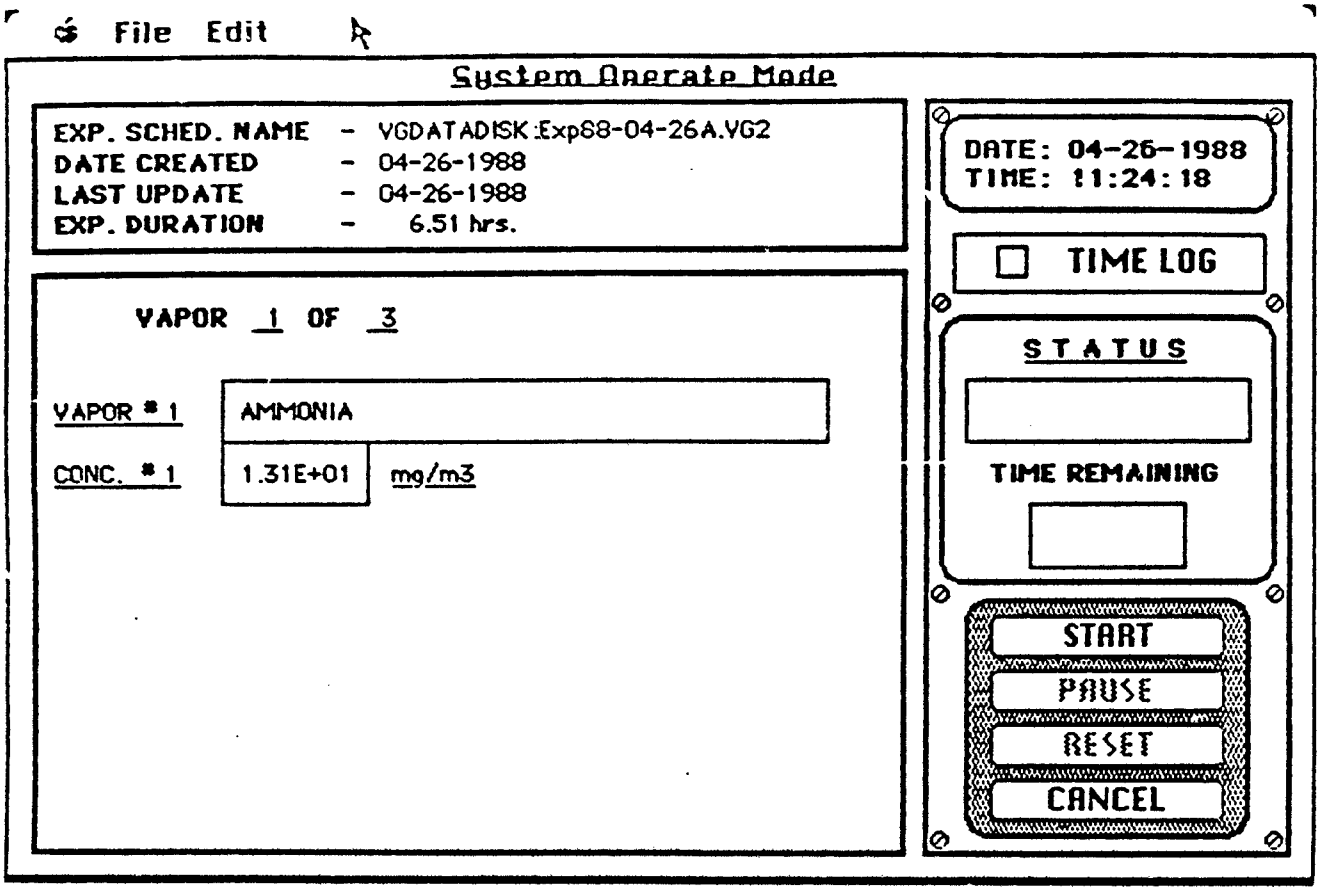
File Edit
System Operate Mode
EXP. SCHED. NAME - VGDATADISK:Exp88-04-26A.VG2
DATE CREATED - 04-26-1988
LAST UPDATE - 04-26-1988
EXP. DURATION - 6.51 hrs.
DATE: 04-26-1988
TIME: 11:24:18
TIME LOG
VAPOR 1 OF 3
VAPOR # 1
AMMONIA
CONC. # 1
1.31E+01
mg/m3
STATUS
TIME REMAINING
START
PAUSE
RESET
CANCEL

File Edit

MICROSENSOR SYSTEMS, INC.
Automatic Vapor Generating System

SELECT OPERATING MODE

SYSTEM DEFINITION

EXPERIMENT SCHEDULE

SYSTEM CHECK

SYSTEM CALIBRATE

SYSTEM OPERATE

IMMEDIATE OPERATE

EXIT VAPOR GENERATOR

File Edit

System Definition Mode — Date Created : 04-25-1988

# of Transfer Containers 8	Material	Saturated Conc. (mg/m3)
GAS # 1	GAS 1	100
GAS # 2	GAS 2	100
GAS # 3	GAS 3	100
GAS # 4	GAS 4	100
GAS # 5	GAS 5	100
GAS # 6	GAS 6	100
GAS # 7	GAS 7	100
GAS # 8	GAS 8	100
# of Gas Cylnders 4	Material	Conc. (mg/m3)
GAS # 1	GAS 9	100
GAS # 2	GAS 10	100
GAS # 3	GAS 11	120
GAS # 4	GAS 12	100

Carrier Gas Flow Rate (cc/min) (0 to 300): 100

System Temp. (°C): 15

System Defaults
10 Sec. Int. (1-999)

Equil.Pd.	180
Exp.Pd.	30
Off Pd.	30
No. Exp.Cycles	10

ACCEPT

CANCEL

PRINT

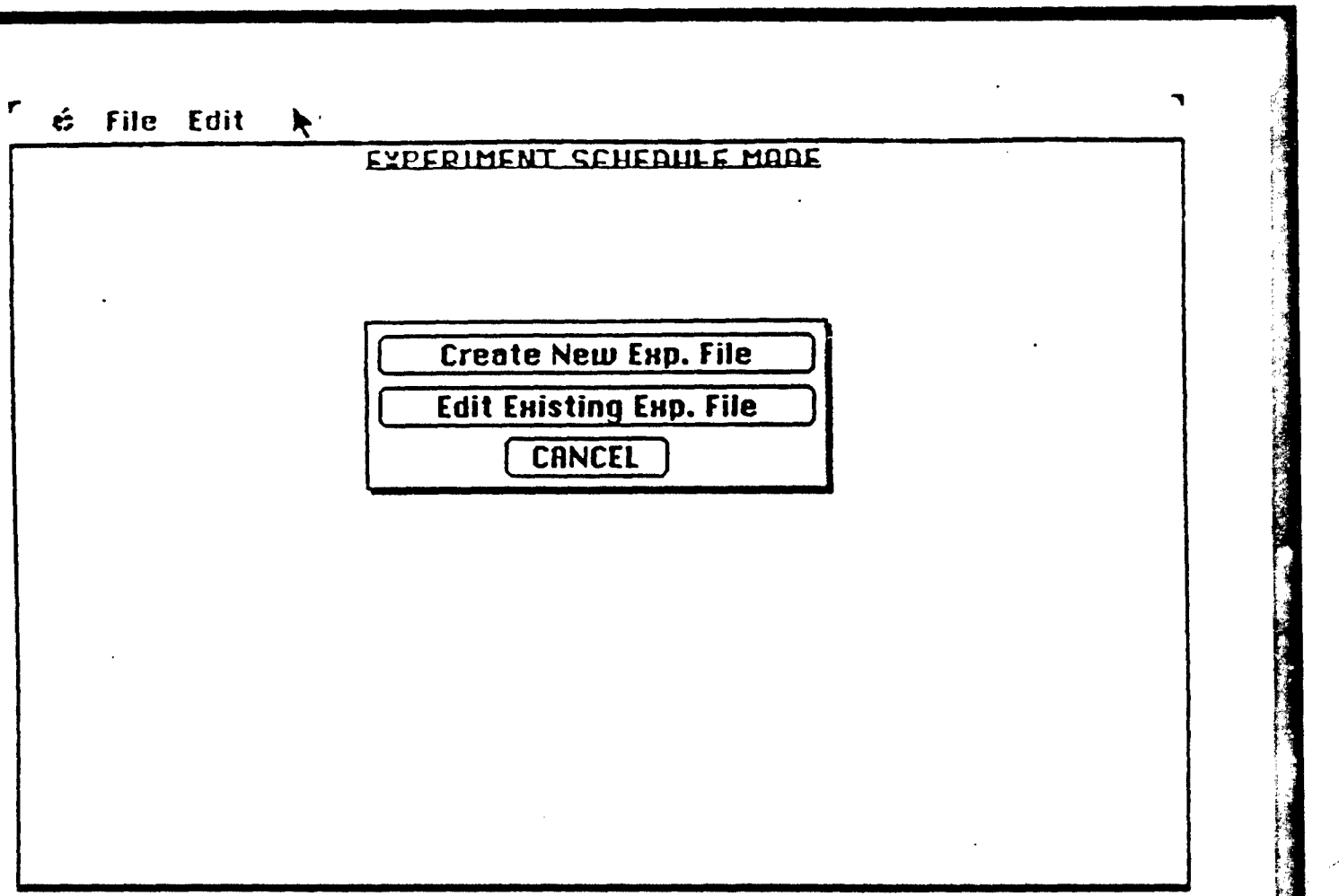
File Edit
EXPERIMENT SCHEDULE MODE
Create New Exp. File
Edit Existing Exp. File
CANCEL

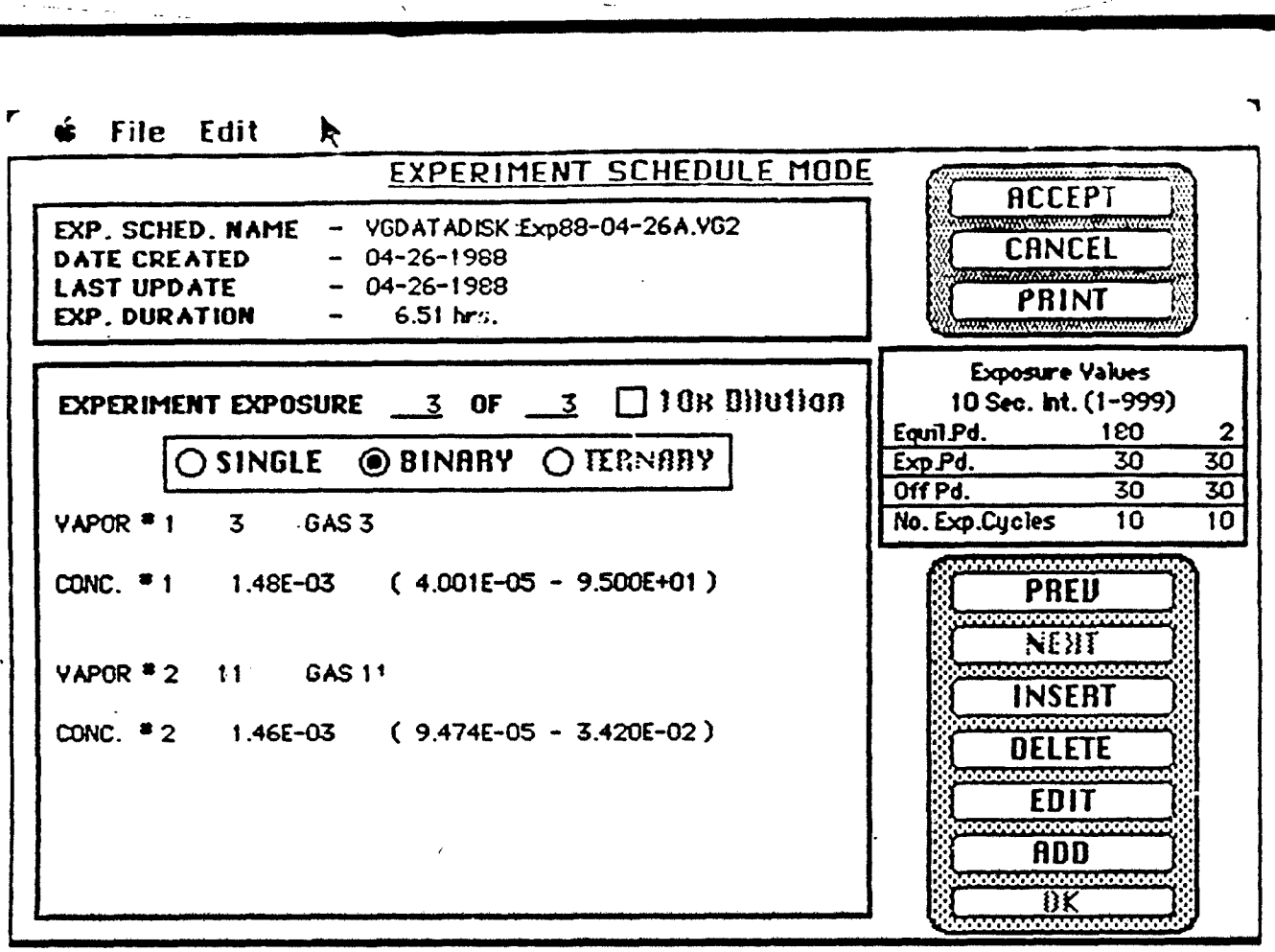
File Edit
EXPERIMENT SCHEDULE MODE
EXP. SCHED. NAME - VGDATADISK:Exp88-04-26A.VG2
DATE CREATED - 04-26-1988
LAST UPDATE - 04-26-1988
EXP. DURATION - 6.51 hrs.
ACCEPT
CANCEL
PRINT
EXPERIMENT EXPOSURE 3 OF 3
10X Dilution
SINGLE
BINARY
TERNARY
VAPOR # 1 3 GAS 3
CONC. # 1 1.48E-03 (4.001E-05 - 9.500E+01)
VAPOR # 2 11 GAS 11
CONC. # 2 1.46E-03 (9.474E-05 - 3.420E-02)
Exposure Values
10 Sec. Int. (1-999)
Equil.Pd. 180 2
Exp.Pd. 30 30
Off Pd. 30 30
No. Exp.Cycles 10 10
PREV
NEXT
INSERT
DELETE
EDIT
ADD
OK

File Edit

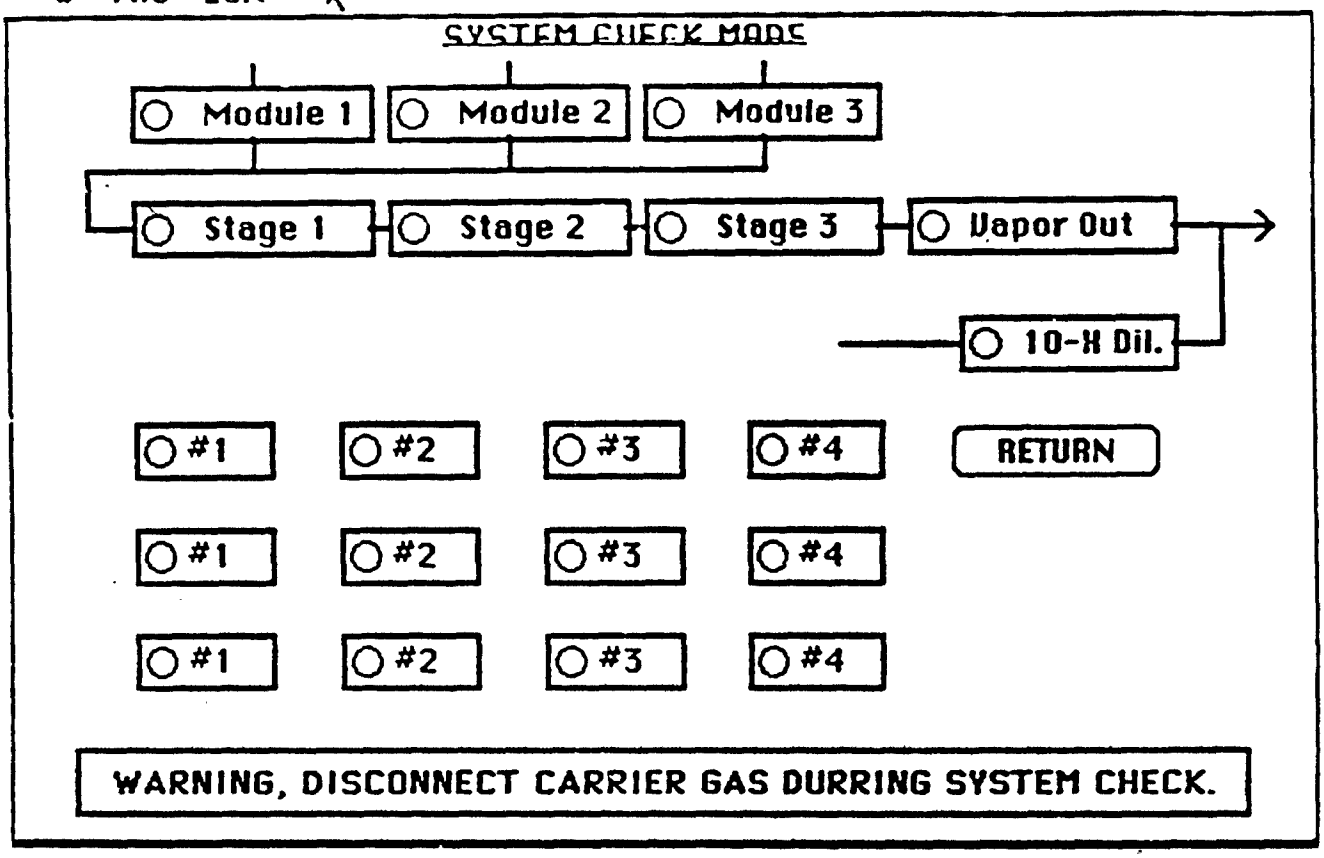
SYSTEM CHECK MODE
Module 1
Module 2
Module 3
Stage 1
Stage 2
Stage 3
Vapor Out
10-X Dil.
#1
#2
#3
#4
RETURN
#1
#2
#3
#4
#1
#2
#3
#4
WARNING, DISCONNECT CARRIER GAS DURRING SYSTEM CHECK.

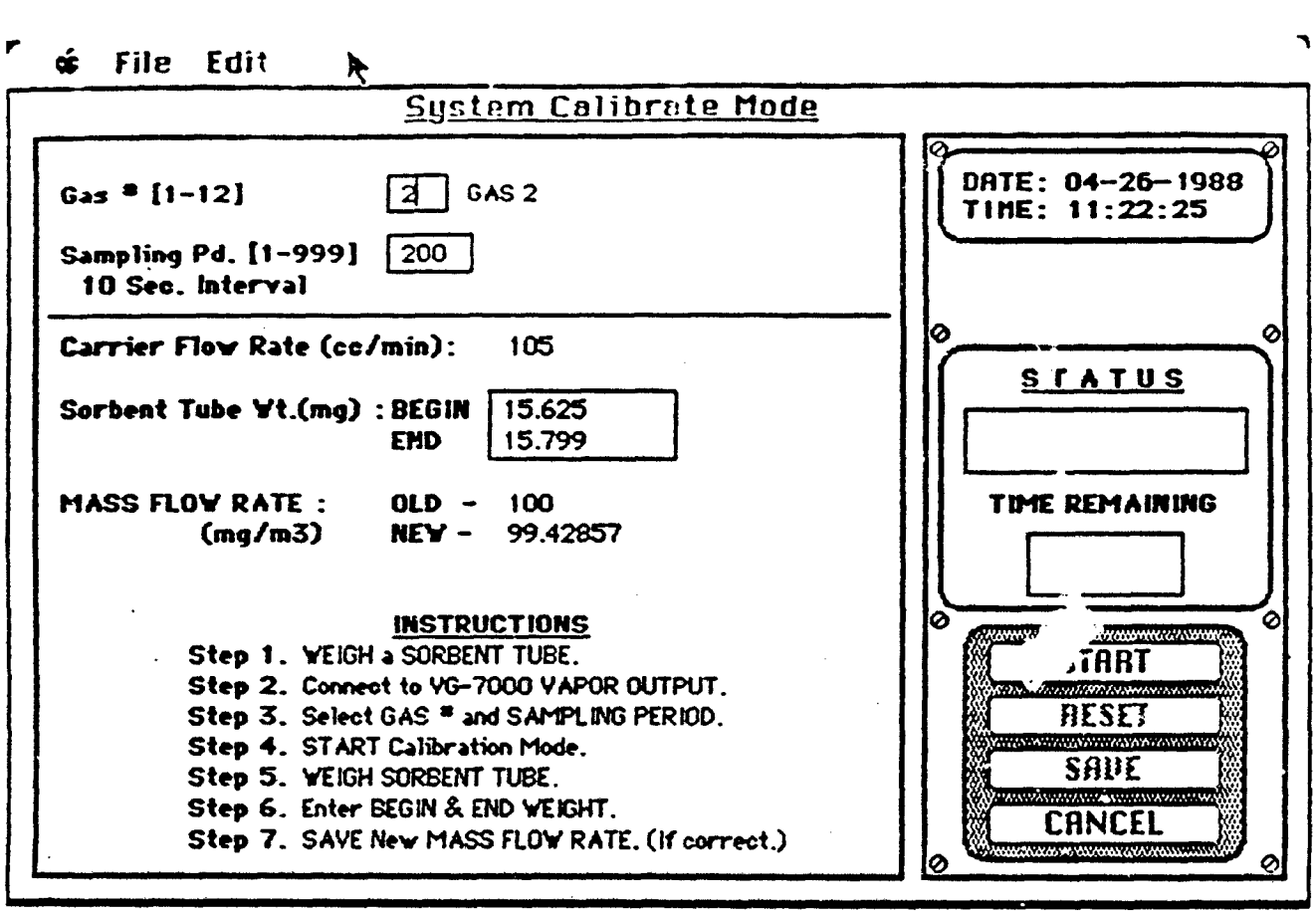
File Edit
System Calibrate Mode
Gas # [1-12]
2
GAS 2
Sampling Pd. [1-999]
10 Sec. Interval
200
Carrier Flow Rate (cc/min): 105
Sorbent Tube Wt.(mg) : BEGIN 15.625
END 15.799
MASS FLOW RATE : OLD - 100
(mg/m3) NEW - 99.42857
INSTRUCTIONS
Step 1. WEIGH a SORBENT TUBE.
Step 2. Connect to VG-7000 VAPOR OUTPUT.
Step 3. Select GAS # and SAMPLING PERIOD.
Step 4. START Calibration Mode.
Step 5. WEIGH SORBENT TUBE.
Step 6. Enter BEGIN & END WEIGHT.
Step 7. SAVE New MASS FLOW RATE. (If correct.)
DATE: 04-26-1988
TIME: 11:22:25
STATUS
TIME REMAINING
START
RESET
SAVE
CANCEL

APPENDIX C.

VG-7000 Pneumatic Flow Diagram

MICROSTRUCTURE SYSTEMS, INC.

VG-7000 AUTOMATIC VAPOR GENERATION SYSTEM

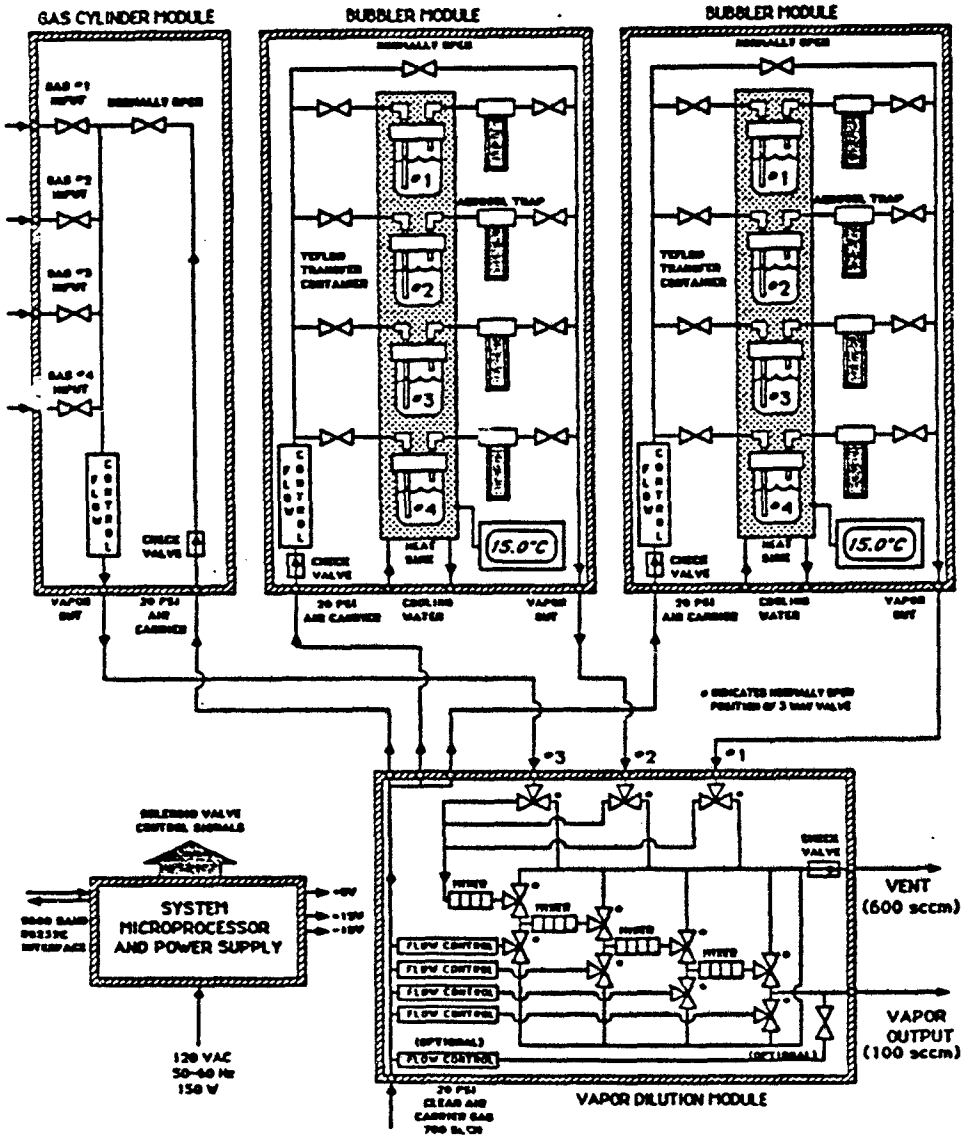

APPENDIX D.

Connector Cable Pin Assignments

DILUTION MODULE CONNECTOR PIN ASSIGNMENTS

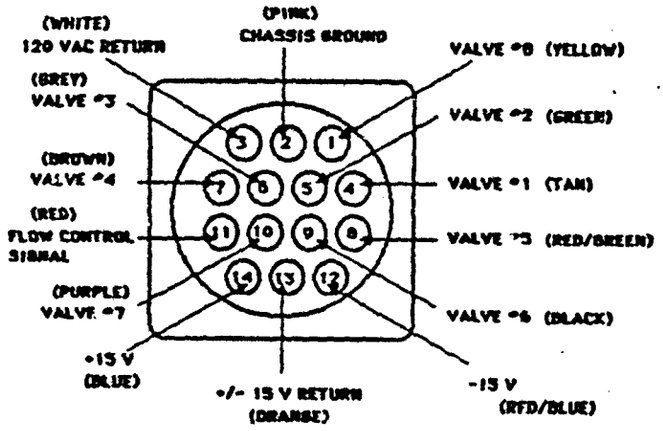

CYLINDER MODULE CONNECTOR PIN ASSIGNMENTS

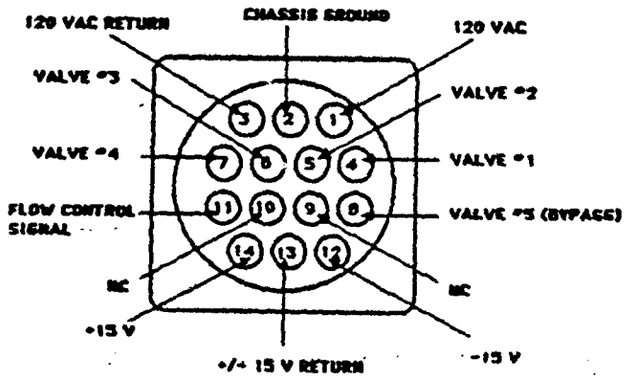

BUBBLER MODULE CONNECTOR PIN ASSIGNMENTS

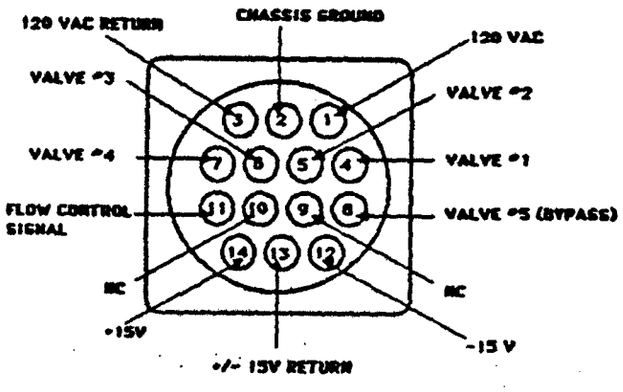

APPENDIX E.

Time Log Sample Printout

VG-7000 VAPOR GENERATOR SYSTEM OPERATE TIME LOG
EXPERIMENT SCHEDULE : HARD DISK:BAS COMP:Exp88-04-24A.VG2
DATE CREATED : 04-24-1988 Run Date : 04-24-1988
LAST UPDATE : 04-24-1988 Time : 22:35:14

Number of Vapors : 5
Approximate Experiment Duration : 25260

GAS 1 : 2 : GAS 2
GAS 2 : 0 : GAS 2
GAS 3 : 0 : GAS 2
Equilibrium Pd. : 120
Exposure Pd. : 30
Off Pd. : 30
No. Exposure Cycles : 10

VAPOR NUMBER : 1
Concentration Gas 1 : 5.30E+01
Concentration Gas 2 : 0.00E+00
Concentration Gas 3 : 0.00E+00
Duty Cycles : 100 0 0 53 100 100

SYSTEM WARMUP BEGIN -> 04-24-1988, 22:35:33

SYSTEM OPERATE BEGIN -> 04-24-1988, 22:55:33

CYCLE No.: 1 ON :22:55:33 OFF :23:00:33
CYCLE No.: 2 ON :23:05:33 OFF :23:10:33
CYCLE No.: 3 ON :23:15:33 OFF :23:20:33
CYCLE No.: 4 ON :23:25:33 OFF :23:30:33
CYCLE No.: 5 ON :23:35:33 OFF :23:40:33
CYCLE No.: 6 ON :23:45:33 OFF :23:50:33
CYCLE No.: 7 ON :23:55:33 OFF :00:00:33
CYCLE No.: 8 ON :00:05:33 OFF :00:10:33
CYCLE No.: 9 ON :00:15:33 OFF :00:20:33
CYCLE No.: 10 ON :00:25:33 OFF :00:30:33

GAS 1 : 7 : GAS 3
GAS 2 : 3 : GAS 3
GAS 3 : 0 : GAS 3
Equilibrium Pd. : 120
Exposure Pd. : 30
Off Pd. : 30
No. Exposure Cycles : 10

VAPOR NUMBER : 2
Concentration Gas 1 : 5.31E+01
Concentration Gas 2 : 2.39E+01
Concentration Gas 3 : 0.00E+00
Duty Cycles : 31 69 0 77 100 100

SYSTEM WARMUP BEGIN -> 04-25-1988, 00:35:46